

# UNIVERSITY OF SOUTHAMPTON



DEPARTMENT OF SHIP SCIENCE

FACULTY OF ENGINEERING

AND APPLIED SCIENCE

THE DESIGN, CONSTRUCTION AND CALIBRATION  
OF A FIVE-COMPONENT STRAIN GAUGE  
WIND TUNNEL DYNAMOMETER

by A.F. Molland, November 1976

Ship Science Report No 1/77

THE DESIGN, CONSTRUCTION AND CALIBRATION OF  
A FIVE-COMPONENT STRAIN GAUGE  
WIND TUNNEL DYNAMOMETER

A. F. Molland  
November 1976

## SUMMARY

The Report describes the design, construction and calibration of a five-component strain gauge dynamometer suitable for the free-stream testing of control surfaces in a wind tunnel at a Reynold's Number of up to  $1.5 \times 10^6$  .

The dynamometer has been designed primarily for the testing of ship control surfaces including, in particular, skeg rudders; it has facilities for the independent adjustment of angle of attack, and the derivation of the forces and moments, on both rudder and skeg.

A review is made of background design philosophy and design requirements, leading to the choice of strain gauged shear flexures incorporated in a fabricated structure; a full description of the dynamometer follows, together with the relevant design calculations.

A report on the complete calibration leading to the interaction correction equations is given; assessments of the magnitudes and origins of the interactions and overall measuring accuracy of the dynamometer confirm the choice of overall design concept.

Brief comments are made on the operation of the dynamometer following successful commissioning experiments in the wind tunnel.

SUMMARY								
1	INTRODUCTION	...	...	...	...	...	...	1
2	DESIGN REQUIREMENTS							
2.1	Components	...	...	...	...	...	...	2
2.2	Loading	...	...	...	...	...	...	2
2.3	Accuracy	...	...	...	...	...	...	3
2.4	Dimensional Requirements	...	...	...	...	...	...	3
2.5	Independent Measurement of Rudder and Skeg Forces	...	...	...	...	...	...	4
2.6	Angular Adjustment	...	...	...	...	...	...	4
3	PHILOSOPHY OF DESIGN AND OUTLINE OF PRINCIPAL DESIGN FEATURES							
3.1	General	...	...	...	...	...	...	5
3.2	Flexure Types	...	...	...	...	...	...	5
3.3	Overall Layout of Flexures and Gauges	...	...	...	...	...	...	6
3.4	Measurement of Forces and Angular Adjustment of Test Models...	...	...	...	...	...	...	7
3.5	Worm Drives	...	...	...	...	...	...	8
3.6	Vernier Scales	...	...	...	...	...	...	8
3.7	Main Lower Rotational Bearing (Skeg and Dynamometer)...	...	...	...	...	...	...	9
3.8	Main Upper Rotational Bearing (Rudder)	...	...	...	...	...	...	9
3.9	Dimensions and Materials of Dynamometer Frame	...	...	...	...	...	...	9
3.10	Dimensions and Materials of Flexures	...	...	...	...	...	...	10
3.11	Warping of Plates Adjacent to Measuring Flexures and Measurement of Torque	...	...	...	...	...	...	12
4	STRAIN GAUGES, ELECTRICAL CIRCUITS AND INSTRUMENTATION							
4.1	General	...	...	...	...	...	...	15
4.2	Selection and Mounting of Strain Gauges	...	...	...	...	...	...	15
4.3	Bridge Circuits	...	...	...	...	...	...	17
4.4	Instrumentation	...	...	...	...	...	...	18
4.5	Bridge Supply Voltage	...	...	...	...	...	...	18

5	CALIBRATION						
5.1	General	...	...	...	...	...	22
5.2	Calibration Rig, Application and Alignment of Calibration Forces						22
5.2.1	Rig	...	...	...	...	...	22
5.2.2	Calibration Masses	...	...	...	...	...	23
5.2.3	Application of Forces	...	...	...	...	...	23
5.2.4	Locking of Chosen Skeg and Rudder Angles	...	...	...	...	...	23
5.2.5	Alignment of Forces	...	...	...	...	...	23
5.3	Proof Loads	...	...	...	...	...	25
5.4	Deflections	...	...	...	...	...	26
5.5	Calibration Data and Discussion	...	...	...	...	...	26
5.5.1	Bridge Voltages and Electrical Zero Stability	...	...	...	...	...	26
5.5.2	Derivation of True Roll Centre of Dynamometer	...	...	...	...	...	27
5.5.3	Component Calibration Slopes	...	...	...	...	...	28
5.5.4	Comparison Between Measured and Predicted Sensitivities	...	...	...	...	...	29
5.5.5	Interactions	...	...	...	...	...	31
5.5.6	Second Order Interactions	...	...	...	...	...	31
5.5.7	Calibration Matrix	...	...	...	...	...	33
5.5.8	Origins of Interactions	...	...	...	...	...	35
5.5.9	Secondary Interactions Caused by Loads on Skeg	...	...	...	...	...	36
5.6	Hysteresis and Creep	...	...	...	...	...	38
5.7	Repeatability and Accuracy	...	...	...	...	...	39
5.8	Calibration Time	...	...	...	...	...	41
5.9	Sixth (Z-Direction) Component	...	...	...	...	...	41
5.10	Summary of Calibration Results	...	...	...	...	...	42
6	OPERATION						
6.1	General	...	...	...	...	...	45
6.2	Attachment of Rudder to Dynamometer and Dynamometer to Ground..						45
6.3	Check Calibration Facilities...	...	...	...	...	...	46
6.4	Details of Tunnel Operation	...	...	...	...	...	46
6.5	Maximum Allowable Loads and Moments	...	...	...	...	...	48
6.6	Maximum Angular Adjustments of Rudder and Skeg	...	...	...	...	...	48
6.7	Corrections Caused by Changes in Bridge Voltages	...	...	...	...	...	49
6.8	Resolution of Measured Loads and Moments caused by Rotation of Dynamometer, hence Dynamometer Axes	...	...	...	...	...	49
6.9	Note on Units	...	...	...	...	...	50

						PAGE
7	CONCLUSIONS.	...	...	...	...	52
	ACKNOWLEDGEMENTS	...	...	...	...	55
	NOMENCLATURE	...	...	...	...	56
	REFERENCES	...	...	...	...	58
APPENDIX	A1	SUMMARY OF FLEXURE TYPES AND CHOICE OF FLEXURES				
	A1.1	Summary of Flexure Types	...	...	...	60
	A1.2	Choice of Type of Flexure	...	...	...	60
APPENDIX	A2	OUTLINE OF OPERATION OF THE SHEAR FLEXURE	...			63
APPENDIX	A3	CALCULATIONS FOR DIMENSIONS OF FLEXURES				
	A3.1	Summary of Formulae and Data Applicable to the Design of the Shear Flexures	...			64
	A3.2	Dimensions of Flexures	...	...	...	65
APPENDIX	A4	ERRORS IN STRAIN DUE TO ERRORS IN FLEXURE DIMENSIONS	...	...	...	75
APPENDIX	A5	SUMMARY OF PROPERTIES OF THE RESISTANCE STRAIN GAUGE AND UNBALANCED BRIDGE...				77
APPENDIX	A6	RE-ANALYSIS OF STRAIN AND SENSITIVITY PREDICTIONS	...	...	...	80

## 1. INTRODUCTION

A proposed series of free-stream tests in the wind tunnel (Ref. 1 ) at the University of Southampton on models of ship control surfaces including, in particular, the case of the semi-balanced skeg rudder, called for the use of a dynamometer specifically designed and constructed for this purpose.

The proposed experiments required that the dynamometer should be suitable for mounting the models through the floor of the 7' x 5' section of the wind tunnel (Fig. 1 ), be capable of the measurement of five components, measure the rudder and skeg forces either separately or combined and allow independent adjustment of angle of attack of both control surface and skeg about a common axis.

Design parameters for the dynamometer including components, dimensions, loading and angular adjustments were basically derived from the projected control surface test series; where practicable, account was also taken of possible future extensions to its use including the testing of other ship control surfaces such as stabiliser fins and other control surfaces and half (or reflection-plane) models in general.

Following a review of wind tunnel balances using strain gauge techniques, and the determination of some desirable design features from the calibration of a small three-component dynamometer constructed by the writer for supplementary test work, a final design was evolved and subsequently constructed and calibrated.

The design, construction and calibration of the dynamometer was carried out in imperial units; suitable conversion factors are presented as necessary in the Report enabling the results of tests with the dynamometer to be analysed in S.I. units.

## 2. DESIGN REQUIREMENTS

### 2.1 Components:

The dynamometer was to be capable of the measurement of five components (two forces and three moments) Fig. 2 , comprising lift, drag, torque (hence derivation of control surface centre of pressure chordwise) and moments about X and Y axes (hence derivation of control surface centre of pressure spanwise).

### 2.2 Loading:

A control surface mean chord of 450 mm (17.7 in ) and span of 900 mm (35.4 in ) was chosen as being the largest size possible for the University wind tunnel commensurate with acceptable limits on corrections due to blockage. The maximum working loads on the dynamometer were therefore estimated assuming the largest anticipated model and assuming  $C_L \text{ max.} = 1.2$ ,  $C_D \text{ max.} = 0.6$ ,  $CP_z = 6 \text{ in}$  ,  $CP_s = 17 \text{ in}$  and a maximum wind speed of 160 ft/sec.

The proposed design load and moment requirements were therefore as follows:

Lift	L	....	170 lbf
Drag	D	....	85 lbf
Torque	MZ	....	1200 lbf in *
Moment about X axis	MX	....	4100 lbf in **
Moment about Y axis	MY	....	2100 lbf in **

\* about vertical centre axis of dynamometer

\*\* about horizontal roll axis of dynamometer

In order to take account of rotation of the skeg and hence dynamometer axis (the need for rotating the dynamometer is discussed later in SECTION 3.4 ), the dynamometer has to carry



the following maximum loads and moments relative to its own rotational axes:

Transverse load	$N_{\beta}$ ....	190 lbf
Axial load	$A_{\beta}$ ....	140 lbf
Torque	$MZ_{\beta}$ ....	1200 lbf in
Moment about longitudinal axis	$MX_{\beta}$ ....	4600 lbf in
" " transverse axis	$MY_{\beta}$ ....	3400 lbf in

Design calculations and proof loads take account of these maximum values. It is to be noted that these maximum loads and moments can occur individually due to positive and negative rotation of the whole dynamometer; the dynamometer is however not designed to carry all the maximum loads and moments simultaneously. An outline of some permissible combinations of these maxima is given in SECTION 6.5.

### 2.3 Accuracy:

Published literature indicates that accuracies of the order of 0.1% to 0.5% of the full scale loads are attainable with dynamometers utilising strain-gauge flexures. It was considered that, for this dynamometer, accuracies of the order of  $\frac{1}{2}\%$  would be desirable. Accuracy, however, is closely related to sensitivity which is itself related to flexure stiffness. APPENDIX A3.2 outlines the background reasons for the choice of skin strains and sensitivities for the various flexures, and SECTION 5.7 discusses the resulting accuracies for the calibration loads.

### 2.4 Dimensional Requirements:

The distance between attachment points of rudder and skeg models formed the only physical limitations on size; this was restricted to a maximum of 6.25 in to accommodate the limiting case of envisaged rudder/skeg combinations.

## 2.5 Independent Measurement of Rudder and Skeg Forces:

In order to investigate variations such as skeg size and angle of attack and the contribution made by the skeg, it was required that the forces and moments on rudder and skeg could be determined either separately or combined, Fig. 3 .

## 2.6 Angular Adjustment:

The projected experiments required that independent adjustment of angle of attack for both control surface and skeg about a common axis could be made, Fig. 4 , and that the rudder angle  $\delta$  could be varied through  $\pm 35^\circ$  and the skeg angle  $\beta$  through  $\pm 25^\circ$ .

### 3. PHILOSOPHY OF DESIGN AND OUTLINE OF PRINCIPAL DESIGN FEATURES

#### 3.1 General:

The measurement of forces and moments by means of strain-gauged flexures was adopted since, with careful design, force and moment readings of sufficient magnitude can be achieved with very small absolute deflections of the dynamometer. This criterion was important in the case of the proposed tests which would include control surfaces whose component parts (rudder plus skeg) were required to be separated by a small, but constant, gap during testing. Also, a small constant gap is required between the control surface and the tunnel base, or groundboard, during testing. Such a near rigid system is also capable of coping with the fluctuating loadings which can occur on a control surface near stall.

Fig. 5 illustrates the principal features of the completed dynamometer and Figs. 6, 7 and 8 show overall views.

The following Sections outline the philosophy of design of the various features.

#### 3.2 Flexure Types:

Refs. 2 to 19 were surveyed in respect of applications of strain gauges to the measurement of forces and moments.

In respect of Refs. 8 to 16 it should be noted that whilst strain gauge technology itself has progressed considerably since the publication of these reports, the overall concepts and requirements of balance or dynamometer design remains unchanged. Refs. 8 and 9 contain useful design information and Ref. 16 contains useful information on calibration of balances. Whilst Refs. 10 to 14 are not referred to specifically in this Report they are included in the list of references since it is considered that they formed useful background reading.

An outline summary of principal flexure types and choice of flexures is given in APPENDIX A1.

The size of the proposed dynamometer, and available manufacturing facilities, called for a design of fabricated construction; this compares with the possibility of machining thick end plates and flexures from one solid piece of material. It should also be noted that fabricated construction does allow the future exchange of flexures to suit a different range of loading requirements for the dynamometer; e.g. dynamometers designed on this principle are discussed in Ref. 19.

Due to the possible incompleteness of end fixing in fabricated construction, and the desire for flexures of simple design and hence construction, force and moment measurement by flexures gauged to measure the direct strain resulting from simple shear was adopted. Some typical applications of the shear plate principle, and its advantages, are given in Refs. 17 and 18.

### 3.3 Overall Layout of Flexures and Gauges:

The overall design layout may be considered as two distinct platform arrangements, the lower measuring lift, drag and torque and the upper measuring moments about X and Y axes. (This assumes  $\beta = 0$ , Fig. 4 b, i.e. dynamometer axis is on flow axis).

The combination of the lower and upper platforms, Fig. 9 a, yields the measurement of the five components. Lower Platform (Fig. 9 b):- This comprises two rigid plates separated by the four force flexures ( $c_1, c_2, d_1, d_2$ ) and four supplementary pillar flexures ( $s_1, s_2, s_3, s_4$ ). The gauges are arranged at  $45^\circ$  to horizontal whereby they measure linear strain due to shear. When flexures  $d_1$ , and  $d_2$  record, say, drag, flexures  $c_1$  and  $c_2$  bending in contraflexure offer relatively little resistance, and outputs from bridge circuits on  $c_1$  and  $c_2$  are arranged to cancel. Similarly, when flexures  $c_1$  and  $c_2$  record, say, lift,  $d_1$  and  $d_2$  cancel. Torque is measured by further gauges on  $d_1, d_2, c_1$  and  $c_2$  which are arranged to record the difference of forces on  $d_1$  and  $d_2$ , and  $c_1$  and  $c_2$ .

Since the applied forces are some distance above the mid plate, the measuring flexures in the lower platform are also subjected

to tensile and compressive loading, Fig. 9 c . If the gauges are perfectly aligned the influence of tension and compression in these flexures will be cancelled in the bridge circuits; however, since the tensile and compressive loads are relatively high, even small misalignment of the gauges coupled with the high skin strains could lead to incomplete cancellation and unwanted interaction effects. In order to minimise the possibility of these effects, supplementary pillar flexures ( $s_1$  ,  $s_2$  ,  $s_3$  and  $s_4$  ), which are not gauged, are located at the corners to share these loads with the measuring flexures. These pillars, Fig. 9 d , are designed whereby they will share the tensile and compressive loads, but offer very little resistance to the horizontal shear loads.

Upper Platform (Fig. 9 e ):- This comprises a rigid centre portion through which the moments are transmitted, separated from the rigid mid-plate by the four moment flexures. The gauges are arranged at  $45^\circ$  to the effective forces (assumed linear) at flexure ends whereby they measure linear strain due to shear. When flexures  $a_1$  and  $a_2$  record, say, moment MY, flexures  $b_1$  and  $b_2$  warp, offering relatively little resistance, and outputs from bridge circuits on  $b_1$  and  $b_2$  are arranged to cancel. Similarly when flexures  $b_1$  and  $b_2$  record, say, MX,  $a_1$  and  $a_2$  cancel. In this arrangement little resistance to torque is offered; hence whilst the bridge circuits are arranged to cancel torque response, supplementary anti-torque flexures ( $T_1$  and  $T_2$  ), which are not gauged, are required to minimise angular deflection. These flexures are basically thin plates arranged in a horizontal plane between the rigid centre portion and the mid-plate whereby they offer high resistance to torque and very little resistance to MX or MY.

### 3.4 Measurement of Forces and Angular Adjustment of Test Models:

The design requirements call for independent adjustment of angle of attack for rudder and skeg and independent measurement of forces on rudder and skeg; the achievement of these two basic design requirements is illustrated in the simplified diagrams, Fig. 10 , which show alternative working arrangements of the dynamometer.

In case (a), the skeg is attached to the 'active' side of the dynamometer and the system will measure the forces and moments on the rudder plus skeg combination. In case (b), the skeg is fixed direct to the base (rotational) by means of an 'insert piece' whereby only the forces and moments on the rudder are measured.

In cases (a) and (b) the rudder and skeg angles are adjusted about a common axis. Rudder angle is adjusted relative to dynamometer, and skeg (and dynamometer) angle adjusted relative to a fixed base plate. Hence in the case of rotation of the skeg there is a change in the direction of the measuring axes; the resolution of the forces for this case is described in SECTION 6.8 . It should be added that the possibility of rotating the skeg relative to the dynamometer (for cases (a) and (b) ) was investigated in the early design stages. Whilst possible, such a system would have necessitated a very sophisticated design involving running bearings within bearings and demanded manufacturing tolerances to very fine limits in order to minimise play in the increased number of moving parts; such a system would also have required a further worm drive and angular measurement quadrant. In order to keep the overall design relatively simple, and since the resolution of axial and normal forces described in SECTION 6.8 is a relatively straightforward task, the system described above was adopted for the angular adjustment of rudder and skeg.

### 3.5 Worm Drives:

Angular adjustment is carried out by manually driven worm gears for which one revolution of the worm drive results in 0.83 deg. radial movement of the worm wheel for both rudder and skeg; the wheels are constructed of brass and the drives of steel. These gears allow very small changes in angle to be made if desired. In order to preclude the possibility of any backlash in the worm drives having an influence on the angles tested, small bolts with wing-nuts are provided to lock the chosen angles for rudder and skeg.

### 3.6 Vernier Scales:

Vernier scales (20:1 ratio) moving over the radial

quadrants allow adjustment of rudder and skeg angles to  $0.025^\circ$ . This order of resolution is required since an error of  $0.025^\circ$  in angular measurement yields an error of approximately  $\frac{1}{2}\%$  in lift at  $10^\circ$  and at  $5^\circ$  a similar angular error yields an error in lift of approximately  $\frac{1}{2}\%$ .

### 3.7 Main Lower Rotational Bearing (Skeg and Dynamometer):

For the lower steel bolt attaching the rotational base to the fixed base a simple sleeved bearing is used; since the stainless steel sleeved rotational base runs on the centre bolt which is fixed by virtue of a press fit into the fixed base, play in the bearing is minimised.

### 3.8 Main Upper Rotational Bearing (Rudder):

The upper main steel bolt carrying the rudder runs in tapered roller bearings whereby play is minimised. Roller bearings were preferred in this case since the rudder is likely to have many more angular adjustments, hence wear, than the lower bearing; further, the rigid centre portion of the upper platform is fabricated from three layers of materials which would have led to complicated fitting and reaming if, say, a sleeved bearing system had been employed.

### 3.9 Dimensions and Materials of Dynamometer Frame:

Incorporating the limitation that the maximum distance between attachment points for rudder and skeg should be 6.25 in, the dynamometer was sized to space the flexures at a maximum distance apart. A wide spacing of flexures is desirable in order to minimise interactions, reduce unwanted stresses in non-reading directions (e.g. tension/compression in lift and drag flexures, Fig. 9 c), minimise error due to misalignment (e.g. effect on torque, SECTION 3.11) and help provide the moment flexures with end effects which are closer to the linear case, Fig. 9 e. The final dimensions evolved on this basis gave a spacing of force flexures

(in lower platform) of 7.75 in , and a spacing to outside of moment flexures (in upper platform) of 9.0 in ; the final overall layout is shown in Fig. 5 .

In order to minimise the overall mass, the basic material chosen for the dynamometer framework was aluminium alloy, the fixed base, rotational base, mid plate and upper structure being machined from NP8 plate. Steel was used where high strength and minimum deflections were required such as the brackets attaching the moment flexures to mid plates, the rotational centre bolt (running in tapered roller bearings) carrying the rudder stock, the upper quadrant arm carrying the angular adjustment gear and measuring scale, the lower sleeved bolt connecting the rotational base to fixed base and the arm attaching the skeg direct to the top of dynamometer. Bare steel surfaces such as the upper quadrant arm and moment flexure brackets were cadmium plated after construction; the remaining steel surfaces and some chosen aluminium surfaces were stove enamelled.

Connections of flexures to adjacent structures:

Each end of each flexure is bolted to its adjacent structure by 6 2BA screws. It is considered that the fineness of the screw threads and the method of attachment will provide adequate friction to prevent slip. The use of pegs (or dowels) was investigated but it was felt that unless perfect in dimensions and location (which, if feasible, would prove very expensive in manufacture) pegs offer little, if any, advantage over the method chosen.

### 3.10 Dimensions and Materials of Flexures:

The forces and moments acting on each flexure were determined by resolving the estimated maximum loadings for the dynamometer. Acceptable maximum skin strains were determined from published data, and hence dimensions of the flexures derived.

Aluminium alloy was chosen for the flexures; its satisfactory use for this purpose (provided stresses are limited to about 5 tonf/in<sup>2</sup> ) is reported in Ref.6. Since the modulus of elasticity of aluminium is about  $\frac{1}{3}$  that of steel then for the same load and required



sensitivity (hence strain), the sectional area for aluminium will be about 3 times that for steel. Hence for the same manufacturing tolerances the possible percentage error in cross-sectional area in way of strain gauges will be reduced, and measuring accuracy increased. Outline calculations indicating the order of error in strain due to errors in flexure dimensions for both aluminium and steel are given in APPENDIX A4. The flexures are required to have a relatively large breadth/thickness ratio in order to bend in contra-flexure and offer little resistance when loaded at right angles to the breadth (non-measuring direction); the use of aluminium of 3 times the area but with the same breadth/thickness ratio and the same strain as steel, will provide increased resistance to buckling.

Refs. 6, 8 and 19 recommend a maximum skin strain at gauge stations of up to 0.001 (0.1% or  $1000 \mu\epsilon$ ), which leads to a stress of about 5 tonf/in<sup>2</sup> in aluminium alloy. Whilst the limit of proportionality for aluminium alloys is not clearly defined, inspection of stress-strain results for the HE 30 material used would suggest an approximate value of about 12 tonf/in<sup>2</sup>; hence in order to provide a satisfactory factor of safety in respect of hysteresis, the limitation of design stresses to about 5 tonf/in<sup>2</sup> would appear satisfactory.

The flexures were manufactured from HE 30 aluminium alloy (0.1% Proof Stress of 17 tonf/in<sup>2</sup>, Tensile Strength 20 tonf/in<sup>2</sup>, Ultimate Shear Stress 14 tonf/in<sup>2</sup>), since it had satisfactory properties for the envisaged loadings, and was readily available; care was taken to ensure that all flexures were cut in the same grain direction from the same extrusion, Fig. 11. Manufactured thickness in way of gauge stations was maintained to within  $\pm 0.001$  in; the need for this tolerance is illustrated in the outline calculation in APPENDIX A4.

Fig. 11 shows the principal dimensions of the flexures (including supplementary non-gauged flexures), and an outline of the calculations for the derivation of flexure dimensions is given in APPENDIX A3.2

### 3.11 Warping of Plates Adjacent to Measuring Flexures, and Measurement of Torque:

This Section outlines some design features derived from the construction and calibration of a small supplementary dynamometer. A small three-component dynamometer (Fig. 12 ) had been constructed by the writer for the purpose of carrying out supplementary rudder tests in the test tank at Southampton College of Technology; the measuring section consisted basically of two steel plates separated by four flexures gauged to measure linear strain due to shear. The construction of the dynamometer ran concurrent with the early design period for the larger five-component dynamometer described in this Report, and experience derived from its design and calibration was incorporated in the larger wind tunnel dynamometer. The final design of this small three-component dynamometer was satisfactory in that all calibration curves, including interactions between components, were linear within acceptable limits; some limitations in the measurement of torque (to be discussed later) exist, but otherwise the dynamometer has proved satisfactory in use for the preliminary experiments carried out so far in the test tank. Further, it is considered that an important overall conclusion from these tests was that the results confirmed the feasibility and suitability of the employment of flexures gauged to measure linear strain due to shear for such multi-component dynamometers.

#### Warping of end plates:-

It had been the original intention to measure rudder forces relative to the test tank axes, and preliminary calibration of the force measuring unit (by hanging masses) entailed rotating the measuring unit relative to a base plate. Severe interaction between the applied force and torque was recorded, the largest interaction being at the limiting angle of  $45^{\circ}$  (Fig. 13 b) which would have precluded the measurement of torque with sufficient accuracy. The interaction was eventually located as being due to 'restricted' warping of the force measuring unit end plate, Fig.13 c ; the insertion of a small washer between these two surfaces completely eliminated the problem, allowing what is effectively 'symmetrical' warping, Fig.13 d . However, in the case of this small dynamometer, since manufacturing tolerances and some slack in the washer/bolt design did not allow the construction to proceed

by this method, it was decided to use rudder body axes. This entailed incorporating the measuring unit in the rotational part of the dynamometer column, and to bolt it to thick machined pads which were themselves welded to tubes above and below the measuring unit, Fig. 12 ; this is the design which was consequently used with success in the test tank.

The discovery of the restricted warping of the end plate was important in that it allowed modifications to be made to the five-component wind tunnel dynamometer early in the design stage, since a flat rotational base plate rotating on a flat fixed base plate had been originally envisaged. Ideally, the flexures of the lower platform of the dynamometer should be contained between two infinitely rigid plates which would preclude any warping. An actual thickness of 1 in aluminium alloy for the plates had been estimated as adequate, based partly on the reported satisfactory operation of approx. 0.5 in steel plates used in the dynamometer described in Ref. 18. In order to alleviate the possibility of problems due to warping, therefore, the rotational base plate was increased in thickness from 1 in to  $1\frac{1}{4}$  in aluminium alloy and a 3 in dia. x 0.05 in thick stainless steel washer incorporated between the rotational and fixed base plates.

#### Torque measurements:-

Calibration of the small dynamometer also indicated further problems which concerned the measurement of torque. From an early stage in the calibration, asymmetry was evident in the results, these being different (although still linear) for the clockwise and anti-clockwise applications of torque. Considered reasons for this included the possibility that there could be some asymmetry in the flexure unit itself (e.g. flexures on opposite sides not identical in section), and that since the flexures were only spaced 2.5 in apart, any small errors in symmetry of the unit would become very apparent in the measurement of torque. Further, torque gauges were only attached to two flexures, and it was considered that this problem would have at least been minimised if all four flexures had been gauged for torque and their outputs included in the same bridge.

Based on these conclusions, therefore, the following criteria were incorporated in the new five-component wind tunnel dynamometer:

(a) The flexures between the rigid plates of the lower platform (measuring lift, drag and torque) were spaced as far apart as other physical limitations would allow (further reasons for this wide spacing were discussed in SECTION 3.9) and,

(b) Torque gauges were incorporated on all four flexures (8 gauges in all) and their outputs included in the one torque bridge (the torque bridge is described in more detail in SECTION 4.3).

#### 4. STRAIN GAUGES, ELECTRICAL CIRCUITS AND INSTRUMENTATION

##### 4.1 General:

The principal strain gauges employed in force measurement dynamometers are semi-conductor gauges where very high sensitivity is required (gauge factors  $k$ , see later, of up to about 120 are attainable) and the wire or foil resistance strain gauge. A preliminary investigation indicated that, for the envisaged flexure sizes and estimated strain levels, adequate sensitivity would be achieved by the use of resistance strain gauges. Due to this, and considerations of the possible compensation techniques required for non-linear responses and temperature effects with semi-conductors, and their high cost (up to twelve times that of an equivalent resistance gauge), the use of semi-conductors was not considered further. For more detailed information the reader is referred to Ref.3 in which useful comparisons are made between semi-conductor and resistance strain gauges.

##### 4.2 Selection and Mounting of Strain Gauges:

###### Gauge length:-

Refs. 3, 5, 6, 7 and 15 all recommend the use of the largest possible gauge for dynamometer applications. The larger gauge has the capability of greater sensitivity, improved bonding, decreasing the effect of creep, a larger area leading to greater heat dissipation and hence capability of carrying higher currents, and lends itself to easier installation and more accurate alignment. (It is desirable to restrict gauge length if actual strain is required at a point in an area with a relatively high strain gradient; the dynamometer requirement, however, calls only for a function of strain). Inspection of the final dimensions of the flexures, with an allowance for the gauge backing base size, indicated that a gauge length of 10 mm would be suitable. The location of the gauges and bases, and their size relative to the flexures is shown in Fig. 14 .

###### Gauge Material:-

Although temperature compensation is provided by the full

bridge circuits in which the gauges are employed, since there was a free choice of gauge material, gauges offering temperature compensation when mounted on aluminium flexures were selected.

Particulars of Gauges Used:-

Make : TML - Tokyo Sokki Kenkyujo Co. Ltd.  
 Type : FCA - 10 - 23 (Crossed foil Two-Gauge Rosette)  
 Gauge Length : 10 mm  
 Base Size : 16 mm x 16 mm  
 Gauge Resistance : 120ohm  $\pm$  0.5 ohm  
 Gauge Factor : 2.13, 2.14

Temperature compensation when test object is aluminium

Number of Gauges:-

Each of the eight flexures has a Two-Gauge 45° Rosette on each of its sides, totalling 16 rosettes or 32 gauges in all.

The gauges are deployed as follows:-

Lift Circuit	-	4	Gauges	(2 on each of the 2 lift flexures)
Drag "	-	4	"	(2 on each of the 2 drag flexures)
Torque "	-	8	"	(2 on each of the 2 lift flexures) (2 on each of the 2 drag flexures)
MX	-	4	"	(2 on each of the 2 MX flexures)
MY	-	4	"	(2 on each of the 2 MY flexures)

There is a further Two-Gauge Rosette on each of the four moment flexures (8 gauges in all); in the present configuration these are treated as spare gauges, although they could be suitably wired and calibrated to provide a sixth (Z - direction) component for the dynamometer.

Location of Gauges:-

The gauges are located in the centre of each side of each flexure with their axes at 45° to the vertical or horizontal axes of the flexures; dimensional particulars of their locations are shown in Fig. 14 .

## Bonding and Protection:-

The gauges were bonded to the flexures using TML P-2 Polyester Adhesive, since this adhesive should provide a long term of use for the bonded gauges; the gauges were applied using the gauge and adhesive manufacturers recommendations for cleansing, clamping pressures and curing times. After bonding, all gauges were coated with R.S. Silicone Rubber Compound (clear) to give physical as well as humidity protection.

### 4.3 Bridge Circuits:

The wiring of the various component bridges is shown in Fig. 15 . The gauges were wired in each bridge whereby the maximum signal output was produced, as outlined in APPENDIX A5 . Key diagrams showing gauge numbering relative to flexures, and relating to the bridge circuits (Fig. 15 ), are shown in Fig. 16 .

Possible inaccuracies in torque readings due to possible asymmetry between flexure units were discussed in SECTION 3.11 ; hence, in order to increase the accuracy of the torque bridge, gauges on both the lift and drag flexures (8 in all) are employed, with two gauges in series in each arm of the bridge. It is to be noted that connecting gauges in series such as for the torque bridge will only improve the accuracy (or average value) of response for each bridge arm, but will not increase the sensitivity or output signal; the increased total equivalent resistance of the series bridge does however allow an increased supply voltage for the same gauge current (see calculations in SECTION 4.5), with consequent increase in total bridge sensitivity.

The terminal wires for the 32 gauges are firstly led to 64 terminals on two tag boards mounted on the dynamometer; the component bridges are made up by suitable connection of these 64 gauge terminals to the 34 bridge terminals below. This arrangement is shown in Fig. 17 .

The lead wires carrying the inward supply voltage and output response signals are led from the dynamometer bridge terminal boards to the recording instrumentation by means of a multi-core cable (with an approximate length of 40 ft ); the cable is attached to the instrumentation

by means of a standard multi-pin plug. The plug terminal reference numbers are related to the equivalent bridge terminal numbers (Figs.15 and 17 ) as listed in Fig. 18 .

Wires are led from the bridge supply voltage pins in the multi-pin plug box direct to the data transfer unit in order to monitor the supply voltage for each bridge; these lead wires are numbered according to the bridge terminal numbers, Fig. 15 .

The polarities of the connections between the bridge unit and the data transfer unit are shown in Fig. 19 .

#### 4.4 Instrumentation:

The dynamometer is designed to be electrically linked with the existing wind tunnel recording equipment; this consists of a strain gauge bridge unit coupled to a data transfer unit and a digital voltmeter.

The strain gauge bridge unit is capable of accepting up to 8 full bridges, and of balancing each bridge independently. The bridge unit provides a stabilised overall input voltage of between 0.2 volts D.C. and 32 volts D.C., leading to actual stabilised supply voltages at the strain gauge bridge terminals of up to approximately 8v for a four ( $\times 120 \Omega$  ) gauge bridge and approximately 13v for an eight ( $\times 120 \Omega$  ) gauge series bridge, see Fig. 15 . Whilst the overall input supply voltage to the bridge unit can be adjusted, the supply voltage to each individual bridge cannot be adjusted separately.

The data logger has 20 channels and the voltmeter can measure down to  $1 \mu\text{v}$ ; the system has facilities for output either by visual digital voltmeter, or by recording on automatic paper print out or high speed punched tape. A typical example of a calibration data print out for the dynamometer, with various components labelled, is shown in Fig. 20 .

#### 4.5 Bridge Supply Voltage:

The output voltage and hence sensitivity of the unbalanced bridge is proportional to the supply voltage as shown by equation A5.3 hence maximum bridge excitation level is desired in order to maximise the



sensitivity of the load measurements. Excess bridge voltage can, however, lead to overheating of the gauges with consequent zero or no-load instability. The most important factors which determine the acceptable excitation level are the power dissipation capability of the gauge which varies approximately with the size of the grid, and the heat sink properties of the mounting surface; in this case the gauges are foil and relatively large (10 mm x 2.5 mm) and the mounting surface is aluminium alloy which provides a good heat sink.

The current carrying capacity of foil gauges is frequently quoted as the power dissipated per unit grid area: for example, Ref. 3 suggests an accepted value for static measurements when mounted on metals as 6.5 watts/in<sup>2</sup>, Ref. 5 suggests an accepted value as 5 watts/in<sup>2</sup>. Ref. 20 suggests 2 to 5 watts/in<sup>2</sup> for high accuracy static measurement with excellent heat sink conditions (e.g. heavy aluminium or copper specimens) although a small derating factor should be allowed due to the stacking effect of the rosette gauge; Ref. 21 suggests 1 to 5 watts/in<sup>2</sup> whilst Ref. 22 suggests that the values quoted in Ref. 21 are conservative.

Ref. 2 suggests that most wire strain gauges will carry approximately 0.030 amp. (30 m.a.) without overheating and that foil gauges, because of their heat dissipation characteristics, will have two to three times the current-carrying capacity of wire gauges (i.e. 60 - 90 m.a.). For the foil gauges in question, and assuming the lower value of 0.060 amps.:

For balanced case (Fig. 21.):

$$I_1 = I_2 = 0.06 \text{ amps}$$

$$\text{and } I = I_1 + I_2 = 0.12 \text{ amps.}$$

$$\text{Equivalent total resistance of bridge} = 120 \Omega$$

$$\text{hence limiting voltage } v = 0.12 \times 120$$

$$= 14.4 \text{ volts}$$

For the torque bridge, two gauges in series are used in each arm, hence for balanced case (Fig. 22 ):

$$I_1 = I_2 = 0.06 \text{ amps}$$

$$\text{and } I = I_1 + I_2 = 0.12 \text{ amps}$$

$$\text{Equivalent total resistance of bridge} = 240 \Omega$$

$$\begin{aligned} \text{hence limiting voltage } v &= 0.12 \times 240 \\ &= 28.8 \text{ volts} \end{aligned}$$

In order to provide ample margin against gauge overheating, a maximum supply voltage of 7 volts is assumed for the 'four gauge' bridges (L, D, MX and MY) and 11 volts for the 'eight gauge' bridge (MZ). (The value of 11 volts for MZ is the approximate value obtained when 7 volts is supplied to the other bridges, as discussed in SECTION 4.4 ).

$$\text{Also power dissipated in grid, watts/in}^2 = \frac{v_g^2}{R \times A_g}$$

where  $v_g$  = voltage across each gauge

$A_g$  = grid area

$$\text{and } A_g = 0.4 \text{ in} \times 0.1 \text{ in}$$

$$= 0.4 \text{ in} \times 0.1 \text{ in}$$

$$= 0.04 \text{ in}^2$$

hence for bridge voltage of 7 volts

and gauge voltage of 3.5 volts

$$\text{power dissipated} = \frac{3.5^2}{120 \times 0.04} = 2.55 \text{ watts/in}^2$$

$$\text{and current in each gauge} = v/R = 3.5/120 = 29 \text{ m.a.}$$

for the bridge voltage of 11 volts

and gauge voltage of  $11/4 = 2.75$  volts

$$\text{power dissipated} = \frac{2.75^2}{120 \times 0.04} = 1.57 \text{ watts/in}^2$$

$$\text{and current in each gauge} = 2.75/120 \text{ (or } = 1/2 \times 11/240)$$

$$= 23 \text{ m.a.}$$

These power densities lie within the range of limits for static measurement suggested by Refs. 3, 5, 20, 21 and 22 and the upper current values suggested by Ref. 2 and the gauge manufacturer Ref. 23.

The original estimates for strain and hence signal voltage output (APPENDIX A3.2) were based on 5 volts supply; the use of 7 volts supplies will, therefore, lead to increases of 40% in output signals, and the use of 11 volts for the torque bridge supply lead to a 120% increase in torque output signal.

## 5. CALIBRATION

### 5.1 General:

For a dynamometer of this type there is a requirement for comprehensive calibration involving the evaluation of the usual component calibration slopes, together with the derivation of interaction effects between the five components; components are firstly applied individually in order to determine calibration slopes and first order interactions, and pairs of loads are then applied to determine the magnitude of the second order interactions. Fig.23 lists the loads and combinations of loads for the derivation of the first and second order interactions.

Measurements are also required in order to derive linear and rotational deflections when loaded, proof loads and sensitivities, and checks are required for defects such as play of assembly, hysteresis and creep. A check is also required in order to determine whether applications of loads on the skeg when connected to base will have an influence on any of the components.

### 5.2 Calibration Rig, Application and Alignment of Calibration Forces:

#### 5.2.1 Rig

A calibration frame was designed and constructed which allows forces and moments of known magnitude and direction to be applied individually or combined by means of pulleys and known masses under gravity. In order to obtain rigidity and stability during calibration the frame was constructed of welded heavy mild steel angle which was suitably machined and drilled after welding to take the dynamometer and calibration mass beams. Figs.24 and 25 illustrate the complete calibration rig; Fig. 26 shows the loading points in the calibration arm for the application of moments, and in the calibration plate for the application of torque; Fig.27 shows diagrammatically how the various forces and moments, and their combinations, may be applied in the calibration rig.

### 5.2.2 Calibration Masses.

The calibration masses were all checked relative to certified standards. Some small corrections were necessary such that all the 20 lb masses were correct within  $\pm 0.0044$  lb and the 10 lb masses within  $\pm 0.0022$  lb ; this amounts to  $\pm 0.022\%$  in each case.

### 5.2.3 Application of Forces

The application of forces and moments in Fig.27 are shown idealised and, since it was not possible to apply loads or offset loads through the dynamometer roll centre, it was necessary to apply both the load and its offset on the calibration arm; thus moments (MX and MY) were obtained by applying equal loads at different levers, Fig. 28 (a), and loads (L and D) were obtained by applying dissimilar loads at levers inversely proportional to their values, Fig. 28 (b).

### 5.2.4 Locking of Chosen Skeg and Rudder Angles

During the early stages of calibration it was noted that tightening of the skeg/dynamometer angle clamping wing nut caused small but erroneous meter readings due to deflections in the rotational base plate; (due to design differences, the same problem could not occur with the rudder angle clamping screw). The gap between the rotational and fixed bases at the clamping screw was suitably shimmed with stainless steel washers and the problem was completely overcome. For consistency, however, all further calibrations were carried out with the wing nuts for both angular adjustments tightened and, as a calibration as well as backlash precaution, it is recommended that both wing nuts be tightened at all chosen angles during wind tunnel testing.

### 5.2.5 Alignment of Forces

Early calibration results indicated poor alignment of the calibration rig relative to the dynamometer. This did not have a significant influence on the direct calibration slopes since errors are proportional to  $\cos\psi$ , where  $\psi$  is the angular error in the direction of the applied force. Small errors in horizontal alignment were however seen to have a significant effect on interactions. This was discovered

by the appearance of dissimilar interaction slopes positive and negative, and then a change in these slopes during re-calibration following changes in the positions of the calibration beams (such as for calibration in other direction, or for torque). The problem was magnified by the need to apply loads and moments with offset loads as discussed earlier, and shown in Figs. 28 (a) and 28 (b).

It should be added that erroneous and sometimes very large interactions on torque were observed in the early stages of the calibration. It was obvious in hindsight that even the smallest of errors in alignment of the 12 in. x 12 in. calibration plate would cause the transmission of incorrect and unwanted torque via the calibration arm. This particular problem was successfully overcome by transmitting the forces to the calibration arm via ball races within plates which were then able to self-centre under load; this system is shown diagrammatically in Fig. 29. The 12 in. x 12 in. calibration plate was of course retained and used for the torque calibration.

The effect of the rig mis-alignment described above is illustrated in Fig. 30 (a) which shows diagrammatically the typical curves produced for one of the interactions. Curve ① shows a typical interaction calibration and curve ② a later repeat calibration for the same interaction; both curves indicated a similar deviation from the correct curve ③ for both positive and negative loads. At this stage the need for very accurate alignment became evident. The position of the dynamometer relative to the calibration frame was checked carefully and, prior to calibrations in the X or Y direction, the calibration mass beams and pulleys were carefully adjusted whereby they were perfectly in line per case ③, Fig. 30 (b), hence producing a correct result per curve ③ in Fig. 30 (a). The procedure adopted to achieve this alignment for the X direction was to vary the position of the calibration beams and at the same time monitor one or two check spots for the influence of MX on MY (or MY on MX for the Y direction) for both positive and negative values; when equal values for both positive and negative check spots were obtained, complete calibration of the interaction effects was carried out. This procedure proved to be entirely satisfactory, producing the interaction results shown in Figs. 37 to 41. Repeat calibrations using the above alignment procedure, following changes in

position of calibration beams, gave data within the experimental scatter shown in Figs. 37 to 41 .

It is considered therefore that the alignment procedure adopted for the rig and described above will prove satisfactory for any future repeat or check calibrations.

### 5.3 Proof Loads :

In order that the flexures should not be subjected to unnecessarily high stresses, only approximately 5% overload was used above the maximum loads and moments listed in SECTION 2.2. The dynamometer was therefore subjected to the following individual proof loads and moments at  $\beta = 0$  :

Lift	±	200	lbf
Drag	±	150	lbf
MZ	±	1200	lbf in
MX	±	4775	lbf in
MY	±	3775	lbf in

The dynamometer is not designed to carry all the maximum loads and moments simultaneously, as mentioned in SECTION 2.2 and discussed in SECTION 6.5. The combination of maximum lift, drag and torque does not cause any problems, but limitations exist in the combinations of MX and MY due to combined stresses and the following maximum combinations of moments were tested for proof purposes at  $\beta = 0$  :

MX	+	MY
4775 lbf in	+	500 lbf in
4500 lbf in	+	1000 lbf in
4275 lbf in	+	2100 lbf in
3275 lbf in	+	3325 lbf in

The response readings were recorded for all proof loads and combinations. Small amounts of hysteresis and gauge creep were observed in different components. Sustaining the maximum loads over short periods of time did not increase the creep. The effects of hysteresis and

creep are discussed in more detail in SECTION 5.6.

From the point of view of structural integrity all the proof loadings proved to be satisfactory and the detailed calibrations reported on in the following Sections were proceeded with.

#### 5.4 Deflections:

Deflections for maximum loads and moments were recorded at points 5 in. above the dynamometer roll centre for the dynamometer and skeg (approximately where dynamometer penetrates wind tunnel floor). It was not possible to obtain accurate deflections at a greater height due to deflections in the calibrating beam itself; it is assumed that the projected models will be of solid laminated construction, and will therefore deflect by negligible amounts.

Deflections were monitored relative to fixed base (e.g. relative to wind tunnel floor) and relative to rotational base; the latter indicates the likely deflections of the rudder relative to the skeg.

The measured deflections are summarised in Fig. 31 . It is considered that the linear deflections are within acceptable limits. The influence of the angular deflection of  $0.00013^{\circ}/\text{lbf in}$  in torque can be neglected up to about 200 lbf in since it is less than the minimum measurable angle on the dynamometer; above this torque, however, an angular correction of  $0.00013^{\circ}/\text{lbf in}$  will be required in the model data analysis.

#### 5.5 Calibration Data and Discussion:

##### 5.5.1 Bridge Voltages and Electrical Zero Stability

The lift bridge voltage was set as close to 7.000 volts as was possible (the choice of 7.0 volts was discussed in SECTION 4.5). The typical repeated drift of the stabilised voltage in the course of a complete day's calibration was from 6.999 volts to 7.002 volts; this amounts to only 0.04% change in voltage and no corrections to calibration



slopes for this order of voltage drift were necessary.

After the instrumentation and gauges had been allowed to warm up completely (approximately 1 hour maximum), and settling time allowed after adjustment to voltmeter zero and/or bridge balance, zero stability was found to be very satisfactory. The electrical zero checks were made over periods of up to half an hour and no significant shifts were recorded. This time period well exceeded the time for any of the calibration runs; tunnel running time for a series of angles (or conditions) is not expected to exceed this approximate limit.

Instability effects due to temperature changes will be insignificant. Temperature compensation is provided by the full bridge circuits as discussed in SECTION 4.2.; also, the dynamometer is completely external to the wind tunnel working section and will be subjected only to the relatively small changes in laboratory temperature.

#### 5.5.2 Derivation of True Roll Centre of Dynamometer

For the purpose of the design of the calibration rig the roll centre was assumed to be at mid height of the moment flexures, i.e. 2.885 in below the top of the dynamometer as shown in Fig. 26. Throughout the calibration process, therefore, loads were applied to the calibration arm at assumed levers of 5 in , 10 in , 15 in and 20 in .

In order to firstly derive the true roll centre prior to analysing the calibration data, loadings were applied at each of the assumed levers of 5 in , 10 in , 15 in and 20 in ; the data was regressed and a mean value obtained for the application of 100 lbf at each of the assumed levers. These values were cross plotted and regressed, as shown in Fig. 32.

The intercepts of the graphs in Fig. 32 indicate that the true roll centre for moment MX is 0.0476 in below the assumed roll centre and for MY is 0.0666 in . This difference between the two moments is probably accounted for by the asymmetry created by the Anti-Torque flexures which are located on the Y-Y axis only. Since one common roll axis is required, a mean correction value of 0.0571 in was assumed; the use of this mean value between 0.0476 in and 0.0666 in for MX and MY leads to errors of less than 0.1% in moments MX and MY for levers

greater than about 10 in .

Hence derived true roll centre  
below top of dynamometer = 2.885 + 0.057  
= 2.942 in

The analysis of all the following calibration data has therefore been based where necessary on the use of this true roll centre.

### 5.5.3 Component Calibration Slopes

The data for the five components are shown plotted in Figs. 33, 34 and 35, and all slopes are linear within acceptable limits. Positive and negative calibration slopes were investigated separately leading to the following differences: Lift 0.32%, Drag 0.21%, Torque 1.52%, MX 0.56% and MY 0.19%. The values for L, D, MX and MY are very satisfactory. The value for torque, whilst high, is considered acceptable; this had been 1.7% for all data, but a plot of errors indicated bigger errors at the larger values of torque. Data within  $\pm 720$  lbf in , representing the practical limits of torque, were therefore considered which led to the difference of 1.52% between the positive and negative slopes; this is of course an effective difference of 0.76% between the mean slope for either the negative or positive data compared with the mean slope for the combined data.

Simple torque was obtained by the application of couples created by offset loads in both the lift and drag directions; the differences in torque response resulting from the application of the loads in the two directions was insignificant and all data (up to  $\pm 720$  lbf in ) were included in the final mean regression line.

Mean calibration slopes for the five components for combined positive and negative data obtained by least squares linear regression and shown on the respective calibration curves Figs. 33, 34 and 35 are summarised in SECTION 5.10.

True errors in actual measured data for each component compared with the regression lines are shown plotted in Fig. 36. The relatively even positive and negative distribution of errors indicates good linearity for each component. The scatter of data is generally within the limits of  $\pm 1\%$  of true values; lift has some positive data a little outside

these limits although it had been observed throughout the calibration process that the voltmeter readings for lift had always been the least stable of the components. Torque errors lie within  $\pm 1.2\%$ , these being due mainly to the difference in slopes of negative and positive data as discussed above.

The reasons for the difference in slopes for positive and negative torque are not altogether clear. The identical results obtained by the application of couples in the lift and drag directions suggest that there are no mechanical or dimensional defects in the dynamometer itself. The calibration plate may not have been exactly correct in the X-Y plane and, since the loads were applied at the edges of the plate, small rotational errors would have led to an increase in the moment arm and hence torque in one direction and a decrease in the other; a check on the accuracy of alignment was very difficult and proved inconclusive. Further, due to the pin attachment between the calibration plate and arm the plate was seen to rotate a small amount under load relative to the arm. The machining tolerances between the calibration plate pin and holes indicated that rotation may not have been the same for positive and negative torques, hence leading to asymmetry in application of loads. The results do therefore suggest that there was probably some asymmetry in the application of torque through the calibration plate and rig, in which case the mean calibration slope for torque is closer to the correct result than the errors suggest.

#### 5.5.4 Comparison Between Predicted and Measured Sensitivities

It is useful, from the point of view of completeness and possible future design purposes, to compare the measured calibration slopes, or sensitivities, with those predicted in APPENDIX A3.2. A summary of the predicted and measured sensitivities is given below, together with the percentage difference in measured values compared with predicted values:

(Measured values are obtained from the reciprocal of the calibration slopes summarised in SECTION 5.10 and predicted values are obtained using the values of strain in APPENDIX A3.2, the voltages shown in SECTION 5.10 and a gauge factor of 2.14 ).

	PREDICTED $\mu\text{V/lbf}$ or lbf in	MEASURED $\mu\text{V/lbf}$ or lbf in	DIFFERENCE %
L	9.35	13.16	+41%
D	12.98	17.61	+36%
MZ	2.15	2.85	+33%
MX	1.19	1.78	+50%
MY	1.50	2.33	+55%

The increased sensitivities recorded are desirable from the point of view of the resolution and accuracy of the dynamometer.

The likelihood of some increase in measured sensitivities over the predicted values was recognised in the design stage, APPENDIX A3.2.

The size of the disparity between the measured and predicted values does however question the use of average shear stress in the estimates of strain and hence sensitivity.

A problem did exist in the design stage in that mean direct strains were assumed in order to derive flexure dimensions; the derived flexure dimensions then allowed a choice of gauge size to be made. An iterative process would have been necessary in order to relate with the assumed strain the integration over the chosen gauge length of the true shear stress (and hence direct strain) distribution for the derived flexure size.

Following the availability of the actual measured data, a more detailed analysis of the predicted values was carried out using the true shear stress distribution; the results of the analysis are given in APPENDIX A6.

The calculations in APPENDIX A6 indicate that the use of the true shear stress distributions give predictions close to the measured values; the residual differences are considered to be due to the restraint of the lift and/or drag flexures bending in contra-flexure and the application of small amounts of rotation to the moment flexures as well as simple shear.

The use of average shear stress in the estimates of maximum principal stresses in the flexures has a relatively small influence on the

estimated values, particularly since in all cases the shear stress is small compared with the superimposed tensile/compressive stresses.

The foregoing discussion does however suggest that for the prediction of sensitivities in flexures subjected to pure shear, and with gauge size relative to flexure size employed in this case, an iterative process using the integration of the true shear stress distribution is desirable at the design stage.

#### 5.5.5 Interactions

Except torque caused by MX (to be discussed later under second order interactions) all first order interactions are linear and are, in the main, of small magnitude. Interaction data and slopes are shown plotted in Figs.37 - 41 ; interaction slopes were obtained by least squares linear regression. Lift and drag were applied by offset loads set at levers inversely proportional to their magnitude, as explained in SECTION 5.2.3 ; these levers were based on the assumed roll centre, hence since the true roll centre is 0.057 in below this, a residual MX existed when L was applied and a residual MY existed when D was applied. Corrections which account for this are shown in the interaction of MX caused by L and the interaction of MY caused by D.

The experimental scatter of the interaction data in Figs.37 to 41 is considered to be satisfactory since each interaction response is very small compared with the direct response of the forces producing the interaction. The scatter of the plotted data can be misleading since the scales used for interaction  $\mu v$  are necessarily very large compared with those used for the component calibration slopes.

It is also to be noted that the true roll centre of the moment flexures (upper platform) and hence centre about which MX or MY is recorded is not the same as the 'roll centre' of the lift and drag flexures (lower platform) when subjected to MX and MY and their possible interaction effects. A cross plot of interaction data for a fixed load indicated a vertical difference in these roll centres of about 1 in (due to the small size of the interactions this exercise was necessarily approximate). The calibration results, Figs.40, 41 do however indicate that this disparity of roll centres can be neglected; the interactions of MX and MY on Lift, Drag and Torque are of such small magnitude that corrections to MX or MY due to such a correction in roll centre lie within the experimental scatter of the recorded interactions.

#### 5.5.6 Second Order Interactions

Checks were made by comparing the second order (combined

loading) interaction with the sum of the first order interactions caused by each of the two individual components, together with an intermediate spot to check the linearity of the interactions caused by combined loadings. This entailed checking the two components and interaction readings for each of the ten combinations of loadings.

The torque interaction caused by  $(MX + MY)$  was unsatisfactory, and is discussed in more detail later; all remaining second order interactions were found to be satisfactory, being within  $\frac{1}{2}\%$  of the sum of the first order interactions.

Considering the interactions as a whole, therefore, torque caused the only real problem. Its first order interaction caused by  $MX$  is non-linear (Fig. 40 b); its second order interaction caused by  $(MX + MY)$  is also non-linear (Fig. 42) but, more important, the interaction caused by combined  $(MX + MY)$  exceeds by a significant amount the summation of the first order interactions caused by  $MX$  and  $MY$ . (This is illustrated in Fig. 42 for the  $60^\circ$  case). For a precise solution this would entail introducing a correction term in the torque equation which would be a non-linear function of  $(MX + MY)$ . The function would also be required to tend to zero as  $MX$  or  $MY$  tend to zero. Since the complete solution of the calibration involves the inversion of a matrix of five linear simultaneous equations, the introduction of second order terms would nullify this relatively simple process, and solution would require a lengthy computerised iterative process. Further, the introduction of second order terms in the calibration matrix is undesirable from the point of view of processing the raw wind tunnel data. For simplicity, therefore, the use of assumed larger linear torque first order interactions caused by  $MX$  and  $MY$  were investigated and subsequently adopted. These assumed compromise slopes, shown in Figs. 40 b and 41 b were obtained by iteration whereby a satisfactory balance between the errors at small and large moments and at different angles was obtained; the assumed second order interactions (formed by the sum of the assumed first order interactions) compared with the measured second order interactions are shown in Fig. 42. The polar plots in Fig. 43 indicate the compromise corrections adopted for different resultant moments and angles of application.

Depending on the siting of the stock and movement of its centre of pressure, absolute torque for a control surface can tend to zero in which case errors in torque tend to infinity. However, one of the basic objectives is to obtain  $CP_{\bar{z}}$  and inspection of Fig. 43 indicates that for a resultant moment of 800 lbf in (due to say 40 lbf applied at 20 in lever) the worst error is for  $60^\circ$  case and is  $5\mu v$ ; this amounts to about 1.8 lbf in error in torque; if the normal force is

assumed to be approximately the same as the 40 lbf resultant then error in  $CP_{\bar{z}}$  =  $1.8/40 = 0.044$  in , which for a lifting surface chord of say 18 in amounts to an error in  $CP_{\bar{z}}$  of 0.25% ; for a resultant of 3200 lbf in (due to say 160 lbf applied at 20 in lever) a similar calculation indicates the worst error in  $CP_{\bar{z}}$  to be about 0.17%. It should be added that these changes in torque, caused by the assumed changes in interactions, have an insignificant effect on the other components.

By inspection of Fig.43 it is seen that one area in which erroneous torque readings can still exist is that when Drag and MY alone are being recorded, or the very low angle of attack case when D/L ratio > approx. 7. The errors in torque in this range are however not large enough to have any significant effect on the interaction corrections to the other components caused by torque. The derivation of  $CP_{\bar{z}}$  at zero angle of attack and  $L = 0$  for a lifting surface is in any case indeterminate, hence it is seen that errors in torque in this low angle range are unlikely to cause any restrictions in the use of the dynamometer for most kinds of lifting surface work.

#### 5.5.7 Calibration Matrix

Using the derived component calibration slopes and interaction constants, it was possible to build up the complete matrix ;

e.g. From Fig. 38 , Lift interaction caused by

$$\text{Drag} = +0.0595455 \mu\text{V Lift/unit Drag}$$

$$\text{from Fig. 33 , Lift} = 0.0759968 \text{ lbf}/\mu\text{V}$$

hence the negative correction to lift caused by the simultaneous

$$\begin{aligned} \text{application of drag} &= -0.0595455 \times 0.0759968 \\ &= -0.0045253 \text{ lbf lift} / \text{lbf drag} \end{aligned}$$

$$\text{i.e. correction to lift} = -0.0045253 \times \text{DRAG}$$

Similar calculations were carried out for all interactions and the following matrix derived :

$$\begin{aligned} L_c &= +1.0000000 & L_u &= -0.0045253 & D_c &= -0.0003059 & MZ_c &= -0.0005983 & MX_c &= -0.0017064 & MY_c &= \\ D_c &= +0.0000000 & L_c &= +1.0000000 & D_u &= -0.0003688 & MZ_c &= +0.0006713 & MX_c &= -0.0005192 & MY_c &= \\ MZ_c &= -0.0213727 & L_c &= +0.0436227 & D_c &= +1.0000000 & MZ_u &= +0.0021053 & MX_c &= +0.0065793 & MY_c &= \\ MX_c &= +0.0797404 & L_c &= +0.0000000 & D_c &= -0.0858513 & MZ_c &= +1.0000000 & MX_u &= +0.0049306 & MY_c &= \\ MY_c &= +0.0000000 & L_c &= +0.0987331 & D_c &= +0.0000000 & MZ_c &= -0.0048043 & MX_c &= +1.0000000 & MY_u &= \end{aligned}$$

Where  $L_c$ ,  $D_c$ , ... represent the corrected or true loads (lbf or lbf in)  
 $L_u$ ,  $D_u$ , ... represent the uncorrected loads (lbf or lbf in)

In appraising the magnitude of the interaction constants it should be noted that the various components are not of equal numerical magnitude, hence it is more realistic to consider each correction based on its typical expected full load value; e.g. Ref.7 suggests that the sum of the interaction corrections should not exceed 3 - 5% of the limiting value of the component being considered.

Taking as an example the dynamometer basic load and moment requirements as :  $L = 170$  lbf,  $D = 85$  lbf,  $MZ = 1200$  lbf in ,  
 $MX = 4100$  lbf in ,  $MY = 2100$  lbf in , then the sum total of corrections to each respective component, as a percentage of the above design component values are as follows:

Correction to	L = + *	- 0.23%	- 0.22%	- 1.44%	- 2.11%	= 4.00%
"	" D = + 0	+ *	- 0.52%	+ 3.24%	- 1.28%	= 5.04%
"	" MZ = - 0.30%	+ 0.31%	+ *	+ 0.72%	+ 1.15%	= 2.48%
"	" MX = + 0.33%	+ 0	- 2.51%	+ *	+ 0.25%	= 3.09%
"	" MY = + 0	+ 0.40%	+ 0	- 0.94%	+ *	= 1.34%

The individual and sum total corrections for each component are seen to be relatively small and are therefore acceptable. Further, the relatively small size of the interaction corrections endorse the validity of the overall dynamometer design concept for the measurement of five components.

Since torque could be relatively small and drag smaller relative to lift, as compared with the maximum loadings, the following loadings were also considered, these representing a typical working case, and the calculations repeated :  $L = 100$  lbf,  $D = 30$  lbf,  $MZ = 150$  lbf in ,  
 $MX = 2000$  lbf in ,  $MY = 600$  lbf in .

Correction to	L = + *	- 0.14%	- 0.05%	- 1.20%	- 1.02%	= 2.41%
"	" D = + 0	+ *	- 0.18%	+ 4.48%	- 1.04%	= 5.70%
"	" MZ = - 1.42%	+ 0.87%	+ *	+ 2.81%	+ 2.63%	= 7.73%
"	" MX = + 0.40%	+ 0	- 0.64%	+ *	+ 0.15%	= 1.19%
"	" MY = + 0	+ 0.49%	+ 0	- 1.60%	+ *	= 2.09%

As would be expected, there is a marked increase in the correction to torque. It is desirable, therefore, that a reasonably large



torque be maintained on the lifting surface. This is feasible by the careful choice of stock location for the all-movable control surface although this freedom of choice of stock location does not exist for the skeg rudder type.

It is to be noted that the derived matrix is in terms of the corrected values of L, D, MZ, MX and MY whereas uncorrected values are obtained from experiments and are therefore required in the equations. The matrix was therefore inverted leading to the following equations:

$$\begin{aligned}
 L_c &= +0.9999580 L_u -0.0047048 D_u -0.0002532 MZ_u -0.0005938 MX_u -0.0017085 MY_u \\
 D_c &= +0.0000628 L_u +0.9999300 D_u -0.0004266 MZ_u +0.0006728 MX_u -0.0005188 MY_u \\
 MZ_c &= -0.0211999 L_u +0.0443621 D_u +0.9998090 MZ_u +0.0021156 MX_u +0.0066016 MY_u \\
 MX_c &= +0.0815552 L_u -0.0036968 D_u -0.0858532 MZ_u +0.9997480 MX_u +0.0042273 MY_u \\
 MY_c &= -0.0003856 L_u +0.0987439 D_u +0.0003704 MZ_u -0.0047367 MX_u +0.9999280 MY_u
 \end{aligned}$$

Where  $L_u, D_u, \dots$  represent the uncorrected or measured loads (lbf or lbf in)  
and  $L_c, D_c, \dots$  represent the corrected or true loads (lbf or lbf in)

#### 5.5.8 Origins of Interactions

The gauges on all flexures are arranged to measure only simple shear. By observation, all gauges are also subjected to tensile/compressive stresses, contraflexure, torsion and bending in greater or lesser degrees of magnitude. All forces, other than shear, are arranged to be electrically cancelled in the bridge circuits, although complete cancellation does not depend on the bridge circuit alone.

Although the recorded interactions are of relatively small magnitude, it is considered worthwhile to attempt to assess briefly the reasons for them. Ref.16 summarises the origins of linear interactions as being construction errors, improper positioning of gauges and variation in gauge factor and attributes non linear interactions to deflections in the structure.

Due to the high accuracy of manufacture (within  $\pm 0.001$  in), it is considered that any interactions due to constructional errors are likely to be very small.

The gauge manufacturer indicates a variation in gauge factor for the gauges used of up to  $\frac{1}{2}\%$ , hence the cumulative effect of four gauges

in one bridge can lead to incomplete cancellation and relatively large interactions; an attempt was made to minimise this problem by following the normal practice of selecting, whenever possible, the gauges for one bridge from one manufactured batch of gauges.

Due to the design of the flexures (with relatively large end connection pads) some difficulty in the accurate marking off of gauge positions and subsequent fixing and clamping was reported. It is therefore concluded that most of the interactions are probably due to improper positioning of the gauges.

One non-linear interaction was recorded (that of MZ caused by MX, Fig.40 b); this can be attributed to the asymmetric deflection of the rotational base plate which in turn is caused by the necessary presence of the angular adjustment clamping screw (described in SECTION 3.5). It follows that this asymmetric deflection also leads to the non-linear second order interactions when the dynamometer is subjected to the combined load (MX + MY).

The general conclusion reached is that most of the interactions are probably due to improper positioning of the gauges, but that some contribution to the interactions may be made by possible variation in gauge factors.

#### 5.5.9 Secondary Interactions Caused by Loads on Skeg (For case when skeg is attached direct to rotational base)

A preliminary investigation indicated that forces on the skeg, when attached to rotational base, produced interactions on some of the components which were too large to be neglected.

Moments caused by forces on the skeg, leading to warping of the rotational base, do produce some interactions, hence forces were applied to the skeg/base attachment in the X and Y directions at varying levers. It can be assumed that direct forces and moments in the plane of the  $l_1$  in rotational base itself will have an insignificant effect on the components.

Since the roll centre of the skeg attached to base differs from that of the dynamometer itself, the first part of the analysis entailed the derivation of the roll centre for the skeg attached to base. The cross plots, Fig. 44, of responses caused by the application of 50 lbf at

varying levers in the X and Y directions led to a mean roll centre 4.547 in below the true roll centre of dynamometer; hence skeg roll centre is approximately at the mid height of the  $1\frac{1}{2}$  in rotational base.

The plotting and analysis of interactions due to skeg moments is based on this correct roll centre.

Skeg moments about the true roll axis are defined as follows:-

MXs = Skeg moment in Y direction = skeg moment about X axis  
through skeg roll centre

MYs = Skeg moment in X direction = skeg moment about Y axis  
through skeg roll centre

Interactions are shown plotted in Figs. 45 and 46, and the corrections caused by skeg (when attached to base) are as follows:

Correction to L = -0.0011003 MXs  
D = -0.0019334 MYs  
MZ = +0.0371777 MXs -0.0015583 MYs  
MX = -0.0106430 MXs  
MY = +0.0067007 MXs

It is to be noted that the influence of MXs on torque is quite large, which is evidently caused by warping of the  $1\frac{1}{2}$  in rotational base plate. This possibility was discussed in SECTION 3.11 and steps were taken at the design stage to minimise this effect. The results do suggest, however, that whilst the changes made in the design stage have obviously led to a workable situation, only by the total isolation of the skeg from the rotational base would the interactions be completely eliminated.

It should be added, however, that corrections to components caused by skeg loads have an insignificant effect on the corrections to other components.

Derivation of MXs and MYs and hence corrections caused by them is required to be carried out by iteration since :

$$MXs = [MX_1 - MX_2] + 4.547 [L_1 - L_2]$$

where  $L_1$  and  $MX_1$  = Lift and moment about X axis respect. of Rudder + Skeg  
 $L_2$  and  $MX_2$  = " " " " " " " " Rudder Alone  
 4.547 in = Difference in roll centres of MX or MY and MXs or MYs  
 and  $L_2$  and  $MX_2$  will themselves be corrected by MXs

Similarly,

$$MYs = [MY_1 - MY_2] + 4.547 [D_1 - D_2]$$

#### 5.6 Hysteresis and Creep:

Hysteresis means that after a material is loaded it does not return to its original length when the load is removed. The phenomenon can apply to the gauges or the flexure material on which they are mounted.

Creep is time dependent and is possible in flexures if material enters plastic region; gauge creep is the term used to describe slip of the strain gauge relative to the surface on which it is bonded. These phenomena are described in more detail in Refs.2, 3 and 4.

After removal of the load the effect of hysteresis is to leave a small positive strain reading and the effect of gauge creep is to leave a small negative strain reading.

It is apparent from the above definitions that the effects on strain output of hysteresis and creep can counteract each other, and in some cases cancel.

The same effect as hysteresis can be exhibited by friction in calibration pulleys; slight agitation of the pulleys will usually overcome this particular problem.

For the known maximum loadings hysteresis in the flexure material is unlikely, and creep very unlikely; for the known maximum strains hysteresis and creep in the gauges, if present, was expected to be small.

It is to be noted that hysteresis and creep are different from electrical zero stability; as reported in SECTION 5.5.1, no significant drift of zeros due to instrumentation effects or gauge heating was recorded.

Creep and hysteresis were observed to be worst during the early stages of calibration, particularly during the proof (and hence high) loadings (as discussed in SECTION 5.3).

Creep and hysteresis both generally decrease following cyclic loading, e.g. as discussed in Refs.2, 3 and 4; this proved to be the case for the dynamometer and by the time the final calibration tests were carried

out creep and hysteresis had diminished to small amounts; e.g. during the final calibration programme hysteresis of up to 0.5% of full scale was observed following loading up to maximum, but no hysteresis was recorded for  $L < 100$  lbf,  $D < 50$  lbf,  $MX < 2000$  lbf in and  $MY < 1000$  lbf in and no creep was recorded during the final calibration.

Due to the small size of the hysteresis and/or creep which occurred, zeros after off-loading were used as necessary for decreasing readings, and effective slopes were therefore the mean of the increasing and decreasing readings.

In summary, therefore, it was observed that after some cyclic loading hysteresis and creep diminished to very low levels. Only in the highest parts of the load and moment ranges is hysteresis and creep likely to be encountered; their values are relatively small and it is considered that satisfactory corrections can be made using post-run zeros.

#### 5.7 Accuracy and Repeatability:

True errors in actual measured calibration data for each component compared with the regression lines are shown plotted in Fig. 36. The scatter of the data is generally within  $\pm 1\%$  of the true values, torque being within  $\pm 1.2\%$ .

The above errors (or inaccuracies) are true errors; the errors for each component as a percentage of full scale are as follows:

$L : \pm 0.39\%$  ;  $D : \pm 0.32\%$  ;  $MZ : \pm 1.2\%$  ;  $MX : \pm 0.33\%$  ;  $MY : \pm 0.30\%$

These accuracies are satisfactory, but they do illustrate the need for a sensitivity of the order of 0.1% of full measured range (as discussed in APPENDIX A3.2). Resolution of the electrical equipment is claimed to be  $1\mu\text{V}$  ; in practice with some instability and local noise, instruments appeared stable only to within 2 to  $3\mu\text{V}$  . Due to the choice of flexure sizes and bridge voltages, this decreased resolution still leads to sensitivities better than 0.1% for each component. The instability of measuring equipment was relatively consistent over the complete load range, hence accounting for the relatively larger percentage errors at smaller readings.

The above discussion considers the errors of readings about predicted lines; repeatability, in this case the ability to repeat the mean curves, is good and comparison between calibration slopes derived in the earlier stages and those derived in the final calibration programme gave the following differences in mean slopes:

	Approx. 2 weeks earlier	Approx. 2 months earlier
L	+ 0.16%	+ 0.51%
D	+ 0.11%	+ 0.44%
MZ	+ 0.06%	+ 0.27%
MX	+ 0.12%	+ 0.40%
MY	- 0.14%	+ 0.19%

As an overall check the dynamometer was loaded with all five components simultaneously (per Fig. 27 ) up through a range of loadings leading to simultaneous maxima of L = 156 lbf, D = 90 lbf, MZ = 1080 lbf in , MX = 3897 lbf in and MY = 2250 lbf in . Measured values were corrected using the interaction equations; it was determined that corrected L, D, MX and MY values were within  $\pm 0.6\%$  of applied full scale loads and MZ within  $\pm 2\%$ . MZ was within  $\pm 0.75\%$  for the range up to half full load; the larger errors for the higher loadings are attributed to misalignment in the application of torque due to deflections (discussed in SECTION 5.5.3); there was no means of checking MZ alignment for the simultaneous five-component case.

It is difficult to compare the absolute accuracies (or more correctly inaccuracies) with other dynamometers since little is published on the subject. The accuracy is to a greater extent governed by the principal design parameters including mechanical and electronic sensitivity and flexure stiffness. In the ultimate the accuracy desired does of course depend on the purposes for which the dynamometer is to be employed; in this context, the accuracy is considered to be very satisfactory and, with the exception of torque, within the desired limits outlined in SECTION 2.3. Whilst a little outside these limits, torque is also considered to be satisfactory; errors in the higher range of the torque component were probably due to asymmetry in, and deflections during, the application of torque (discussed in SECTION 5.5.3) and actual errors are therefore likely

to be less than the  $\pm 1.2\%$  obtained during calibration.

#### 5.8 Calibration Time:

The complete calibration described in this Report took a total of approximately three months.

It is not intended to labour the reader further with the detailed problems, which were many and varied, which delayed the calibration process at various stages. A number of the problems have already been described in the preceeding Sections; a further problem was the unreliability of some of the electronic measuring equipment which caused considerable delays. However, on studying the reports on the calibration of numerous other multi-component strain gauge balances, it is some consolation that the various difficulties encountered with the calibration of this dynamometer, and the considerable overall time taken, are far from being peculiar to this dynamometer alone.

It should be added that, taking into account the developed knowledge and techniques for the calibration of this dynamometer and assuming good reliability of instrumentation, it is estimated that any future complete calibration check or re-calibration should be possible in a total of about ten full working days.

#### 5.9 Sixth (Z-Direction) Component:

Since its magnitude will be of insignificant value the measurement of the Z (vertical) component is not called for in the proposed series of tests on control surfaces, hence the dynamometer was designed and calibrated only for the other five components.

Since very little extra work or cost was involved the gauges for the sixth component were bonded to the reverse side of the moment flexures, as described in SECTION 4.2 ; leads from these gauges were carried as far as the tag board on the dynamometer. Whilst the moments  $M_X$  and  $M_Y$  are proportional to the difference of forces on the moment flexures, the vertical force will be proportional to the sum of these forces and the spare gauges would therefore be appropriately arranged in their bridge circuit.

The calibration rig was designed only for the five component case, and some additions to the rig would be required in order to calibrate

the sixth component. However, as an outline check to take account of possible small extraneous Z forces, loads up to -40 lbf in the Z direction were applied by simply stacking the calibration masses on the top pad of the dynamometer; the interactions recorded in the other five components were negligible and following the symmetry of the foregoing calibration data no interaction would be expected from positive Z loading.

#### 5.10 Summary of Calibration Results:

##### Roll Centres of Dynamometer and Skeg Attachment:

True Roll Centre of Dynamometer Below Top

of Rudder/Skeg Attachment Pads = 2.942 in  
(74.7 mm)

True Roll Centre of Skeg when Attached to Rotational

Base Below Top of Rudder/Skeg Attachment Pads = 7.489 in  
(190.2 mm)

These Roll Centres are illustrated graphically in Fig. 47.

##### Calibration Slopes:

Component		Slope		Supply Voltage
LIFT	... $k_L$	=	0.0759968 lbf/ $\mu$ v	... 7.000 v
DRAG	... $k_D$	=	0.0567712 lbf/ $\mu$ v	... 6.998 v
TORQUE	... $k_{MZ}$	=	0.3508955 lbf in/ $\mu$ v	... 10.962 v
MX	... $k_{MX}$	=	0.5621218 lbf in/ $\mu$ v	... 7.009 v
MY	... $k_{MY}$	=	0.4290317 lbf in/ $\mu$ v	... 7.008 v

##### Interaction Matrix:

$L_c = +0.9999580$   $L_u = -0.0047048$   $D_u = -0.0002532$   $MZ_u = -0.0005938$   $MX_u = -0.0017085$   $MY_u$   
 $D_c = +0.0000628$   $L_u = +0.9999300$   $D_u = -0.0004266$   $MZ_u = +0.0006728$   $MX_u = -0.0005188$   $MY_u$   
 $MZ_c = -0.0211999$   $L_u = +0.0443621$   $D_u = +0.9998090$   $MZ_u = +0.0021156$   $MX_u = +0.0066016$   $MY_u$   
 $MX_c = +0.0815552$   $L_u = -0.0036968$   $D_u = -0.0858532$   $MZ_u = +0.9997480$   $MX_u = +0.0042273$   $MY_u$   
 $MY_c = -0.0003856$   $L_u = +0.0987439$   $D_u = +0.0003704$   $MZ_u = -0.0047367$   $MX_u = +0.9999280$   $MY_u$

Where  $L_c, D_c, \dots$  represent the corrected or true loads (lbf or lbf in)  
and  $L_u, D_u, \dots$  represent the uncorrected or measured loads (lbf or lbf in)

also,  $L_u = k_L \cdot R_L$  ;  $D_u = k_D \cdot R_D$  ;  $MZ_u = k_{MZ} \cdot R_{MZ}$  ;  $MX_u = k_{MX} \cdot R_{MX}$  ;  
 $MY_u = k_{MY} \cdot R_{MY}$



Where  $k_L, k_D \dots$  represent the component calibration slopes (lbf/ $\mu$ v or lbf in/ $\mu$ v)

and  $R_L, R_D \dots$  represent the uncorrected meter readings ( $\mu$ v)

**Corrections Caused by Skeg Loadings when Skeg Attached to Rotational Base:**

Correction to L = -0.0011003 MXs  
 D = -0.0019334 MYs  
 MZ = +0.0371777 MXs -0.0015583 MYs  
 MX = -0.0106430 MXs  
 MY = +0.0067007 MXs

MXs and MYs are skeg moments in X and Y directions about true roll centre of skeg when attached to rotational base,

and  $MX_s = [MX_1 - MX_2] + 4.547 [L_1 - L_2]$

where  $L_1$  and  $MX_1$  = Lift and Moment about X axis respect of Rudder + Skeg  
 $L_2$  and  $MX_2$  = " " " " " " " " Rudder Alone  
 4.547 in = Difference in roll centres of MX or MY and MXs or MYs

Similarly,  $MY_s = [MY_1 - MY_2] + 4.547 [D_1 - D_2]$

**Summary of Sensitivities and Accuracies:**

Component	Sensitivity (based on 1 $\mu$ v)	Accuracy		
		Actual	: % True	: % Full Scale
L	0.076 lbf	$\pm 0.74$ lbf	: $\pm 1\%$	: $\pm 0.39\%$
D	0.057 lbf	$\pm 0.45$ lbf	: $\pm 1\%$	: $\pm 0.32\%$
MZ	0.35 lbf in	$\pm 14.40$ lbf in	: $\pm 1.2\%$	: $\pm 1.2\%$
MX	0.56 lbf in	$\pm 15.18$ lbf in	: $\pm 1\%$	: $\pm 0.33\%$
MY	0.43 lbf in	$\pm 10.20$ lbf in	: $\pm 1\%$	: $\pm 0.30\%$

**CONVERSION TO S.I. UNITS:**

For conversion of the forces  $L_c$  and  $D_c$ , their interaction equations in terms of uncorrected meter readings should be multiplied throughout by 4.4482 to yield NEWTONS.

For conversion of the moments  $MZ_c$ ,  $MX_c$  and  $MY_c$ , their interaction equations in terms of uncorrected meter readings should be multiplied throughout by 0.11298 to yield NEWTON METRES.

Consequently the constant in the equations for the derivation of  $MX_s$  and  $MY_s$  should be changed from 4.547 in to 0.1155 m .

Using  $MX_s$  and  $MY_s$  in N.m derived above, skeg corrections to L and D (N) should be multiplied by  $4.4482/0.11298 = 39.3716$  to yield corrections in N ; the skeg corrections to  $MZ$ ,  $MX$  and  $MY$  (N.m) should be multiplied by  $0.11298/0.11298 = 1.0$  to yield corrections in N.m, and hence remain unchanged.

#### NOTE ON SKEG CORRECTIONS:

The corrections caused by skeg loads, when skeg is connected to rotational base, require that the rudder with skeg case has always to be tested as well as the case of rudder without skeg; it is suggested that, for the convenience of the data analysis, the same skeg and rudder angles at the same speed should be tested for both cases.

#### NOTE ON AXES AND RESOLUTION OF FORCES:

Calibration was carried out at  $\beta = 0$  and, for convenience, in the discussion and presentation of calibration data, results and interaction matrix the five components are referred to (correctly for  $\beta = 0$ ) as L, D,  $MZ$ ,  $MX$  and  $MY$ . The components are similarly referred to in the design, description, discussion and notation of flexures, gauges, bridge circuits and wiring.

It is to be noted however that when tests are carried out with the dynamometer (and hence skeg) rotated through some angle  $\beta$  (Fig.54), the interaction matrix and skeg corrections will then apply to the uncorrected and corrected values of the forces and moments relative to the dynamometer axes, namely  $N_\beta$ ,  $A_\beta$ ,  $MZ_\beta$ ,  $MX_\beta$  and  $MY_\beta$ ; these components relative to the dynamometer axes  $X_\beta - X_\beta$ ,  $Y_\beta - Y_\beta$  (Fig.54) are therefore firstly corrected by means of the interaction matrix (and skeg corrections as necessary) prior to their resolution to wind tunnel axes  $X - X$ ,  $Y - Y$  (Fig.54) as described in SECTION 6.8.

## 6. OPERATION

### 6.1 General:

This Section outlines the various outstanding items of information required for the complete setting up and operation of the dynamometer in the wind tunnel. Brief comments on the first wind tunnel tests in respect of dynamometer operation are also included.

### 6.2 Attachment of Rudder to Dynamometer and Dynamometer to Ground:

The model rudder and skeg are bolted to  $3\frac{1}{2}$  in dia. attachment pads at the top of the dynamometer; each pad has four  $\frac{3}{8}$  in studs and two location pegs. The models are therefore all provided with  $3\frac{1}{2}$  in dia. x  $\frac{3}{4}$  in pads suitably drilled for attachment to the dynamometer pads; details of the dynamometer pads and their location relative to the wind tunnel floor are given in Fig. 48 .

The dynamometer is bolted to a fabricated stand; the stand has the facility of vertical adjustment of approximately 3 in whereby dynamometer (and model) can be raised relative to tunnel base hence allowing control surface/tunnel base gap variations to be made, or a groundboard to be used. Fig. 48 illustrates the range of the vertical adjustment relative to wind tunnel floor. The fabricated stand and dynamometer holding down bolts are designed symmetrical about the tunnel longitudinal centreline whereby dynamometer, and hence rudder plus skeg, can be turned through  $180^\circ$  for astern testing. (This is not necessary for an all movable control surface model which can simply be turned through  $180^\circ$  and re-bolted on the main attachment pad).

The fabricated stand is bolted to a heavy cast steel pedestal which in turn is bolted to the concrete floor beneath the wind tunnel, leading to a very rigid fixture. Outline details of the pedestal, fabricated stand and dynamometer in its working position are given in Fig. 49 . Figs. 50, 51, 52 illustrate the dynamometer in its working position with skeg rudder attached.

### 6.3 Check Calibration Facilities:

Calibration checks can be made with the dynamometer in its working position under tunnel and with model fitted. Checks can be made on lift or drag independently or on all components simultaneously by a spot load applied to the dynamometer in a rotated position (per Fig. 27 ).

A portable calibration frame and pulley is bolted to the fabricated stand; the arrangement allows the application of calibration forces either to the dynamometer 1 in aluminium mid plate for lift or drag, or to the top of the dynamometer attachment pad via a 4 in torque arm for the five-component case. These check calibration features are outlined in Fig. 49 .

### 6.4 Details of Tunnel Operation:

The first tests in the wind tunnel were successfully carried out on a skeg rudder, the results for which form a separate report. The rudder had a span of 675 mm ( $\approx$  27 in ) and a mean chord of 450 mm ( $\approx$  18 in ). Maximum test wind speed was 43 m/s (140 ft/sec), resulting in a  $R_n \approx 1.4 \times 10^6$  . At maximum wind speed typical recorded maximum values of lift and drag were 325 N (73 lbf) and 151 N (34 lbf) respectively. The following observations were made and are reported briefly since they contribute to the successful operation of the dynamometer during future tests:

Angular adjustments of the rudder were possible with the wind on; the torques recorded for the skeg rudder were however not high.

The practice was adopted of starting and stopping the wind with the rudder at zero angle of attack, especially for the high speed tests, since turbulence in the tunnel air stream can be relatively high during these conditions; the angular adjustment clamping wing nuts were always tightened after the desired skeg and rudder angles had been set.

Oscillations were observed in the rig at certain angles of attack and appeared to be caused primarily by turbulence in the wind tunnel flow;

care was taken to limit the experiments as necessary (e.g. near stall) when the oscillations became severe.

The oscillations in the rig led to fluctuations in the meter readings; however, investigation indicated that the arithmetic mean of five readings for each rudder angle setting produced satisfactory repeatable data. (Data from repeat tests on last day of testing, compared with data derived on first day, repeated within  $\pm 1\%$  full scale).

A short investigation was made into filtering the meter fluctuations electrically. This proved to be only partially successful at the first attempt, and time did not allow further investigation. It is however considered that electrical filtering can be applied successfully for future tests; this will require an initial investigation into the natural frequency of rudder and dynamometer whence values for the filter components can be derived.

Since little change can be made to the mass and natural frequency of the dynamometer, changes could only be made by substantial changes in the mass of the rudders (e.g. rudder in above tests was laminated in jelaton and weighed 30 lbf; a significant saving in weight would be achieved by manufacturing in G.R.P.). The rudders in the test series are all of approximately the same weight hence no greater problems than those encountered in the first tests are expected.

Some creep was observed in the initial readings which suggested that the gauges were creeping considerably more under fluctuating loadings than the worst recorded under static load conditions; it was found that the creep was largest when the loads were high and/or the oscillations severe. Investigation showed, however, that by limiting the wind-on test time for each run, the creep diminished to negligible amounts. Hence the test programme which was found to be successful restricted the number of angles tested in any one run to about 7 (less for higher angles hence loads); a typical sequence of wind-on runs and rudder angles within each run for a particular skeg angle was as follows:

RUN No. 1	:	0 °	,	5 °	,	10 °	,	15 °	,	20 °	,	0 °				
2	:	0 °	,	25 °	,	30 °	,	35 °	,	40 °	,	0 °				
3	:	0 °	,	- 5 °	,	- 2 $\frac{1}{2}$ °	,	2 $\frac{1}{2}$ °	,	7 $\frac{1}{2}$ °	,	12 $\frac{1}{2}$ °	,	17 $\frac{1}{2}$ °	,	0 °
4	:	0 °	,	22 $\frac{1}{2}$ °	,	27 $\frac{1}{2}$ °	,	32 $\frac{1}{2}$ °	,	37 $\frac{1}{2}$ °	,	0 °				

Total time for collecting the set of data for one skeg angle for rudder angles from  $-5^{\circ}$  to  $+40^{\circ}$  in  $2\frac{1}{2}^{\circ}$  increments, allowing say four sets of runs with zeros before and after each run, amounted to approximately  $1\frac{1}{2}$  hours.

#### 6.5 Maximum Allowable Loads and Moments:

Due to rotation of the skeg and hence dynamometer axis the dynamometer has to carry maximum individual loads greater than the basic lift and drag requirements. These maximum values have been taken into account in the design calculations (APPENDIX A3.2) and proof loadings (SECTION 5.3).

The dynamometer is however not designed to carry all the maximum loads and moments simultaneously (simultaneous maximum loading is not a requirement of the envisaged control surface tests) hence, based on an assessment of the stresses obtained in APPENDIX A3.2, maximum COMBINED loads and/or moments were evolved and the proof loading programme took account of these combinations. The recommended maximum allowable combinations of loads and moments are shown in Fig. 53 .

It is to be noted that the maximum loads and moments quoted in Fig. 53 , as for the proof loads and complete calibration programme, are all STATIC loads and moments; suitable allowances will have to be made when dynamically fluctuating loadings occur under test conditions.

#### 6.6 Maximum Angular Adjustments of Rudder and Skeg:

Whilst the basic design requirements called for the facility to vary the rudder angle  $\delta$  through  $\pm 35^{\circ}$  and skeg angle  $\beta$  through  $\pm 25^{\circ}$ , the final constructed worm drive arrangements allow adjustment to the following maximum angles:

Rudder Angle  $\delta$  :  $\pm 35^{\circ}$  ;  $\pm 40^{\circ}$  if vernier scale used as an extension  
Skeg Angle  $\beta$  :  $\pm 31^{\circ}$

## 6.7 Corrections caused by Changes in Bridge Voltages.

Calibration was carried out with the Lift bridge supply voltage set at 7.0 volts (the choice of 7.0 v was discussed in SECTION 4.5); due to the properties of the data logger bridge unit and the gauge bridge circuits, this resulted in the following calibration supply voltages for the five components:

L	...	7.000 v
D	...	6.998 v
MZ	...	10.962 v
MX	...	7.009 v
MY	...	7.008 v

Since all bridge voltages are adjusted simultaneously by adjustment of the common supply (Fig. 15 ), variation in any one bridge supply will be proportionally reflected in the remaining four bridges. This property was checked and confirmed during the calibration programme.

Since bridge voltage output is proportional to the supply voltage, the calibration slopes (Force or Moment/ $\mu\text{V}$ ) are inversely proportional to the supply voltages.

Hence if 7.0 volts supply to the Lift bridge is used as the basis for correction, and  $V_0$  is some other chosen (or recorded) supply voltage to the Lift bridge, then the five calibration slopes ( $k_L$ ,  $k_D$ ,  $k_{MZ}$ ,  $k_{MX}$ ,  $k_{MY}$ ) listed in SECTION 5.10 should be multiplied by  $7.0/V_0$ , and the corrected slopes used in the interaction matrix.

## 6.8 Resolution of Measured Forces and Moments caused by Rotation of Dynamometer, hence Dynamometer Axis:

Notation:

(a) Measured components from dynamometer (ref. Fig. 54 )

$N_\beta$	...	Force normal to dynamometer axis when at an angle $\beta$
$A_\beta$	...	Force axial " " " " " " " " $\beta$
$MZ_\beta$	...	Moment about vertical (Z or $Z_\beta$ ) axis
$MX_\beta$	...	Moment about $X_\beta$ axis
$MY_\beta$	...	Moment about $Y_\beta$ axis

(b) Resolved forces and moments

L ... Lift = Force in Y direction  
D ... Drag = Force in X direction  
MZ ... Torque about vertical Z axis  
MX ... Moment about X axis  
MY ... Moment about Y axis

Relationship between measured and resolved components:

$$\begin{aligned}L &= N_{\beta} \cdot \cos \beta - A_{\beta} \cdot \sin \beta \\D &= A_{\beta} \cdot \cos \beta + N_{\beta} \cdot \sin \beta \\MZ &= MZ_{\beta} \\MX &= MX_{\beta} \cdot \cos \beta - MY_{\beta} \cdot \sin \beta \\MY &= MY_{\beta} \cdot \cos \beta + MX_{\beta} \cdot \sin \beta\end{aligned}$$

These equations are correct for  $\pm N_{\beta}$ ,  $A_{\beta}$ ,  $MX_{\beta}$ ,  $MY_{\beta}$   
and  $\pm \beta$  (since  $\sin [-\beta] = -\sin \beta$ )

The use of normal and axial force in their usual form with their usual notation has been avoided since the dynamometer (and skeg) axis moves relative to the flow, and the rudder moves relative to both the dynamometer and the flow; i.e. when  $\beta \neq 0$  the forces normal and tangential to the dynamometer are recorded.

The following equalities exist for certain other conditions:

when  $\beta = 0$ ,  $N_{\beta} =$  rudder lift force, L  
and  $A_{\beta} =$  rudder drag force, D  
when  $+\delta = +\beta$ ,  $N_{\beta} =$  rudder normal force  
and  $A_{\beta} =$  rudder axial force

hence for an all movable control surface, true lift and drag or true normal and axial force may be measured direct.

## 6.9 Note on Units:

For convenience, imperial units were used in the design, construction and calibration of the dynamometer, and in the discussion and general presentation of this Report.



Following current recommended practice, results of tests carried out in the wind tunnel with the dynamometer will be presented in S.I. units or non-dimensionally.

Where necessary, therefore, the appropriate conversions or alternative metric units have been included in the Report and these entail only the following:

The attachment centres of rudder and skeg to dynamometer	}	Included in Fig.47
The roll centres of dynamometer, and skeg attached to base		

Conversion of the calibration matrix to the form of

N or N.m output, given in SECTION 5.10

7.1 The accuracy of the dynamometer is within  $\pm 1.2\%$  of the true values for torque and within  $\pm 1\%$  of the true values for the remaining components; it is within  $\pm 1.2\%$  of full scale for torque and within  $\pm 0.4\%$  of full scale for the remaining components. These orders of accuracy are considered very satisfactory considering the dynamometer type and its operational requirements.

7.2 All calibration slopes were linear within acceptable limits. Component sensitivities of less than 0.1% full scale were achieved; the resulting dynamometer accuracy does however illustrate that sensitivities of this order were a necessary design requirement.

The preliminary design values of strain and hence sensitivity based on average shear stress underestimated the measured values by a significant amount. A re-analysis of the comparison between measured and predicted sensitivities produced very good agreement; the analysis showed that the error is a function of the gauge size relative to flexure size and that, for the accurate prediction of sensitivities in flexures subjected to simple shear, an iterative process using the integration of the true shear stress distribution in way of strain gauge is desirable at the design stage.

7.3 Interactions were all, except one, of linear form and of the same slope for both positive and negative loadings. The non-linear case was of small enough magnitude to be analysed into a linear equivalent without incurring unacceptable error.

The sum of the interaction corrections for each of the five components does not exceed 5% of the limiting value of the component considered; this is a very good achievement, especially if one compares it with more conventional wind tunnel sting balance designs for which considerably larger interactions often have to be accepted.

Following an assessment of the origins of the various interactions it is concluded that, other than those due to deflections of

the rotational base discussed later, the interactions resulted primarily from improper gauge positioning and possibly from variation in gauge factor.

7.4           The measurement of torque is the most inaccurate of all the components, and the torque component was the only one to be subjected to first and second order non-linear interactions. These inaccuracies and interactions are considered to arise from deflections of the  $1\frac{1}{4}$  in rotational base plate.

The results could be interpreted as questioning the method of measuring torque by taking the difference of forces on flexures separated by plates; the problem would of course be eliminated by the use of plates of considerable (and perhaps impractical) thickness.

No simple alternative exists for the isolation of torque measurement in the existing dynamometer. The accuracy for torque is however considered satisfactory for the purposes for which the dynamometer was designed.

7.5           Some interactions were recorded when the skeg was connected direct to rotational base (i.e. non active part of dynamometer); satisfactory correction factors were however derived. These interactions are evidently due to warping of the  $1\frac{1}{4}$  in rotational base, but there is no simple alternative way of isolating the skeg from the rotational base in the existing design concept.

7.6           It was a design requirement that deflections should be small, bearing in mind that certain minimum deflections and hence sensitivities were also required. The measured linear and rotational deflections of the dynamometer under load were found to be well within the requirements of the envisaged free stream rudder tests.

7.7           The measured amounts of hysteresis and creep are considered to be very satisfactory; both characteristics diminished to very low levels following cyclic loading during calibration, and only in the highest parts

of the load and moment ranges was further hysteresis (up to 0.5% full scale) encountered.

7.8           The calibration programme and its findings highlighted the great importance of the need for high accuracy of alignment in the application of loads and moments for the calibration of a multi-component dynamometer of this type.

7.9           Dynamic oscillations of the rudder and dynamometer leading to data output fluctuations were observed during the first high speed tests of a rudder in the wind tunnel. The use of the arithmetic mean of five readings for each test case proved reliable leading to data of satisfactory accuracy and repeatability. However, a preliminary investigation indicated that electrical filtering of the readings should be possible, leading to considerable savings in future test and analysis time.

7.10          It is concluded that the relatively small size of the interaction corrections, small deflections under load and accuracies achieved endorse the validity of the design procedure and overall dynamometer design concept for the measurement of five components.

## ACKNOWLEDGEMENTS

The writer wishes to acknowledge the support and assistance given by the following:

Professor G. J. Goodrich, who supervised the project.

The personnel of the workshops of the Department of Aeronautics and Astronautics, University of Southampton, who were involved in the construction of the dynamometer, particularly Mr. A. Tuck who constructed and assembled all the principal components and items of structure.

Mr. S. Coates, Southampton College of Technology, for his assistance in the construction of the worm wheels and drives, vernier scales and electrical tag boards.

The Science Research Council, who financed the project.

His wife, Andrea, for her support throughout the duration of the project and for typing the Report.

## NOMENCLATURE

The units employed in the Report are discussed in SECTION 6.9.

$A_{\beta}$	-	Force Axial to Dynamometer when at an angle $\beta$
$A_G$	-	Strain gauge grid area
$CP_c$	-	Centre of pressure chordwise measured from leading edge
$CP_s$	-	Centre of pressure spanwise measured from root
$C_D$	-	Drag coefficient
$C_L$	-	Lift coefficient
$D$	-	Drag = force in direction of X - Axis
$E$	-	Modulus of elasticity
$G$	-	Modulus of rigidity
$I$	-	Current
$k$	-	Gauge factor
$k_D$	-	Calibration slope for drag (Force/ $\mu v$ )
$k_L$	-	" " " Lift (Force/ $\mu v$ )
$k_{MX}$	-	" " " MX (Moment/ $\mu v$ )
$k_{MY}$	-	" " " MY (Moment/ $\mu v$ )
$k_{MZ}$	-	" " " MZ (Moment/ $\mu v$ )
$L$	-	Lift = force in direction of Y - Axis
$MX$	-	Moment about X axis through dynamometer roll centre
$MX_{\beta}$	-	Moment about $X_{\beta}$ axis through dynamometer roll centre
$MX_s$	-	Skeg moment about X axis through skeg roll centre
$MY$	-	Moment about Y axis through dynamometer roll centre
$MY_s$	-	Skeg moment about Y axis through skeg roll centre
$MY_{\beta}$	-	Moment about $Y_{\beta}$ axis through dynamometer roll centre
$MZ$	-	Torque = Moment about Z axis

$MZ_{\beta}$	-	Torque = Moment about $Z_{\beta}$ (= Z) axis
$N_{\beta}$	-	Force normal to dynamometer axis when at an angle $\beta$
$q$	-	Shear stress
$R_D$	-	Uncorrected meter reading for Drag ( $\mu v$ )
$R_L$	-	" " " " Lift ( $\mu v$ )
$R_{MX}$	-	" " " " MX ( $\mu v$ )
$R_{MY}$	-	" " " " MY ( $\mu v$ )
$R_{MZ}$	-	" " " " MZ ( $\mu v$ )
$Rn$	-	Reynolds Number
$R$	-	Strain gauge resistance ( $\Omega$ )
$v$	-	Bridge voltage
$v_g$	-	Gauge voltage
X-Axis	-	Air flow axis = longitudinal axis of tunnel
Y-Axis	-	Axis normal to air flow
Z-Axis	-	Vertical axis
$\alpha$	-	Rudder angle relative to flow
$\beta$	-	Dynamometer (and skeg) angle relative to flow
$\delta$	-	Rudder angle relative to dynamometer (or ship, or skeg)
$\epsilon$	-	Direct strain
$\theta$	-	Angle of principal strains
$\sigma$	-	Direct stress
$\phi$	-	Shear strain
$\mu v$	-	Microvolts (Datalogger voltmeter output)

Suffixes : c ... represent the corrected or true loads and moments  
u ... represent the uncorrected or measured loads and moments  
 $\beta$  ... represent the axes, loads and moments  
when dynamometer is at an angle  $\beta$

## REFERENCES

1. Davies P.A.O.L. : 'The New 7' x 5½' and 15' x 12' Low Speed Wind Tunnel at the University of Southampton'. AASU Report No. 202.
2. Perry C.C. and Lissner H.R. : 'The Strain Gage Primer'. McGraw - Hill Book Co.
3. Neubert H.K.P. : 'Strain Gauges - Kinds and Uses'. Macmillan.
4. Potma T. : 'Strain Gauges - Theory and Application'. Iliffe Books Ltd.
5. Beckwith T.G. and Buck N.L. : 'Mechanical Measurements'. Addison Wesley Publishing Co.
6. Pope A. and Harper J.J. : 'Low Speed Wind Tunnel Testing'. John Wiley & Sons Inc.
7. Gorlin S.M. and Slezinger I.I. : 'Wind Tunnels and their Instrumentation'. Israel Program Scientific Translations, Jerusalem 1966 (Translated from Russian, 1964).
8. Anderson J.R. : 'Strain Gage Balances for Wind Tunnels - An Outline of Practice in the United Kingdom'. AGARD Report 5 (1956).
9. Rebuffet P. : 'Some Strain Gage Balances used in French Wind Tunnels'. AGARD Report 6-T (1956).
10. Smith T.L. : 'Special Types of Internal Strain Gauge Balances'. AGARD Report 7 (1956).
11. Lightfoot J.R. and White C.E. : 'Special Applications of Strain Gage Balances used in the Supersonic and Hypersonic Wind Tunnels at the U.S. Naval Ordnance Laboratory'. AGARD Report 8 (1956).
12. Hansen R.M. : 'Mechanical Design and Fabrication of Strain-Gage Balances'. AGARD Report 9 (1956).
13. N.A.E. Canada (Staff) : 'Development of Half-Model Wind Tunnel Balances'. AGARD Report 10 (1956).
14. Lambourne N.C. : 'A Note on a Half-Model Strain-Gauge Balance'. AGARD Report 11 (1956).
15. McFarland K.H. and Dimeff J. : 'Problems involved in Precision Measurements with Resistance Strain Gauges'. AGARD Report 12 (1956).
16. Hansen R.M. : 'Evaluation and Calibration of Wire Strain-Gage Wind Tunnel Balances under Load'. AGARD Report 13 (1956).
17. Boyle H.B. : 'The Shear Plate as a Multi-Component Balance'. Strain, Vol.4, No.2. 1968.



18. Boyle H.B. : "The Strain Gauge: An aid to the Development of Marine Transport". Strain, Vol.6, No.4. 1970.
19. Dubois M. : "Design and Manufacture of High Precision Strain Gauge Dynamometers and Balances at the ONERA Modane Centre". Strain, October 1974.
20. Welwyn Strain Measurement Ltd., MM Tech. Note TN 127 : "Strain Gauge Excitation Levels".
21. Hartrup C.C. : "Bridge Voltages for Strain Gauges". Strain, Vol.8, No.2. 1972.
22. Swan J.W. : Letter referring to Bridge Voltages for Strain Gauges - pgs.35,36. Strain, Vol.9, No.1. 1973.
23. Tokyo Sokki Kenkyujo Co. Ltd., TML Pam. E-1A.

## APPENDIX A1

### SUMMARY OF FLEXURE TYPES AND CHOICE OF FLEXURES

#### A1.1 Summary of Flexure Types:

A summary of the principal flexure types is given in Fig. 55 ; strain gauges can be applied in several locations on the flexures in order that unwanted interactions may be electrically cancelled. The different flexures can be used in many combinations and the reader is referred to the numerous references on the subject, including Refs. 2 to 19 , for detailed discussions of various gauge and flexure applications, their advantages and limitations.

Types ③ and ④ are the most important in respect of this Report since they represent the two principal types most suitable for the new five-component dynamometer.

Type ④ , shear flexures, were chosen for all components of the new dynamometer; total forces are measured directly as the sum of forces on two flexures, and torque and moments measured direct by suitably arranging the bridge circuits whereby the difference of forces on two flexures is recorded.

The next Section, A1.2, gives an outline comparison between the flexure on which strain due to bending in contra-flexure is recorded (Type ③ ), or that which records direct strain due to shear (Type ④ ) and reasons are given for the choice of the latter.

#### A1.2 Choice of Type of Flexure:

The design concept of the dynamometer described in this Report calls for small deflections which include in particular, therefore, deflections in the measuring flexures. Since the dynamometer is of fabricated construction, it was considered that a further feature should be simplicity of design. No particular limitations existed in the vertical dimensions, hence the use of the 'cage' arrangement (or 'elastic parallelogram') with flexures separated by rigid plates was considered the most suitable

layout. The most suitable type of flexure employed in this situation amounts to either that on which strain due to bending on contra-flexure is recorded, Fig. 56 , or that which records direct strain due to shear Fig. 57 .

An important advantage of the flexure bending in contra-flexure is that for the same flexure length, same load and same measured strain at gauge station, its section shape can be arranged whereby its deflection is considerably less than that of the shear plate flexure.

However, shear plate flexures have certain advantages over the flexure bending in contra-flexure, particularly when fabricated construction and simplicity of design are called for, and the following notes give brief outlines of these advantages:

(a) The end fixing conditions for a shear plate are not critical.

This property, which is described and discussed by Boyle, Refs. 17 and 18, is illustrated by comparing Figs. 58 and 59 in which it is seen that the shear force is  $\frac{1}{2}W$  in both the encastré case and for free ends. The measurement of direct strain due to shear is, therefore, independent of end fixity. However, the bending moment at clamped ends is  $W.l/8$ , and for free ends is zero; since the strain at ends due to bending (e.g. in case of contra-flexure) is to be recorded it is important that the ends have either 100% fixity, or some value less than 100% but which should remain unchanged. Either of these conditions is likely to be difficult to obtain in fabricated construction and for this method of construction the shear plate is, therefore, preferable.

A more descriptive way of illustrating this point is by comparing the extreme cases of a plate with very small height in simple shear Fig. 60 in which it is readily apparent that end conditions are not critical, and a beam bending in contra-flexure in which the end fixity is poor, Fig. 61 .

It should be added that the problem of end fixity is, of course, minimised if the end plates and flexures are all machined from one piece of solid material; sophisticated sting and wall mounted wind tunnel balances which employed this manufacturing technique are described by Anderson, Ref. 8 .

(b) The shear plate flexure offers little resistance at right angles to its principal measuring direction.

This is an important property if more than one component of force is to be measured simultaneously by more than one set of flexures situated between the same pair of rigid plates. Flexures bending in contra-flexure can often be arranged with  $D > B$  (Fig. 62 ) whereby less resistance is offered in the non-measuring direction; for the levels of loading being discussed, however, the strain gauge width can put a physical limitation on  $B$ , and the resistance offered in the non-measuring direction will be relatively higher than that for the shear plate in the equivalent situation. If space allows, and superimposed tensile/compressive forces are not large, then contra-flexures can, of course, be employed in two platforms comprised of three rigid plates, Fig. 63 . However, if forces are applied at some height above these platforms then the lever which creates the tensile/compressive forces is increased with consequent increase in these forces.

An alternative approach when employing the measurement of strain in flexures due to bending in contra-flexure (or simple bending) is to use complex cut outs in the flexure (Fig. 64 ) in order that resistance in its non-measuring direction is minimised. A simple diagrammatic example of this is shown; such flexures can call for intricate and highly accurate machining. It is seen, therefore, that the shear plate flexure can be preferable if simplicity of design and manufacture is desired.

(c) With the shear plate flexure the gauge is located at the position of maximum strain, and the strain gradient is small in way of gauge location, hence leading to maximum sensitivity.

(d) The flexure which bends in contra-flexure may suffer interaction due to superimposed compressive forces and moments (Figs. 65 and 66 ), e.g. as discussed in Refs. 6 and 7. In the light of the reasons (particularly (a) and (b) ) outlined above, shear plate flexures were chosen for the new dynamometer described in this Report.

Whilst the deflections of equivalent beams bending in contra-flexure would be considerably less, maximum deflections for the proposed shear plates are estimated to be less than 0.001 in which is within acceptable limits.

APPENDIX A2

OUTLINE OF OPERATION OF THE SHEAR FLEXURE

Resistance strain gauges are arranged at  $45^\circ$  to vertical axis of flexure, and record direct strain due to simple shear, Fig. 67 . A pair of such gauges on each side of one flexure, (or on one side of each of a pair of flexures) may be arranged in one bridge circuit whereby each of its four arms is active, and the outputs from the arms additive, Fig. 68 .

The bridge circuit for the shear flexure may be arranged whereby it is insensitive in all directions other than the measuring direction. This property is, however, dependent on accurate alignment of the strain gauges.

A summary of the outputs from the principal applied forces and moments is, therefore, as follows:-

When flexure is subjected to :

SIMPLE SHEAR	- gauge signals are additive and bridge output is MAXIMUM
TENSION/COMPRESSION	- gauge signals cancel and bridge output is ZERO
BENDING	- " " " " " "
TORSION	- " " " " " "

APPENDIX A3

CALCULATIONS FOR DIMENSIONS OF FLEXURES

A3.1 Summary of Formulae and Data Applicable to the Design of the Shear Flexures (refer Fig. 69 ):

Maximum principal direct stresses in material:

$$\sigma_1 \text{ and } \sigma_2 = \frac{1}{2} (\sigma_x + \sigma_y) \pm \frac{1}{2} \sqrt{(\sigma_x - \sigma_y)^2 + 4 q^2} \dots A3.1$$

Angle of principal planes:-

$$\theta = \frac{1}{2} \tan^{-1} \frac{2 q}{\sigma_x - \sigma_y} \dots A3.2$$

Strain at any angle  $\theta$  is the algebraic sum of the strains resulting from each individual force:-

$$\epsilon_\theta = \epsilon_x \cos^2 \theta + \epsilon_y \sin^2 \theta + \phi \sin \theta \cdot \cos \theta \dots A3.3$$

where  $\phi$  is shear strain

$$\phi = \frac{q}{G} \quad \text{where } G = \text{modulus of rigidity}$$

Principal strains:-

$$\epsilon_1 \text{ and } \epsilon_2 = \frac{1}{2} (\epsilon_x + \epsilon_y) \pm \frac{1}{2} \sqrt{(\epsilon_x - \epsilon_y)^2 + \phi^2} \dots A3.4$$

acting at an angle

$$\theta = \frac{1}{2} \tan^{-1} \frac{\phi}{(\epsilon_x - \epsilon_y)} \dots A3.5$$

The force flexures are subjected to tensile/compressive forces and simple shear forces.

The moment flexures are subjected to tensile/compressive forces, torsion and simple shear forces.

Strains due to tensile/compressive forces and torsion will cancel in proposed gauge configurations (see APPENDIX A2), hence the analysis in respect of gauge signal output is based on the application of simple shear. (Maximum principal stresses are estimated as a check in respect of possible hysteresis in the flexure material).

When shear flexures are subjected to simple shear stress  $q$ , and  $\sigma_x = \sigma_y = 0$ ,

then from equation A3.1

$$\sigma_1 = q$$

" " " A3.2

$$\theta = 45^\circ$$

" " " A3.3 and A3.4 with  $\theta = 45^\circ$  per principal stress and proposed gauge orientation:

$$\epsilon_\theta = \frac{\phi}{2}$$

i.e. Direct strain is half of the shear strain

The material chosen for the flexures was aluminium alloy, Type HE 30, as explained in SECTION 3.10. This alloy has the following particulars:

	Tensile Strength	.....	20	tonf/in <sup>2</sup>
	0.1% Proof Stress	.....	17	tonf/in <sup>2</sup>
	Limit of Proportionality (approx.)...		12	tonf/in <sup>2</sup>
	Ultimate Shear Stress (approx.)...		14	tonf/in <sup>2</sup>
Assumed for calculations	{	Modulus of Elasticity, E	...	10 x 10 <sup>6</sup> lbf/in <sup>2</sup>
		Modulus of Rigidity, G	...	4 x 10 <sup>6</sup> lbf/in <sup>2</sup>

### A3.2 Dimensions of Flexures:

Flexure dimensions are governed on the one hand by the need for a small thickness which will carry the required load with adequate strain but which will offer little resistance to loads in some other directions, and the need for adequate thickness for rigidity and stiffness

in order to minimise deflections and possibly carry loads in other directions. Hence the flexure design problem generally includes the contradictory requirements of sensitivity and stiffness.

Refs. 6, 8 and 19 recommend a maximum skin strain at gauge stations of up to 0.001 (0.1% or  $1000 \mu\epsilon$ ), which leads to a stress of about 5 tonf/in<sup>2</sup> in aluminium alloy. Refs. 7 and 15 suggest a maximum skin strain of up to  $500 \mu\epsilon$  in order to reduce the possibility of hysteresis.

From the point of view of sensitivity, if 0.1% of full measured range is assumed to be required (e.g. this is recommended in Ref. 7 in order to achieve an accuracy of the order of 1% for the aerodynamic loads) and resolution of  $1 \mu v$  is available on measuring equipment, then a minimum full scale reading of  $1000 \mu v$  is required.

$$\Delta v = v \times k \times \epsilon \quad \dots \text{Equation A5.3 (APPENDIX A5)}$$

where  $\epsilon$  is the strain in one arm of a four active arm bridge

$$\text{Hence min. } \epsilon = \frac{\Delta v}{vk} = \frac{1000}{5 \times 2} = 100 \mu\epsilon$$

(assuming supply voltage is 5 volts and gauge factor is 2)

Hence for a sensitivity of 0.1% of full range,  $100 \mu\epsilon$  are required per arm. (Any increases in this value of strain or assumed value of supply voltage will, of course, increase the 0.1% sensitivity).

In view of the above recommendations, a direct strain due to shear at each gauge of  $500 \mu\epsilon$  was assumed in order to initiate the design cycle; the calculations will indicate, however, that without making the flexures complex in design, other constraints such as superimposed tensile/compressive forces and the need for a minimum mechanical thickness lead in the main to values of direct strain due to shear of much less than this.

The flexures are designed to be square in profile in order to minimise the possibility of bending due to shear. The lift and drag flexures have overall depths (D) of 1.75 in (decided by limitations of access) and attachment pad thickness of 0.25 in; the net maximum flexure depth is, therefore, 1.25 in. In order to maintain flexure thickness, the chosen values for  $l$  are less than 1.25 in hence in



order to maintain a square 'working' section (d x l ), the flexures have been suitably radiused (R), Fig. 70 . The moment flexures have overall depths of 1.90 in and attachment pad thicknesses of 0.25 in ; the net maximum flexure depth is, therefore, 1.40 in and this is also used as the width for the moment flexures in order to attain a square 'working' section.

Summary of Calculations:

It is to be appreciated that the calculations for the flexure dimensions followed an iterative process, particularly in the case of the lift and drag flexures which are subjected to relatively high tensile/compressive forces as well as the design shear forces.

For brevity, therefore, an outline of the calculations leading up to the final flexure dimensions is given. The calculations are based on the following maximum (proof) loads:-

Lift	....	200 lbf
Drag	....	150 lbf
Torque	....	1200 lbf in
MX	....	4800 lbf in
MY	....	3600 lbf in

Assumed max. linear skin strain  $\epsilon = 0.0005$  ( =  $500 \mu\epsilon$  )

" for aluminium  $G = 4 \times 10^6$  lbf/in<sup>2</sup>

Since direct strain = half of shear strain

i.e.  $\epsilon = \frac{\phi}{2}$

and  $q/G = \phi$

shear stress  $q = \phi \times G = 2 \cdot \epsilon \cdot G$

=  $2 \times 0.0005 \times 4 \times 10^6$

= 4000 lbf/in<sup>2</sup>

Average shear stress  $q = F/A$

then Area  $A = F/q$

#### MOMENT X FLEXURES

(4800 lbf in ) refer Fig.71

Neglecting bending moment in flexures and resistance due to warping of flexures at right angles (MY Flexures),

$$\begin{aligned}\text{Shear Forces on Flexures } F_1 &= F_2 = 4800/9 \\ &= 533 \text{ lbf} \\ q &= 4000 \text{ lbf/in}^2 - \text{assumed earlier} \\ \text{hence Area} &= F/q = 533/4000 = 0.133 \text{ in}^2\end{aligned}$$

Depth of flexure = 1.4 in , hence thickness would be  $0.133/1.4 = .095$  in proposed to reduce strain to  $380 \mu\epsilon$  , hence  $q = 3040 \text{ lbf/in}^2$

$$\text{and Area} = 533/3040 = 0.175 \text{ in}^2$$

hence thickness will be 0.125 in for  $380 \mu\epsilon$  max. at 533 lbf

Hence MX FLEXURE DIMENSIONS ARE : 1.40 in x 0.125 in

#### MOMENT Y FLEXURES

(3600 lbf in )

$$\begin{aligned}\text{Shear Forces on Flexures } F_1 &= F_2 = 3600/9 = 400 \text{ lbf} \\ \text{and Area} &= 400/4000 = 0.10 \text{ in}^2\end{aligned}$$

hence thickness of flexure would be  $0.10/1.4 = 0.071$  in

proposed to reduce strain to  $360 \mu\epsilon$  , hence  $q = 2880 \text{ lbf/in}^2$

$$\text{and Area} = 400/2880 = 0.139 \text{ in}^2$$

hence thickness will be 0.10 in for  $360 \mu\epsilon$  max. at 400 lbf

Hence MY FLEXURE DIMENSIONS ARE : 1.40 in x 0.10 in

## ANTI-TORQUE FLEXURES (UN-GAUGED)

refer Fig. 72

Load in X - Direction assumed to be substantially carried by MY Flexures in tension/compression

$$\text{hence } F_1 = F_2 = 1200/9 = 133 \text{ lbf}$$

Flexures assumed to have section 1.5 in x 0.1 in = 0.15 in<sup>2</sup>

$$\text{then stress} = 133/0.15 = 890 \text{ lbf/in}^2$$

$$\text{and strain} = \phi = q/G = 890/4 \times 10^6 = 0.00022$$

$$\text{hence approximate shear displacement} = 1.9 \text{ in} \times 0.00022 = 0.00042 \text{ in}$$

hence approximate radial displacement  $\approx 0.00042/4.5 = 0.005^0$  which is assumed to be acceptable

## LIFT FLEXURES

refer Fig. 73

Maximum Shear Force condition approx. as shown where 1200 lbf in max. torque shared approx. as 80 lbf in each lift flexure and 70 lbf in each drag flexure (see following calculations for dimensions).

Hence assumed for design maximum condition, all lift of 200 lbf carried by one flexure.

This assumption also neglects resistance of drag flexures bending in contra-flexure; an estimate suggests this amounts to about 2% of load.

$$\text{Hence assuming lift on one flexure} = 200 \text{ lbf}$$

$$q = 4000 \text{ lbf/in}^2 - \text{assumed earlier}$$

$$\text{hence area} = 200/4000 = 0.05 \text{ in}^2$$

With a depth of flexure of, say, 1.0 in, thickness would be 0.05 in

propose reduce strain to  $250 \mu\epsilon$ , hence  $q = 2000 \text{ lbf/in}^2$

$$\text{and Area} = 200/2000 = 0.10 \text{ in}^2$$

hence thickness will be 0.10 in for  $250 \mu\epsilon$  max. at 200 lbf

Hence LIFT FLEXURE DIMENSIONS ARE : 1.0 in x 0.10 in

Total skin strain on flexure at gauge station due to shear and tension/compression (see following calculations) is  $250 + 160 = 410 \mu\epsilon$ , which corresponds with recommended practice.

Above figure of  $250 \mu\epsilon$  is for one flexure (2 gauges) hence this is equivalent to  $125 \mu\epsilon$  per gauge for complete bridge.

#### DRAG FLEXURES

Due to combined effects of torque and drag, assumed for design maximum condition all drag of 150 lbf carried by one flexure.

This assumption also neglects resistance of lift flexures bending in contra-flexure.

Hence assuming drag on one flexure = 150 lbf

$$q = 4000 \text{ lbf/in}^2 - \text{assumed earlier}$$

$$\text{hence area} = 150/4000 = 0.0375 \text{ in}^2$$

With a depth of flexure of, say, 1.0 in, thickness would be 0.0375 in

Propose reduce strain to  $260 \mu\epsilon$ , hence  $q = 2080 \text{ lbf/in}^2$

$$\text{and area} = 150/2080 = 0.072 \text{ in}^2$$

Propose reduce depth to 0.90 in,

hence thickness will be 0.08 in for  $260 \mu\epsilon$  at 150 lbf

Hence DRAG FLEXURE DIMENSIONS ARE : 0.90 in x 0.08 in

Total skin strain on flexure at gauge station due to shear and tension/compression (see following calculations) is  $260 + 260 = 520 \mu\epsilon$ , which corresponds with recommended practice.

Above figure of  $260 \mu\epsilon$  due to shear is for one flexure (2 gauges), hence this is equivalent to  $130 \mu\epsilon$  per gauge for complete bridge.

## COMPRESSIVE/TENSILE STRESSES IN DRAG FLEXURES DUE TO MX

Roll centre lowered by approximately 3 in (refer Fig. 74 ) and maximum apparent MX acting on drag flexures is  $200 \times (24 + 3) = 5400$  lbf in (as compared with  $200 \times 24 = 4800$  on moment flexures).

Hence compressive or tensile force

$$\text{in Drag flexures is } 5400/7.75 = 697 \text{ lbf}$$

$$\begin{aligned} \text{and compressive/tensile stress} &= 697/.072 = 9680 \text{ lbf/in}^2 \\ &= 4.32 \text{ tonf/in}^2 \end{aligned}$$

$$\begin{aligned} \text{From above, average shear stress in drag flexures } q &= 2080 \text{ lbf/in}^2 \\ &= .93 \text{ tonf/in}^2 \end{aligned}$$

Applying Eqtn. A3.1,

$$\begin{aligned} \text{Max. principal stress} &= \frac{1}{2} (4.32) \pm \frac{1}{2} \sqrt{(4.32)^2 + 4 \times .93^2} \\ &= 2.16 \pm 2.35 \\ &= 4.51 \text{ tonf/in}^2 \end{aligned}$$

This figure is considered satisfactory in respect of strength, although perhaps a little high in respect of possible hysteresis. The strains due to the tensile/compressive forces are, however, high and, although these strains should be cancelled electrically, any misalignment of gauges could lead to serious interaction.

$$\text{i.e. due to tension/compression, } \sigma_y = 9680 \text{ lbf/in}^2$$

$$\text{and } \epsilon_y = 9680/10 \times 10^6 = 968 \mu\epsilon$$

$$\text{and using Eqtn. A3.3, } \epsilon_{45^\circ} = \epsilon_y \sin^2 \theta = 968 \times .5 = 484 \mu\epsilon$$

Further, the total skin strain at gauge station due to tension and shear is  $484 + 260 = 744 \mu\epsilon$ , which is high according to the recommended practice.

It was felt that the section area of the drag flexures should not be increased further since this would have reduced their sensitivity to below the acceptable limits, hence it was decided to introduce supplementary pillars (un-gauged) which would share the tensile/compressive loads, but which would offer little resistance to the shear loads.

SUPPLEMENTARY PILLAR FLEXURES (UN-GAUGED)

An outline of the calculations for the chosen dimensions is as follows:

The design was assumed to be idealised as shown in Fig. 75

$$P = P_a + P_b + P_c = 2P_a + P_b = 697 \text{ lbf}$$

$$\text{hence } P_b = 697 - 2P_a \quad \dots (1)$$

$$\text{Extension } \chi = \chi_a = \chi_b = \chi_c$$

$$\begin{aligned} \chi_a = \chi_1 + \chi_2 + \chi_3 &= 0.2 \varepsilon_1 + 0.85 \varepsilon_2 + 0.2 \varepsilon_3 \\ &= 0.2 \frac{f_1}{E_1} + 0.85 \frac{f_2}{E_2} + 0.2 \frac{f_3}{E_3} \end{aligned}$$

$$\varepsilon_1 = \varepsilon_3, \text{ and } f_1 = f_3, \text{ and } E_1 = E_2 = E_3 = E_{AL}$$

$$\text{hence } \chi_a = \frac{1}{E_{AL}} (0.4 f_1 + 0.85 f_2) \quad \dots (2)$$

$$\chi_b = 1.25 \varepsilon_4 = 1.25 \frac{f_4}{E_4} = 1.25 \frac{f_4}{E_{AL}} \quad \dots (3)$$

$\chi_a = \chi_b$ , hence equating (2) and (3)

$$\frac{1}{E_{AL}} (0.4 f_1 + 0.85 f_2) = 1.25 \frac{f_4}{E_{AL}}$$

$$0.4 \frac{P_a}{.0113} + 0.85 \frac{P_a}{.196} = 1.25 \frac{P_b}{.072}$$

$$\text{i.e. } 39.74 P_a = 17.36 P_b$$

Subst. in (1), whence  $39.74 P_a = 17.36 (697 - 2P_a) = 12100 - 34.72 P_a$

$$P_a = \frac{12100}{74.46} = 162.5 \text{ lbf}$$

$$\begin{aligned} \text{and } f_1 = f_3 &= \frac{162.5}{.0113} = 14380 \text{ lbf/in}^2 \\ &= 6.4 \text{ tonf/in}^2 \end{aligned}$$

This stress is high, but considered acceptable; it will in fact be reduced a little due to the radii on the drag flexures reducing the length of the 0.9 in x 0.08 in section.

$$P_6 = \frac{39.74 \times 162.5}{17.36} = 372 \text{ lbf}$$

$$\text{and } f_4 = \frac{P_6}{.072} = \frac{372}{.072} = 5167 \text{ lbf/in}^2 = 2.3 \text{ tonf/in}^2$$

$$\text{and } \epsilon_A = \frac{f_4}{E_{AL}} = \frac{5167}{10 \times 10^6} = 517 \mu\epsilon$$

$$\text{and } \epsilon_{45^\circ} = 260 \mu\epsilon$$

Hence the strain at gauge station due to tension/compression has been reduced to a little over half of the strain without supplementary pillars, and the total skin strain at gauge station on drag flexures due to tension/compression and shear will be  $260 + 260 = 520 \mu\epsilon$ .

Similar calculations for the two pillars acting in the MY plane, for maximum apparent  $MY = 150 \times (24 + 3) = 4050 \text{ lbf in}$  and lift flexure area of  $1 \text{ in} \times 0.1 \text{ in} = 0.1 \text{ in}^2$ , leads to  $f_1 = 3.98 \text{ tonf/in}$  and, for lift flexure,  $\epsilon_{45^\circ} = 160 \mu\epsilon$ .

Further check calculations were carried out for the extreme combined case of lift = 170 lbf plus drag = 85 lbf leading to apparent  $MX = 170 \times (24 + 3)$  plus  $MY = 85 \times (24 + 3)$ . This leads to approximate combined tensile/compressive stresses in outside pillars of  $5.44 \text{ tonf/in}^2$  due to  $MX$  plus  $2.25 \text{ tonf/in}^2$  due to  $MY$ ; i.e. a total stress of  $7.69 \text{ tonf/in}^2$ .

This stress is high but assumed acceptable. The calculation does, however, illustrate the need to restrict the combinations of maximum loadings (with a large lever leading to large  $MX$  and/or  $MY$ ) to the permissible combinations outlined in SECTION 6.5.

#### TORQUE

This is derived from gauges mounted on the inside of each of the lift and drag flexures, and the magnitude of the torque response is, therefore, dictated by the already determined sizes of the lift and drag flexures.

If 80 lbf is assumed to act on each lift flexure due to

1200 lbf in Torque (see lift flexure calcs.), then this results in 100  $\mu\epsilon$  per gauge for complete torque bridge. A similar calculation for 70 lbf due to torque acting on the drag flexures results in approximately 120  $\mu\epsilon$  per gauge.

The torque series bridge circuit takes account of differences in torque response for lift and drag flexures. The magnitude of these strains due to torque is considered adequate.

#### ESTIMATES OF STRAIN

It should be noted that all the foregoing estimates of strain at gauge stations, resulting from the chosen flexure sizes and design loads, are based on mean values of shear stress. Since the shear stress distribution is parabolic, and has a value at the centre of the flexure section of 1.5 times the mean value which was assumed, some increase in the predicted responses and hence output signals would be expected from the calibrated results. The magnitude of the increase will depend on the size of the chosen gauges relative to the flexure size.

A comparison between the above predicted strains (hence sensitivities) and actual measured strains (hence sensitivities) is contained in the calibration data discussion, SECTION 5.5.3, and APPENDIX A6 contains a more detailed analysis (using the chosen gauge and flexure sizes) of the correlation between more accurate theoretical predictions and the actual measured data.



APPENDIX A4

ERRORS IN STRAIN DUE TO ERRORS IN FLEXURE DIMENSIONS

The following outline calculations indicate the order of error in strain due to errors of  $\pm 0.001$  in in flexure dimensions for both aluminium and steel.

Assume an Aluminium section of 1.0 in x 0.1 in = 0.1 in<sup>2</sup>

$$\text{Direct strain due to shear } \epsilon = \frac{q}{2G} = \frac{F}{A_s \times 2G}$$

$$\text{since } G_A \approx 4 \times 10^6 \text{ and } G_s \approx 12 \times 10^6, \quad G_s = 3 \times G_A$$

hence for same strain, area of equivalent

$$\text{steel flexure} = 0.1/3 = 0.0333 \text{ in}^2$$

Assume steel flexure section of 0.7 in x 0.0476 in = 0.0333 in<sup>2</sup>

For aluminium flexure:-

Due to error in each dimension of + 0.001 in (yielding maximum error in section)

$$\text{Actual area} = 1.001 \times 0.101 = 0.1011 \text{ in}^2$$

$$\text{error in area} = 0.0011/0.1 \times 100 = 1.1\%$$

$$\text{and error in strain} = (1/0.1 - 1/0.1011) \times 0.1/1 \times 100 = 1.09\%$$

For steel flexure:-

Due to error in each dimension of + 0.001 in

$$\text{Actual area} = 0.701 \times 0.0486 = 0.0341 \text{ in}^2$$

$$\text{error in area} = 0.0008/0.0333 \times 100 = 2.4\%$$

$$\text{and error in strain} = (1/0.0333 - 1/0.0341) \times 0.0333/1 \times 100 = 2.35\%$$

Comments on calculations:-

(a) The calculations illustrate the need for accurate machining of flexures (say to within  $\pm 0.001$  in ) in way of strain gauge location. This may not be of importance if one flexure is to be used in isolation, which can, therefore, be calibrated independently. If, however, two flexures of 'identical' section are required, the sum of their strains indicating force and their differences moment (as in the case of the dynamometer described in this Report, see APPENDIX A1) then differences in their dimensions and hence strain lead to asymmetry in layout and an 'electrical' centre not coincident with the designed 'mechanical' centre.

(b) A steel flexure with an area equivalent to aluminium in order to produce the same strain (for chosen dimensions in example) has over two times the error in strain. This indicates an advantage in favour of the use of aluminium flexures for the application in question.

APPENDIX A5

SUMMARY OF PROPERTIES OF THE RESISTANCE STRAIN GAUGE AND UNBALANCED BRIDGE

The resistance strain gauge operates on the principle that its electrical resistance varies with strain. The basic equation relating relative change in resistance  $\Delta R$  and change in length, or strain, is :

$$\text{Strain } \epsilon = \frac{\Delta l}{l} = \frac{1}{k} \cdot \frac{\Delta R}{R}$$

where  $k$  = gauge factor

and  $R$  = nominal gauge resistance

The most suitable circuit for detecting this change in resistance (and that most commonly used) is the bridge circuit, Fig. 68

$$\text{When bridge is balanced } \frac{R_1}{R_2} = \frac{R_4}{R_3}$$

If a single gauge,  $R_1$ , is sensitive to strain, then

$$\text{bridge becomes unbalanced and } \frac{R_1 + \Delta R_1}{R_2} \neq \frac{R_4}{R_3}$$

For strain output, or signal output as a function of force as in the case of the force transducer, the bridge is generally operated as a direct reading instrument when the bridge becomes unbalanced.

From theory of unbalanced bridge (e.g. Ref. 2), when resistance of one arm of equal arm bridge changes by  $\Delta R$ , imbalance voltage  $\Delta v$  across measuring diagonal of bridge is:

$$\begin{aligned} \Delta v &= \frac{v}{4} \cdot \frac{\Delta R}{R} \\ &= \frac{v}{4} \cdot k \cdot \epsilon \end{aligned}$$

where  $v$  is supply voltage

For force transducers it is common to make all four arms of

bridge active whence four times the output and hence sensitivity is achieved. The full bridge also self-compensates for temperature.

If all four arms of bridge are active, and changes in resistance of arms are  $\Delta R_1$ ,  $\Delta R_2$ ,  $\Delta R_3$  and  $\Delta R_4$ , then from unbalanced bridge theory, imbalance voltage  $\Delta v$  across measuring diagonal of bridge, for small values of  $\Delta R$ , can be shown to be:

$$\Delta v = \frac{v}{4} \left( \frac{\Delta R_1}{R_1} - \frac{\Delta R_2}{R_2} + \frac{\Delta R_3}{R_3} - \frac{\Delta R_4}{R_4} \right) \quad \dots A5.1$$

where all four gauges have the same nominal resistance  $R$ .

If all four gauges have same gauge factor  $k$ , then equation A5.1 becomes:

$$\Delta v = \frac{v \cdot k}{4} (\epsilon_1 - \epsilon_2 + \epsilon_3 - \epsilon_4) \quad \dots A5.2$$

It is evident that if gauges  $R_2$  and  $R_4$  are subjected to strain of the same magnitude but opposite sign for that of  $R_1$  and  $R_3$  then the maximum bridge imbalance and hence output signal will occur

$$\text{and } \frac{R_1}{R_2} + \frac{\Delta R_1}{\Delta R_2} \neq \frac{R_4}{R_3} - \frac{\Delta R_4}{\Delta R_3}$$

In this case, for full bridge with four active gauges with equal strains in each, output signal is

$$\Delta v = v \cdot k \cdot \epsilon \quad \dots A5.3$$

where  $\epsilon$  is strain in one arm.

Example:

If supply voltage  $v = 5v$ ,  $\epsilon = 100 \mu\epsilon$  and  $k = 2$  then from equation A5.3,  $\Delta v = v \times k \times \epsilon = 5 \times 2 \times 100 = 1000 \mu v$ . Hence if a maximum load of, say, 200 lbf produces, say, 100  $\mu\epsilon$  per gauge in four arm bridge, then  $\Delta v = 1000 \mu v$ . If instrumentation can measure down to, say, 1  $\mu v$ , then sensitivity (or minimum load that will produce a response) is 0.2 lbf, i.e. 0.1% of maximum load.

Calculations for the dimensions of flexures are shown in APPENDIX A3, and equation A5.3 is used as the criterion for estimating the required sensitivity and hence required strain for a known value of  $k$  for gauges, supply voltage  $v$  and minimum response in  $\mu v$  for measuring instrumentation.

APPENDIX A6

RE-ANALYSIS OF STRAIN AND SENSITIVITY PREDICTIONS

The disparities between the predictions and measured sensitivities were discussed briefly in SECTION 5.5.3, and the values are reproduced below:

	PREDICTED $\mu\text{V/lbf}$ or $\text{lbf/in}$	MEASURED $\mu\text{V/lbf}$ or $\text{lbf/in}$	DIFFERENCE %
L	9.35	13.16	+ 41%
D	12.98	17.61	+ 36%
MZ	2.15	2.85	+ 33%
MX	1.19	1.78	+ 50%
MY	1.50	2.33	+ 55%

Some increase in measured response compared with predicted was envisaged at the design stage due to the use of mean shear stress. The relatively large differences recorded above called for a short investigation into the use of mean shear stress for the determination of strain over the gauge length.

For brevity it was decided not to investigate each numerical prediction in turn but to determine, non-dimensionally for each flexure type, the difference between predictions based on the true integrated strain over the gauge length, and the assumed mean strain value.

The shear stress distribution is parabolic; hence due to simple shear the direct strain distribution along line of principal axis (also gauge axis) will be parabolic.

Gauge length relative to flexure length in direction of principal axes was obtained from Fig. 14 for each flexure type.

The ratios of gauge length/flexure length for each flexure type, together with the results of the integrated stresses over the gauge length compared with assumed mean stress are given in Fig. 76 . The analysis produced the following results:

Lift gauges	:	$q_{actual}$	=	1.46	$q_{mean}$	
Drag gauges	:	$q_{actual}$	=	1.45	$q_{mean}$	
Torque gauges	:	$q_{actual}$	=	1.45	$q_{mean}$	(approx.)
Moment gauges	:	$q_{actual}$	=	1.48	$q_{mean}$	

Hence the predictions using the true strains in way of gauges are within about 10% of the measured values.

The remaining error is due to a small amount of the lift being carried by the drag flexures and supplementary pillars bending in contra-flexure, drag carried by the lift flexures and supplementary pillars, and torque carried by the supplementary pillars, hence accounting for the decrease in measured values. An approximate estimate of the influence of drag flexures on lift indicated that the drag flexures bending in contra-flexure carry about 2% of the load; since the lift flexures are larger than the drag flexures the lift flexures will carry a slightly larger proportion of the drag. Accurate estimates were not attempted concerning the bending of the flexures and pillars in contra-flexure due to the complexities of the end shapes of the lift and drag flexures, and shape of pillars.

There is a further small increase in the moment response and this can be accounted for by the influence of rotation on the moment flexures, Fig. 77 . Due to its complexity, the numerical influence of rotation was not investigated, but the foregoing figures indicate that its effect is relatively small.

The foregoing results and discussion indicate that nearly all of the disparities between original predicted sensitivities and measured values can be accounted for; the analysis also suggests that in the design of flexures subjected to simple shear an iterative process should be adopted at the design stage which takes account of the shear stress distribution and the size of the gauge relative to the flexure.

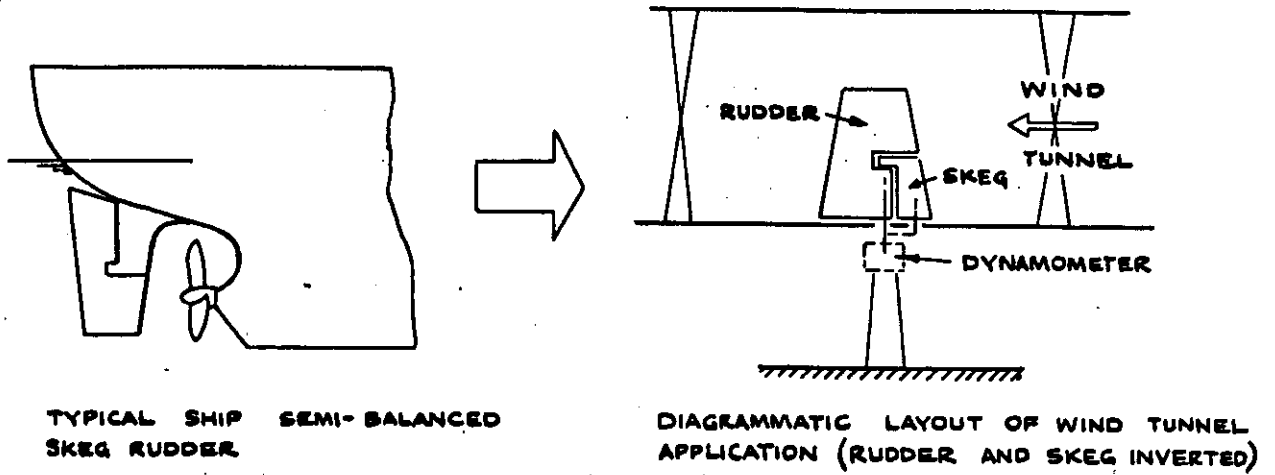
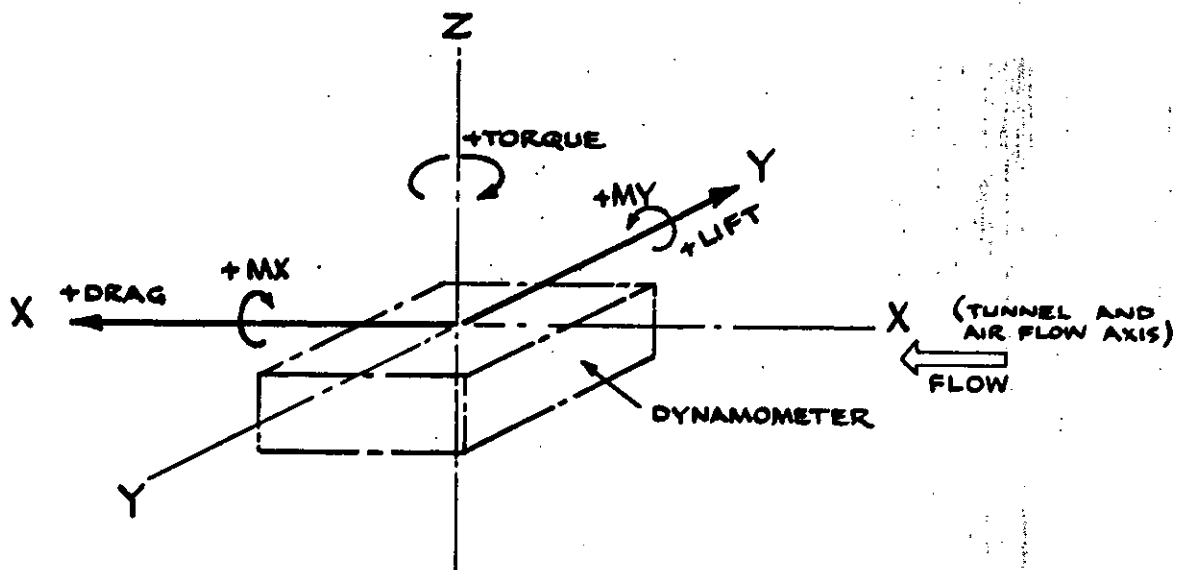


Fig. 1 MOUNTING OF MODEL IN WIND TUNNEL



FIVE COMPONENTS:

LIFT : L

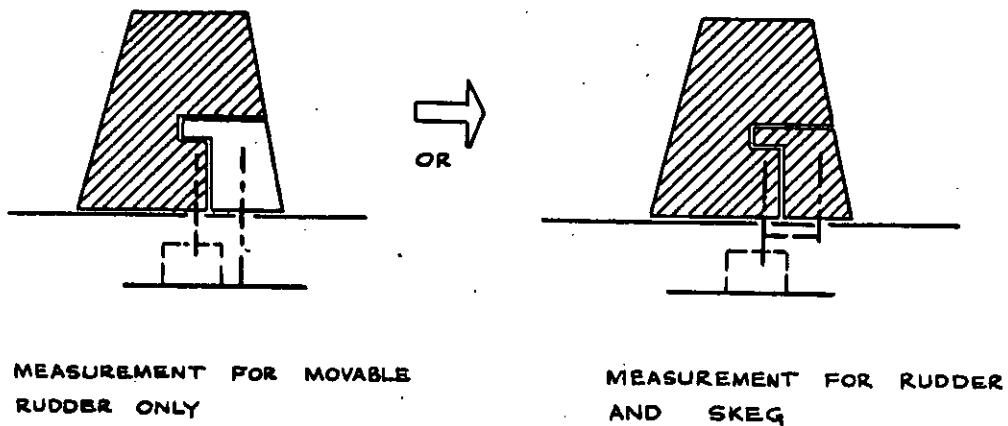
DRAG : D

TORQUE : MZ - HENCE DERIVATION OF CENTRE OF PRESSURE CHORDWISE

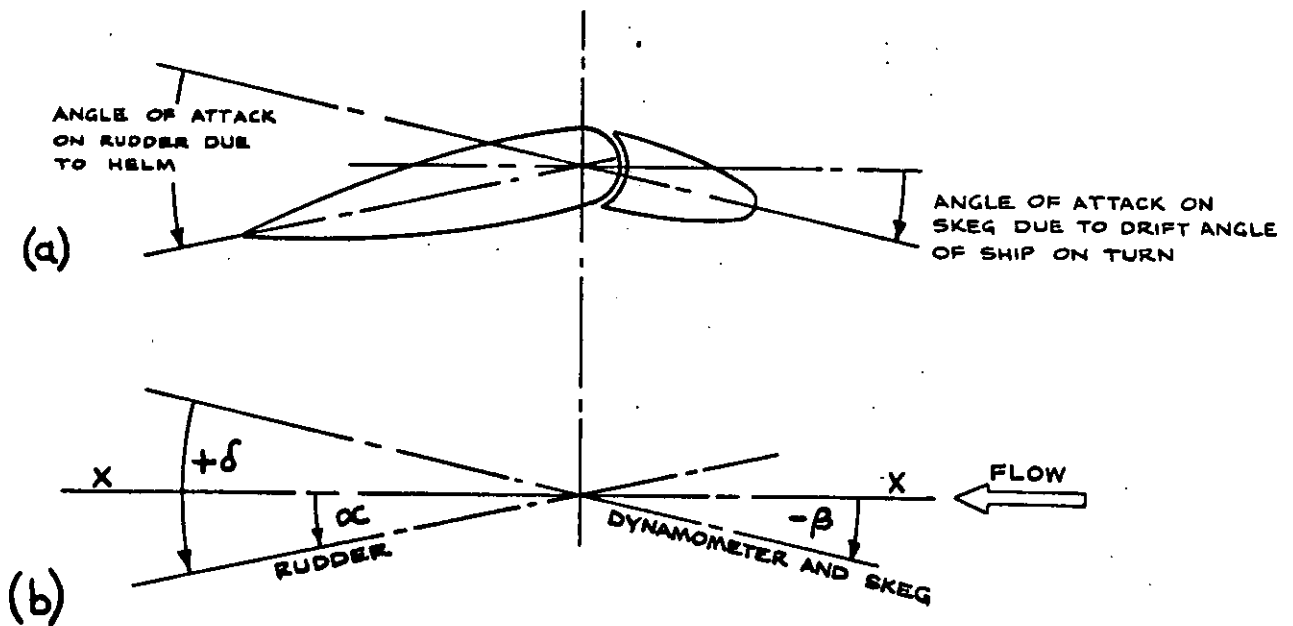
MOMENT ABOUT X-AXIS : MX } HENCE DERIVATION OF CENTRE  
 MOMENT ABOUT Y-AXIS : MY } OF PRESSURE SPANWISE

Fig. 2 COMPONENTS MEASURED





**Fig. 3** RUDDER AND SKEG FORCES



**NOTATION :**

- $β$  = DYNAMOMETER (AND SKEG) ANGLE RELATIVE TO FLOW
- $δ$  = RUDDER ANGLE RELATIVE TO DYNAMOMETER (OR SHIP, OR SKEG)
- $α$  = RUDDER ANGLE RELATIVE TO FLOW
- $α = δ + β$

**Fig. 4** NOTATION OF ANGLES



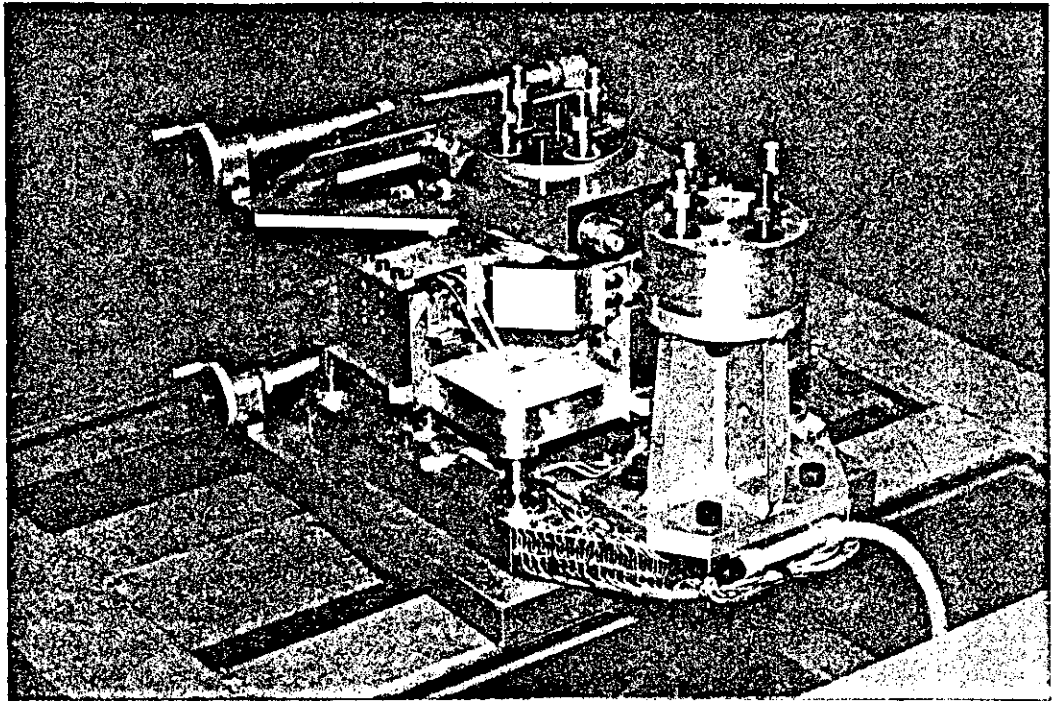


Fig.6 DYNAMOMETER

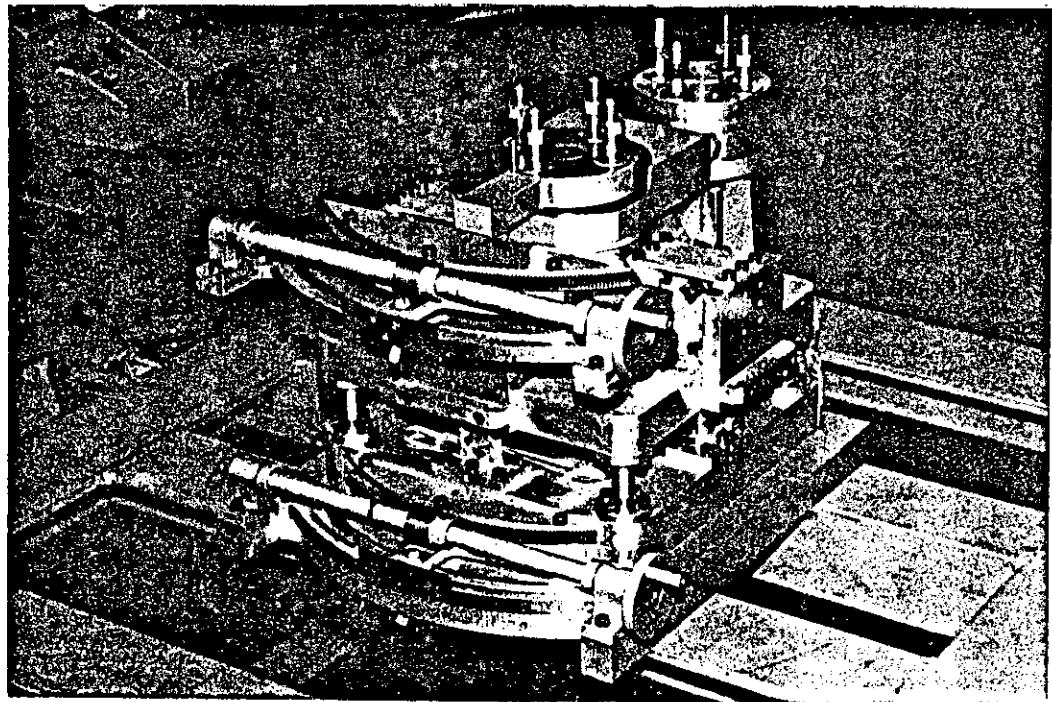


Fig. 7 DYNAMOMETER

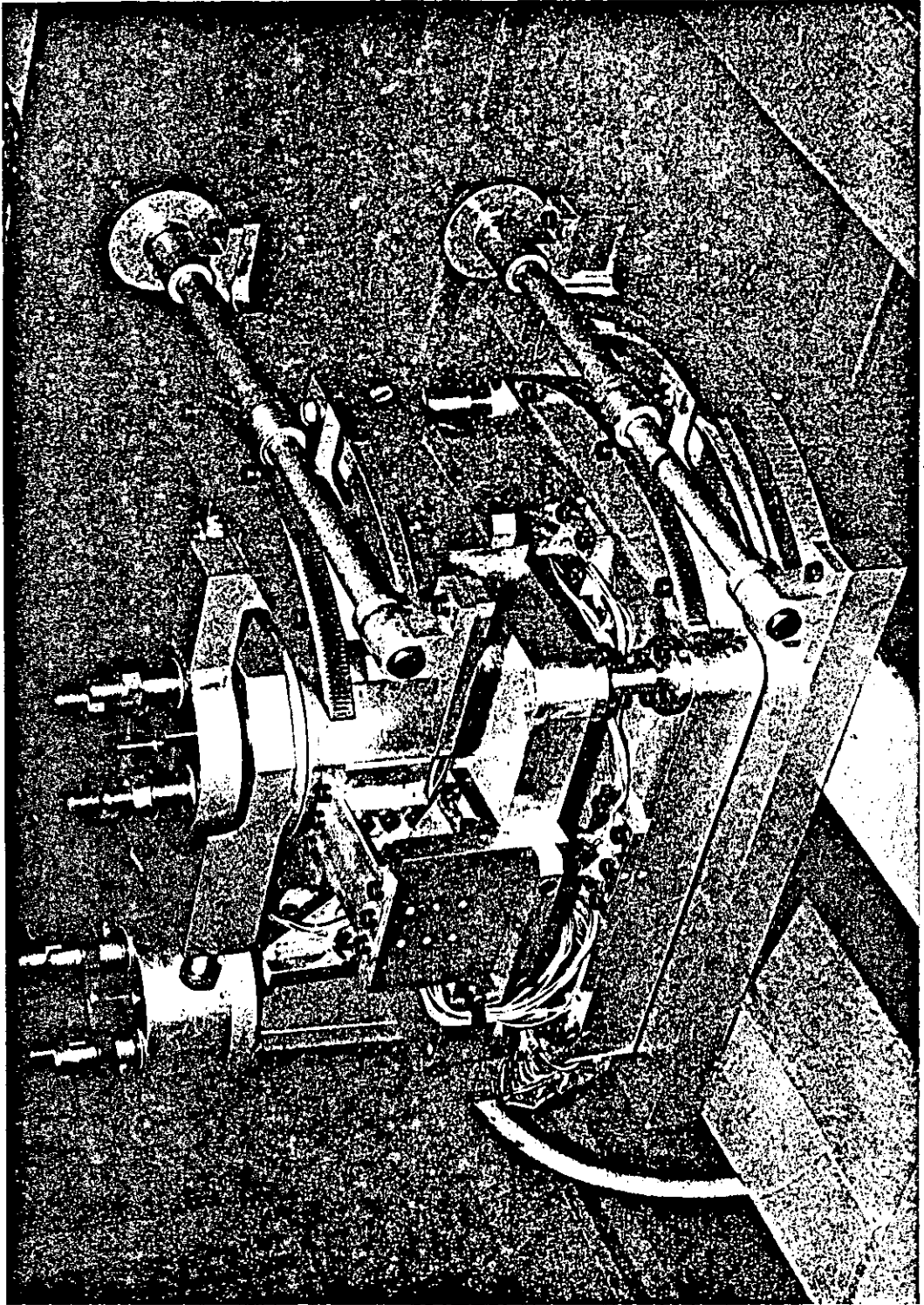


Fig. 8 DYNAMOMETER

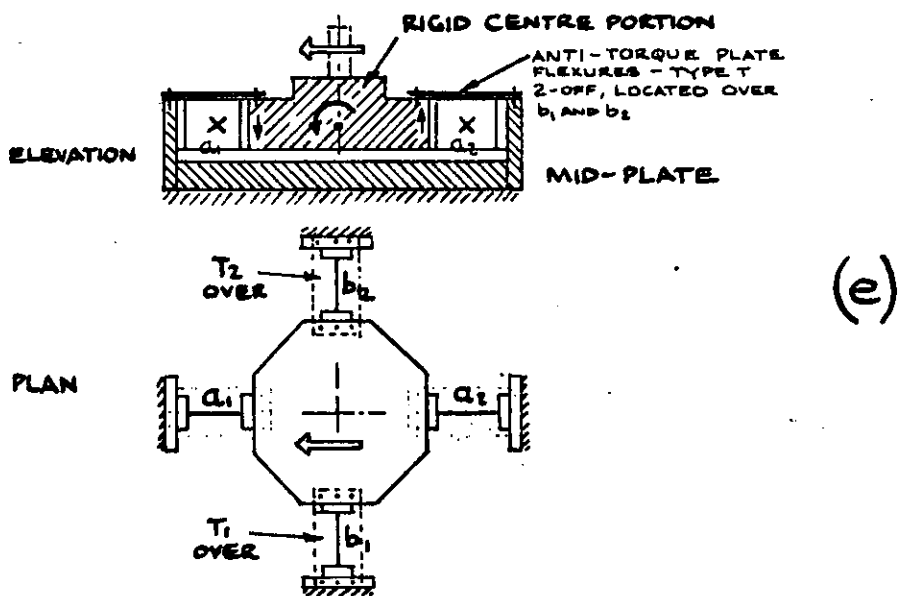
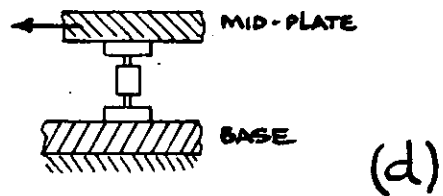
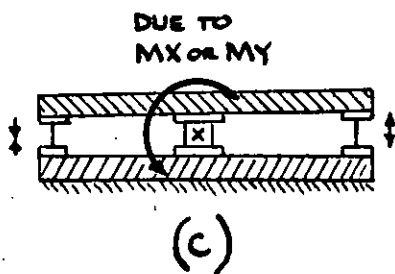
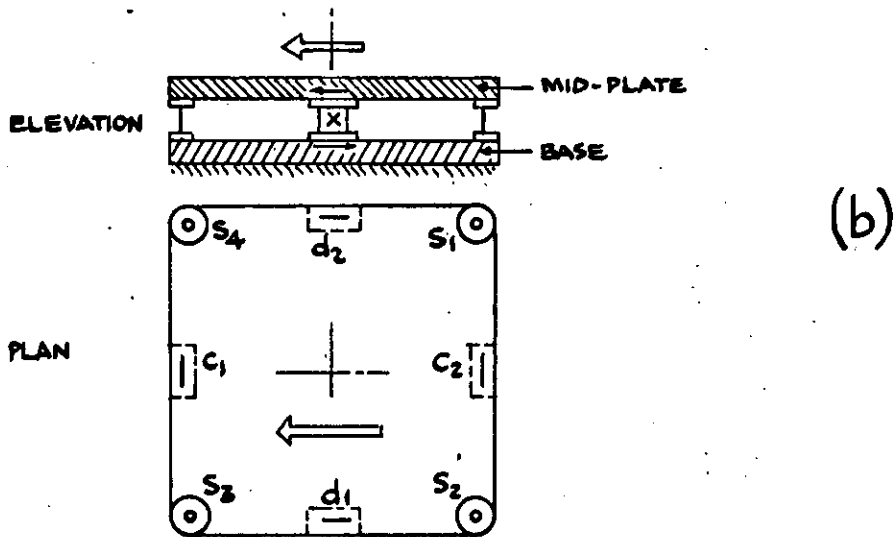
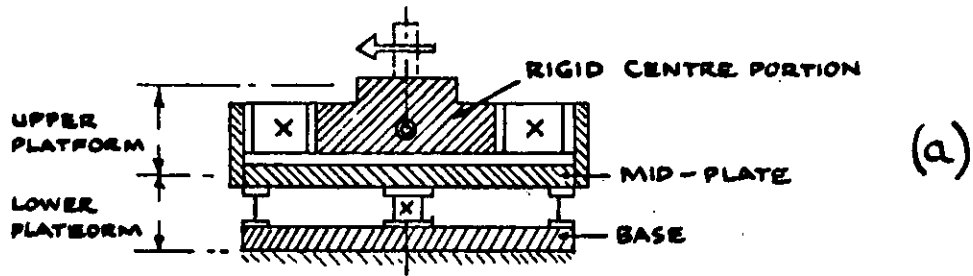


Fig. 9 LAYOUT OF FLEXURES

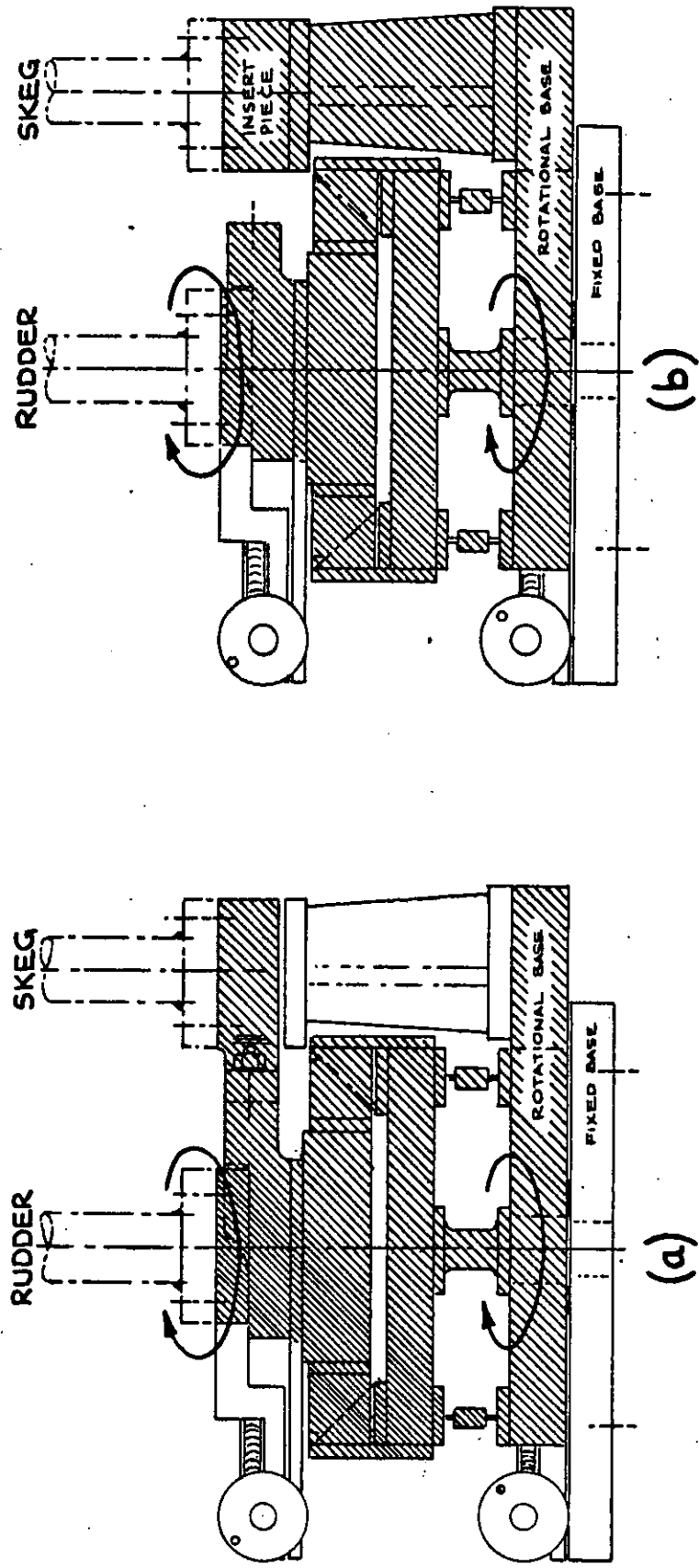
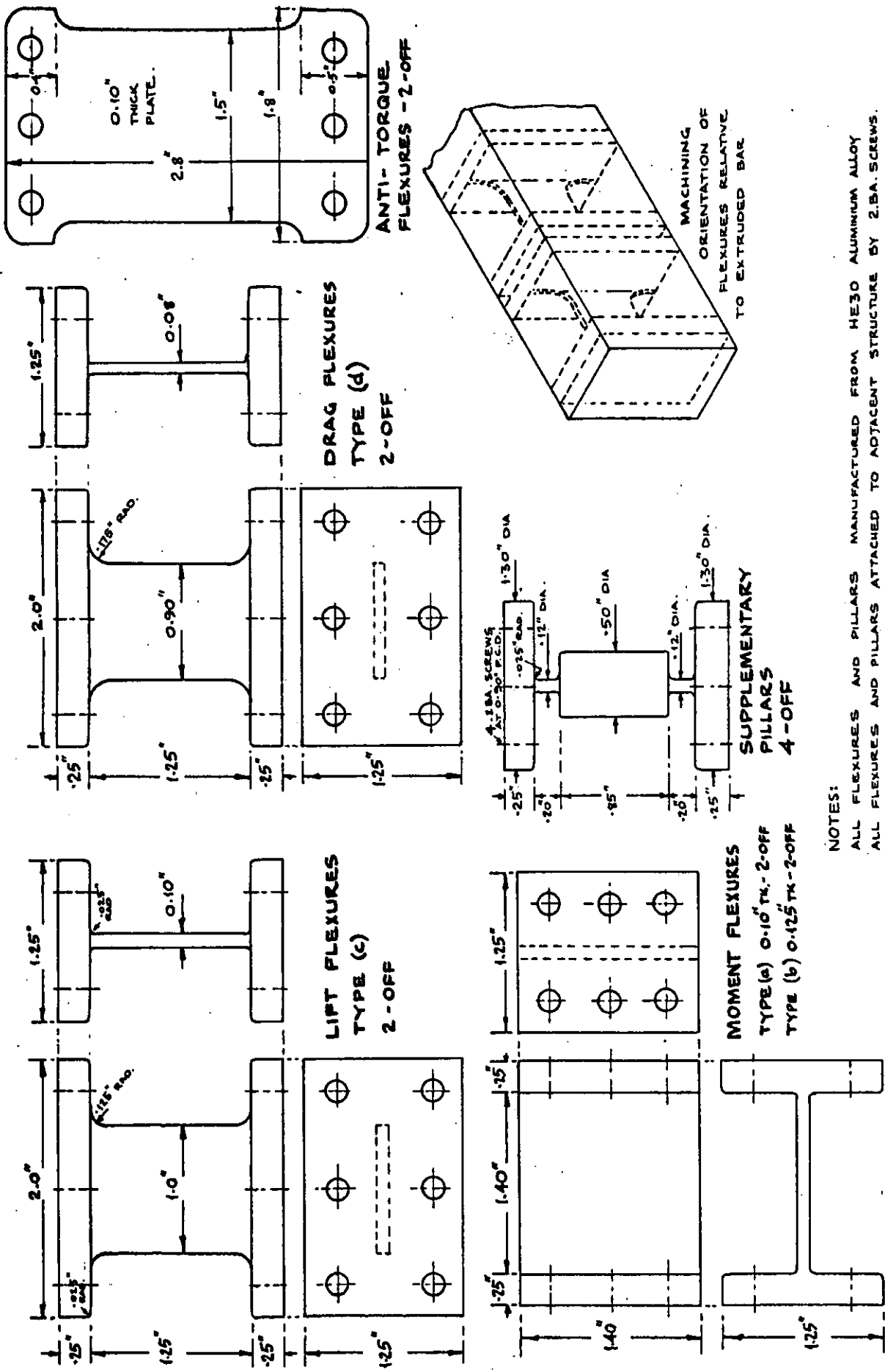


Fig. 10 ALTERNATIVE WORKING ARRANGEMENTS FOR THE DYNAMOMETER



NOTES:  
 ALL FLEXURES AND PILLARS MANUFACTURED FROM HE30 ALUMINUM ALLOY  
 ALL FLEXURES AND PILLARS ATTACHED TO ADJACENT STRUCTURE BY 2.BA. SCREWS.

Fig. 11 PRINCIPAL DIMENSIONS OF FLEXURES AND PILLARS

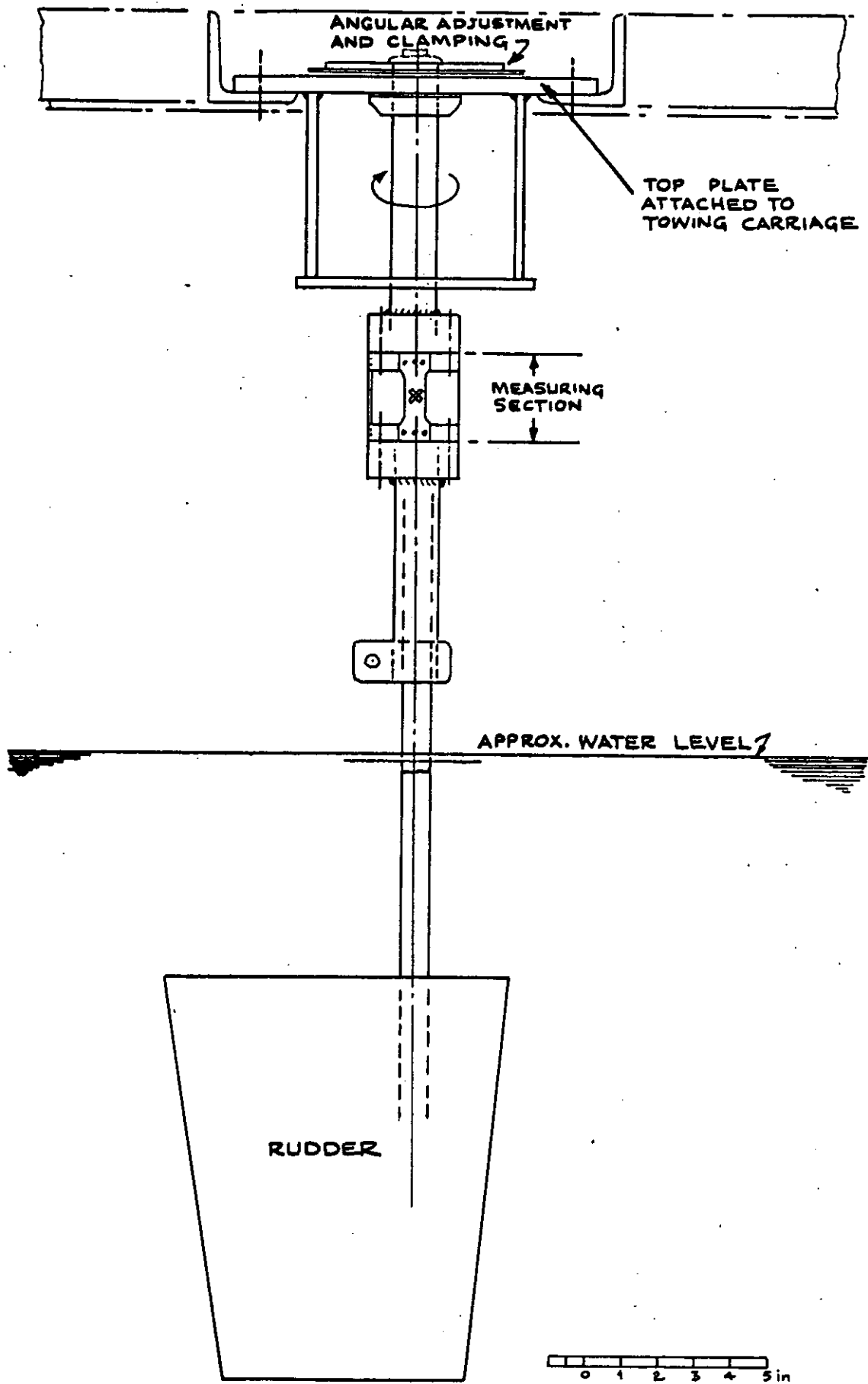


Fig. 12 OUTLINE PARTICULARS OF SMALL THREE-COMPONENT DYNAMOMETER FOR USE IN TEST TANK AT SOUTHAMPTON COLLEGE OF TECHNOLOGY



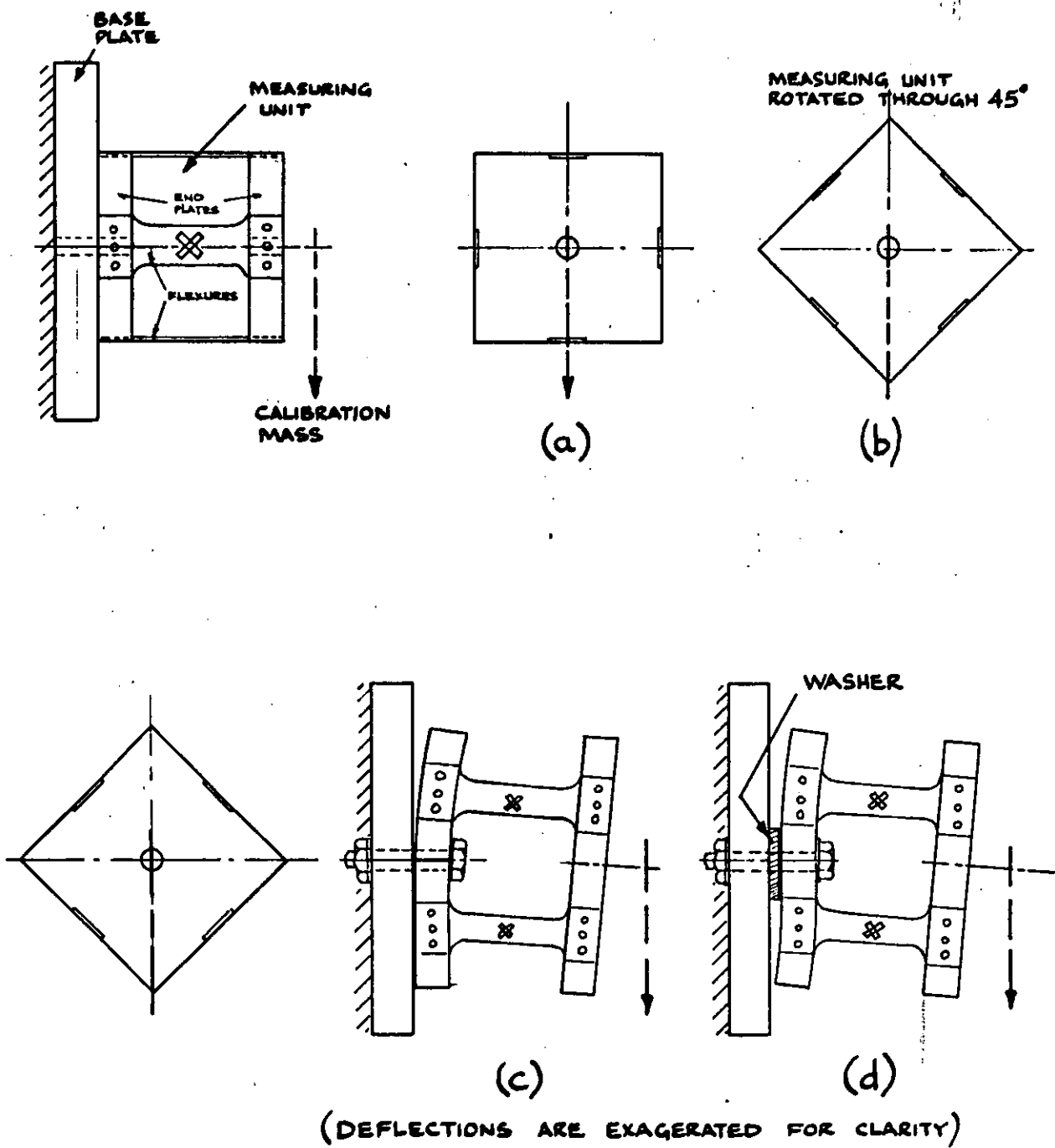
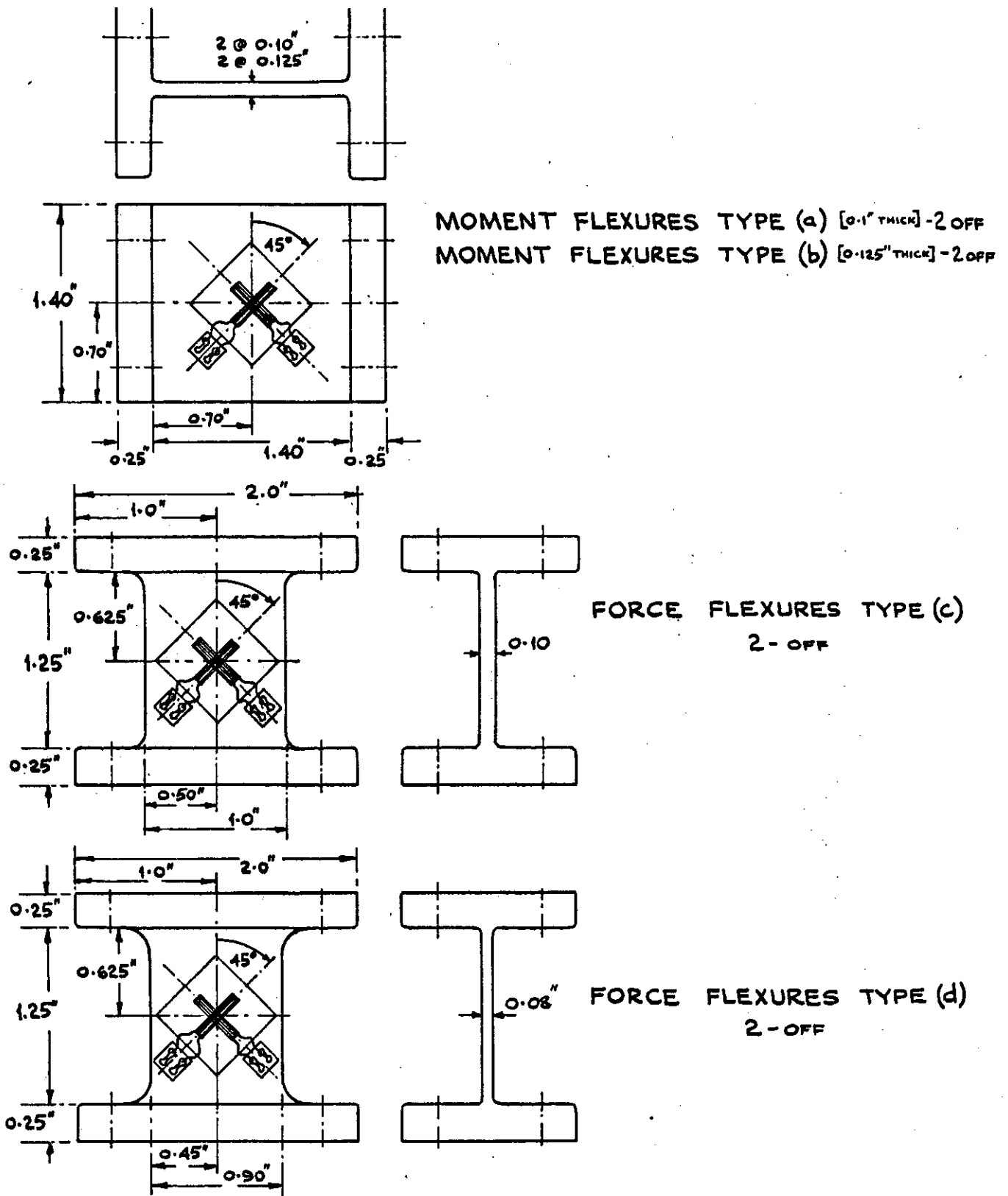


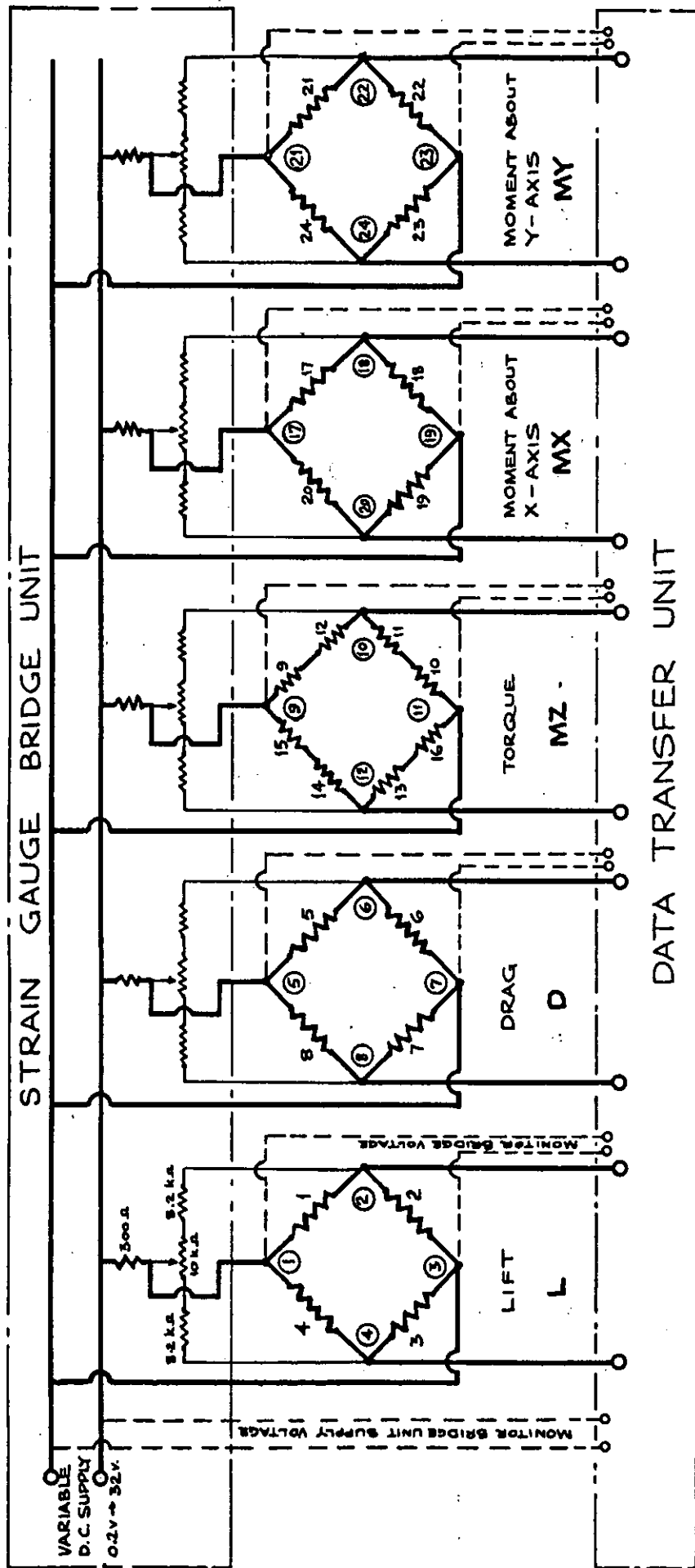
Fig. 13 WARPING OF END PLATE



**NOTES:**

ALL GAUGES : TML TYPE FCA - 10 - 23 , CROSSED FOIL  
GAUGES AND TERMINALS ATTACHED TO EACH SIDE OF EACH FLEXURE.  
SEE Fig.16 FOR LOCATION OF FLEXURE TYPES

**Fig.14 POSITIONS OF STRAIN GAUGES ON FLEXURES**

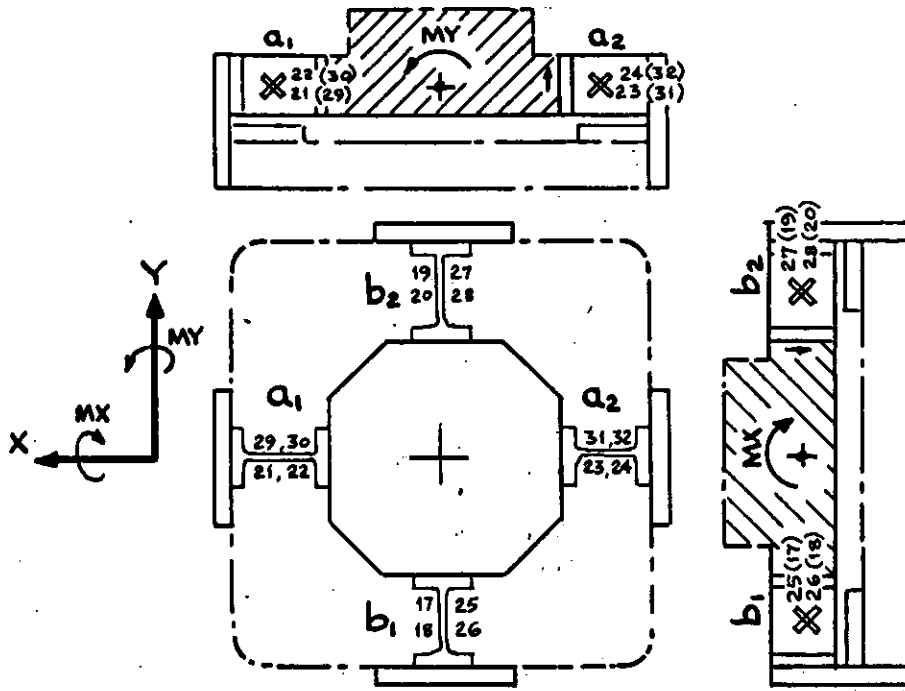


OUTPUT ON DIGITAL VOLTMETER,  
PAPER PRINT OUT OR HIGH  
SPEED PUNCHED TAPE

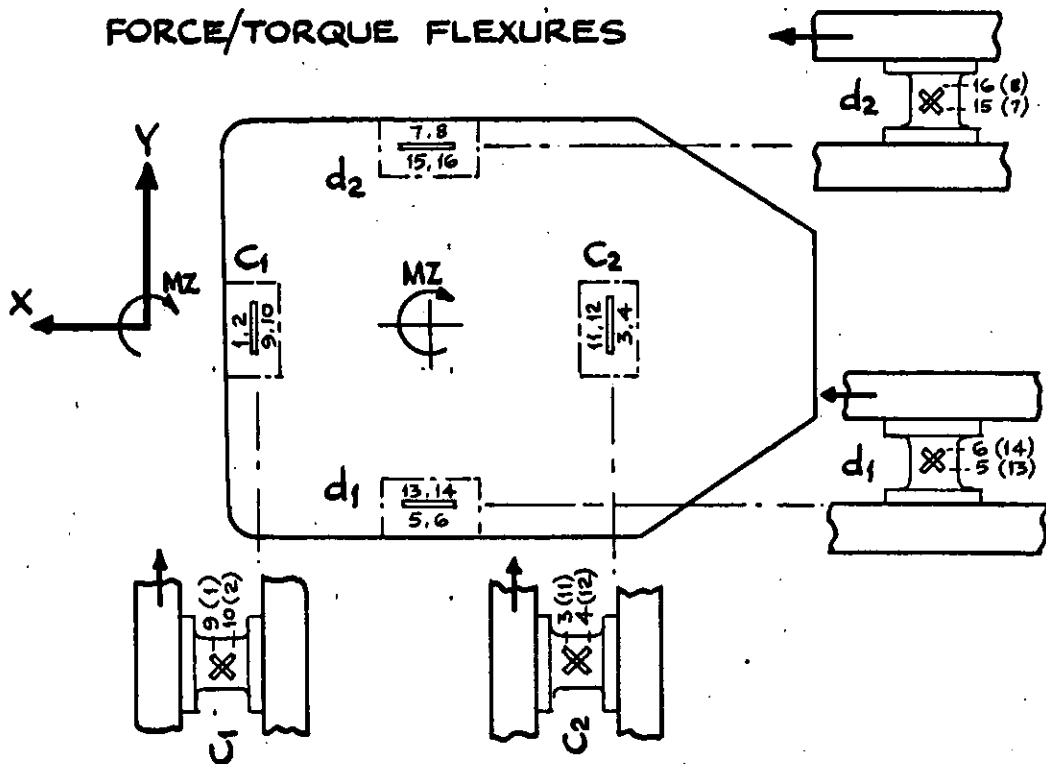
NOTES:  
GAUGES DENOTED AS 1, 2, 3 -----  
BRIDGE TERMINALS DENOTED AS ①, ②, ③ -----  
FOR GAUGE NUMBERING RELATIVE TO FLEXURES SEE KEY DIAGRAMS Fig.16  
( SPARE GAUGES : 25 TO 32  
SPARE BRIDGE TERMINALS : ④ TO ⑩ AND ②⑤ TO ②⑧ )

Fig.15 DIAGRAMMATIC LAYOUT OF STRAIN GAUGE BRIDGE CIRCUITS AND INSTRUMENTATION

**MOMENT FLEXURES**

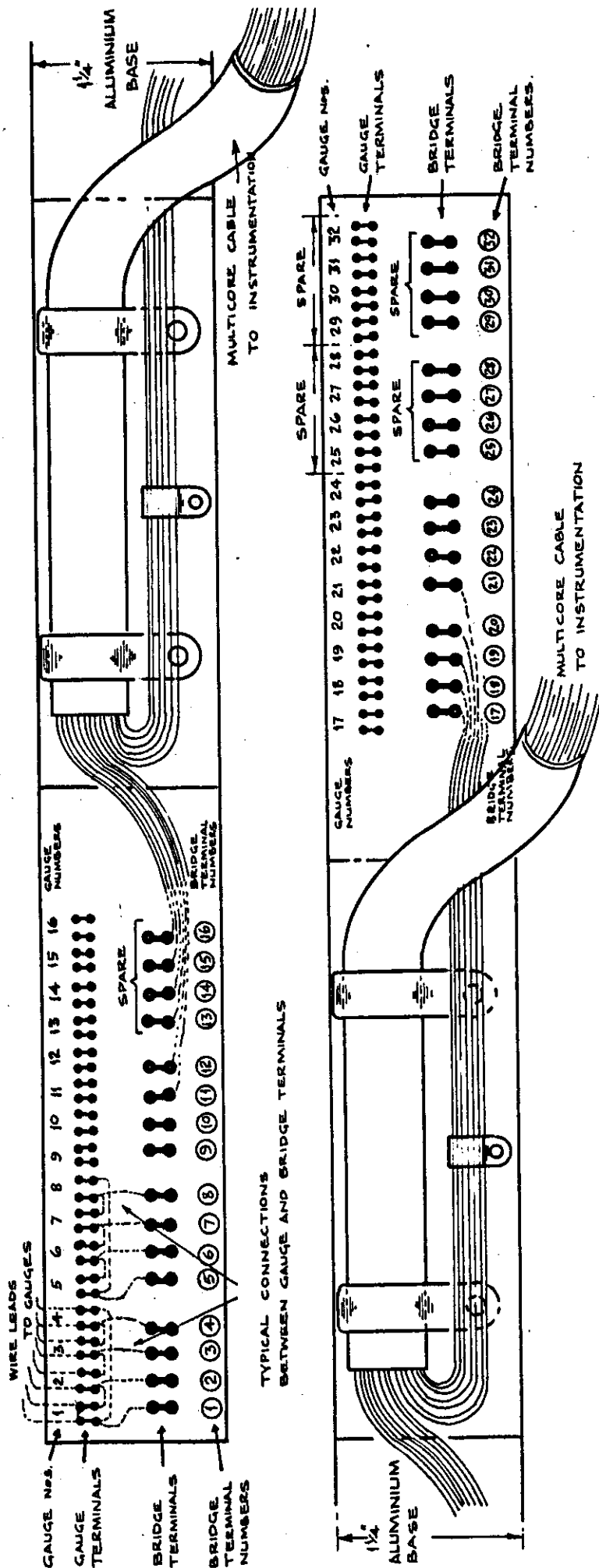


**FORCE/TORQUE FLEXURES**



**NOTES:**  
 FLEXURE REFERENCE LETTERS PER FIG. 11 AND DYNAMOMETER DRAWING  
 SPARE GAUGES : 25 TO 32

**Fig. 16 KEY DIAGRAMS SHOWING GAUGE NUMBERING**



NOTES:  
 GAUGE NUMBERS DENOTED 1, 2, 3, ..... } PER KEY DIAGRAMS, FIG. 16  
 BRIDGE TERMINAL NUMBERS DENOTED ① ② ③ ..... } AND CIRCUIT DIAGRAM, FIG. 15

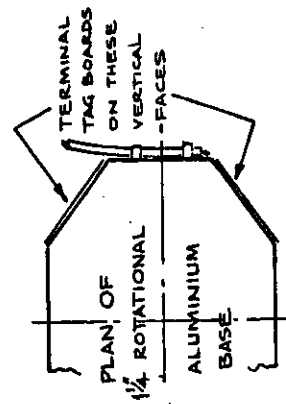


Fig. 17 OUTLINE DETAILS OF TERMINAL TAG BOARDS

BRIDGE CIRCUIT TERMINAL NUMBERS (Ref. Figs. 15 & 17) ON DYNAMOMETER	EQUIVALENT PLUG PIN NUMBERS FOR INSTRUMENTATION CONNECTING PLUG ON MULTI-CORE CABLE	CABLE COLOUR
①	2	BLUE
②	3	GREEN
③	4	YELLOW
④	1	RED
⑤	6	BLACK
⑥	7	BROWN
⑦	8	VIOLET
⑧	5	WHITE
⑨	10	PINK
⑩	11	TURQUOISE
⑪	12	GREY
⑫	9	ORANGE
⑬	22	ORANGE / BLUE
⑭	23	YELLOW / GREEN
⑮	24	WHITE / GREEN
⑯	21	BLUE / BLACK
⑰	14	GREEN / RED
⑱	15	YELLOW / RED
⑲	16	WHITE / RED
⑳	13	RED / BLUE
㉑	18	RED / BROWN
㉒	19	YELLOW / BLUE
㉓	20	WHITE / BLUE
㉔	17	RED / BLACK
㉕	26	GREEN / BLUE
㉖	27	GREY / BLUE
㉗	28	GREEN / BLACK
㉘	25	ORANGE / GREEN
㉙	30	YELLOW / BROWN
㉚	31	WHITE / BROWN
㉛	32	BROWN / BLACK
㉜	29	GREY / GREEN
		YELLOW / VIOLET
		GREY / BROWN
		VIOLET / BLACK
		WHITE / VIOLET

**Fig. 18**  
**TABLE SHOWING RELATIONSHIP**  
**BETWEEN INSTRUMENTATION CONNECTING**  
**PLUG PIN NUMBERS AND DYNAMOMETER BRIDGE TERMINAL NUMBERS**

DATA TRANSFER UNIT CHANNEL NUMBER	POLARITY	CABLE COLOUR	CABLE REFERENCE NUMBER	FUNCTION
0	+	BROWN	0	BRIDGE OUTPUTS
	-	RED		
1	+	ORANGE	1	
	-	YELLOW		
2	+	GREEN	2	
	-	BLUE		
3	+	MAUVE	3	
	-	WHITE		
4	+	BLACK	4	
	-	BROWN		
5	+	MAUVE	③	BRIDGE SUPPLY VOLTAGE MONITORING
	-	WHITE	①	
6	+	GREY	⑦	
	-	YELLOW	⑤	
7	+	BLUE	⑪	
	-	RED	⑨	
8	+	PINK	⑲	
	-	BLACK	⑰	
9	+	ORANGE	⑳	
	-	GREEN	㉑	

Fig.19 TABLE SHOWING POLARITIES OF CABLE CONNECTIONS BETWEEN BRIDGE UNIT AND DATA TRANSFER UNIT





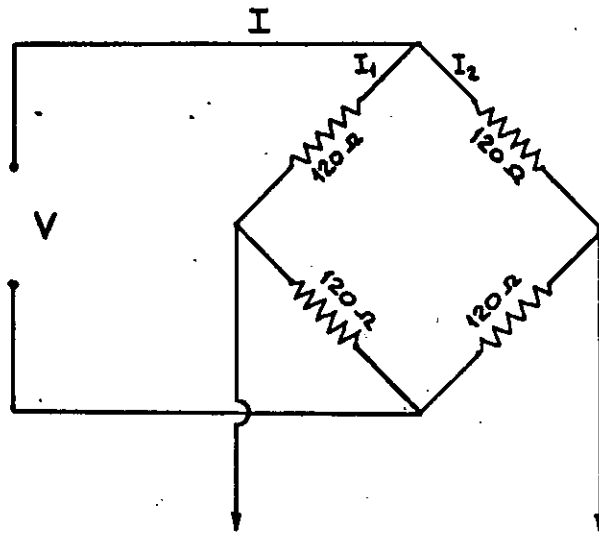


Fig. 21

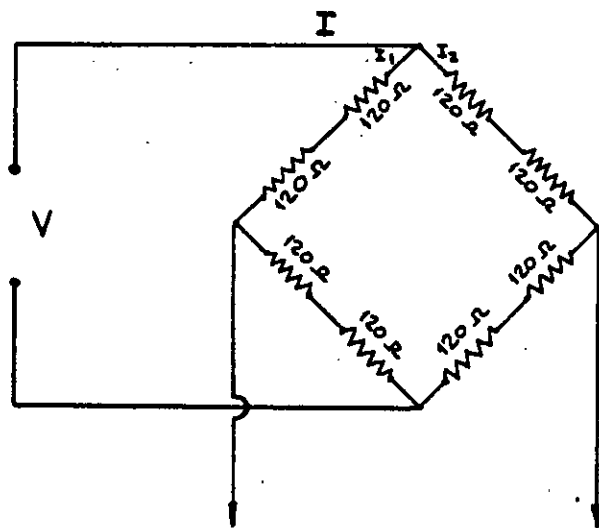


Fig. 22

LOADING OF INDIVIDUAL COMPONENTS FOR DERIVATION OF FIRST ORDER INTERACTIONS	LOADING OF COMPONENTS IN PAIRS FOR DERIVATION OF SECOND ORDER INTERACTIONS
L	L + D
D	L + MZ
MZ	L + MX
MX	L + MY
MY	D + MZ
	D + MX
	D + MY
	MZ + MX
	MZ + MY
	MX + MY

WHERE:

L .... LIFT

D .... DRAG

MZ ... TORQUE

MX ... MOMENT ABOUT X-AXIS

MY ... MOMENT ABOUT Y-AXIS

Fig.23 LOADINGS FOR DERIVATION OF INTERACTIONS

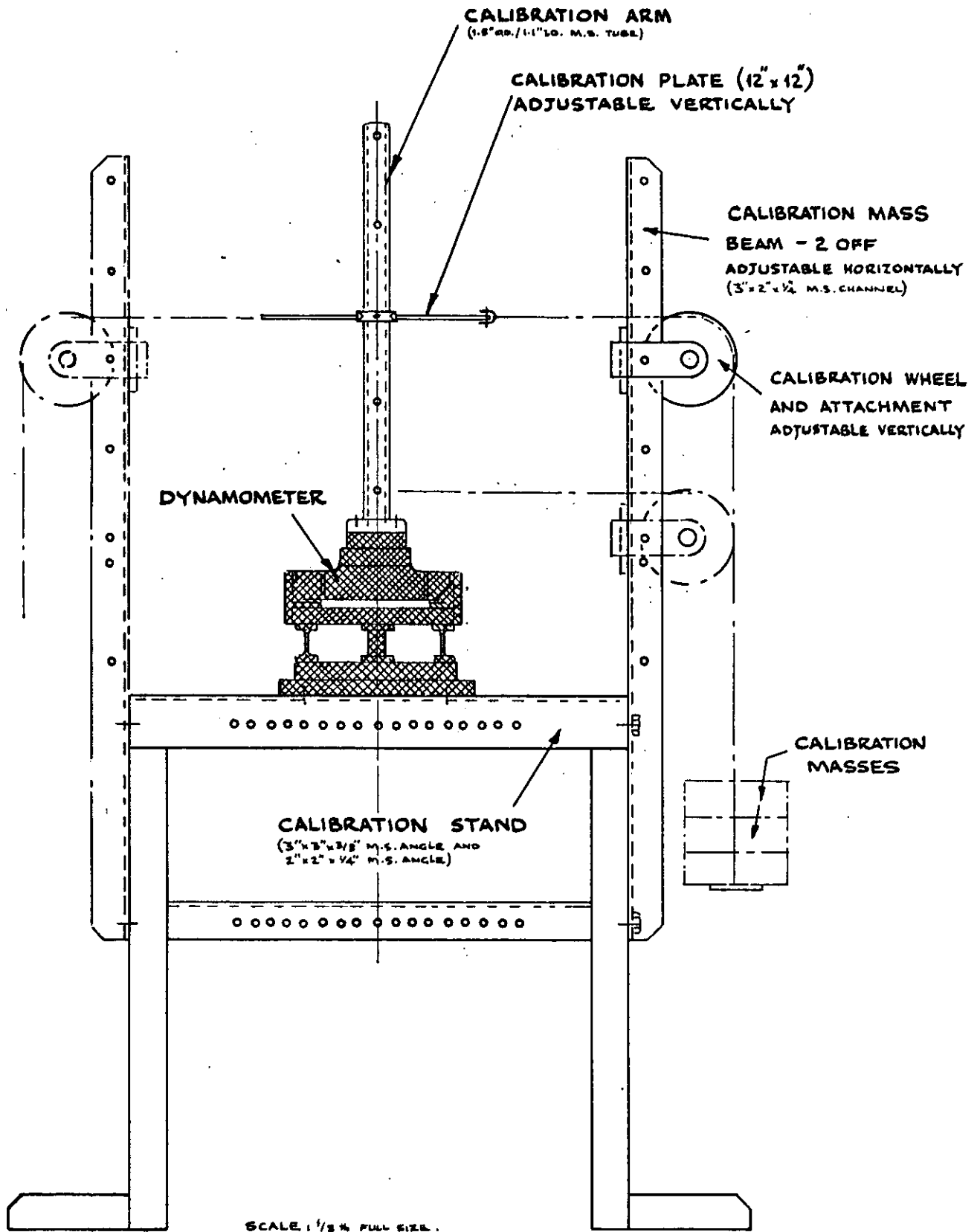


Fig. 24 CALIBRATION RIG

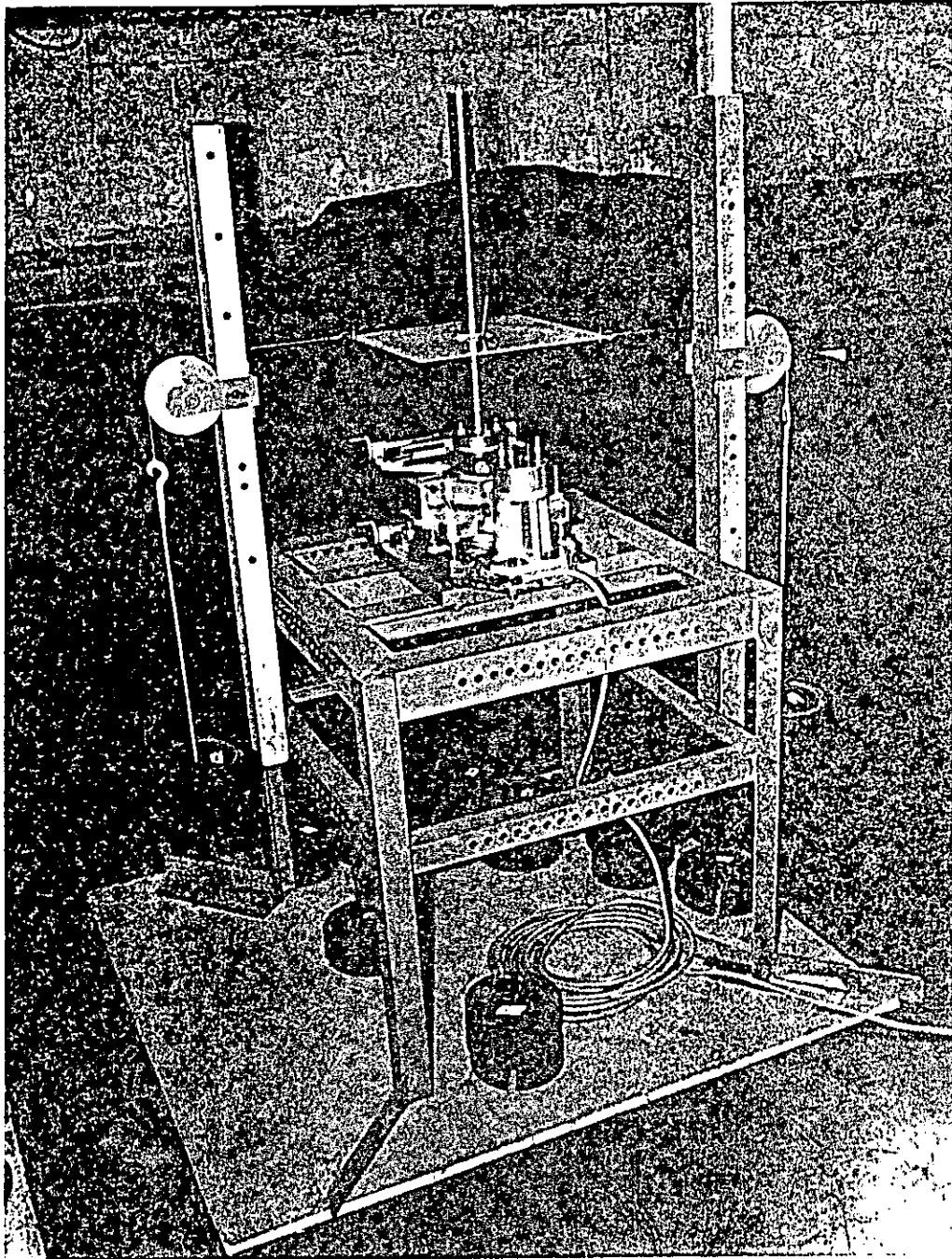


Fig. 25 CALIBRATION RIG

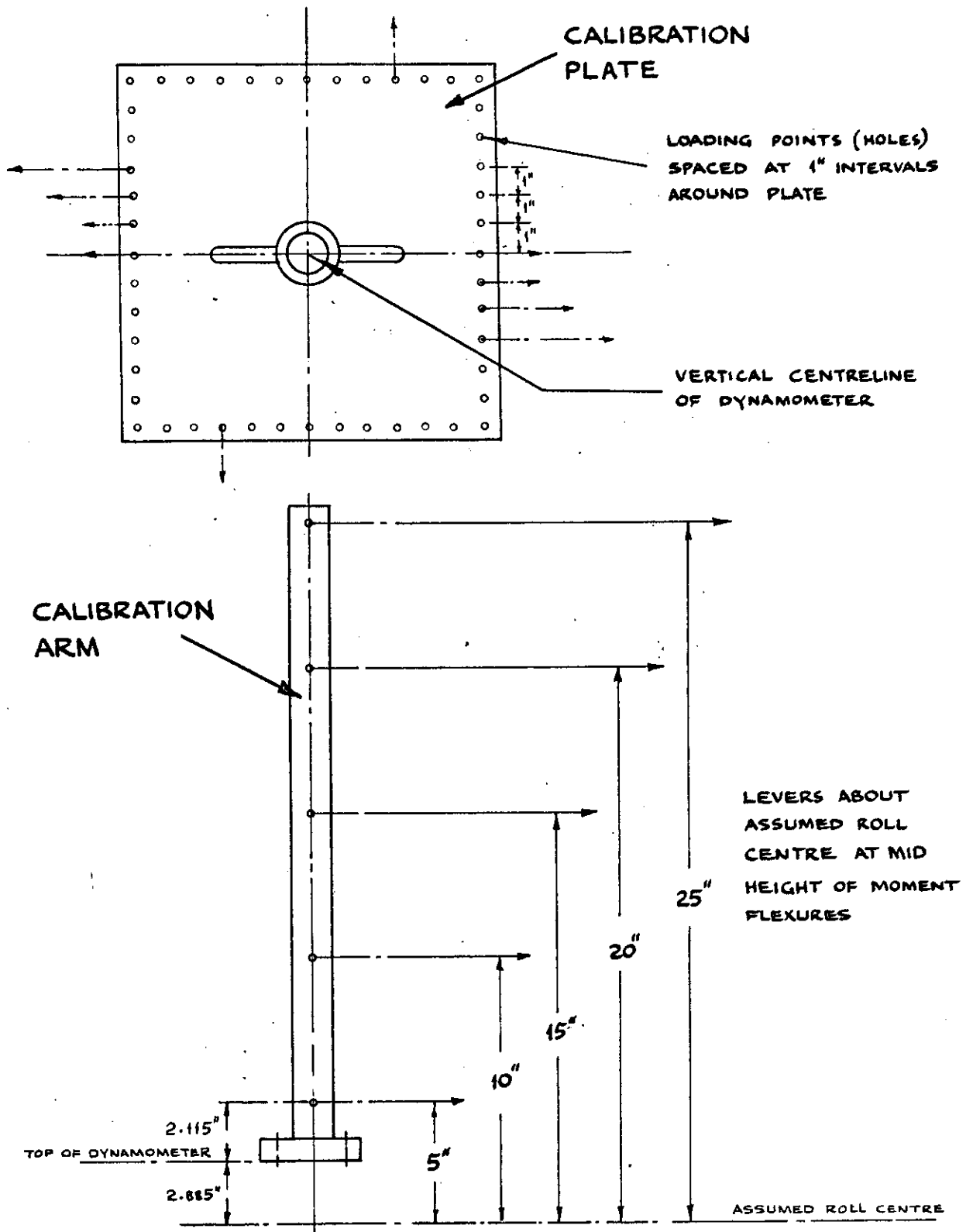


Fig. 26 POSITIONS OF LOADING POINTS ON CALIBRATION PLATE AND CALIBRATION ARM

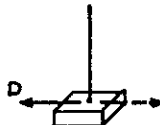

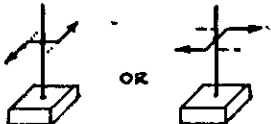
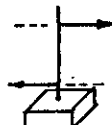
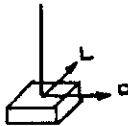

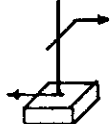

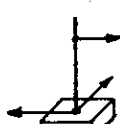
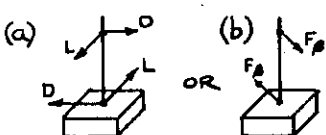

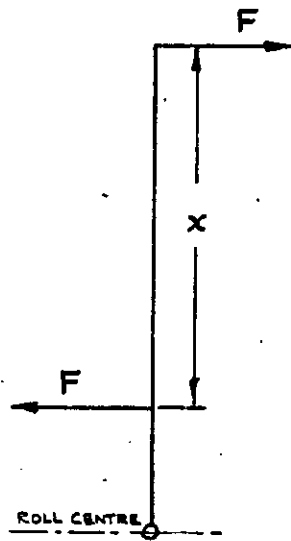
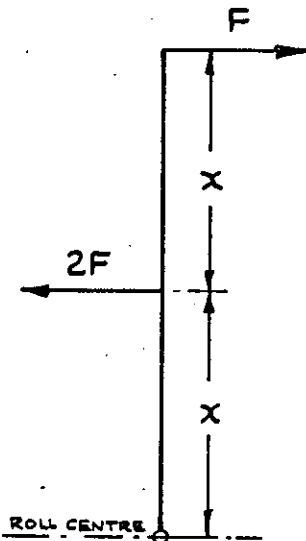
	KEY DIAGRAMS	COMPONENTS	REMARKS
APPLICATION OF SINGLE COMPONENTS		$\pm D$	-
		$\pm L$	-
		$\pm MZ$	NOTE APPLICATION OF COUPLE TO ELIMINATE MX OR MY
		$\pm MX$ $\pm MY$	NOTE EQUAL AND OPPOSITE OFFSET LOAD REQUIRED TO ELIMINATE L OR D
APPLICATION OF COMBINATIONS OF COMPONENTS IN PAIRS		$L + D$	-
		$D + MY,$ $L + MX$	-
		$MZ + MX,$ $MZ + MY$	NOTE EQUAL AND OPPOSITE OFFSET LOAD REQUIRED TO ELIMINATE L OR D
		$MZ + D,$ $MZ + L$	NOTE APPLICATION OF COUPLE TO ELIMINATE MX OR MY, EXTRA PULLEY REQUIRED TO APPLY L OR D SEPARATELY
		$MX + D,$ $MY + L$	EXTRA PULLEY REQUIRED TO APPLY L OR D SEPARATELY
		$MX + MY$	(a) TWO EXTRA PULLEYS REQUIRED TO APPLY LOWER OFFSET LOADS. ALTERNATIVELY, (b) DYNAMOMETER ROTATED IN RIG WHEREBY D AND L ELIMINATED, AND MX AND MY OBTAINED BY RESOLUTION OF MOMENT AT $\beta$
APPLICATION OF ALL FIVE COMPONENTS		$L, D,$ $MZ, MX,$ $MY$	DYNAMOMETER ROTATED IN RIG WHEREBY SUITABLE SINGLE POINT LOAD WILL APPLY ALL FIVE COMPONENTS

Fig.27 KEY DIAGRAMS SHOWING APPLICATIONS OF VARIOUS LOADS AND THEIR COMBINATIONS



(a) MOMENT =  $F \times x$   
 FORCE =  $F - F = 0$



(b) MOMENT =  $2F \times x - F \times 2x = 0$   
 FORCE =  $2F - F = F$

Fig. 28

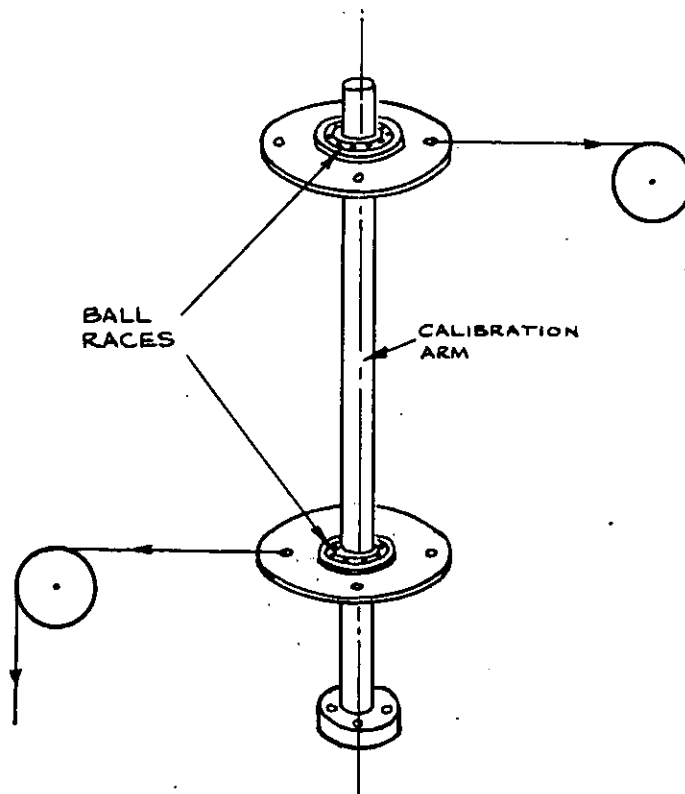


Fig. 29

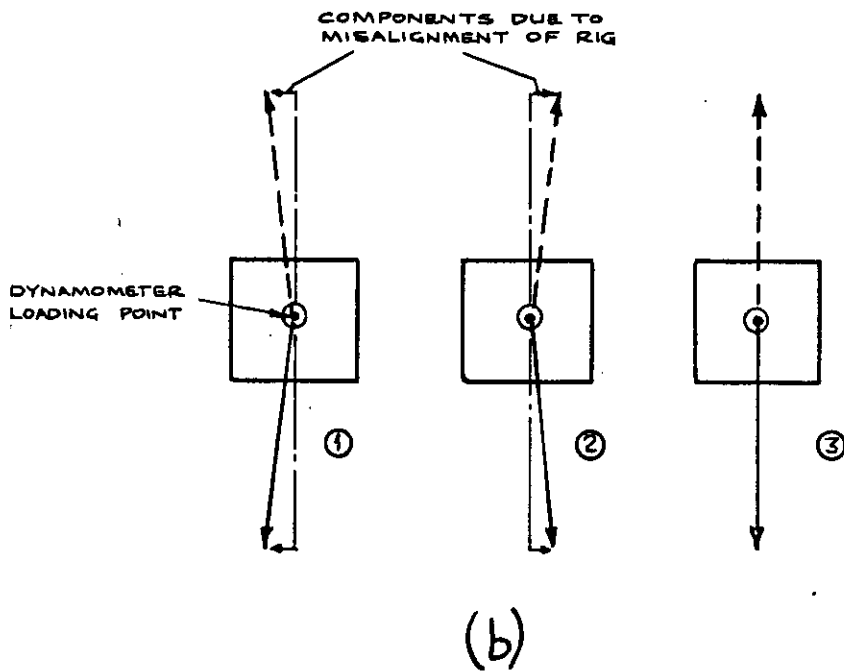
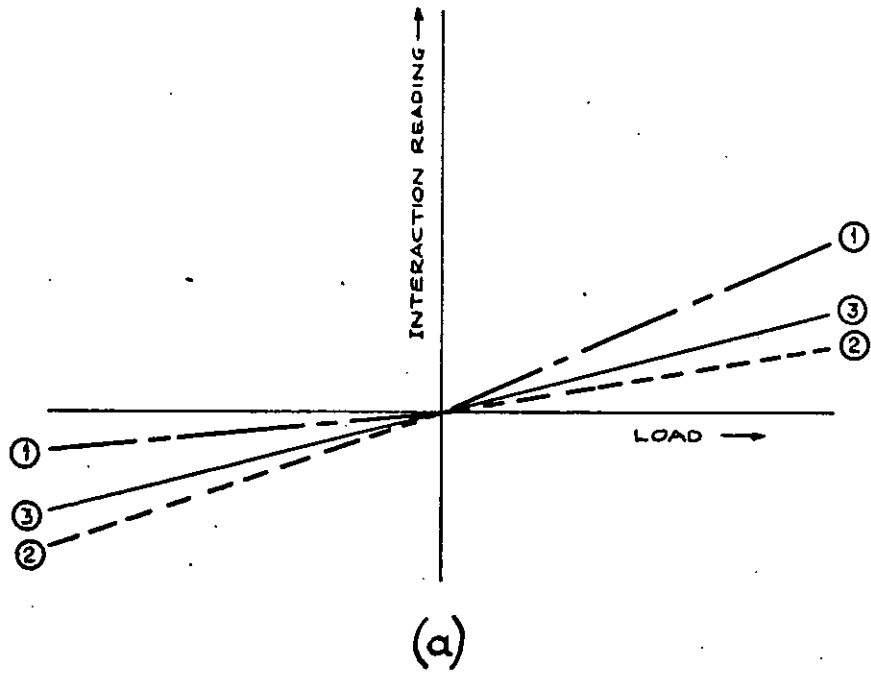


Fig. 30



DYNAMOMETER				SKEG - CONNECTED TO ROTATIONAL BASE	
	LIFT 180 lbf. x 25 in LEVER TO ROLL CENTRE	DRAG 140 lbf. x 25 in LEVER TO ROLL CENTRE	TORQUE ± 1200 lbf.in	LIFT 40 lbf. x 15 in LEVER TO ROLL CENTRE	DRAG 40 lbf. x 15 in LEVER TO ROLL CENTRE
RELATIVE TO FIXED BASE	0.045 in (1.14 mm)	0.044 in (1.12 mm)	MEAN 0.00013°/lbf.in	0.007 in (0.19 mm)	0.010 in (0.25 mm)
RELATIVE TO ROTATIONAL BASE	0.012 in (0.30 mm)	0.010 in (0.25 mm)	—	0.003 in (0.08 mm)	0.005 in (0.13 mm)

Fig. 31 DEFLECTIONS OF DYNAMOMETER 5in ABOVE  
ROLL CENTRE FOR MAXIMUM LOADINGS

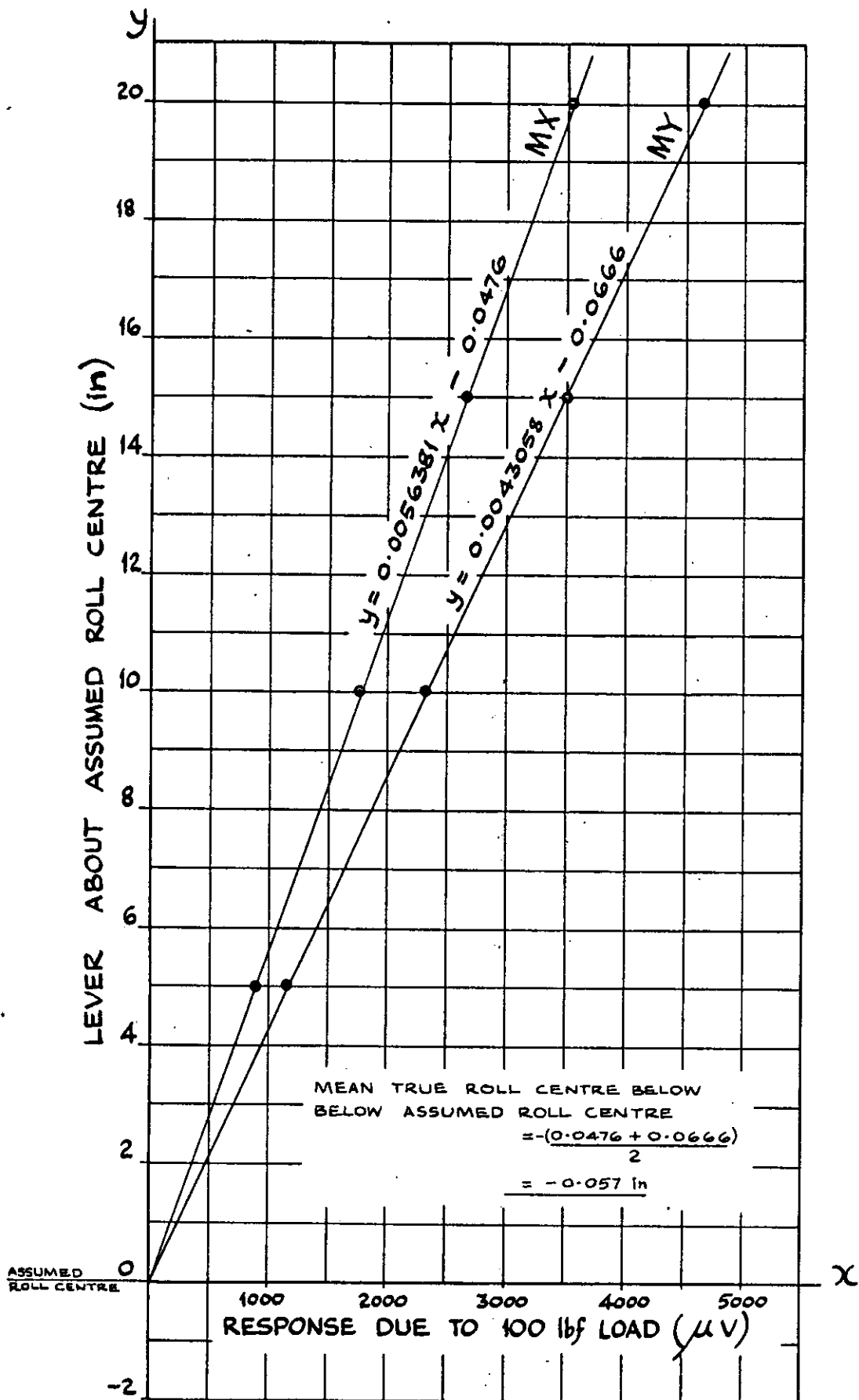


Fig. 32 DERIVATION OF TRUE ROLL CENTRE;  
 CROSS PLOTS OF RESPONSE DUE TO 100 lbf. LOAD  
 APPLIED AT VARYING LEVERS IN X AND Y DIRECTIONS.

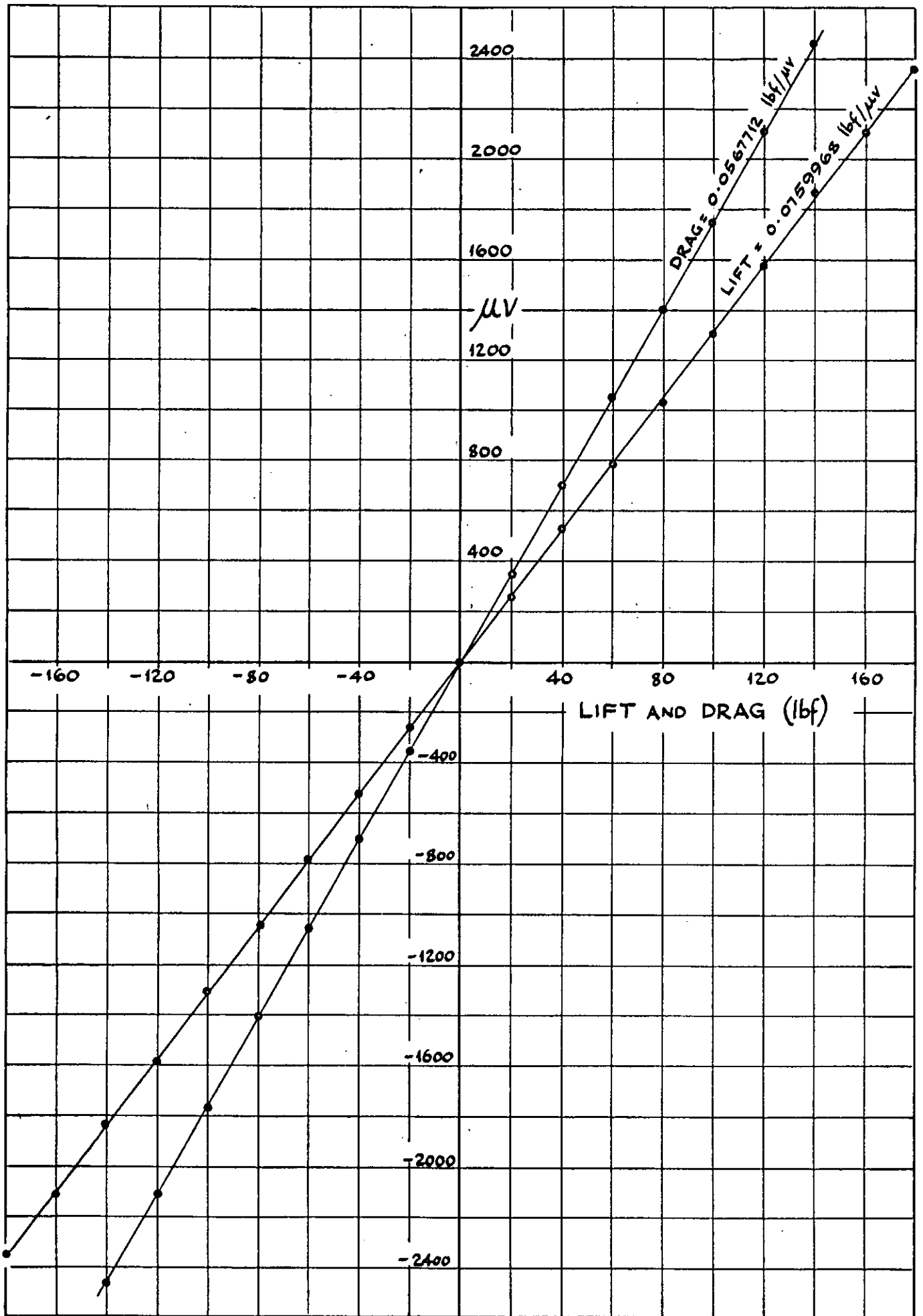


Fig. 33 LIFT AND DRAG CALIBRATION

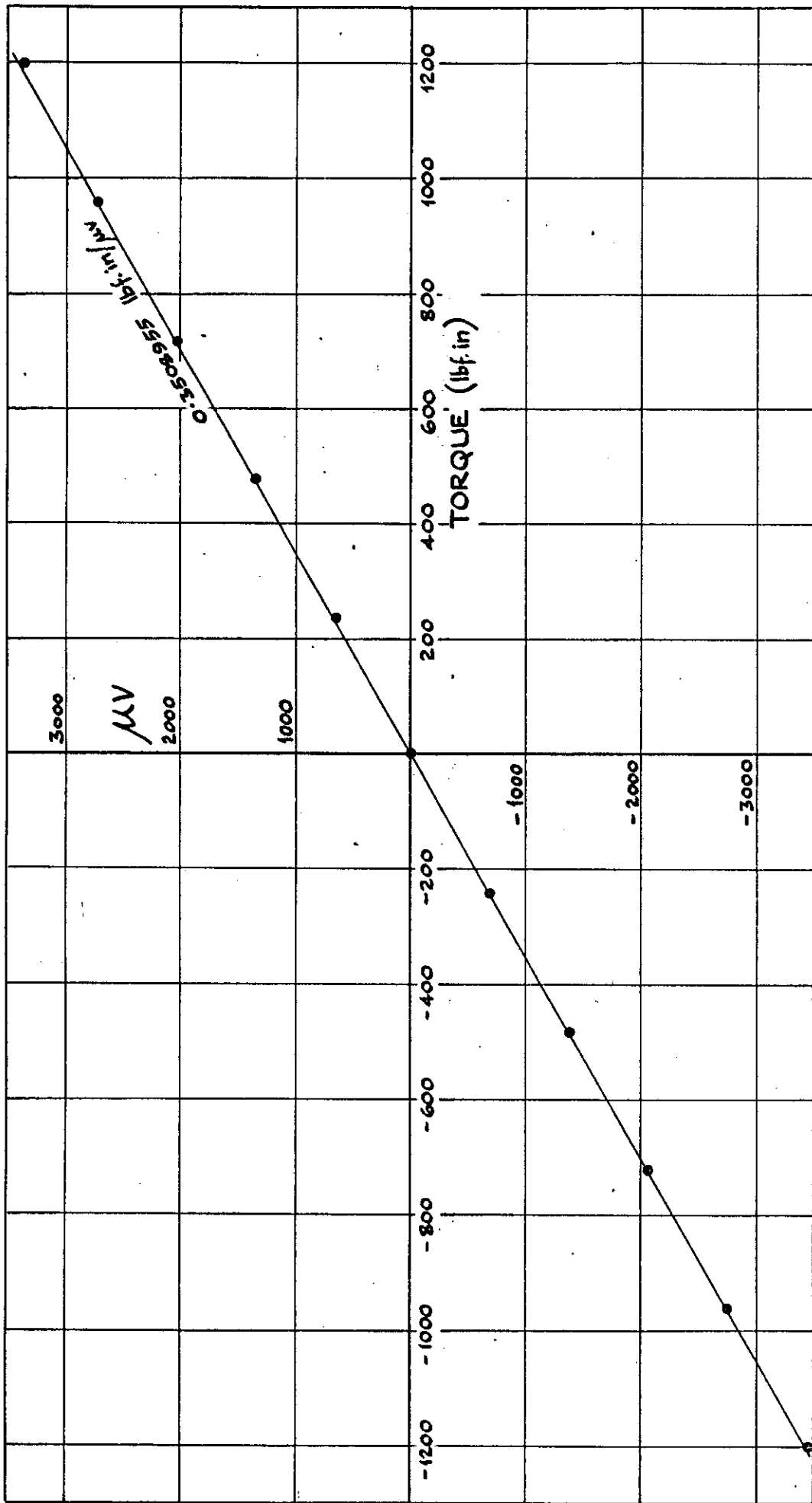


Fig. 34 TORQUE CALIBRATION

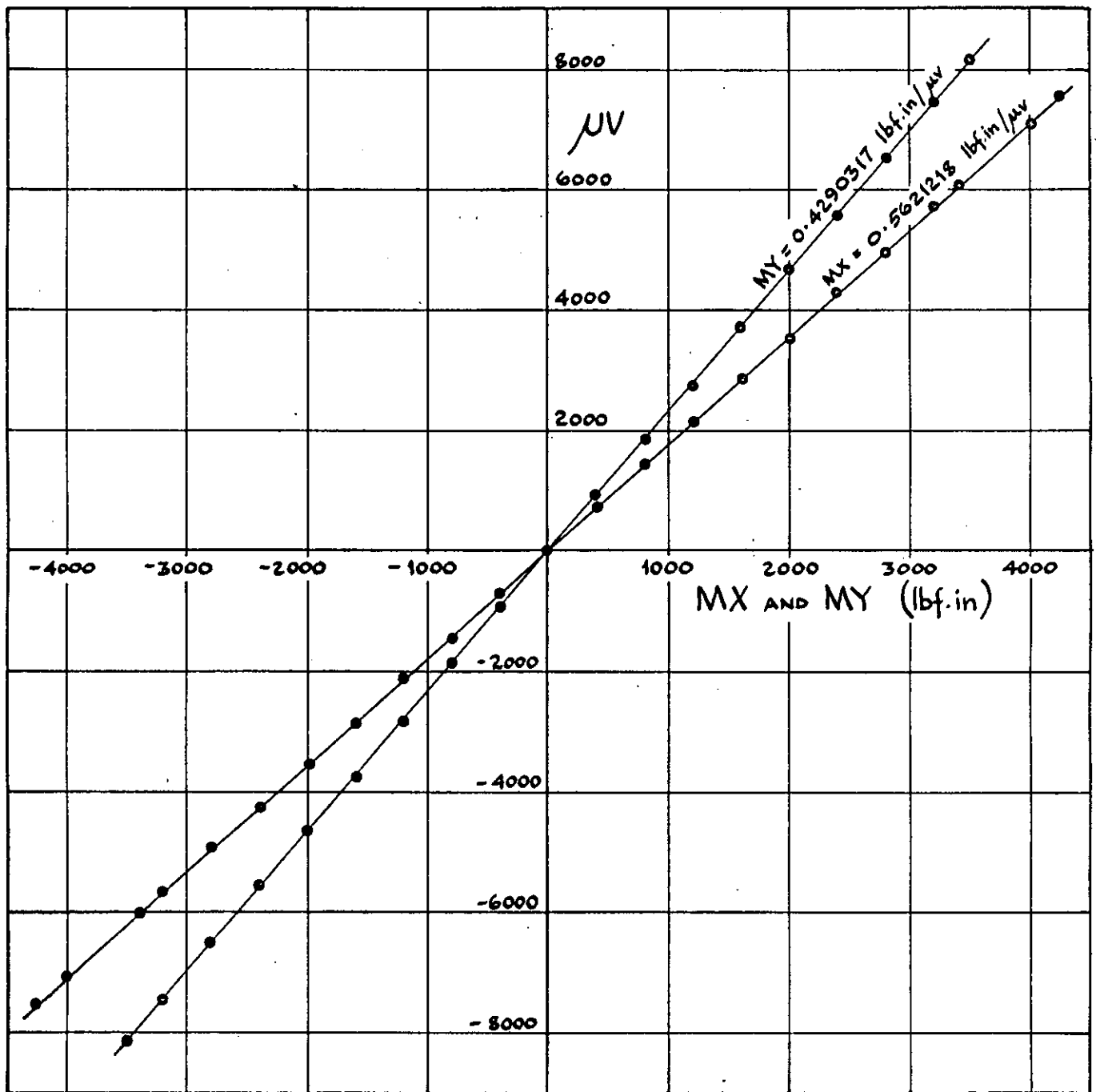


Fig. 35 MX AND MY CALIBRATION

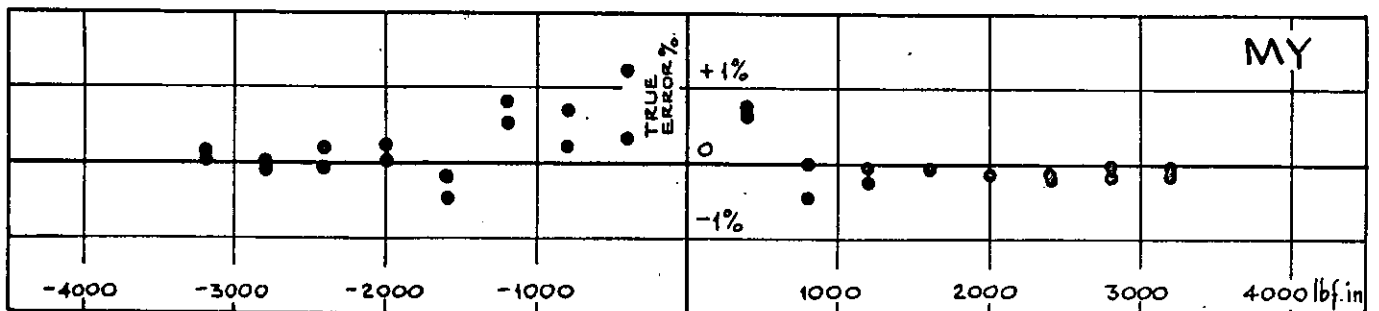
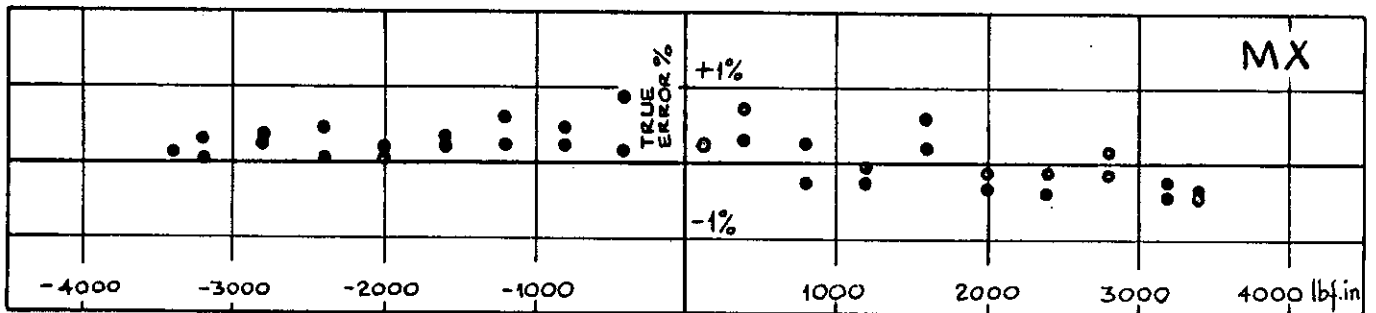
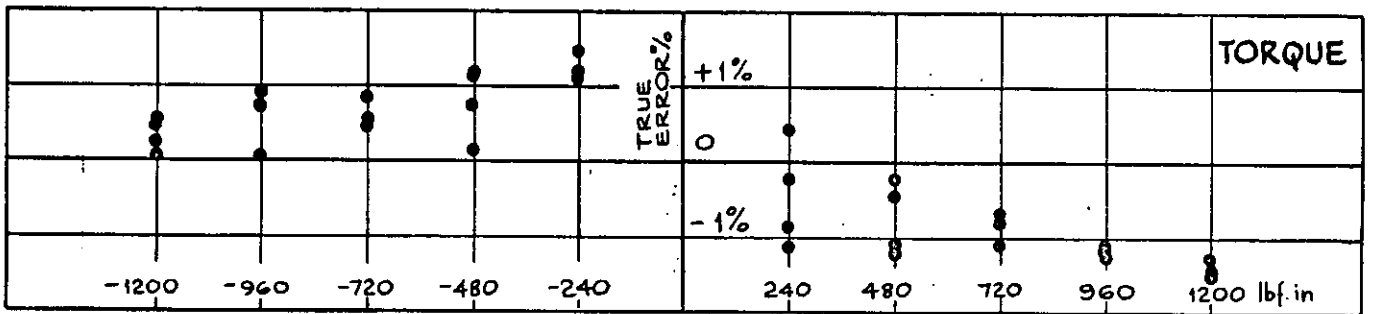
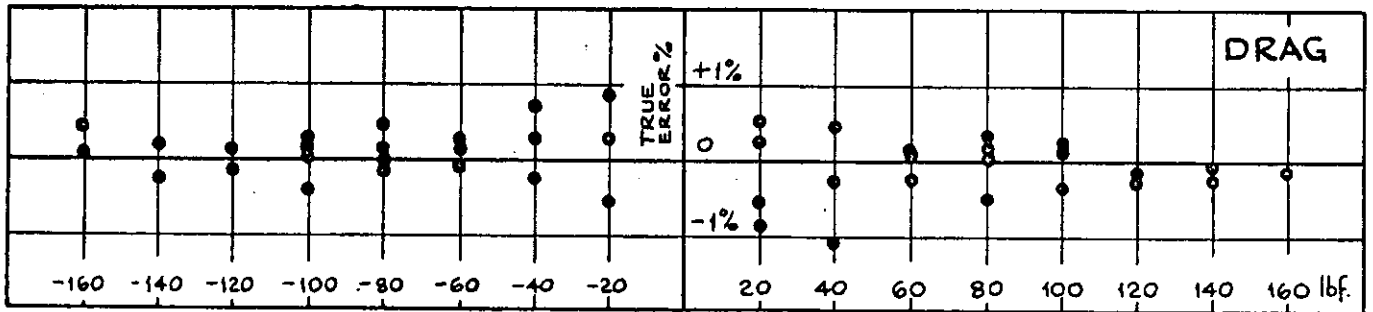
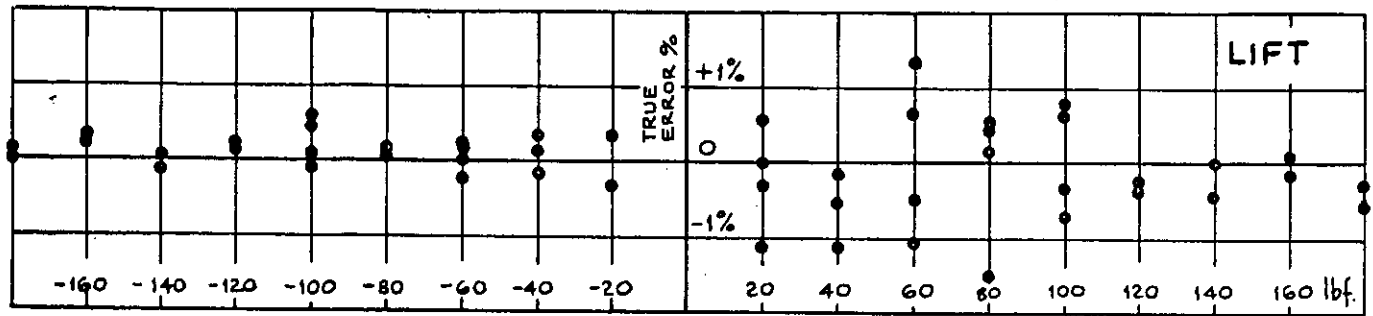


Fig. 36 TRUE ERRORS IN MEASURED DATA FOR EACH COMPONENT COMPARED WITH REGRESSION LINES

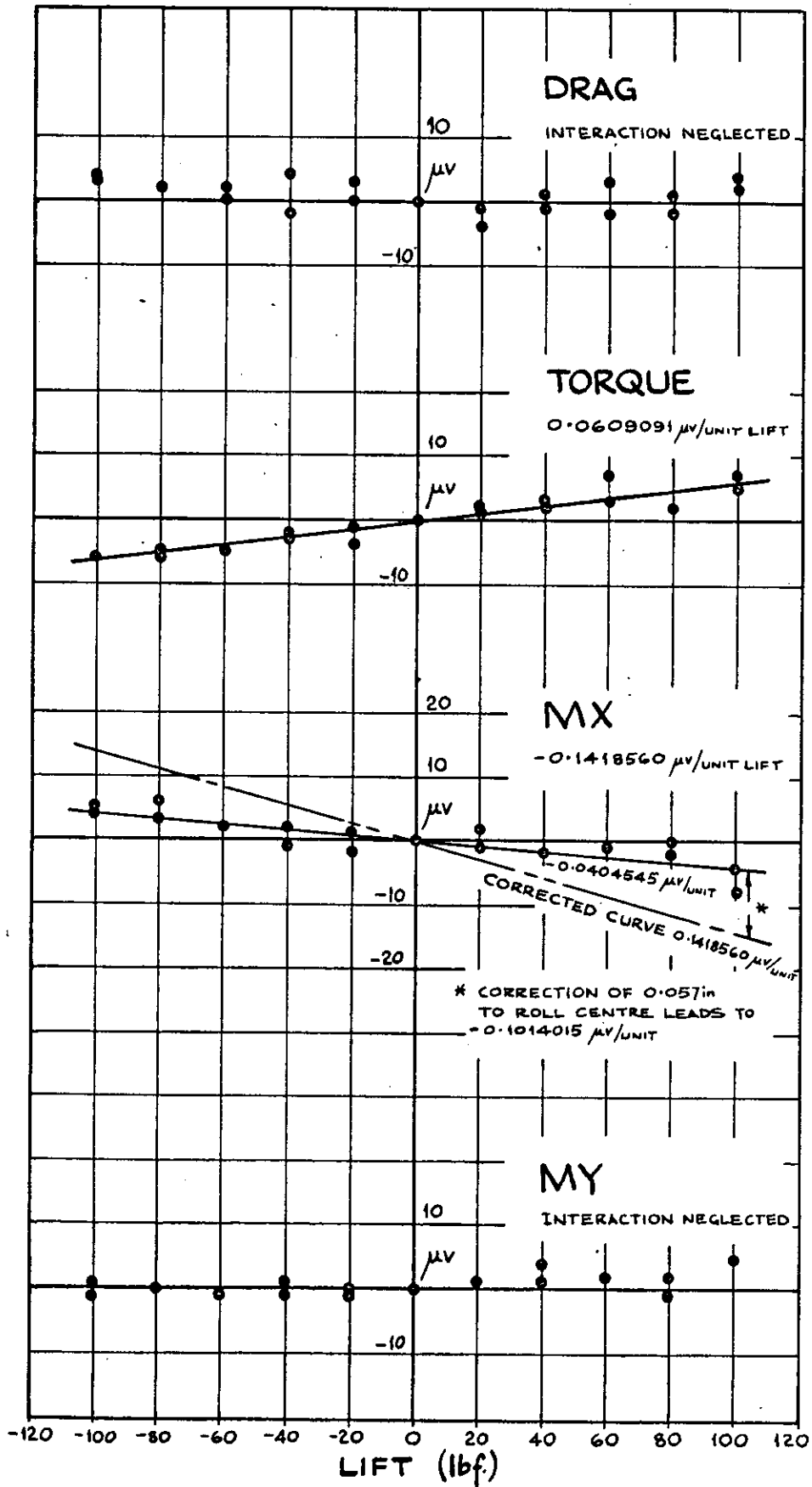


Fig. 37 INTERACTIONS CAUSED BY LIFT CALIBRATION DATA AND MEAN CURVES

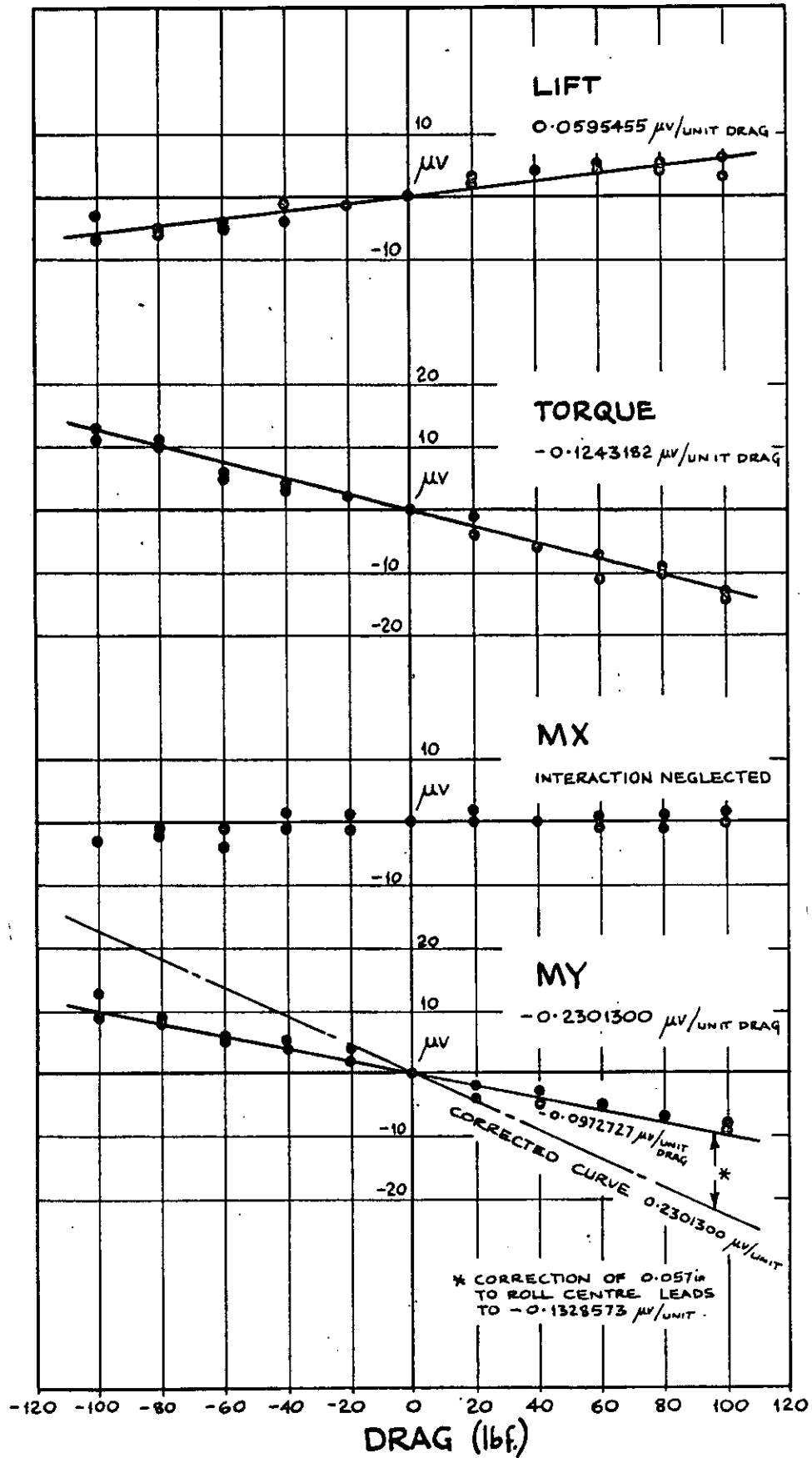


Fig. 38 INTERACTIONS CAUSED BY DRAG  
 CALIBRATION DATA AND MEAN CURVES



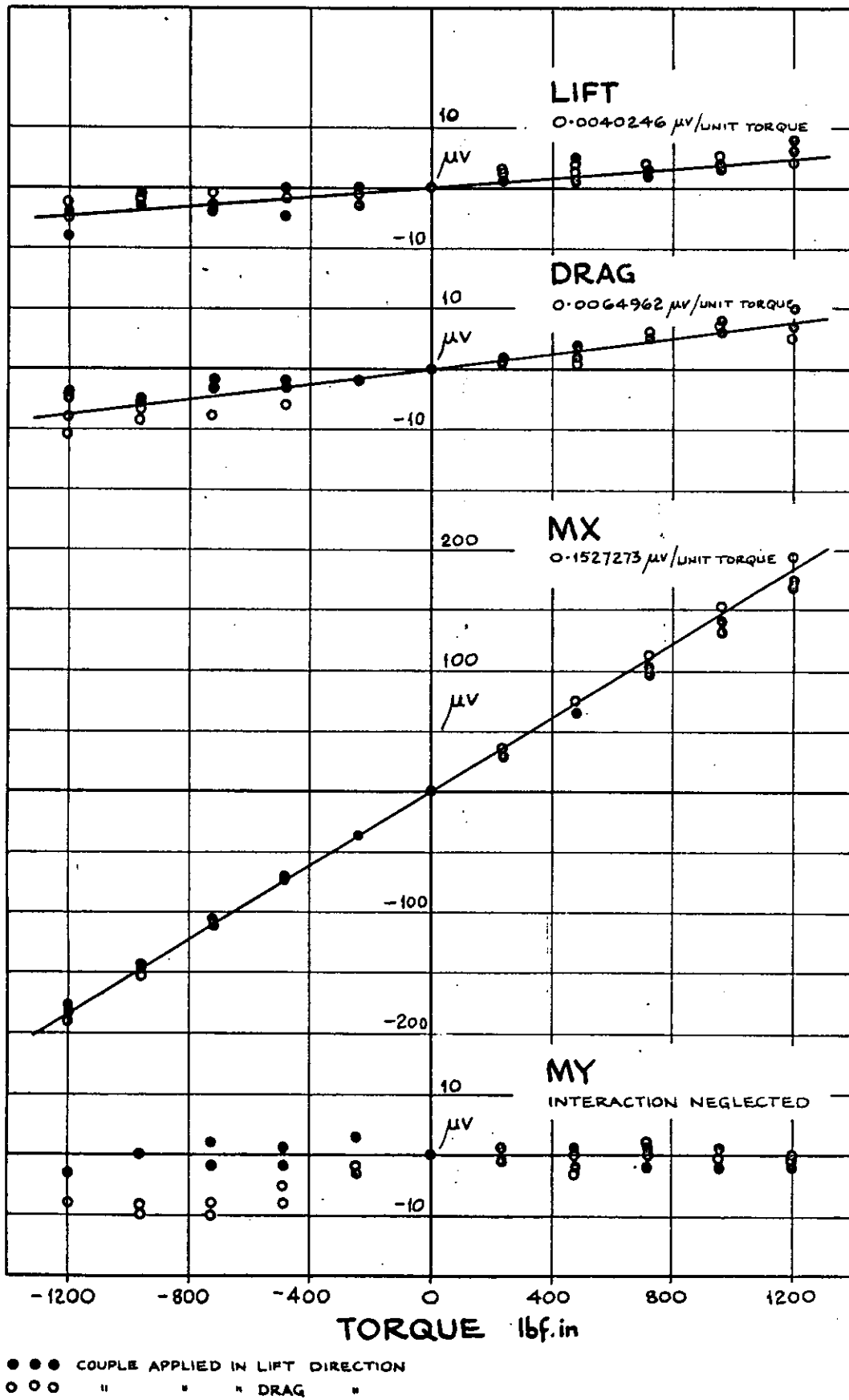


Fig. 39 INTERACTIONS CAUSED BY TORQUE  
CALIBRATION DATA AND MEAN CURVES

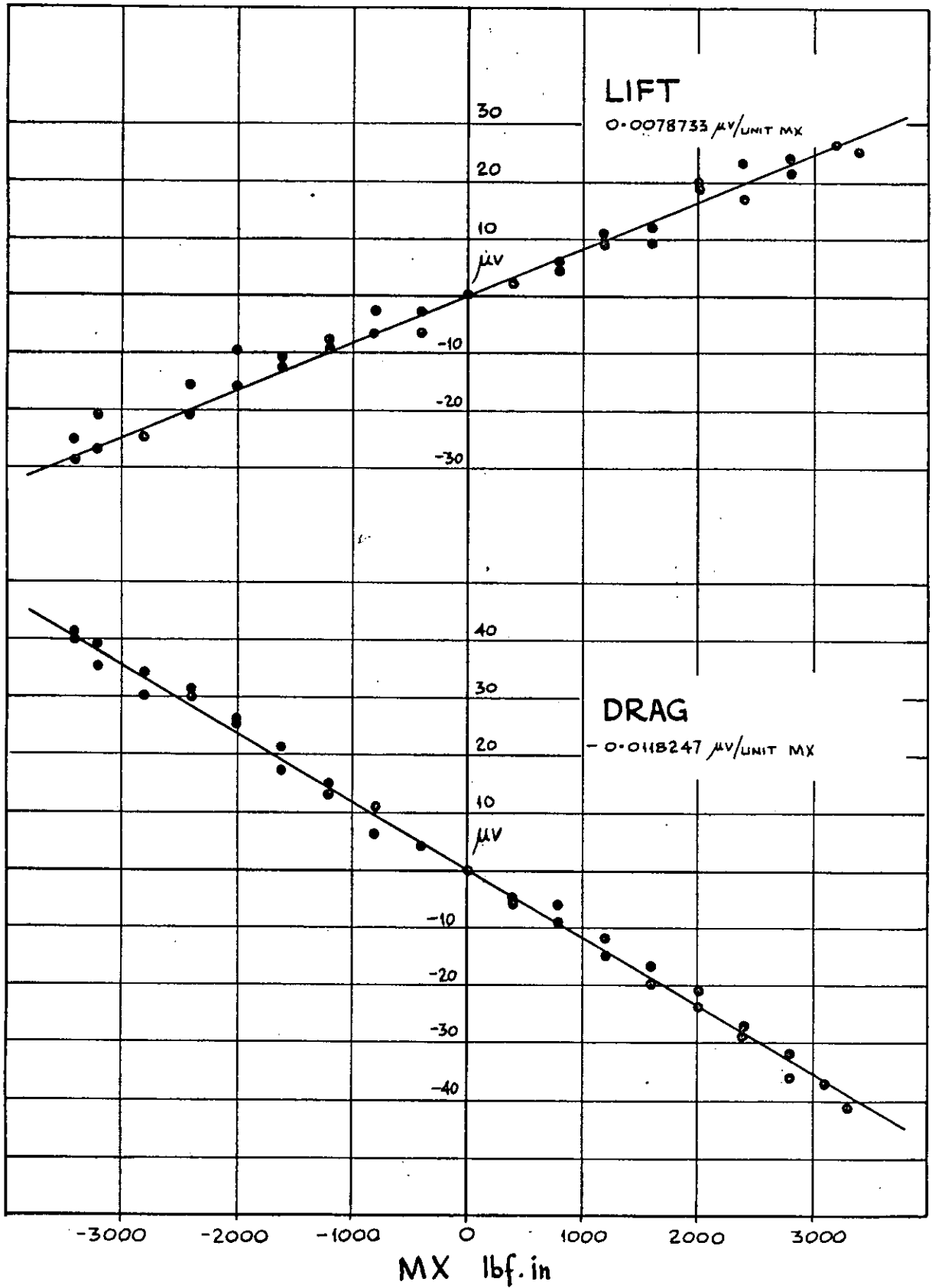


Fig. 40a INTERACTIONS CAUSED BY MX  
 CALIBRATION DATA AND MEAN CURVES

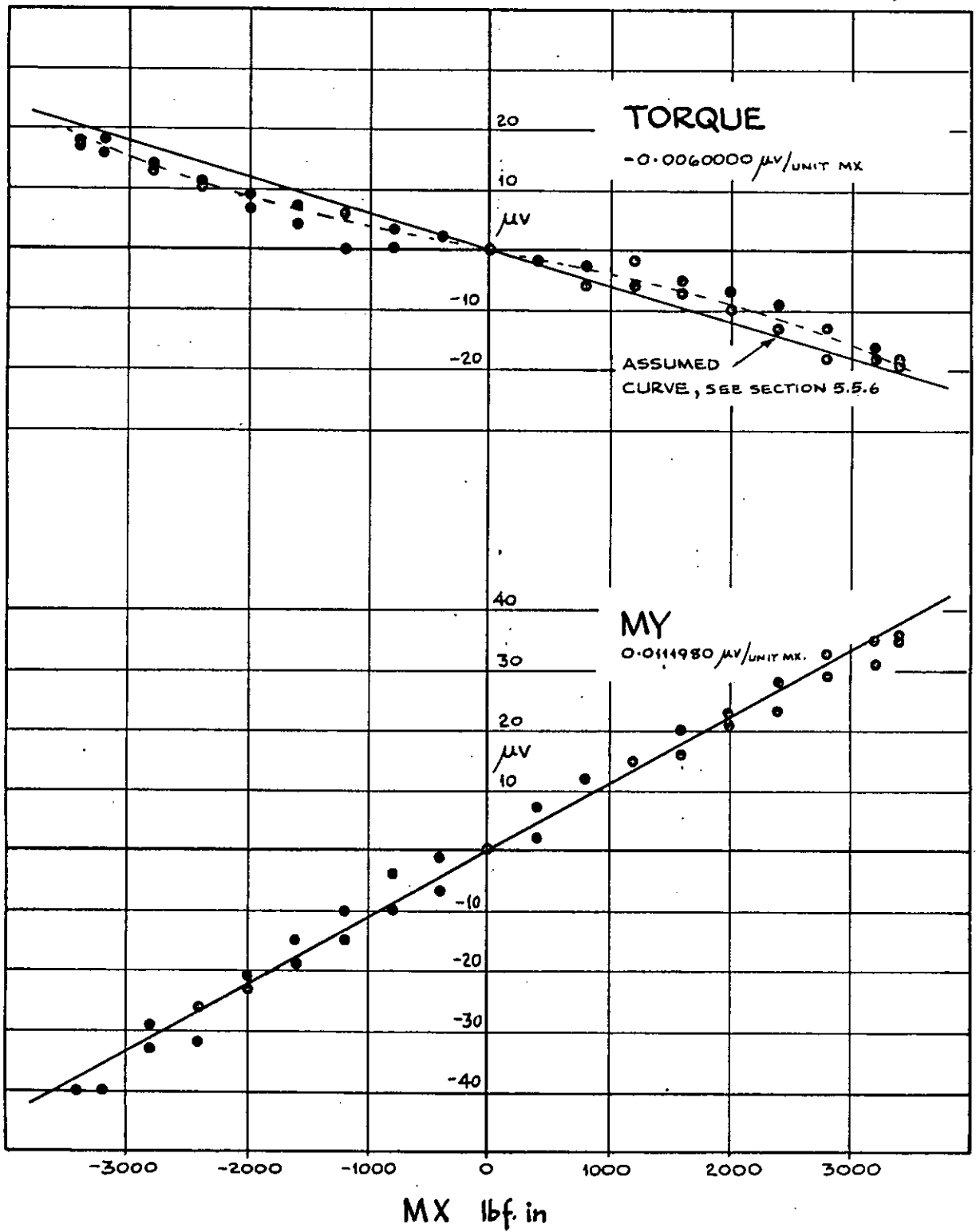


Fig. 40b INTERACTIONS CAUSED BY MX (cont'd)  
 CALIBRATION DATA AND MEAN CURVES

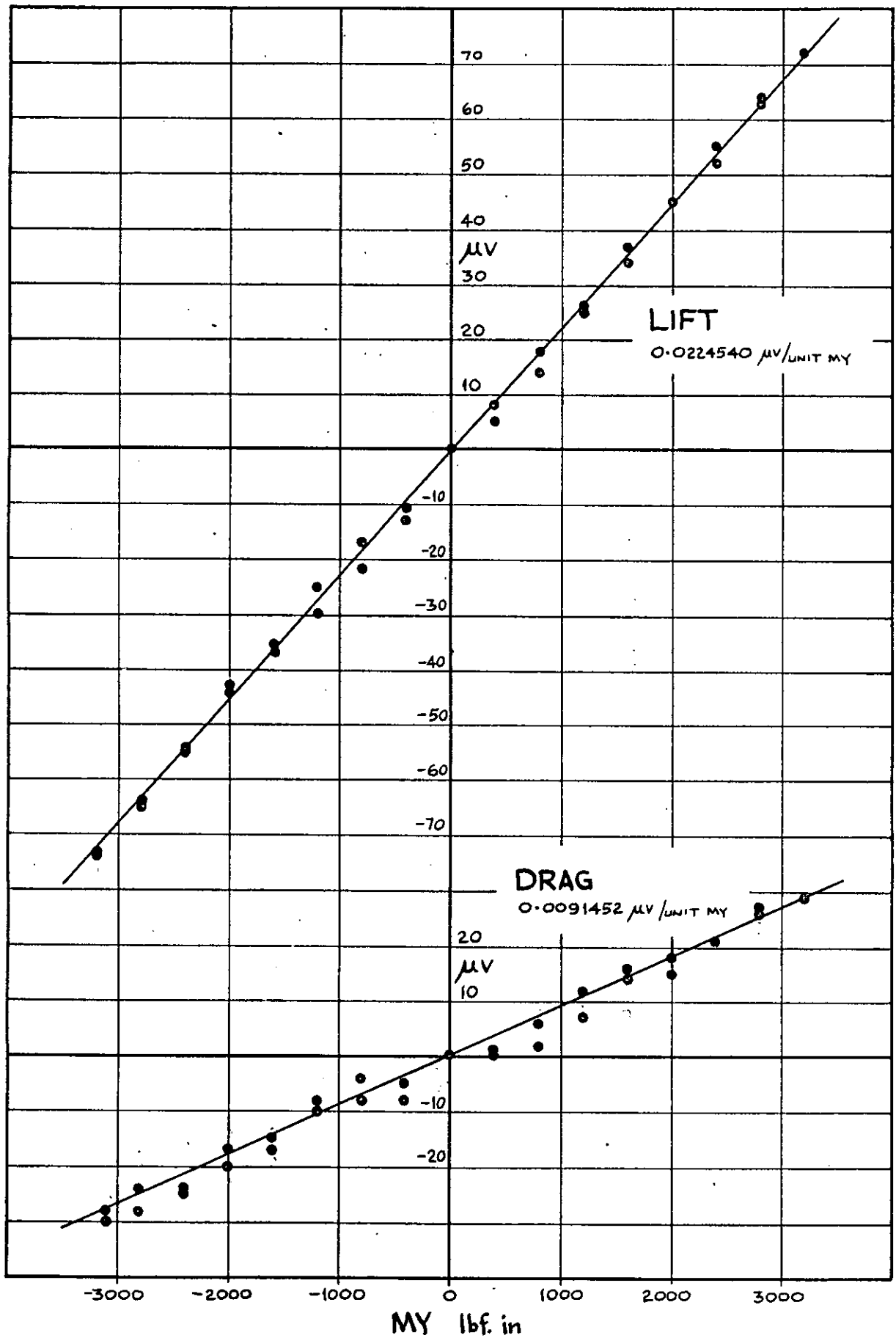


Fig. 41a INTERACTIONS CAUSED BY MY  
 CALIBRATION DATA AND MEAN CURVES

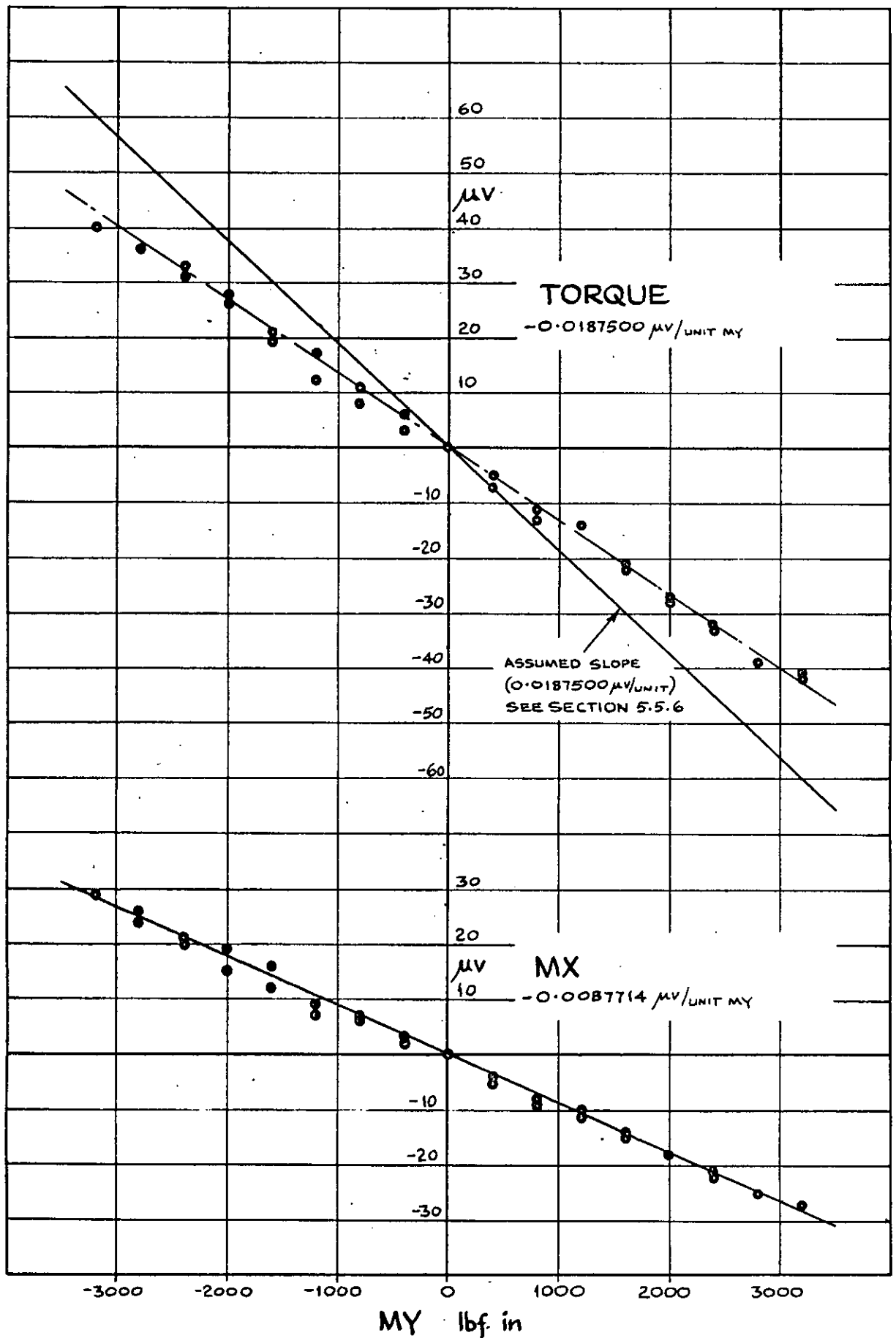
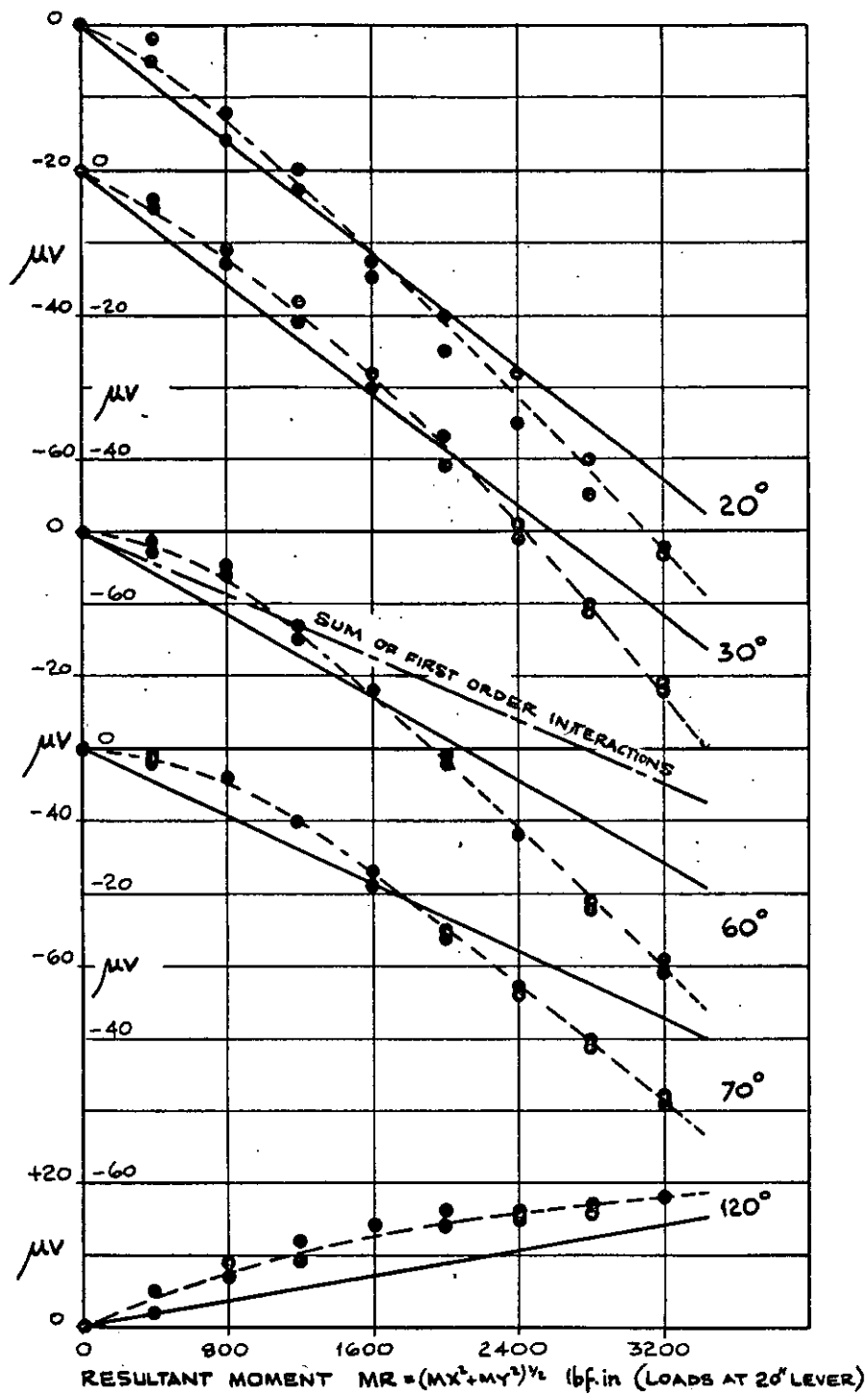


Fig. 41 b INTERACTIONS CAUSED BY MY (cont'd)  
 CALIBRATION DATA AND MEAN CURVES



-●-●-●- MEASURED INTERACTIONS  
 ——— ASSUMED INTERACTIONS

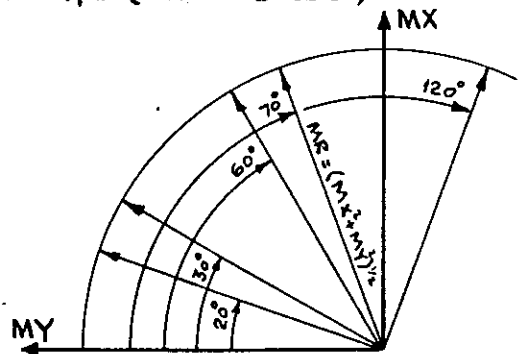
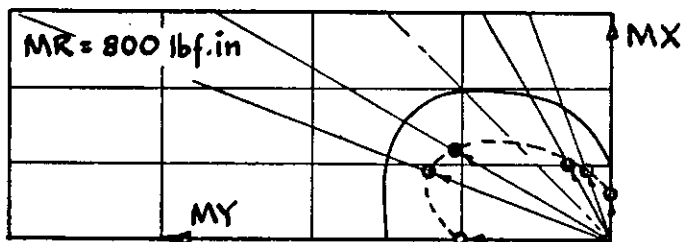
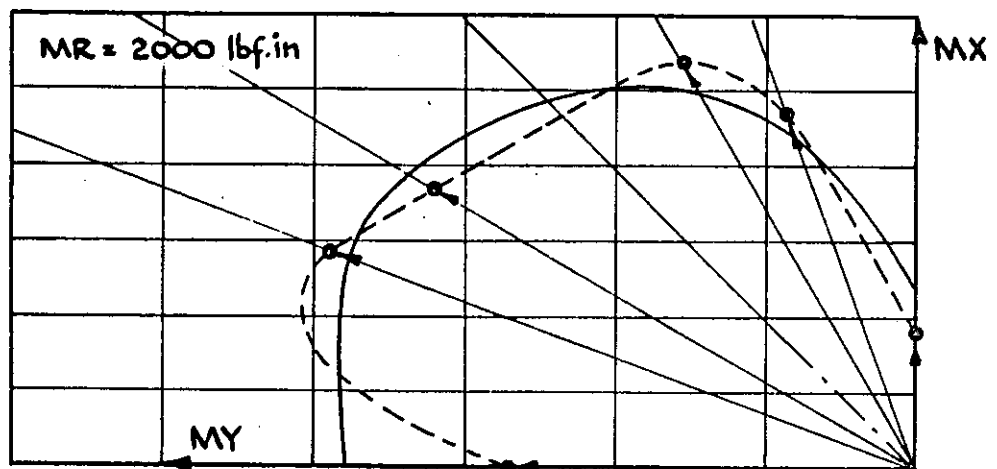
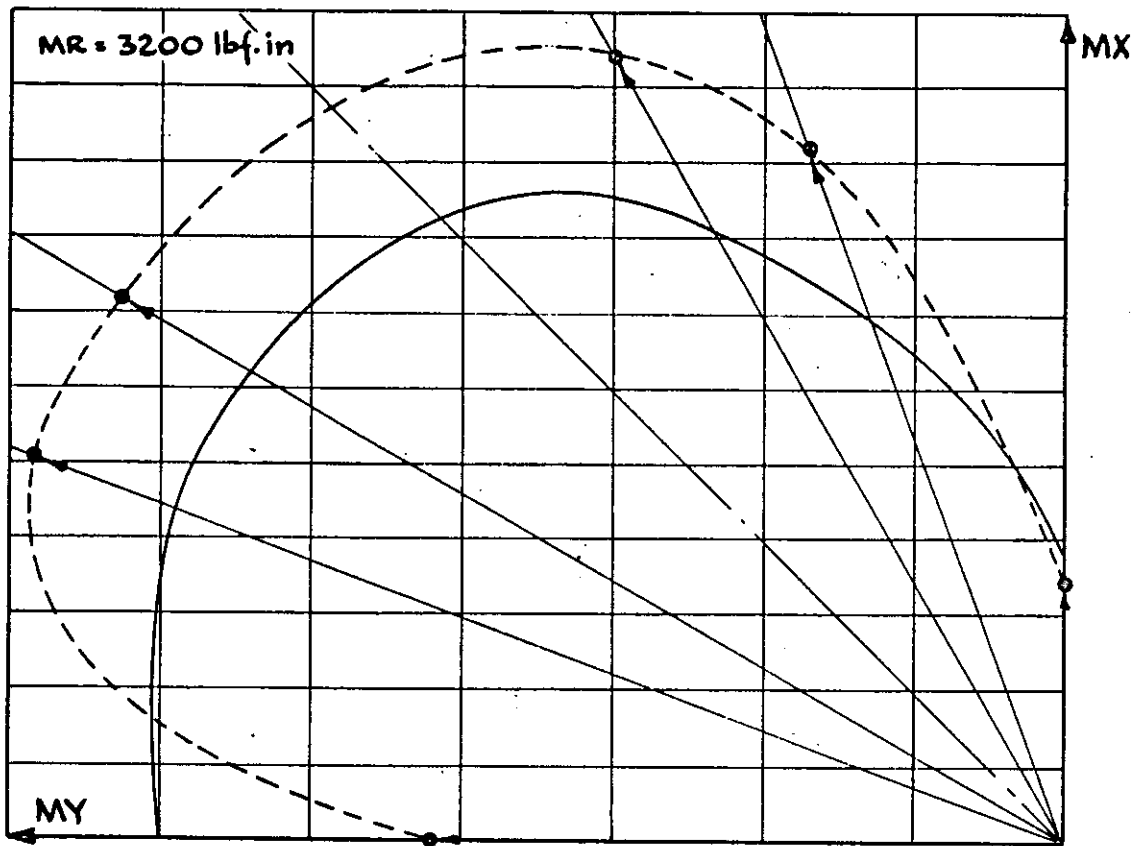


Fig. 42 TORQUE INTERACTIONS CAUSED BY  
 COMBINED MOMENTS (MX + MY)



-●-●-● MEASURED INTERACTION  
 ——— ASSUMED INTERACTION  
 SCALE : 2 mm = 1 μV

Fig. 43 POLAR DIAGRAMS OF TORQUE INTERACTIONS CAUSED BY (MX + MY)  
 (DERIVED FROM Figs. 42, 41b, 40b)

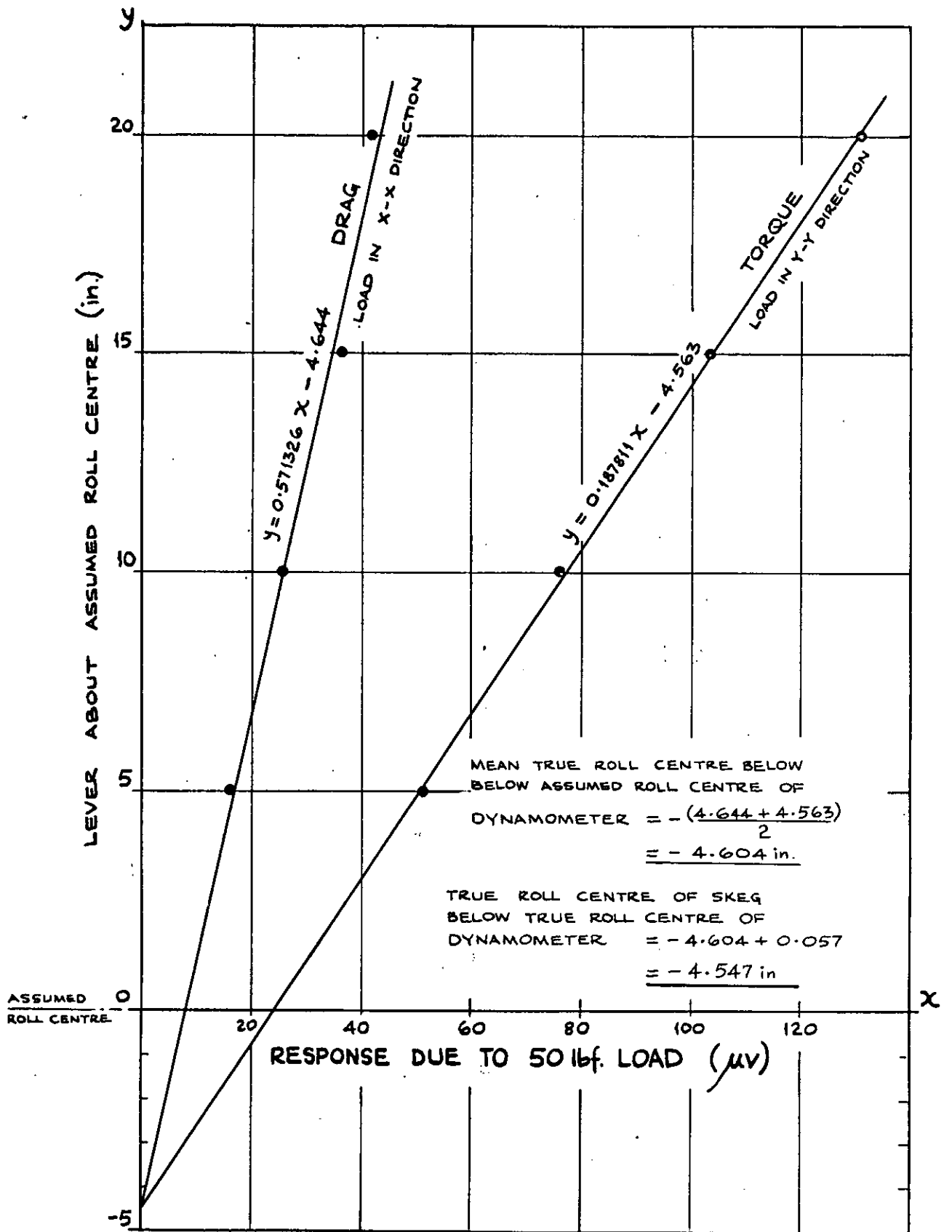


Fig. 44 DERIVATION OF TRUE ROLL CENTRE OF SKEG WHEN ATTACHED TO BASE  
CROSS PLOTS OF DRAG AND TORQUE RESPONSE CAUSED BY 50 lbf. LOAD APPLIED TO SKEG AT VARYING LEVERS IN X AND Y DIRECTIONS



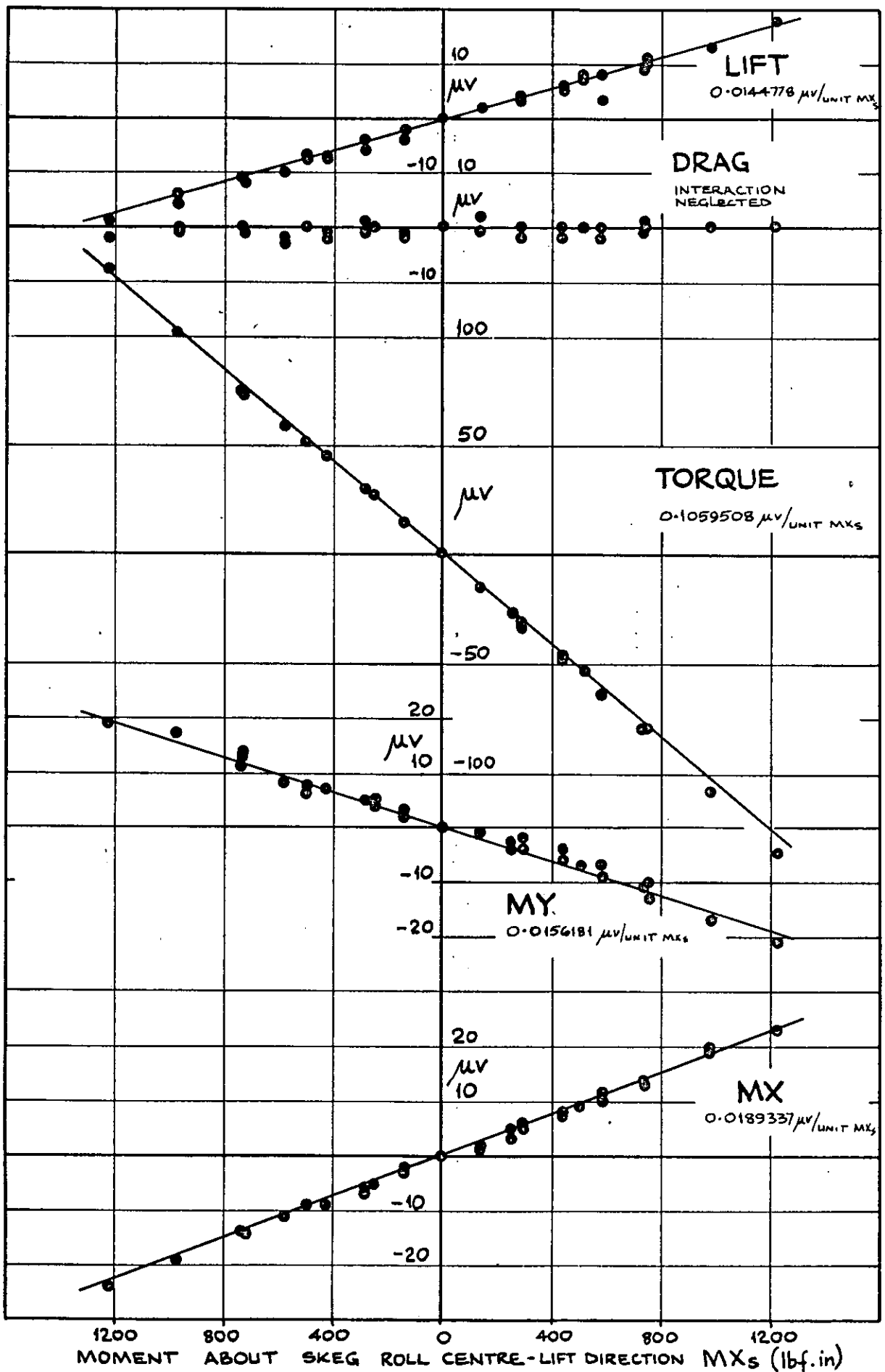


Fig.45 INTERACTIONS CAUSED BY SKEG LOADS:  
LIFT DIRECTION  
CALIBRATION DATA AND MEAN CURVES

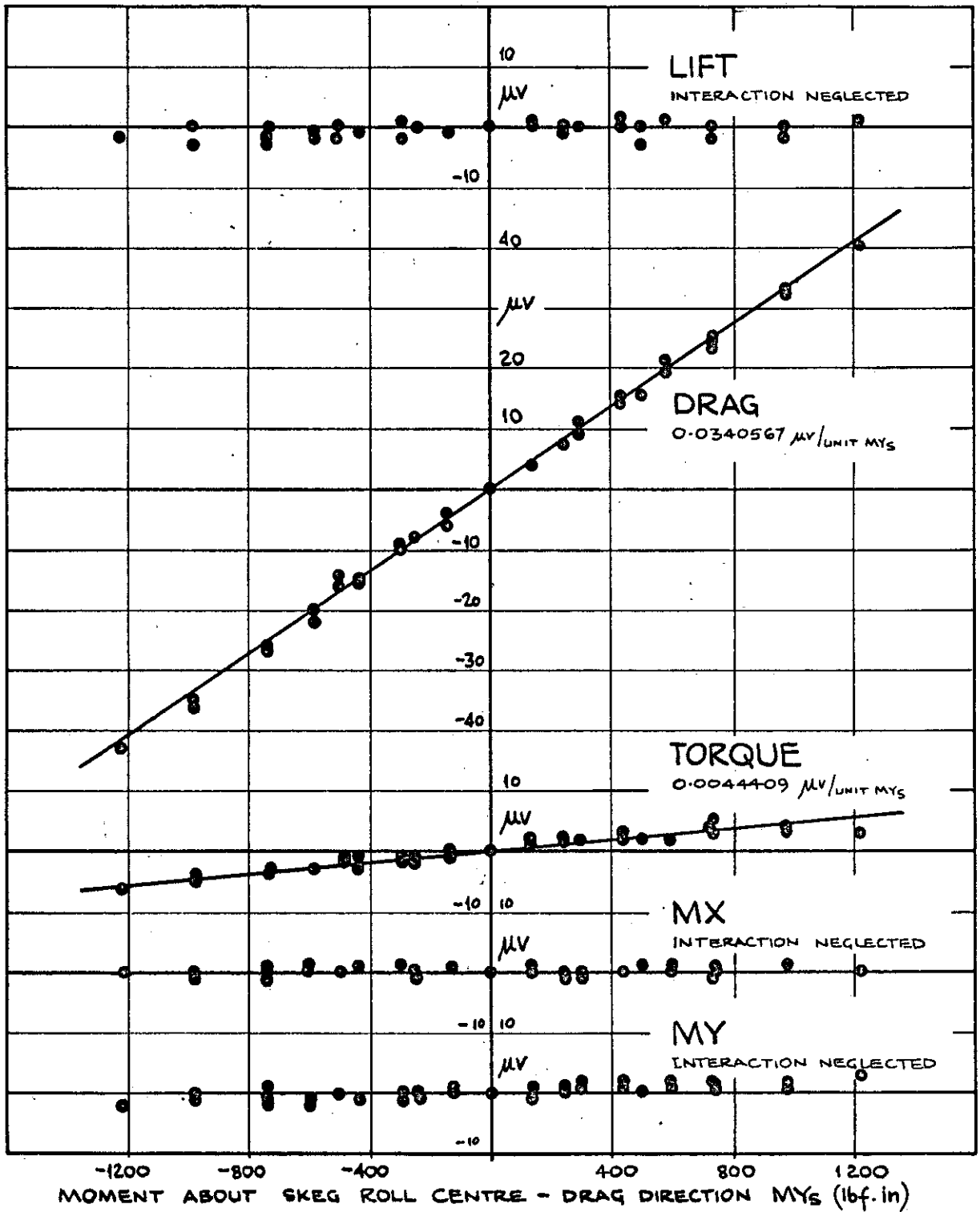


Fig. 46 INTERACTIONS CAUSED BY SKEG LOADS:  
 DRAG DIRECTION  
 CALIBRATION DATA AND MEAN CURVES

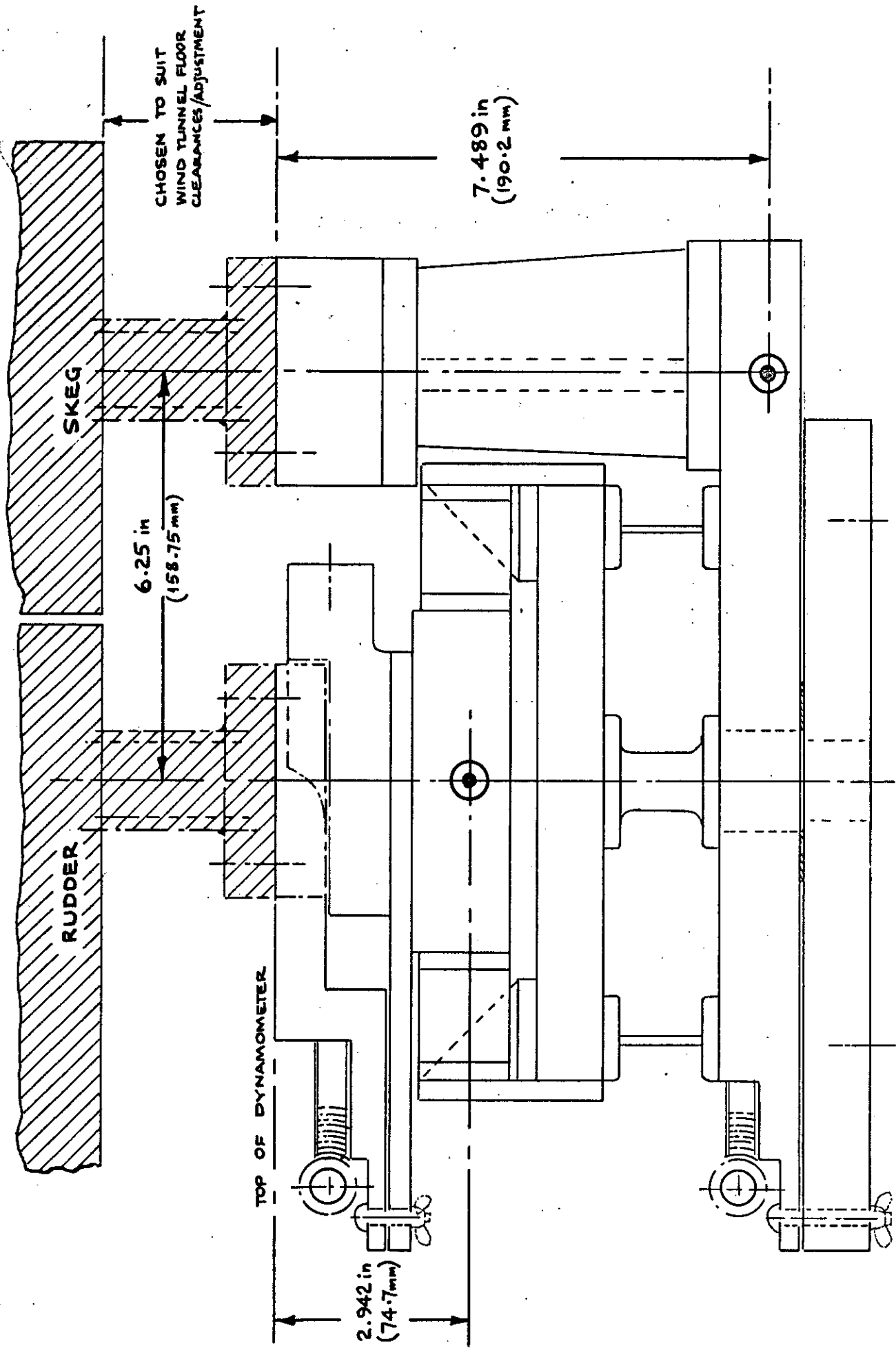


Fig. 47 TRUE ROLL CENTRES OF DYNAMOMETER

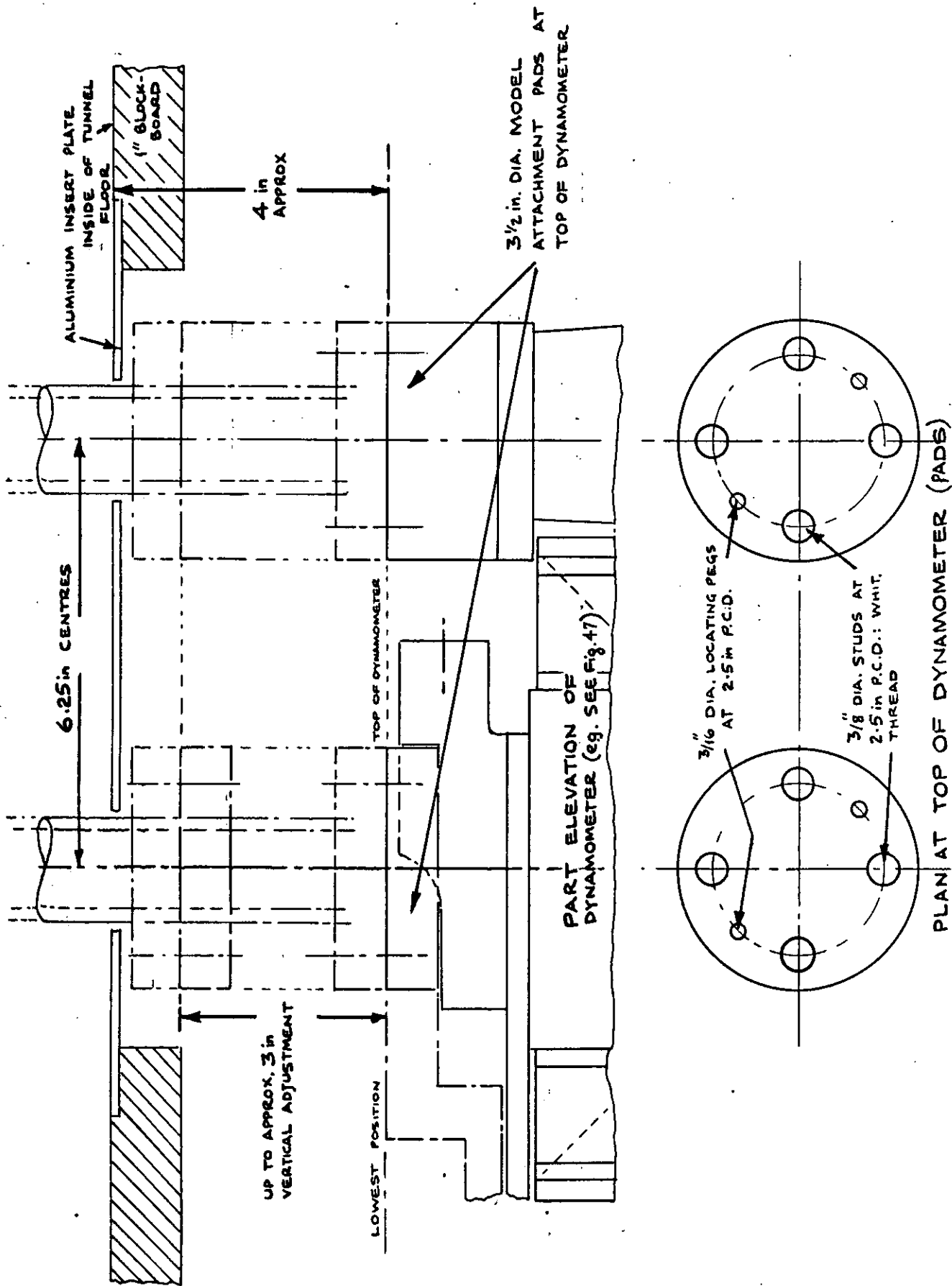


Fig. 48 MODEL CONNECTING PADS ON DYNAMOMETER, AND VERTICAL ADJUSTMENT

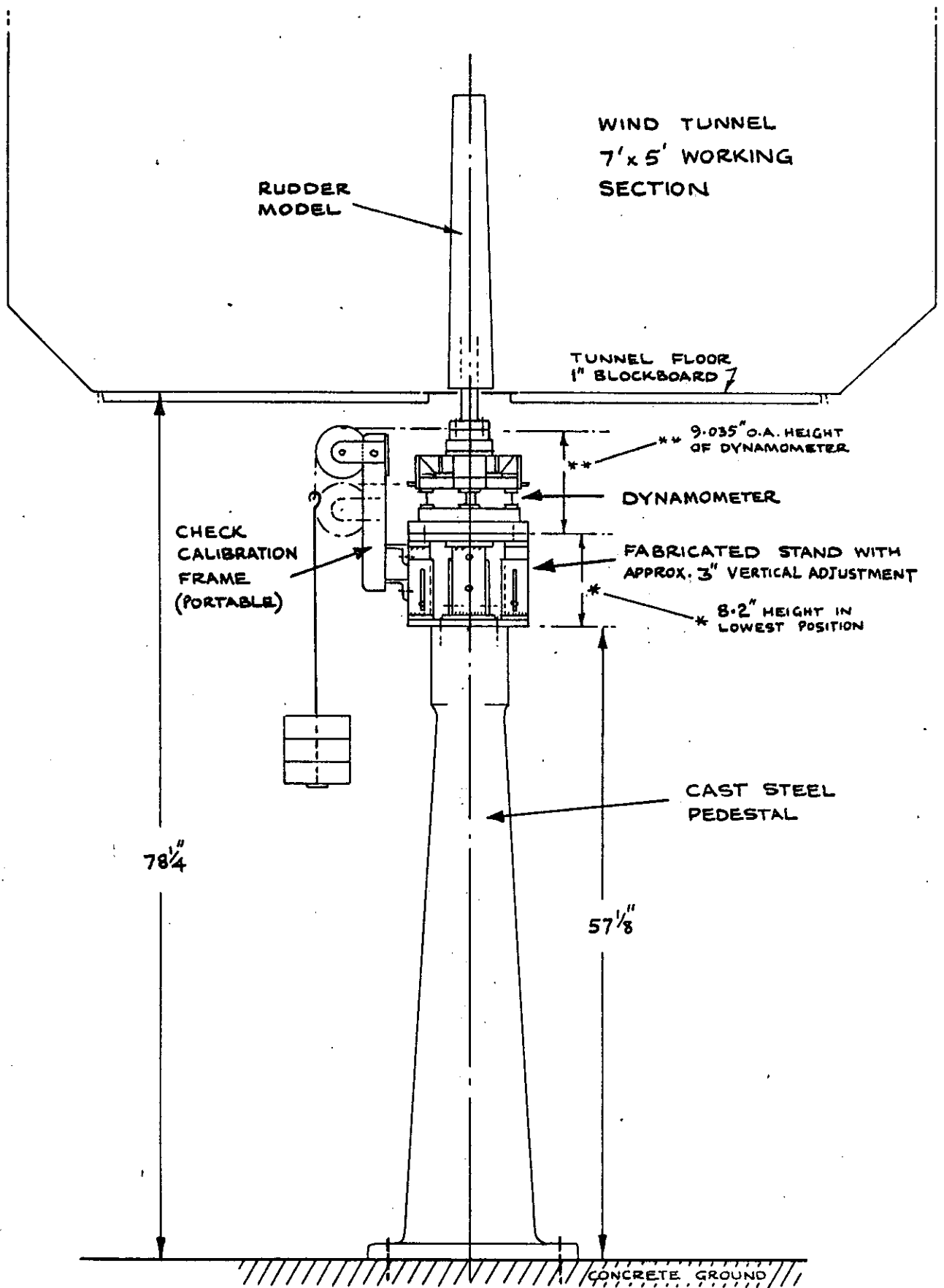


Fig. 49 OUTLINE DETAILS OF DYNAMOMETER  
IN WORKING POSITION

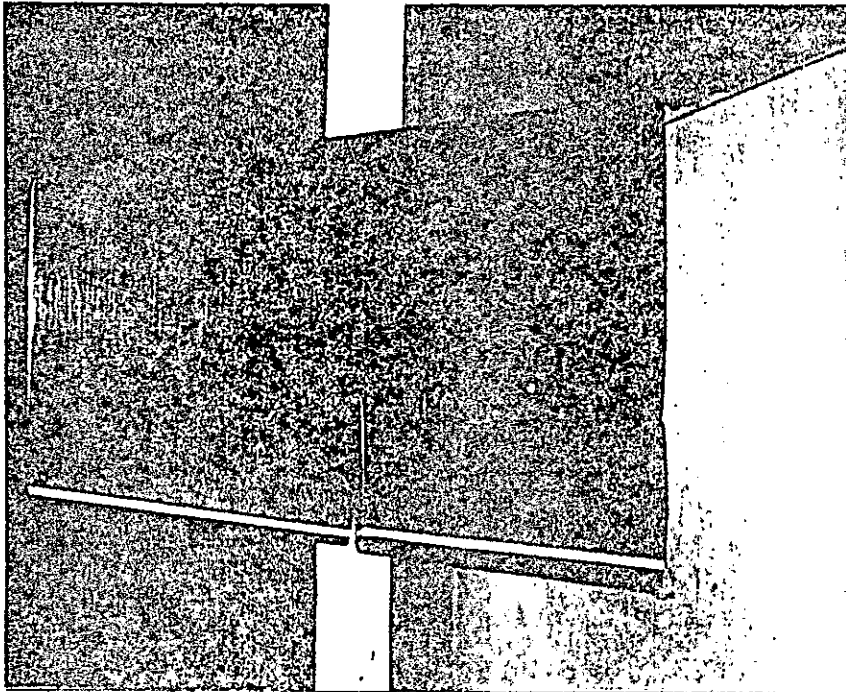


Fig. 50 SKEG RUDDER IN TUNNEL

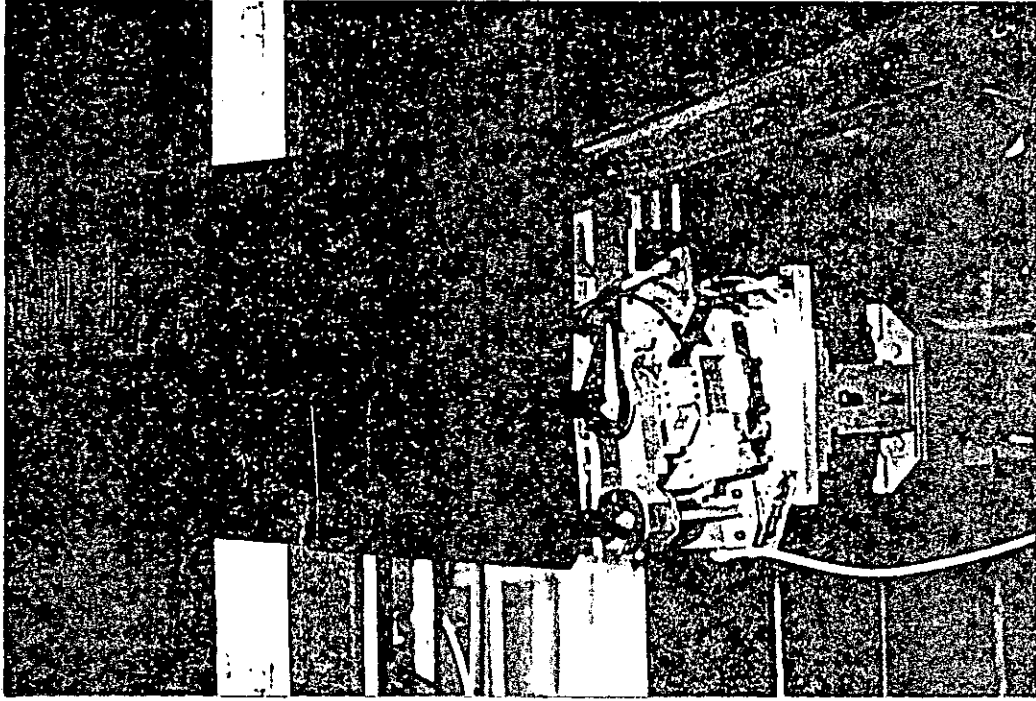


Fig. 51 SKEG RUDDER IN TUNNEL  
(FLOOR REMOVED SHOWING  
DYNAMOMETER)

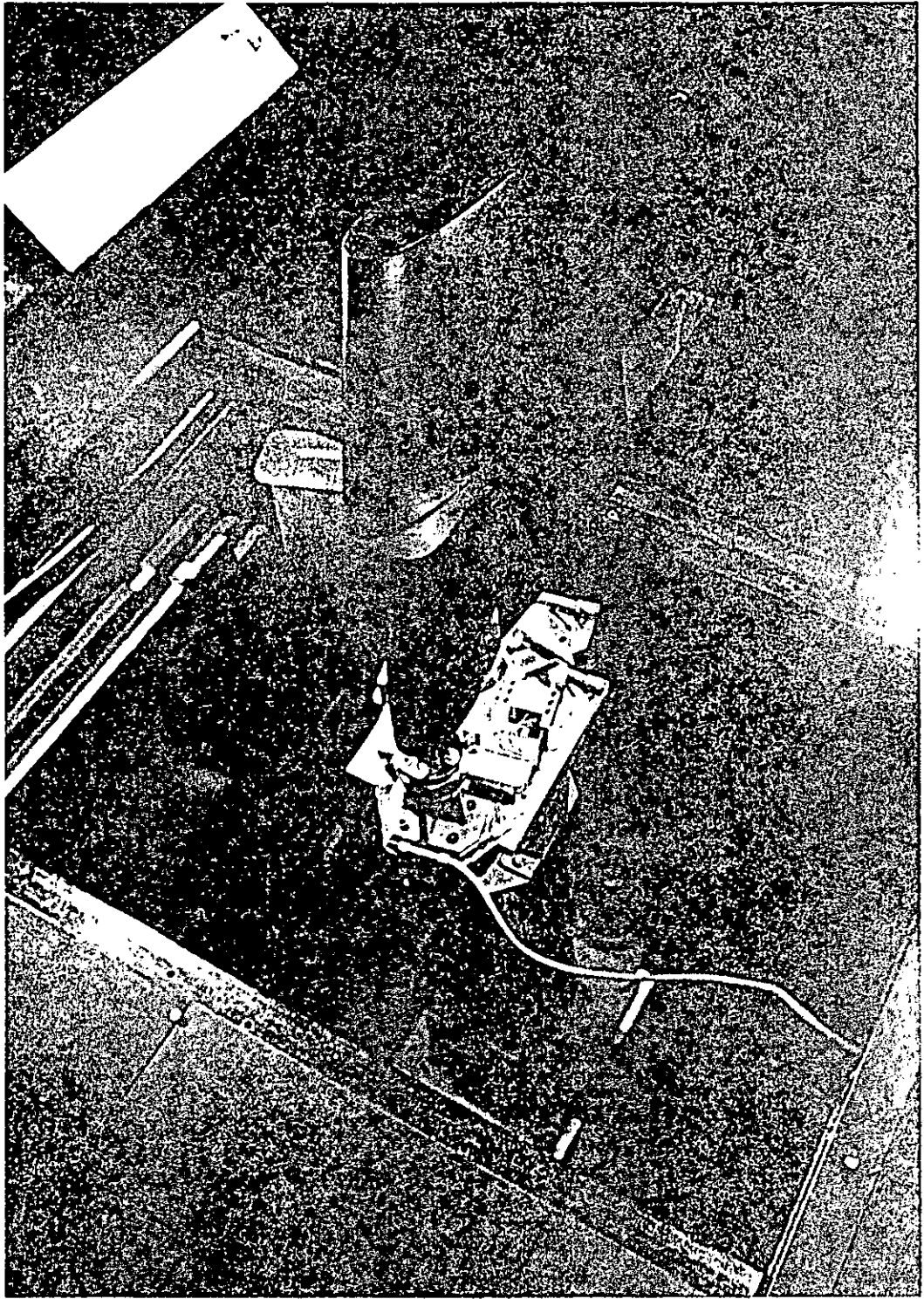
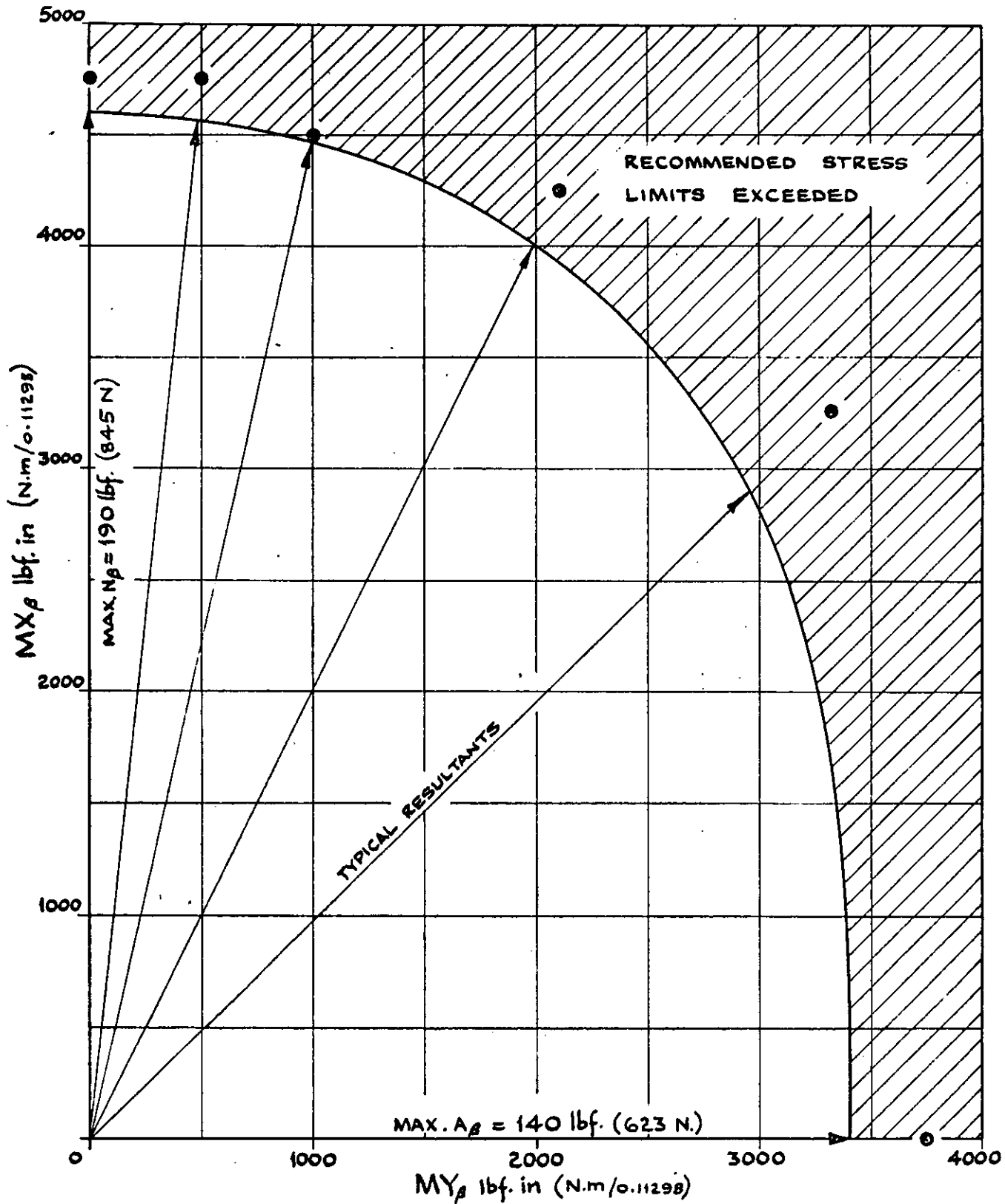


Fig. 52 SKEG RUDDER IN TUNNEL  
(TUNNEL FLOOR REMOVED SHOWING  
DYNAMOMETER AND PEDESTAL ATTACHMENT  
TO GROUND)



NOTES:

ONE QUADRANT SHOWN; COMBINATIONS APPLICABLE TO ALL FOUR QUADRANTS

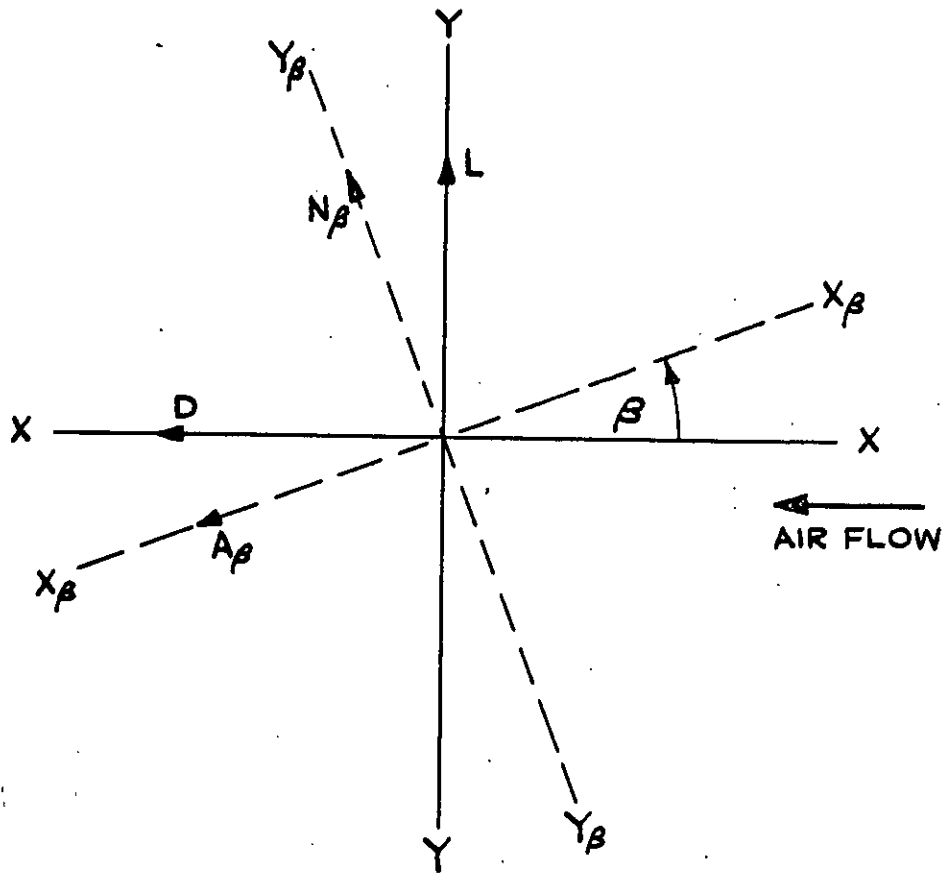
● ● ● PROOF LOAD DATA

MAXIMUM TORQUE OF 1200 lbf.in CAN BE SUPERIMPOSED ON ANY OF ABOVE MAXIMUM COMBINATIONS OF LOADINGS

LOADS CAN BE UP TO  $N_{\beta} = 190$  lbf. OR  $A_{\beta} = 140$  lbf. AND ANY COMBINATION OF THESE MAXIMA PROVIDED ABOVE COMBINATIONS OF MOMENTS ( $M_{X_{\beta}} + M_{Y_{\beta}}$ ) ARE NOT EXCEEDED

Fig. 53 MAXIMUM STATIC LOADS AND MOMENTS



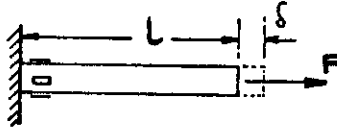


X AND Y ARE TUNNEL AXES  
 $X_\beta$  AND  $Y_\beta$  ARE DYNAMOMETER AXES

Fig. 54 RESOLUTION OF COMPONENTS

## FORCE MEASUREMENT

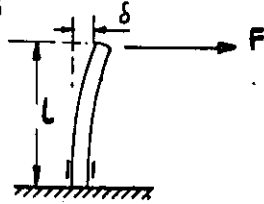
### ① AXIAL



$$\epsilon = \frac{\sigma}{E}$$

$$\delta = L \times \epsilon$$

### ② BENDING

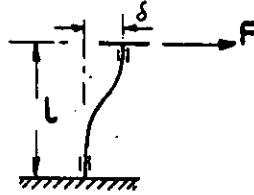


STRAIN AT ROOT DUE TO BENDING:

$$\epsilon = \frac{F \cdot L}{E \cdot I_y}$$

$$\delta = \frac{F L^3}{3 E \cdot I}$$

### ③ CONTRA-FLEXURE

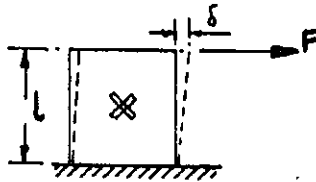


STRAIN AT ROOT DUE TO BENDING IN CONTRA-FLEXURE:

$$\epsilon = \frac{F \cdot L}{2 E \cdot I_y}$$

$$\delta = \frac{F \cdot L^3}{12 E \cdot I}$$

### ④ SHEAR



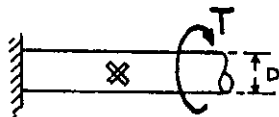
DIRECT STRAIN DUE TO SIMPLE SHEAR:

$$\epsilon_{45^\circ} = \frac{\phi}{2} = \frac{\delta}{2l} = \frac{q}{2G}$$

$$\delta = \frac{l q}{G}$$

## MOMENT OR TORQUE MEASUREMENT

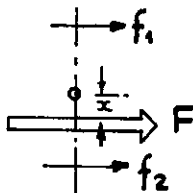
### ⑤ SHEAR



STRAIN DUE TO TORSIONAL SHEAR (ACTING AT 45° TO AXIS):

$$\epsilon_{45^\circ} = \frac{16T}{\pi \cdot D \cdot E}$$

⑥ ALTERNATIVELY, MOMENT OR TORQUE MAY BE DERIVED BY COMPUTING THE DIFFERENCES OF FORCES MEASURED BY ONE OF THE ABOVE METHODS



i.e. TOTAL FORCE =  $F = f_1 + f_2$   
AND MOMENT ( $F \times x$ )  $\propto (f_2 - f_1)$

A SUITABLE ARRANGEMENT OF STRAIN GAUGE BRIDGE CIRCUIT WILL GIVE A DIRECT READING OF MOMENT

Fig. 55

SOME FLEXURE TYPES WITH SUMMARY OF STRAINS AND DEFLECTIONS

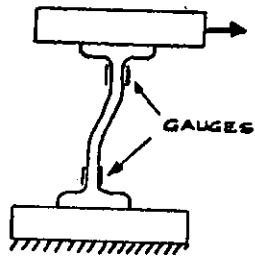


Fig. 56

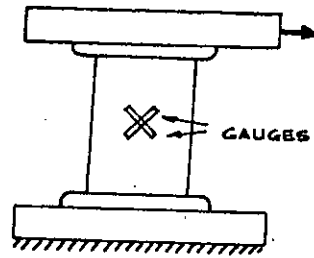


Fig. 57

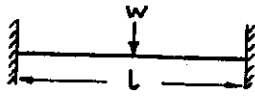


Fig. 58

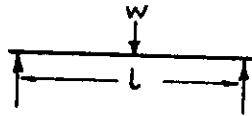


Fig. 59

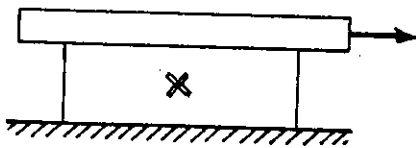


Fig. 60

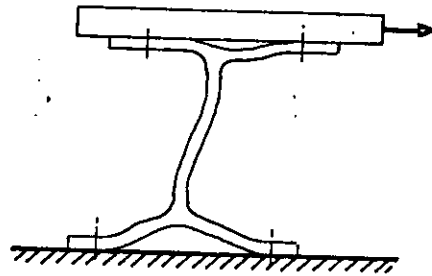


Fig. 61

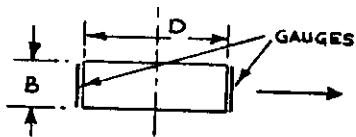


Fig. 62

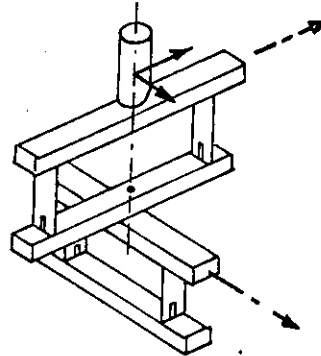


Fig. 63

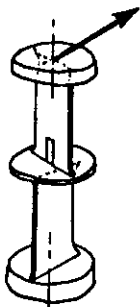


Fig. 64

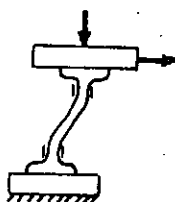


Fig. 65

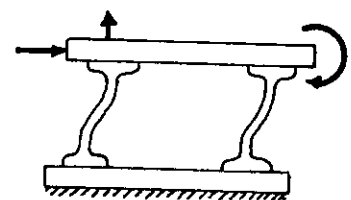


Fig. 66

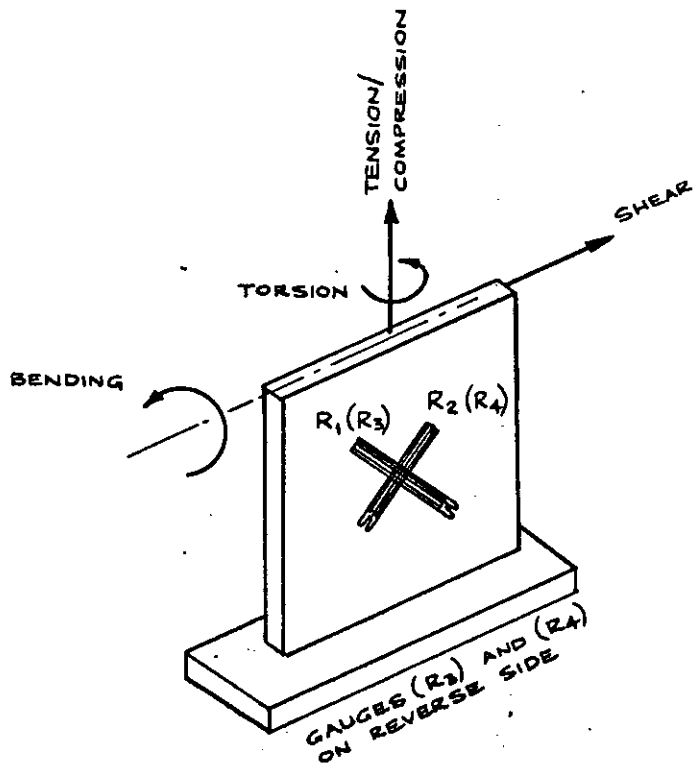
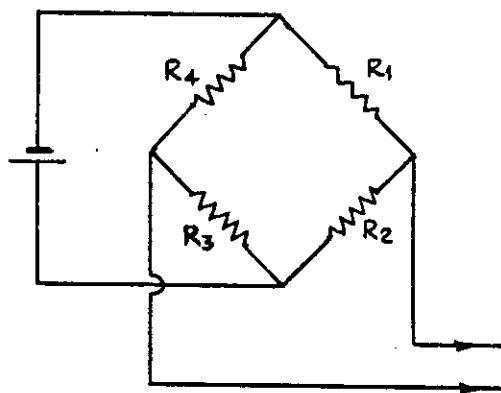


Fig. 67



FOR BRIDGE BALANCE :

$$\frac{R_1}{R_2} = \frac{R_4}{R_3}$$

Fig. 68

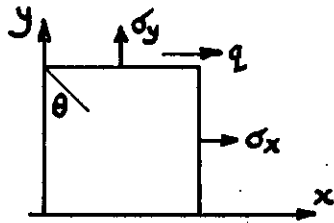


Fig. 69

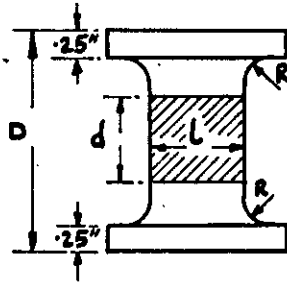


Fig. 70

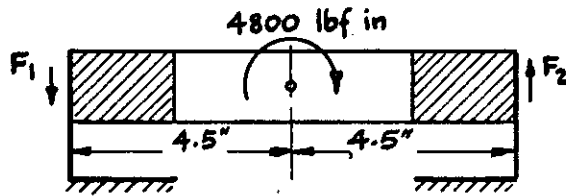


Fig. 71

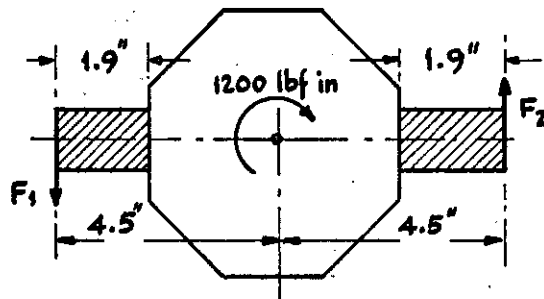


Fig. 72

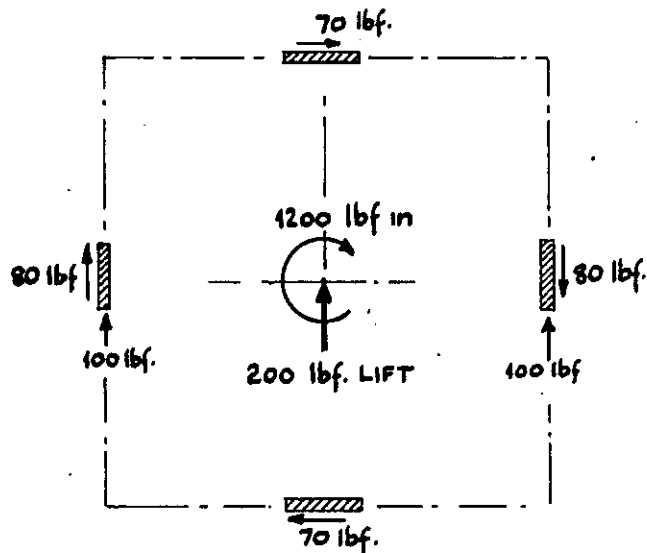


Fig. 73

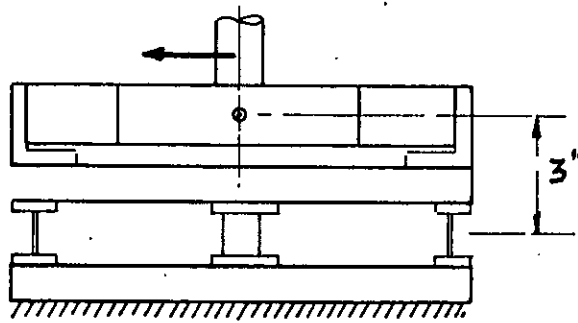


Fig. 74

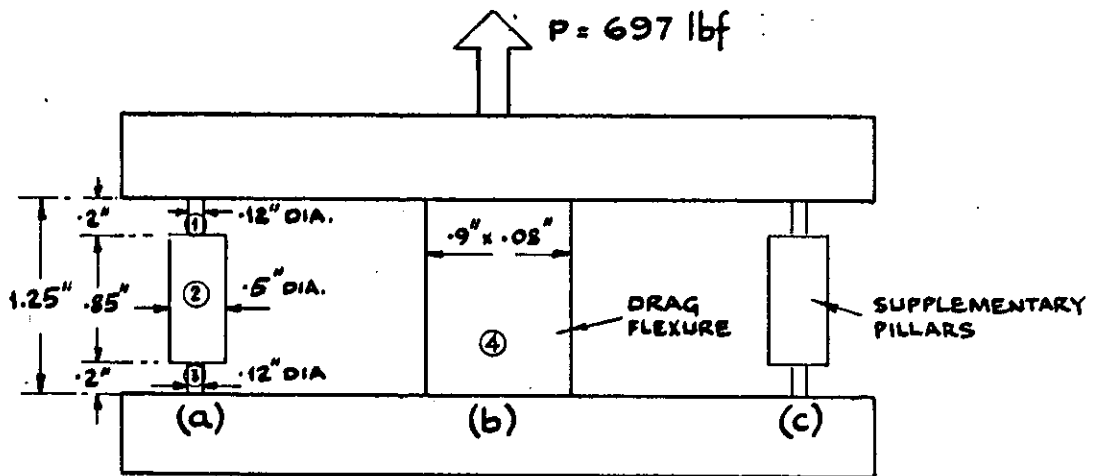
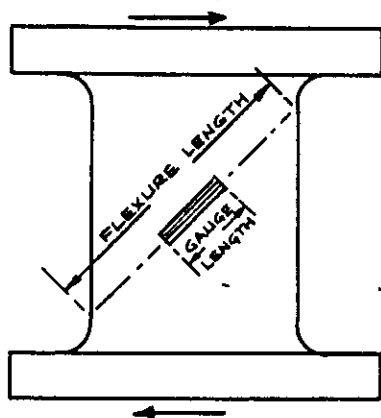
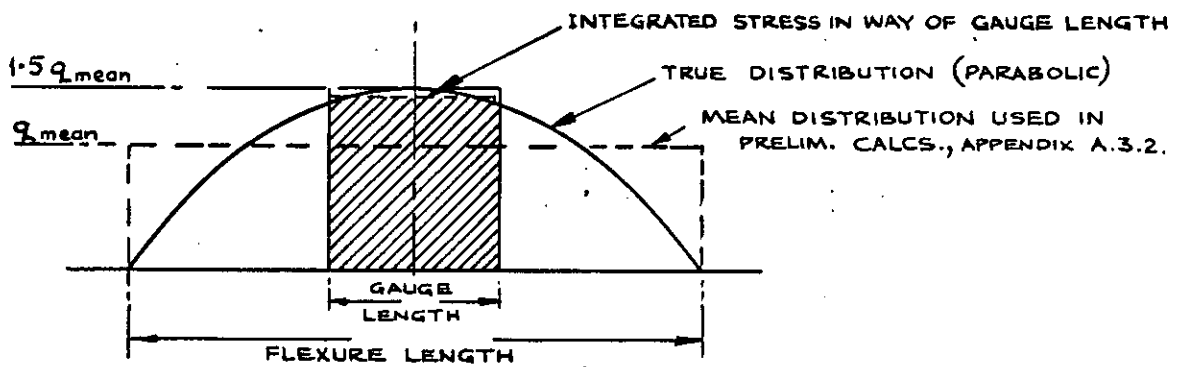


Fig. 75



	GAUGE LENGTH / FLEXURE LENGTH
LIFT FLEXURES	: 0.310
DRAG FLEXURES	: 0.297
TORQUE FLEXURES	: APPROX. AVERAGE OF LIFT AND DRAG
MOMENT FLEXURES	: 0.199



INTEGRATED STRESSES OVER GAUGE LENGTH FOR DIFFERENT FLEXURE TYPES :

LIFT GAUGES	: $q_{actual} = 1.46 q_{mean}$
DRAG GAUGES	: $q_{actual} = 1.45 q_{mean}$
TORQUE GAUGES	: $q_{actual} = 1.45 q_{mean}$ (APPROX.)
MOMENT GAUGES	: $q_{actual} = 1.48 q_{mean}$

Fig.76 STRAIN DISTRIBUTION IN WAY OF GAUGES

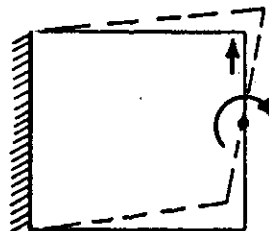


Fig.77 INFLUENCE OF ROTATION ON MOMENT FLEXURES

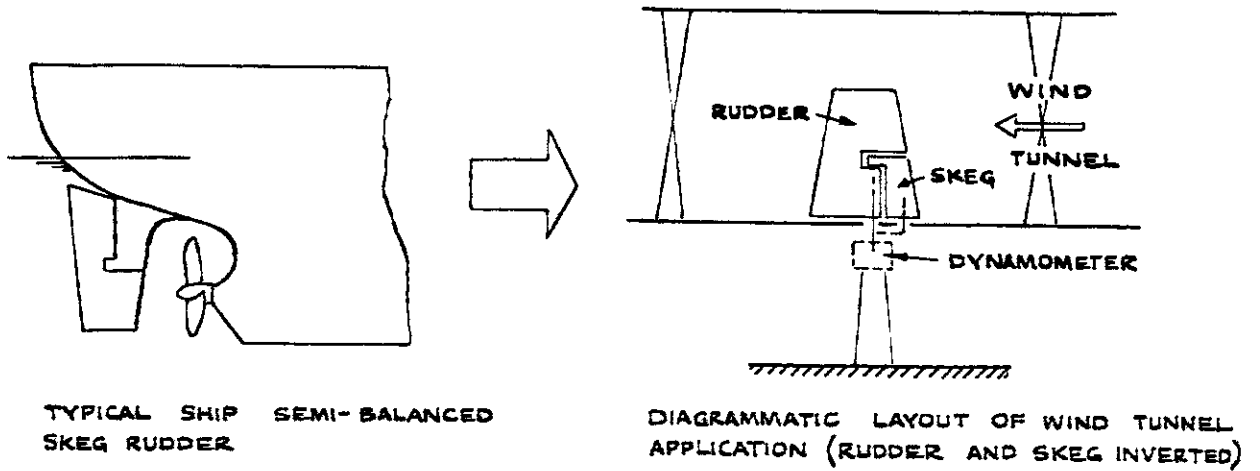
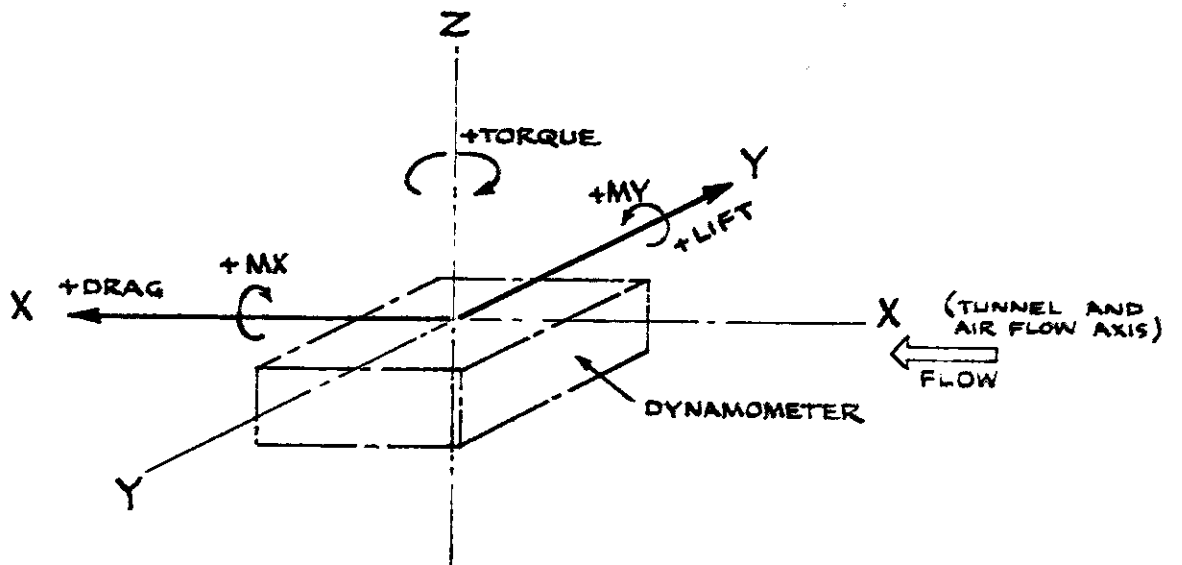


Fig. 1 MOUNTING OF MODEL IN WIND TUNNEL



FIVE COMPONENTS:

LIFT : L

DRAG : D

TORQUE : MZ - HENCE DERIVATION OF CENTRE OF PRESSURE CHORDWISE

MOMENT ABOUT X-AXIS : MX } HENCE DERIVATION OF CENTRE  
 MOMENT ABOUT Y-AXIS : MY } OF PRESSURE SPANWISE

Fig. 2 COMPONENTS MEASURED



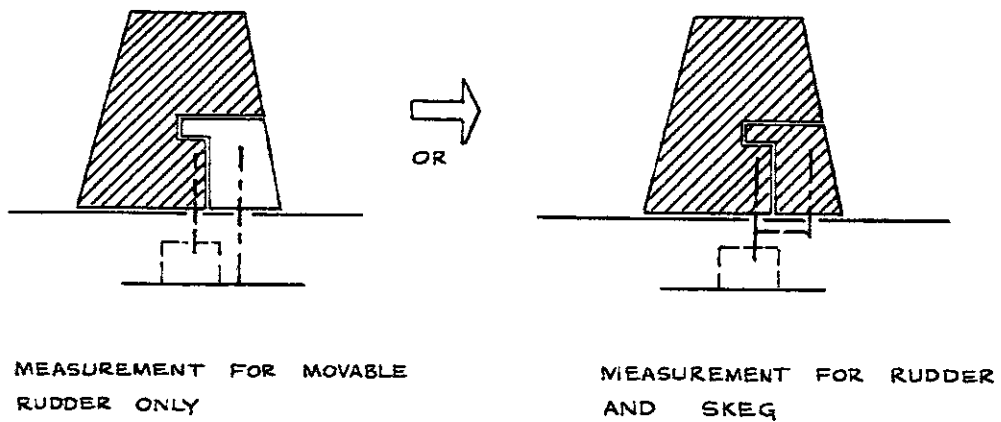
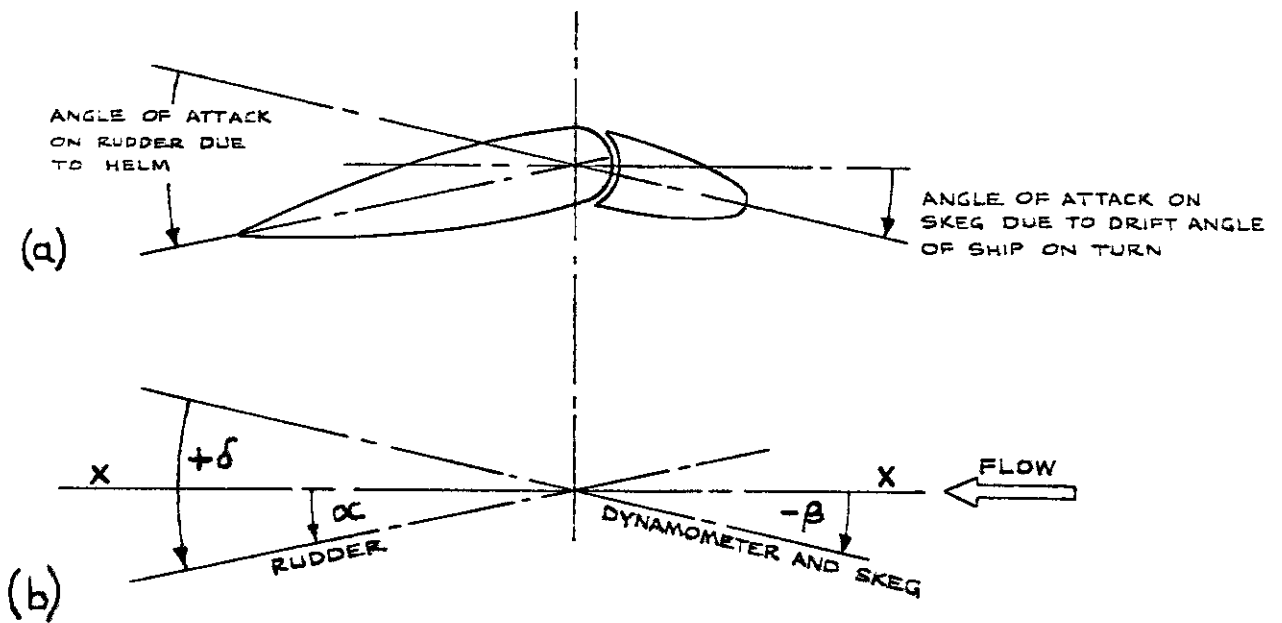


Fig. 3 RUDDER AND SKEG FORCES



NOTATION :

- $\beta$  = DYNAMOMETER (AND SKEG) ANGLE RELATIVE TO FLOW
- $\delta$  = RUDDER ANGLE RELATIVE TO DYNAMOMETER (OR SHIP, OR SKEG)
- $\alpha$  = RUDDER ANGLE RELATIVE TO FLOW
- $\alpha = \delta + \beta$

Fig. 4 NOTATION OF ANGLES

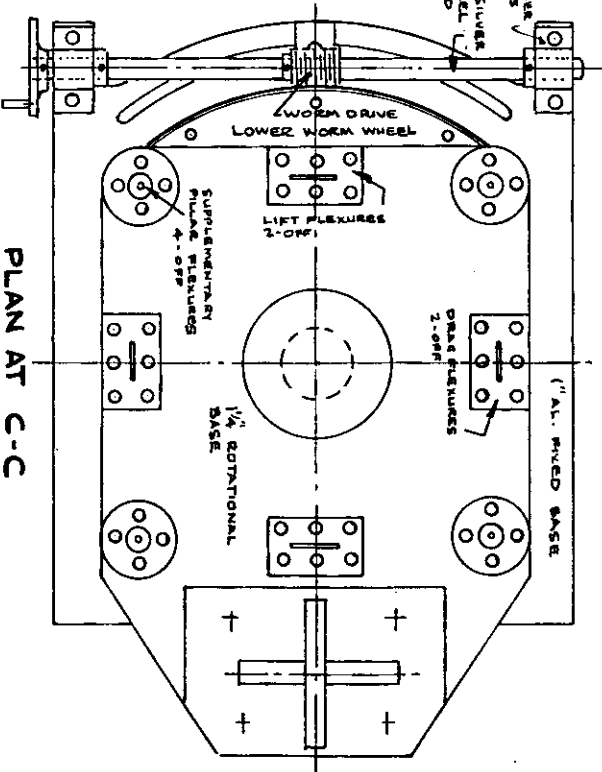
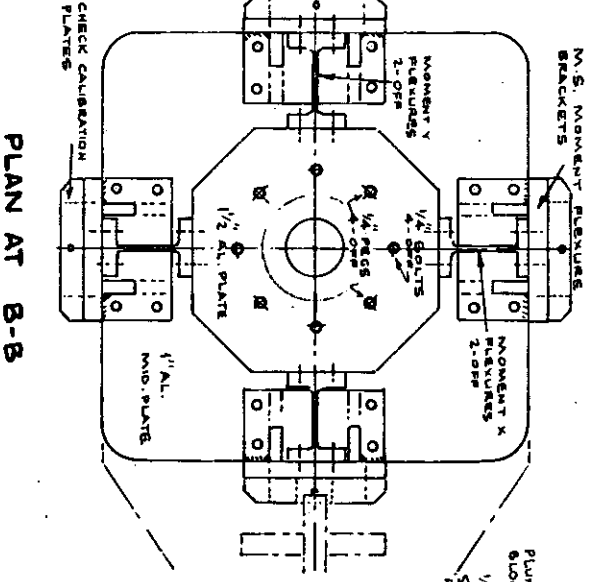
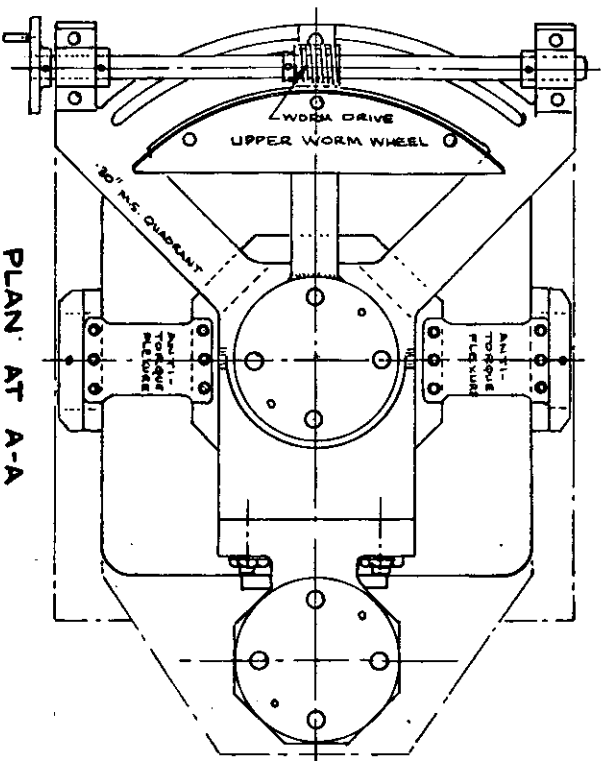
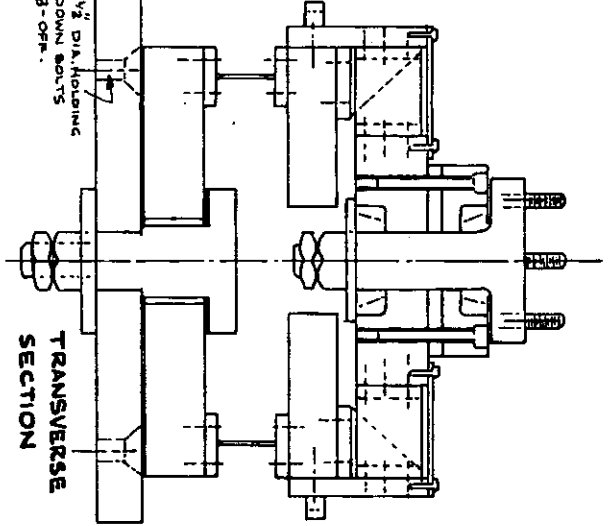
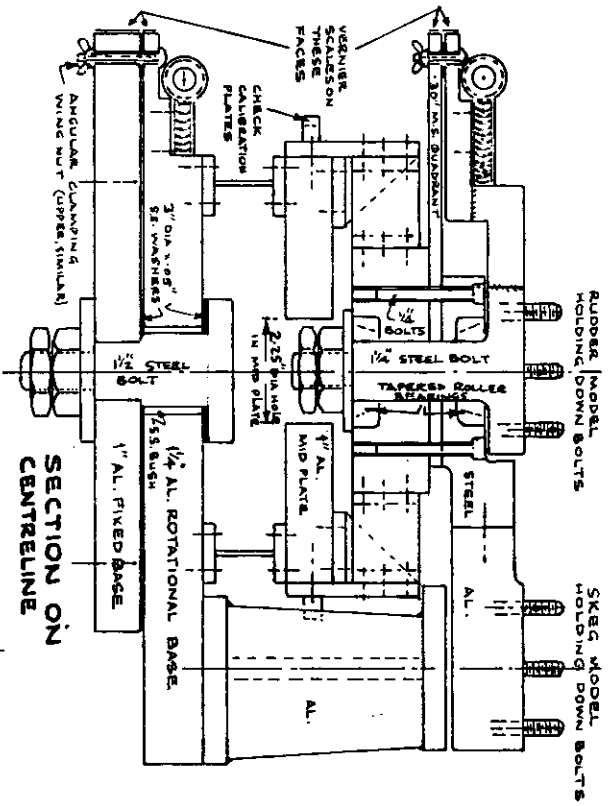
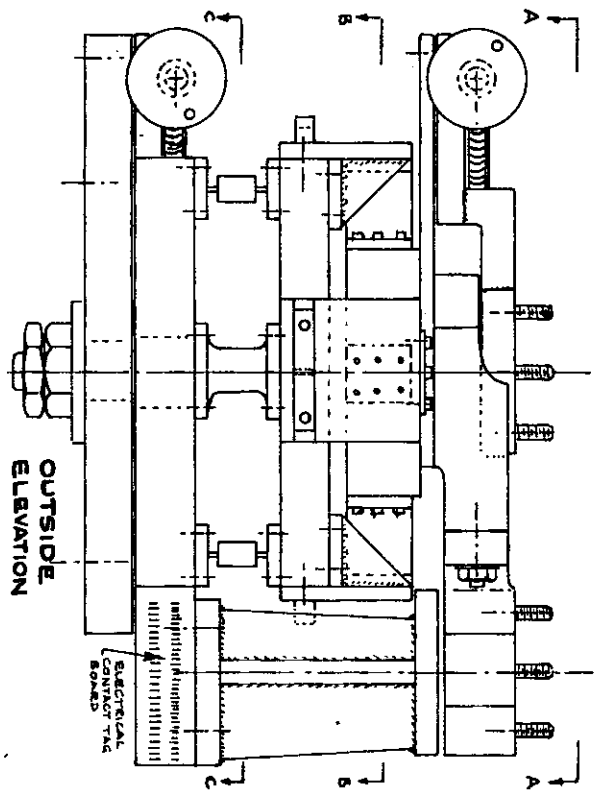


Fig. 5 GENERAL ARRANGEMENT OF DYNAMOMETER

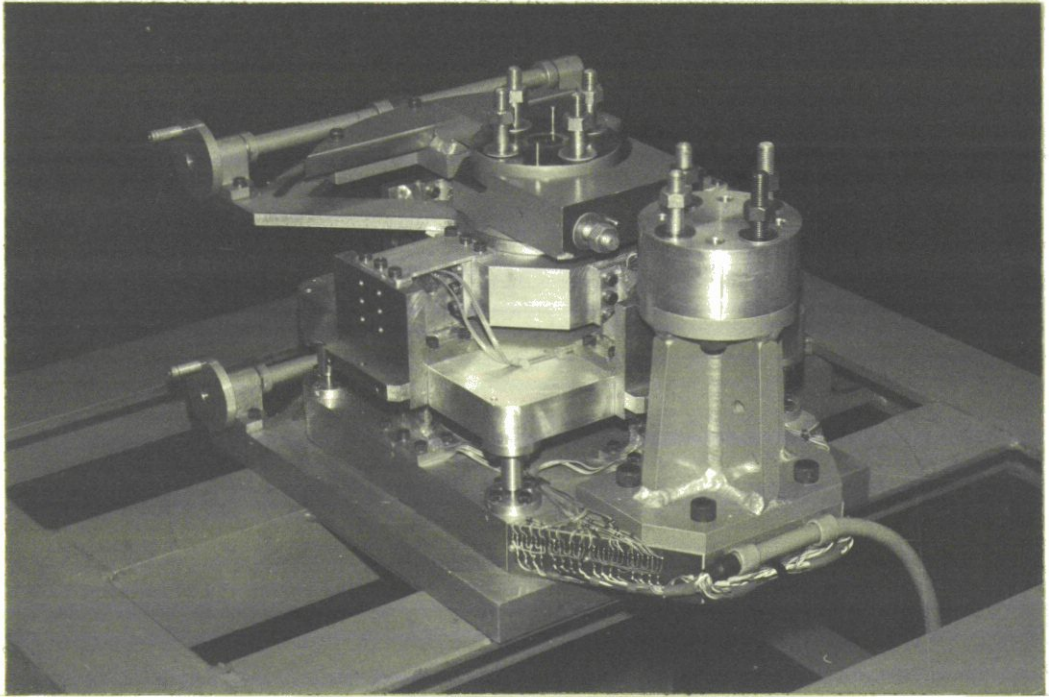


Fig. 6 DYNAMOMETER

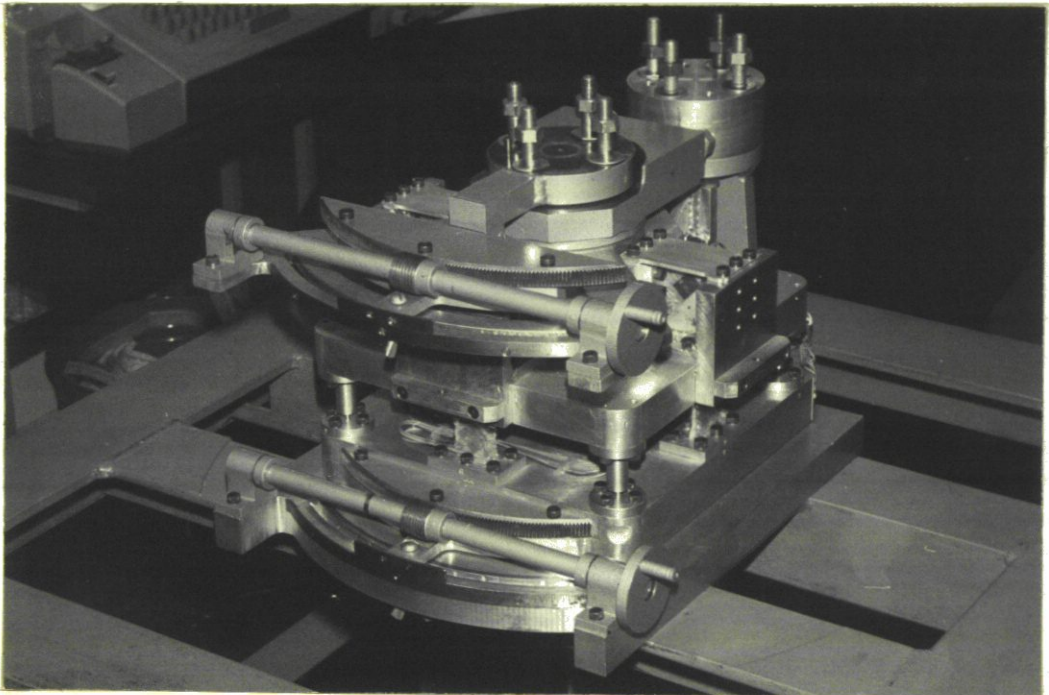


Fig. 7 DYNAMOMETER

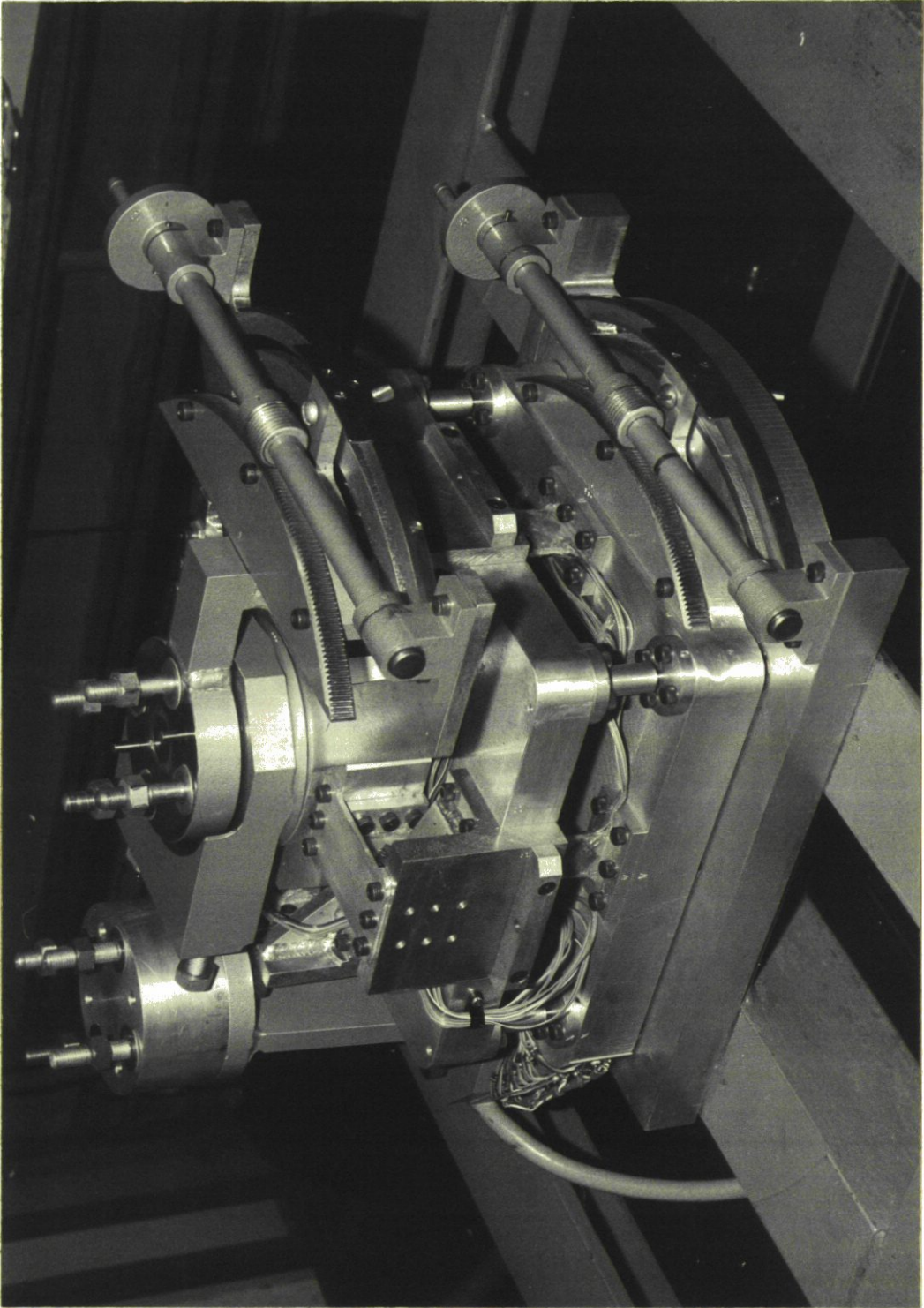


Fig. 8 DYNAMOMETER

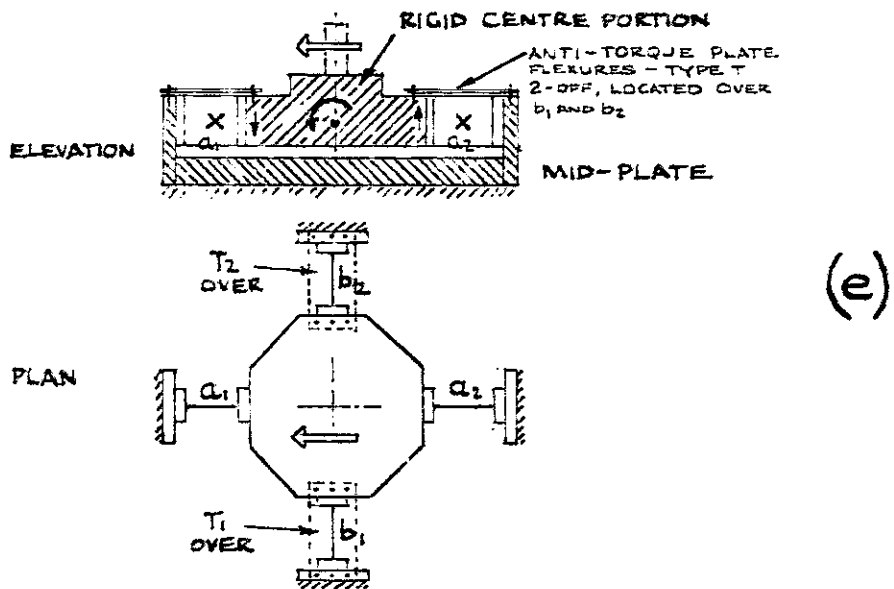
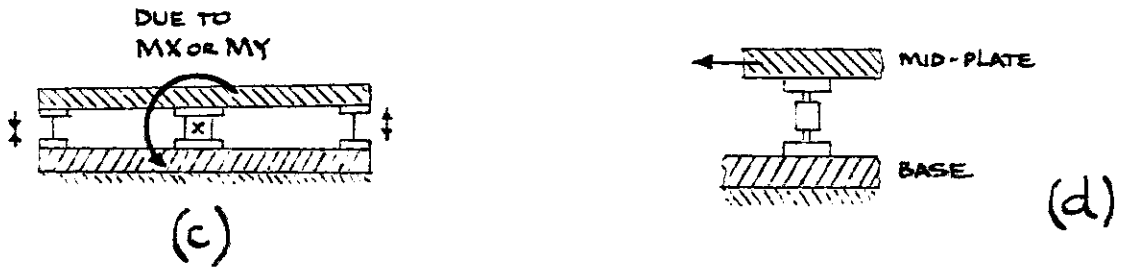
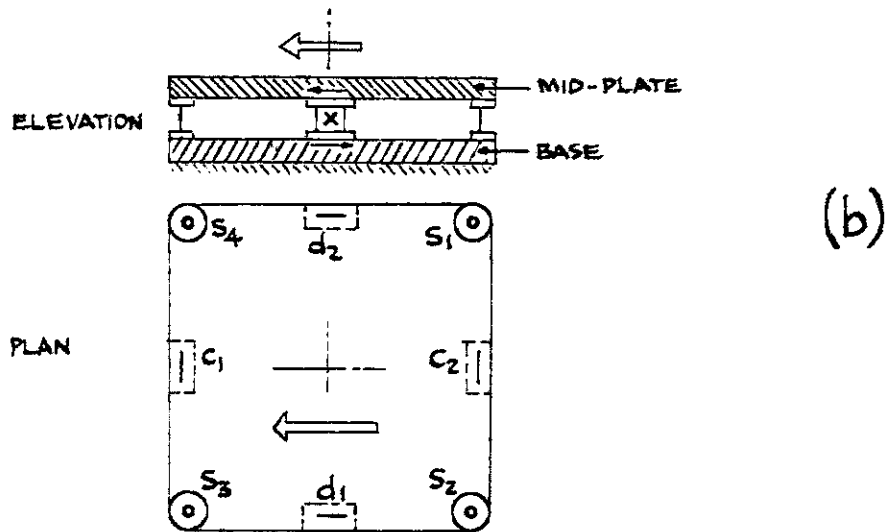
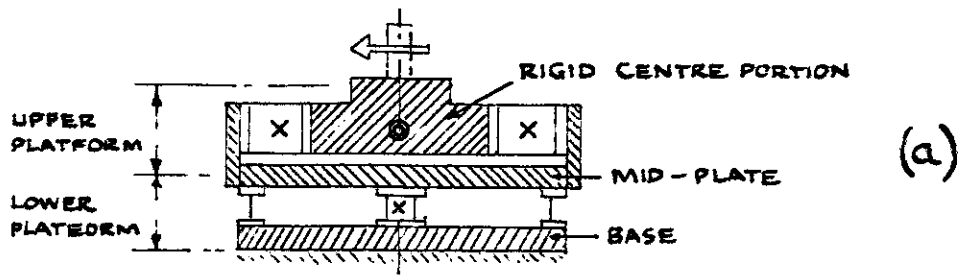


Fig. 9 LAYOUT OF FLEXURES

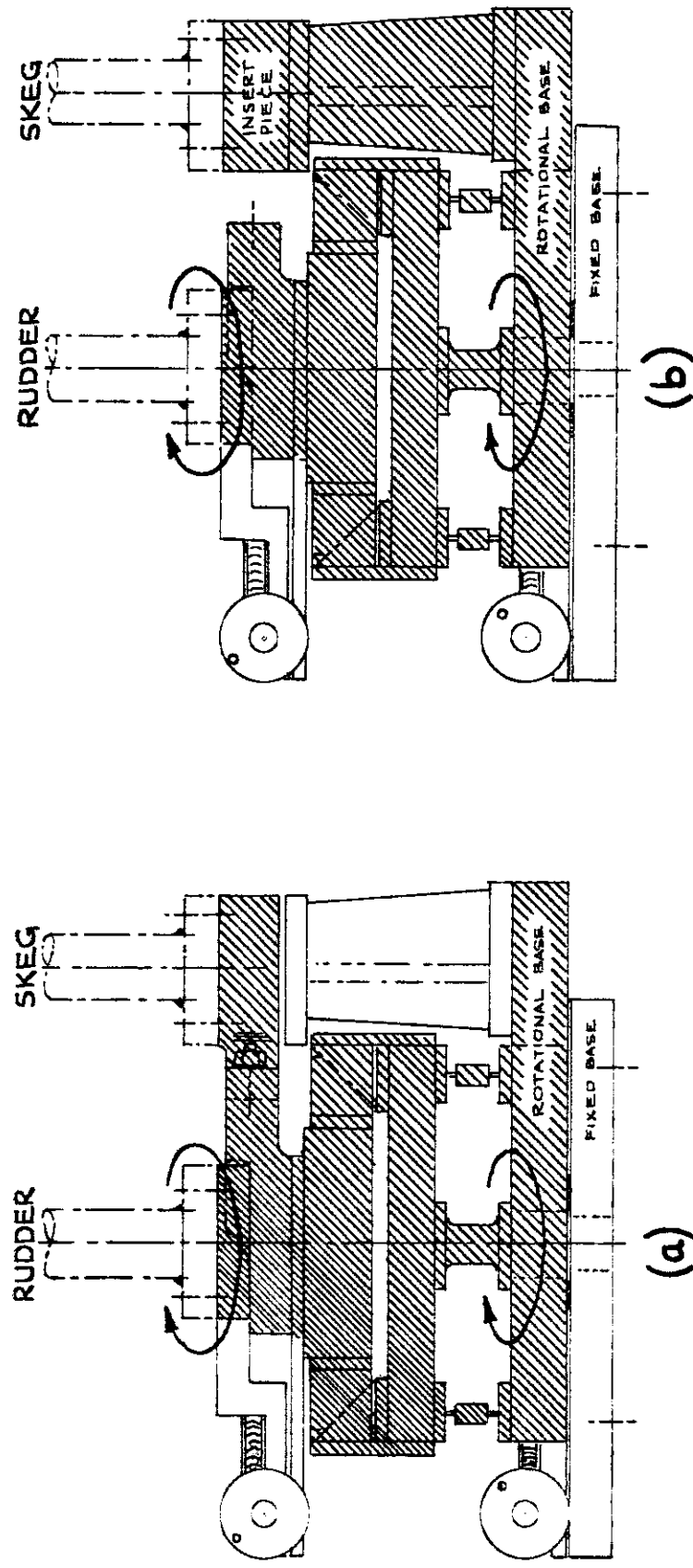
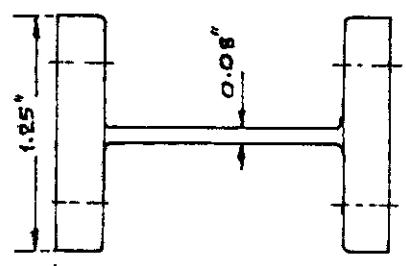
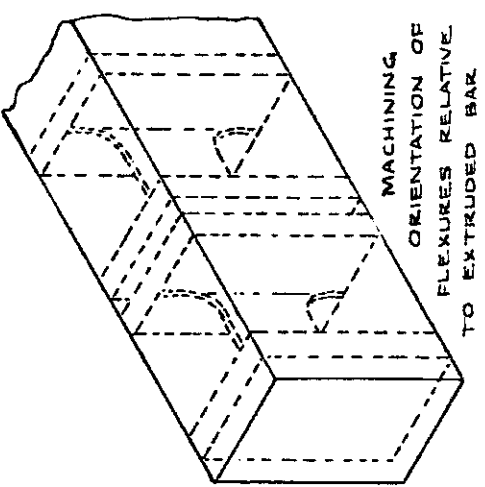
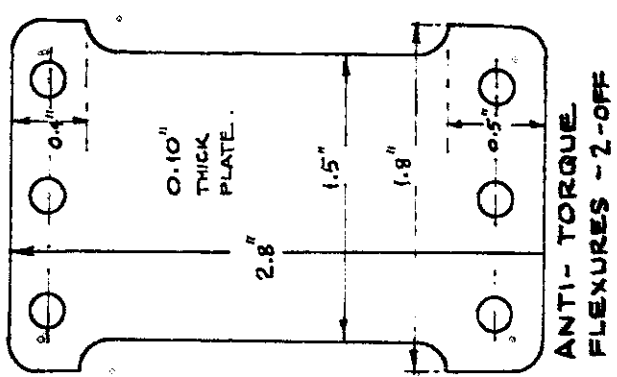
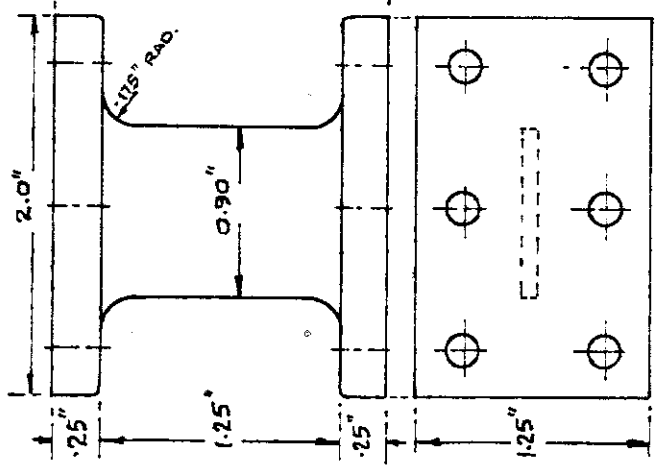


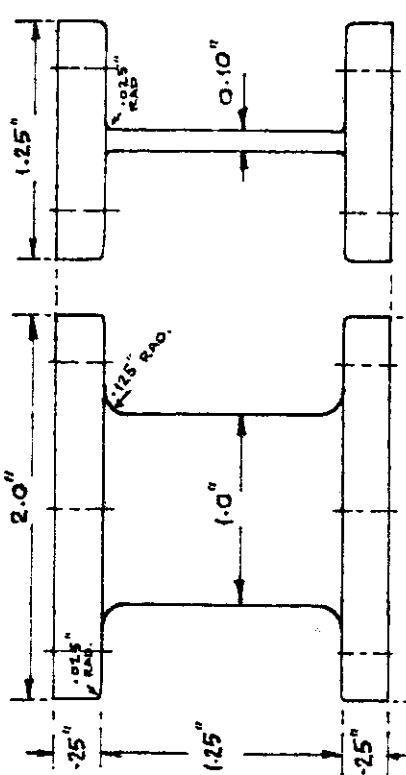
Fig. 10 ALTERNATIVE WORKING ARRANGEMENTS FOR THE DYNAMOMETER



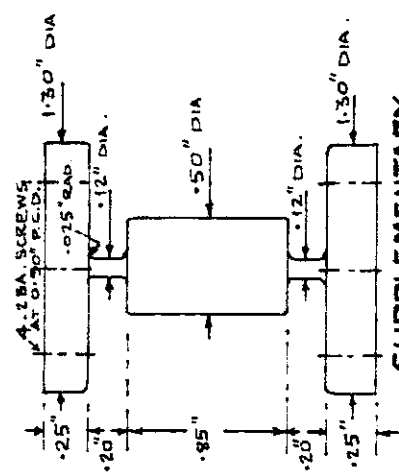
DRAG FLEXURES  
TYPE (d)  
2-OFF



LIFT FLEXURES  
TYPE (c)  
2-OFF



MOMENT FLEXURES  
TYPE (a) 0.10" TH. 2-OFF  
TYPE (b) 0.125" TH. 2-OFF



SUPPLEMENTARY  
PILLARS  
4-OFF

NOTES:

ALL FLEXURES AND PILLARS MANUFACTURED FROM HE30 ALUMINIUM ALLOY  
ALL FLEXURES AND PILLARS ATTACHED TO ADJACENT STRUCTURE BY 2.BA. SCREWS.

Fig. 11 PRINCIPAL DIMENSIONS OF FLEXURES AND PILLARS

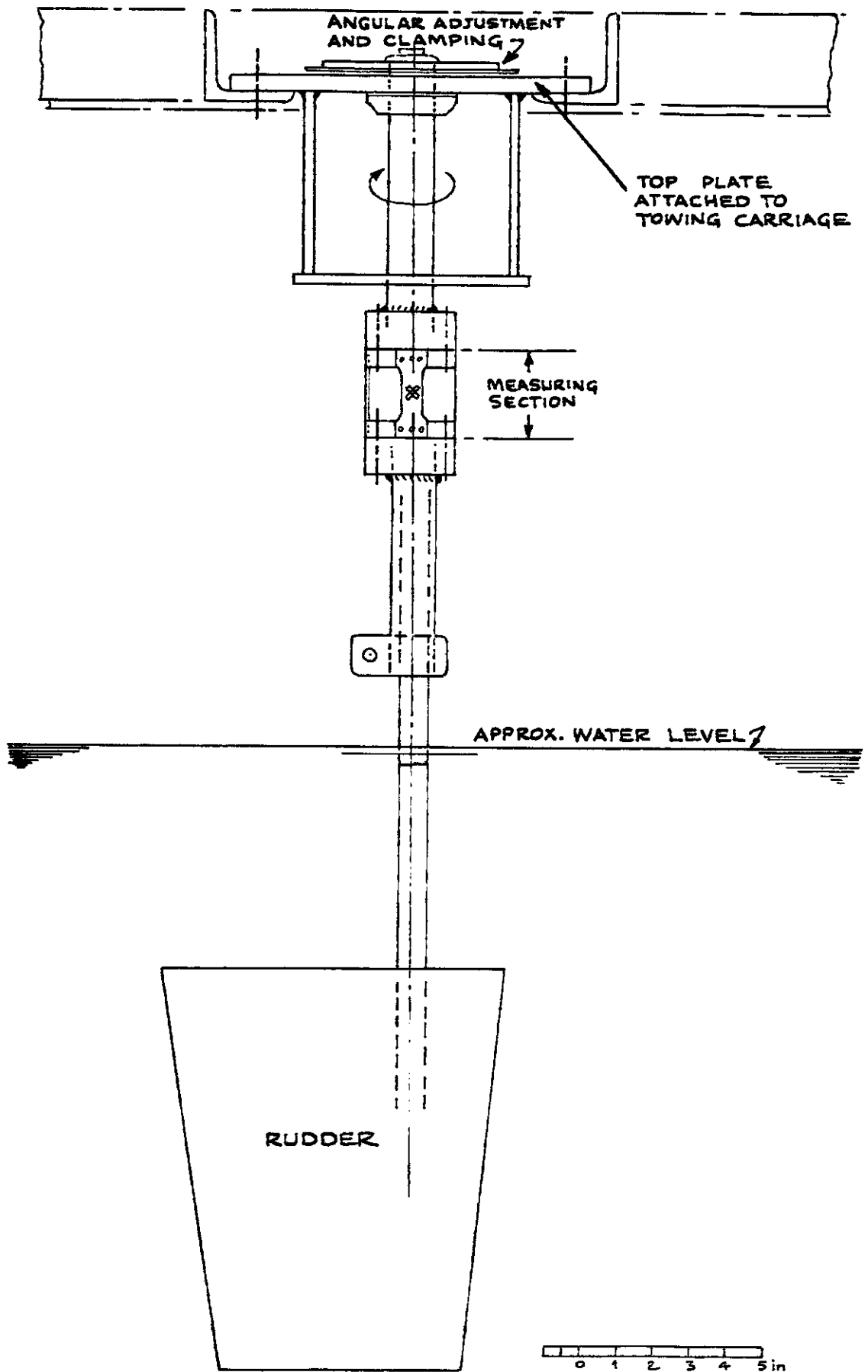


Fig. 12 OUTLINE PARTICULARS OF SMALL THREE-COMPONENT DYNAMOMETER FOR USE IN TEST TANK AT SOUTHAMPTON COLLEGE OF TECHNOLOGY



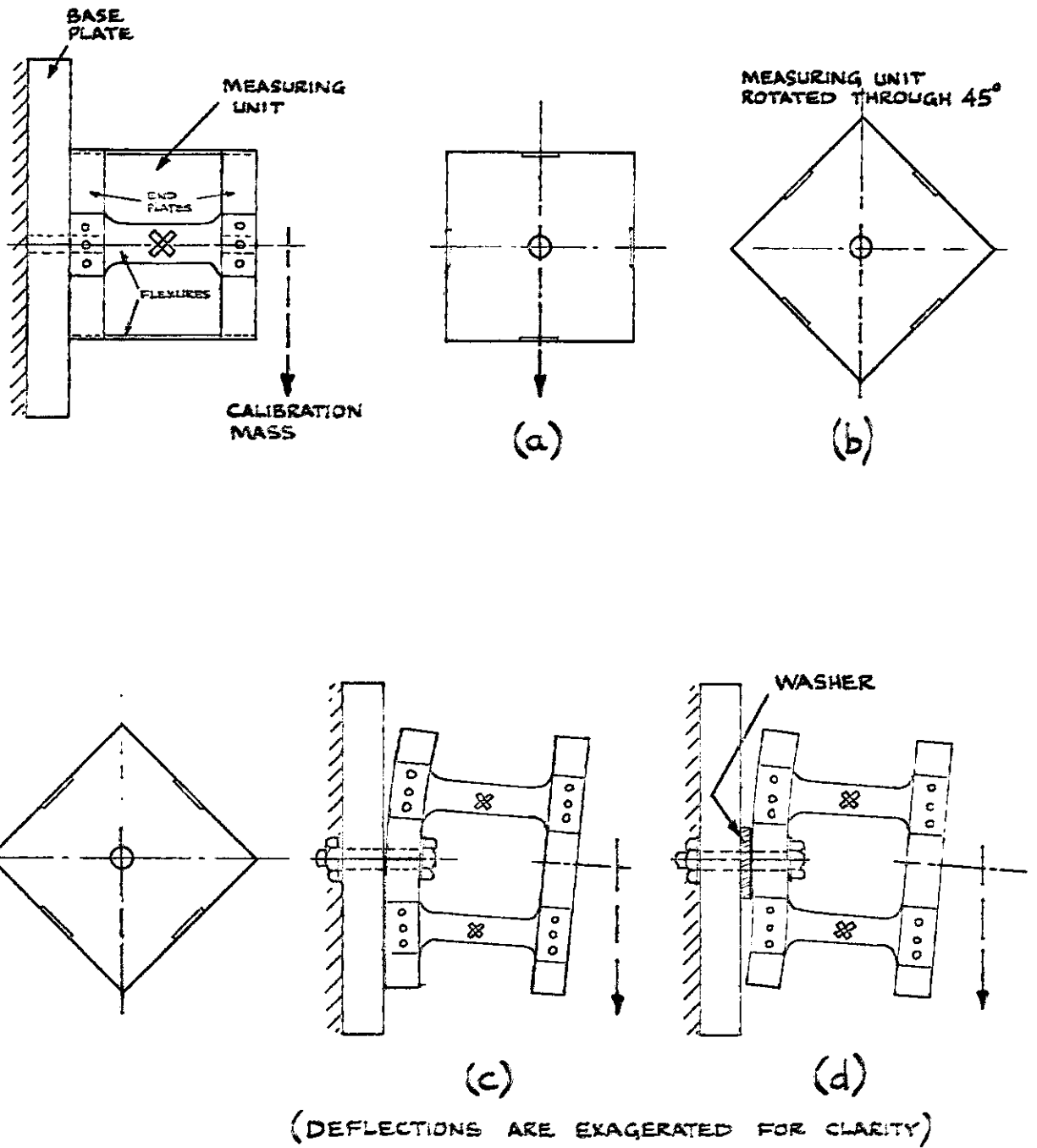
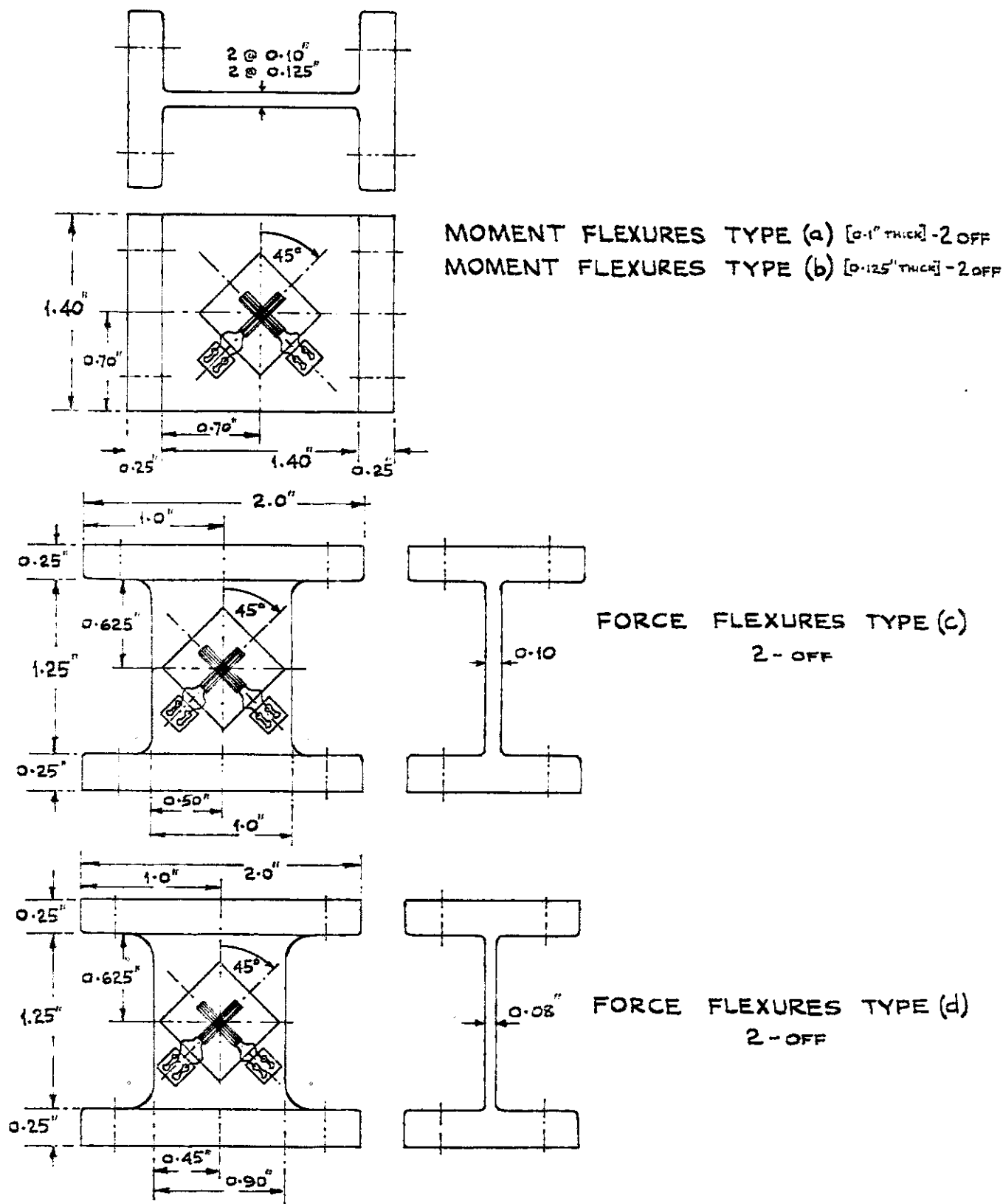


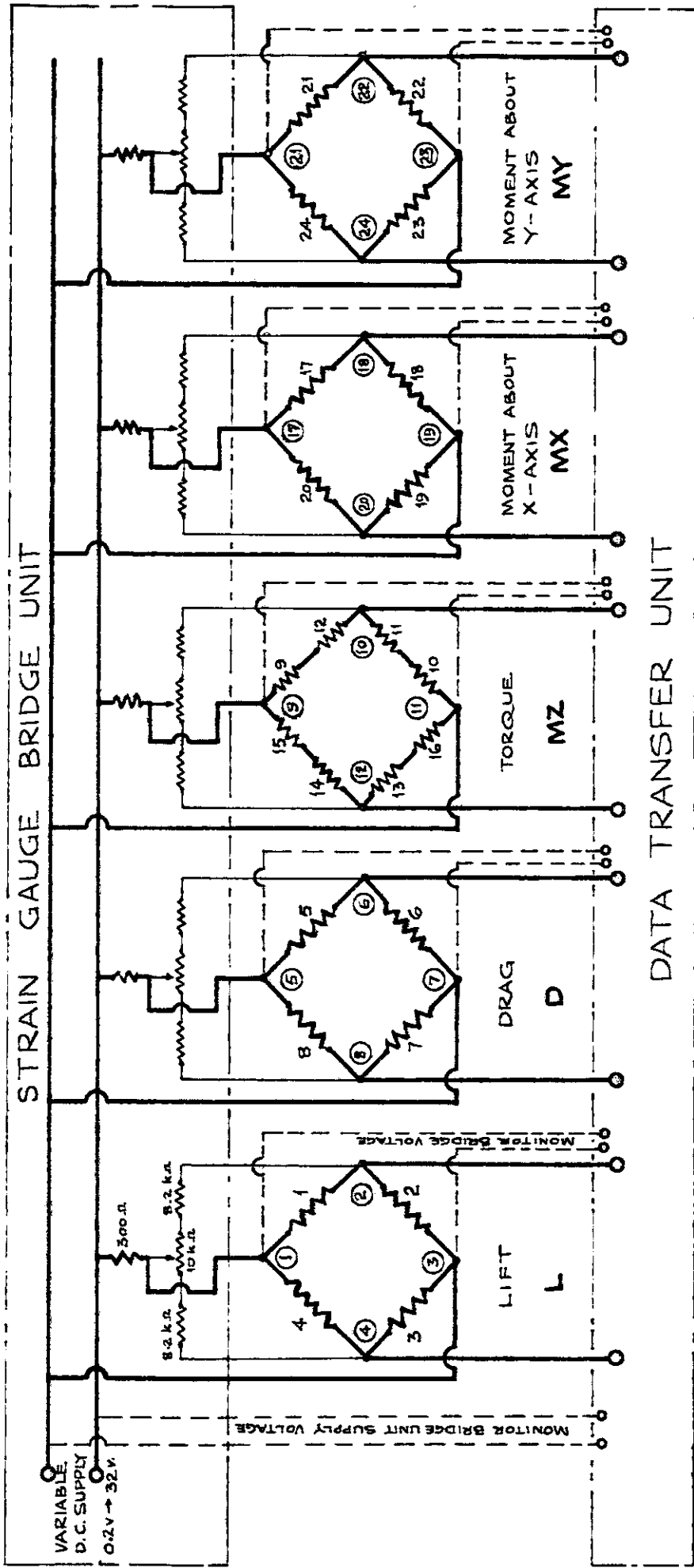
Fig. 13 WARPING OF END PLATE



NOTES:

ALL GAUGES : TML TYPE FCA - 10-23, CROSSED FOIL  
GAUGES AND TERMINALS ATTACHED TO EACH SIDE OF EACH FLEXURE.  
SEE Fig.16 FOR LOCATION OF FLEXURE TYPES

Fig.14 POSITIONS OF STRAIN GAUGES  
ON FLEXURES

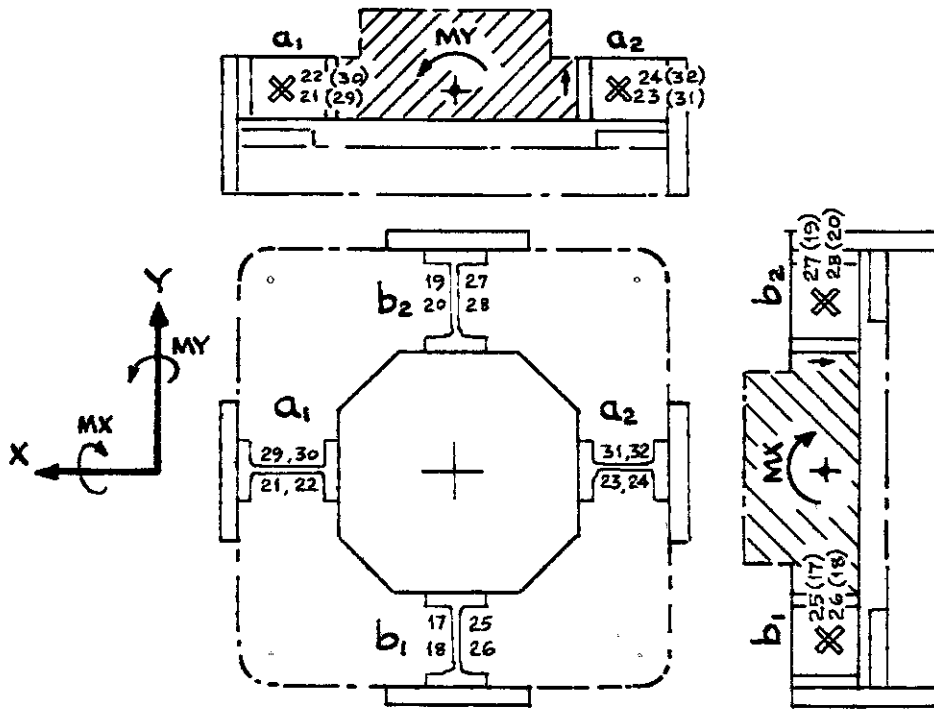


OUTPUT ON DIGITAL VOLTMETER,  
PAPER PRINT OUT OR HIGH  
SPEED PUNCHED TAPE.

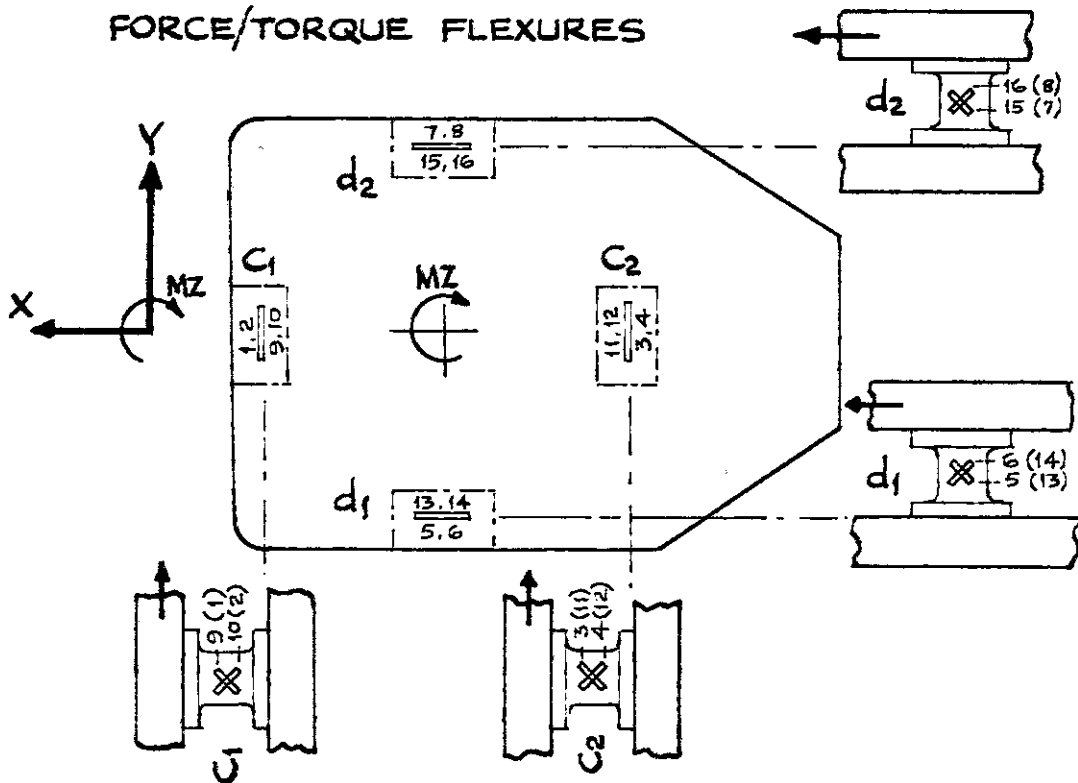
NOTES:  
GAUGES DENOTED AS 1, 2, 3 -----  
BRIDGE TERMINALS DENOTED AS ①, ②, ③ -----  
FOR GAUGE NUMBERING RELATIVE TO FLEXURES SEE KEY DIAGRAMS FIG. 16  
(SPARE GAUGES: 25 TO 32  
SPARE BRIDGE TERMINALS: ④ TO ⑩ AND ②⑤ TO ②⑩)

Fig. 15 DIAGRAMMATIC LAYOUT OF STRAIN GAUGE BRIDGE CIRCUITS AND INSTRUMENTATION

### MOMENT FLEXURES



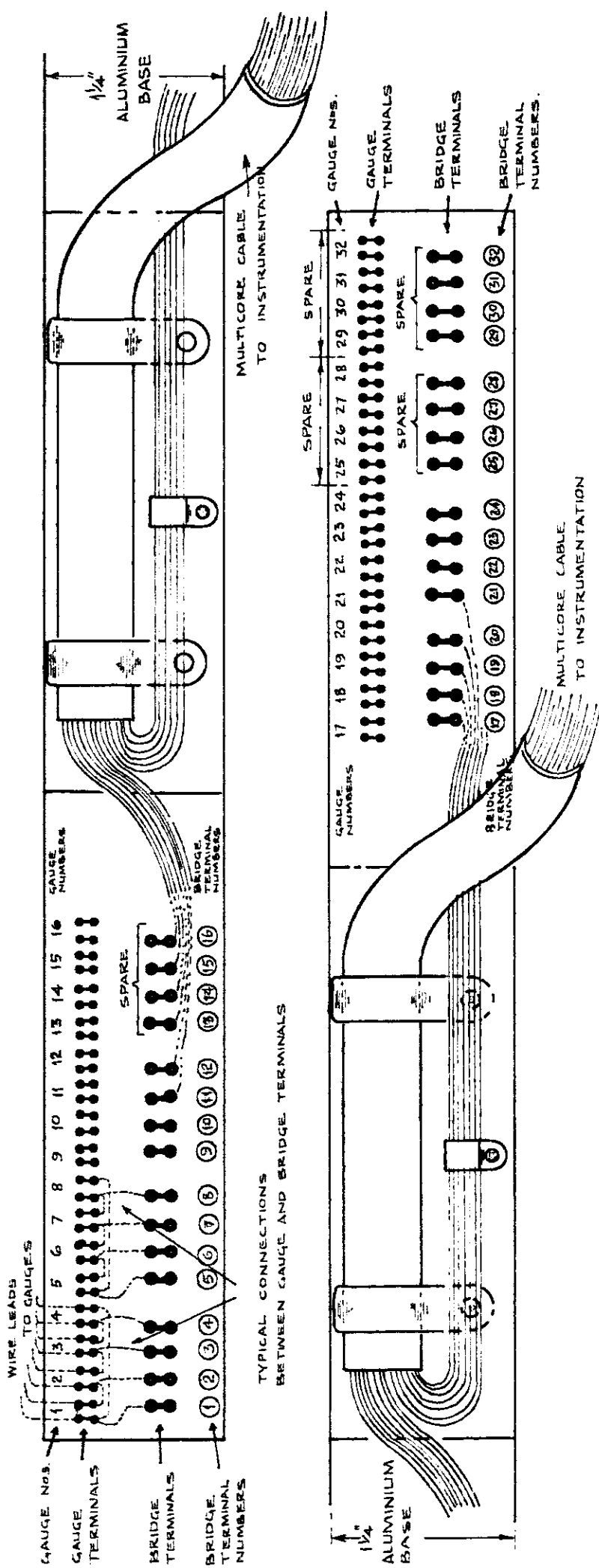
### FORCE/TORQUE FLEXURES



**NOTES:**

FLEXURE REFERENCE LETTERS PER Fig.11 AND DYNAMOMETER DRAWING  
 SPARE GAUGES : 25 TO 32

**Fig.16 KEY DIAGRAMS SHOWING GAUGE NUMBERING**



NOTES:  
 GAUGE NUMBERS DENOTED 1, 2, 3, ..... } PER KEY DIAGRAM, FIG. 16  
 BRIDGE TERMINAL NUMBERS DENOTED ① ② ③ ..... } AND CIRCUIT DIAGRAM, FIG. 15

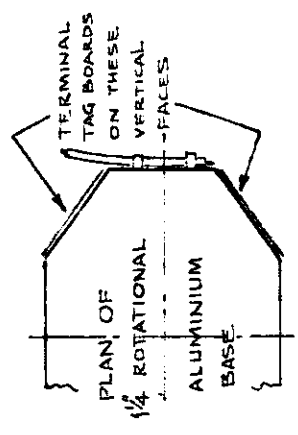


Fig. 17 OUTLINE DETAILS OF TERMINAL TAG BOARDS

BRIDGE CIRCUIT TERMINAL NUMBERS (Ref. Figs. 15 & 17) ON DYNAMOMETER	EQUIVALENT PLUG PIN NUMBERS FOR INSTRUMENTATION CONNECTING PLUG ON MULTI-CORE CABLE	CABLE COLOUR
①	2	BLUE
②	3	GREEN
③	4	YELLOW
④	1	RED
⑤	6	BLACK
⑥	7	BROWN
⑦	8	VIOLET
⑧	5	WHITE
⑨	10	PINK
⑩	11	TURQUOISE
⑪	12	GREY
⑫	9	ORANGE
⑬	22	ORANGE / BLUE
⑭	23	YELLOW / GREEN
⑮	24	WHITE / GREEN
⑯	21	BLUE / BLACK
⑰	14	GREEN / RED
⑱	15	YELLOW / RED
⑲	16	WHITE / RED
⑳	13	RED / BLUE
㉑	18	RED / BROWN
㉒	19	YELLOW / BLUE
㉓	20	WHITE / BLUE
㉔	17	RED / BLACK
㉕	26	GREEN / BLUE
㉖	27	GREY / BLUE
㉗	28	GREEN / BLACK
㉘	25	ORANGE / GREEN
㉙	30	YELLOW / BROWN
㉚	31	WHITE / BROWN
㉛	32	BROWN / BLACK
㉜	29	GREY / GREEN
		SPARES
		YELLOW / VIOLET
		GREY / BROWN
		VIOLET / BLACK
		WHITE / VIOLET

**Fig. 18**  
**TABLE SHOWING RELATIONSHIP**  
**BETWEEN INSTRUMENTATION CONNECTING**  
**PLUG PIN NUMBERS AND DYNAMOMETER BRIDGE TERMINAL NUMBERS**

DATA TRANSFER UNIT CHANNEL NUMBER	POLARITY	CABLE COLOUR	CABLE REFERENCE NUMBER	FUNCTION
0	+	BROWN	0	BRIDGE OUTPUTS
	-	RED		
1	+	ORANGE	1	
	-	YELLOW		
2	+	GREEN	2	
	-	BLUE		
3	+	MAUVE	3	
	-	WHITE		
4	+	BLACK	4	
	-	BROWN		
5	+	MAUVE	③	BRIDGE SUPPLY VOLTAGE MONITORING
	-	WHITE	①	
6	+	GREY	⑦	
	-	YELLOW	⑤	
7	+	BLUE	⑪	
	-	RED	⑨	
8	+	PINK	⑲	
	-	BLACK	⑰	
9	+	ORANGE	⑳	
	-	GREEN	㉑	

Fig. 19 TABLE SHOWING POLARITIES OF CABLE CONNECTIONS BETWEEN BRIDGE UNIT AND DATA TRANSFER UNIT

```

L0
00 +00000 0 01 +00006 0 02 -00002 0 03 +00035 0 04 -00007 0
05 +07001 3 06 +06998 3 07 +10960 3 08 +07011 3 09 +07009 3
00 +00003 0 01 +00006 0 02 -00003 0 03 +00036 0 04 -00006 0
05 +07001 3 06 +06999 3 07 +10960 3 08 +07011 3 09 +07009 3
L40
      L           D           MZ           MX           MY
00 +00004 0 01 +00005 0 02 -00001 0 03 +00751 0 04 +00003 0
05 +07001 3 06 +06999 3 07 +10960 3 08 +07011 3 09 +07009 3
L80
      RESPECTIVE VOLTAGES
00 +00012 0 01 +00006 0 02 -00000 0 03 +01456 0 04 +00017 0
05 +07001 3 06 +06998 3 07 +10960 3 08 +07011 3 09 +07009 3
00 +00010 0 01 +00006 0 02 +00000 0 03 +01450 0 04 +00017 0
05 +07001 3 06 +06999 3 07 +10960 3 08 +07011 3 09 +07010 3
L100
00 +00010 0 01 +00006 0 02 -00000 0 03 +01811 0 04 +00024 0
05 +07001 3 06 +06998 3 07 +10960 3 08 +07011 3 09 +07009 3
00 +00002 0 01 +00008 0 02 -00000 0 03 +01810 0 04 +00025 0
05 +07001 3 06 +06999 3 07 +10960 3 08 +07011 3 09 +07009 3
L80
00 +00005 0 01 +00006 0 02 +00000 0 03 +01454 0 04 +00017 0
05 +07001 3 06 +06999 3 07 +10960 3 08 +07011 3 09 +07009 3
00 +00006 0 01 +00005 0 02 +00000 0 03 +01442 0 04 +00021 0
05 +07001 3 06 +06999 3 07 +10960 3 08 +07011 3 09 +07009 3
L40
00 +00007 0 01 +00004 0 02 +00000 0 03 +00747 0 04 +00004 0
05 +07001 3 06 +06999 3 07 +10960 3 08 +07011 3 09 +07009 3
00 +00007 0 01 +00004 0 02 +00000 0 03 +00748 0 04 +00005 0
05 +07001 3 06 +06999 3 07 +10960 3 08 +07011 3 09 +07009 3
L0
00 +00001 0 01 +00005 0 02 -00002 0 03 +00037 0 04 -00006 0
05 +07001 3 06 +06999 3 07 +10960 3 08 +07011 3 09 +07009 3
00 +00001 0 01 +00007 0 02 -00003 0 03 +00037 0 04 -00007 0
05 +07001 3 06 +06999 3 07 +10960 3 08 +07011 3 09 +07009 3
-MX
L0
00 -00000 0 01 +00005 0 02 -00003 0 03 -00012 0 04 -00011 0
05 +07001 3 06 +06999 3 07 +10960 3 08 +07011 3 09 +07009 3
00 +00003 0 01 +00005 0 02 -00002 0 03 -00011 0 04 -00009 0
05 +07001 3 06 +06999 3 07 +10961 3 08 +07011 3 09 +07010 3
L-40
00 -00001 0 01 +00016 0 02 -00007 0 03 -00726 0 04 -00003 0
05 +07001 3 06 +06999 3 07 +10961 3 08 +07011 3 09 +07010 3
L-80
00 -00000 0 01 +00030 0 02 -00009 0 03 -01435 0 04 +00000 0
05 +07001 3 06 +06998 3 07 +10960 3 08 +07011 3 09 +07009 3
L-100
00 -00009 0 01 +00037 0 02 -00008 0 03 -01788 0 04 +00005 0
05 +07001 3 06 +06999 3 07 +10960 3 08 +07011 3 09 +07009 3
00 -00005 0 01 +00035 0 02 -00009 0 03 -01788 0 04 +00005 0
05 +07001 3 06 +06999 3 07 +10960 3 08 +07011 3 09 +07009 3
L-80
00 -00004 0 01 +00031 0 02 -00009 0 03 -01437 0 04 +00001 0
05 +07001 3 06 +06999 3 07 +10960 3 08 +07011 3 09 +07009 3
L-40
00 -00000 0 01 +00017 0 02 -00006 0 03 -00722 0 04 -00004 0
05 +07001 3 06 +06999 3 07 +10960 3 08 +07011 3 09 +07009 3
L0
00 +00001 0 01 +00003 0 02 -00003 0 03 -00010 0 04 -00010 0
05 +07001 3 06 +06999 3 07 +10961 3 08 +07011 3 09 +07009 3

```

Fig. 20 EXAMPLE OF A CALIBRATION DATA PRINT OUT



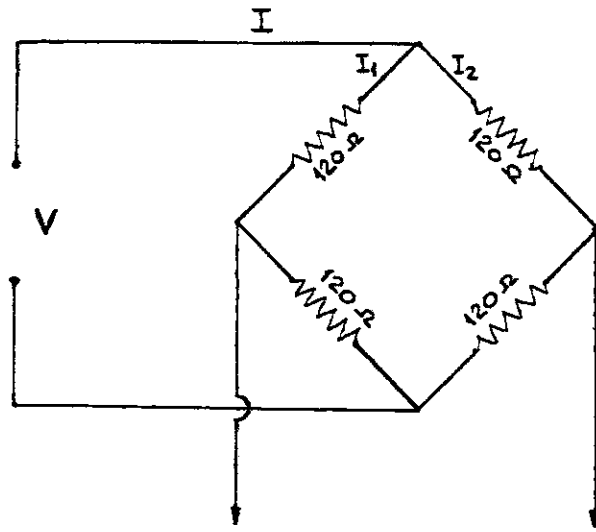


Fig. 21

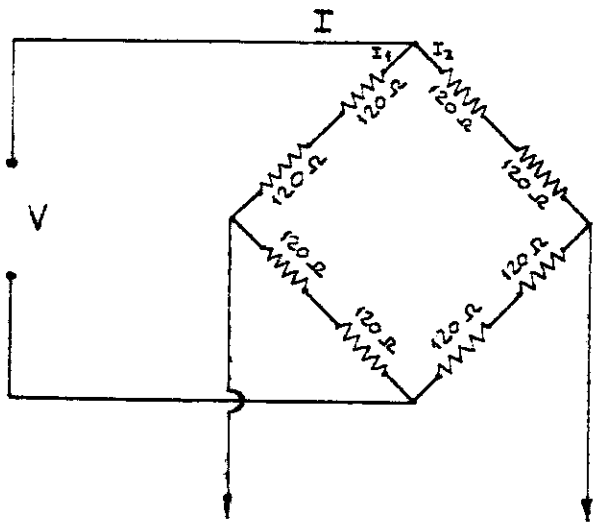


Fig. 22

LOADING OF INDIVIDUAL COMPONENTS FOR DERIVATION OF FIRST ORDER INTERACTIONS	LOADING OF COMPONENTS IN PAIRS FOR DERIVATION OF SECOND ORDER INTERACTIONS
L	L + D
D	L + MZ
MZ	L + MX
MX	L + MY
MY	D + MZ
	D + MX
	D + MY
	MZ + MX
	MZ + MY
	MX + MY

WHERE:

L .... LIFT

D .... DRAG

MZ ... TORQUE

MX ... MOMENT ABOUT X-AXIS

MY ... MOMENT ABOUT Y-AXIS

Fig. 23 LOADINGS FOR DERIVATION OF INTERACTIONS

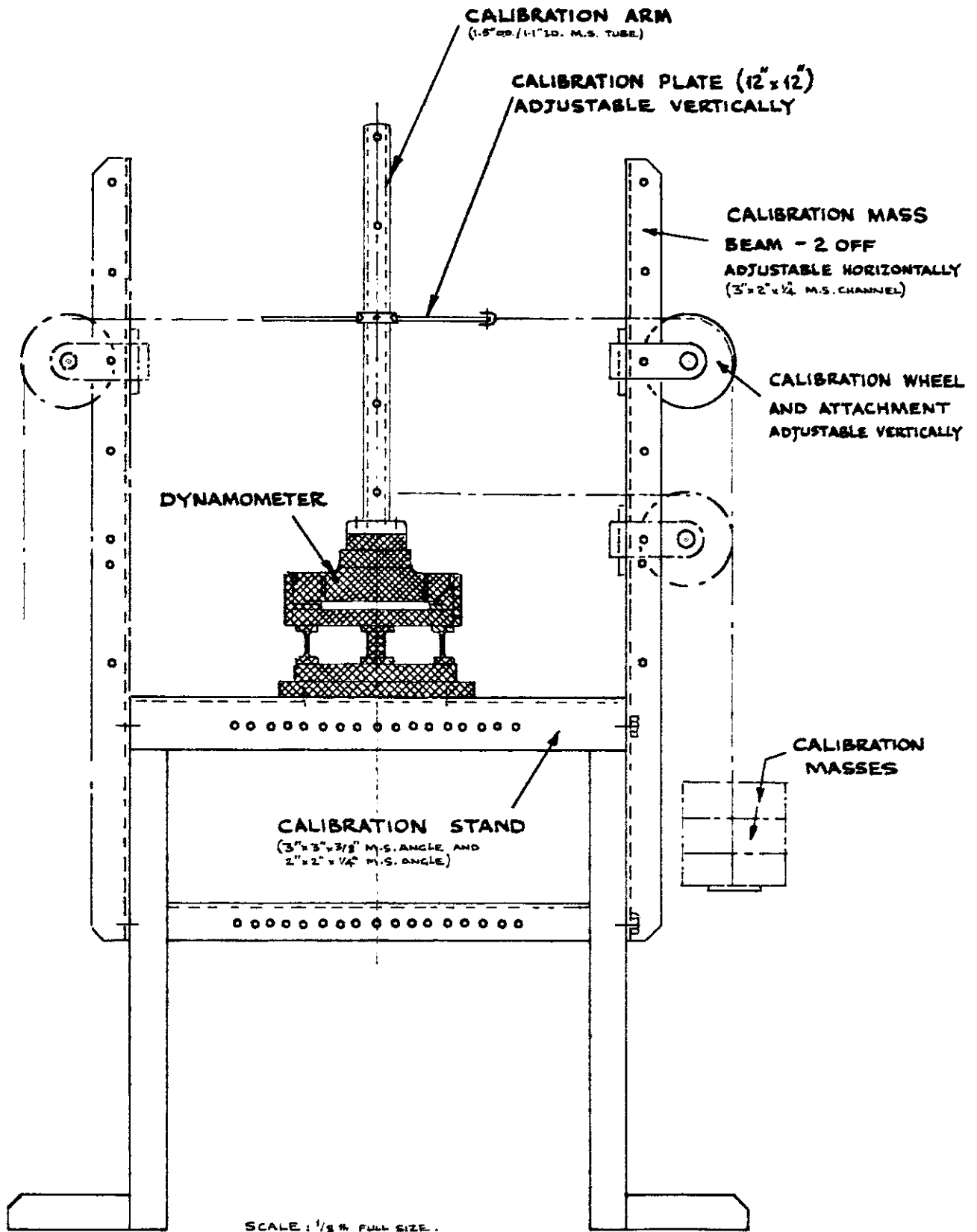


Fig. 24 CALIBRATION RIG

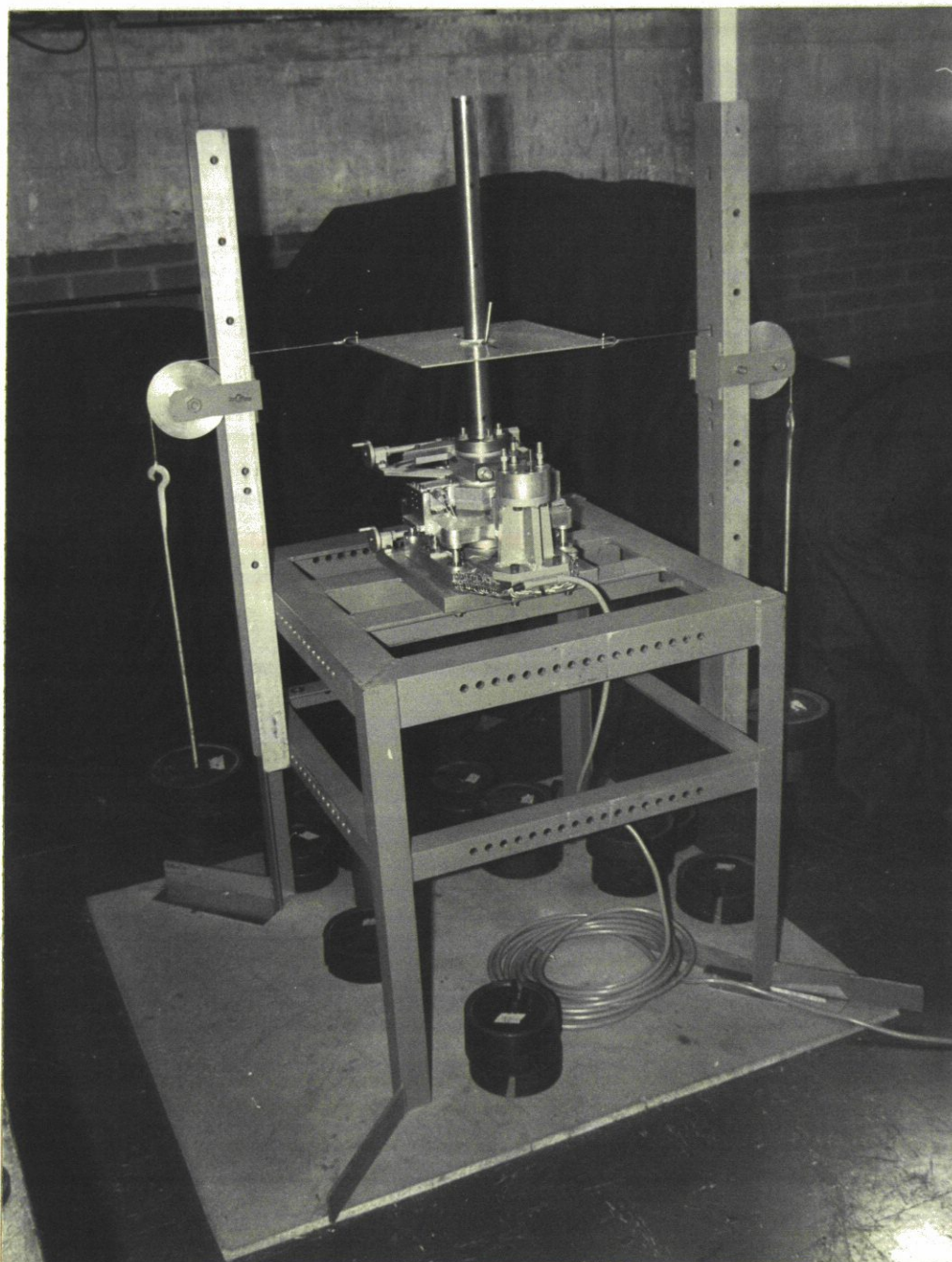


Fig. 25 CALIBRATION RIG

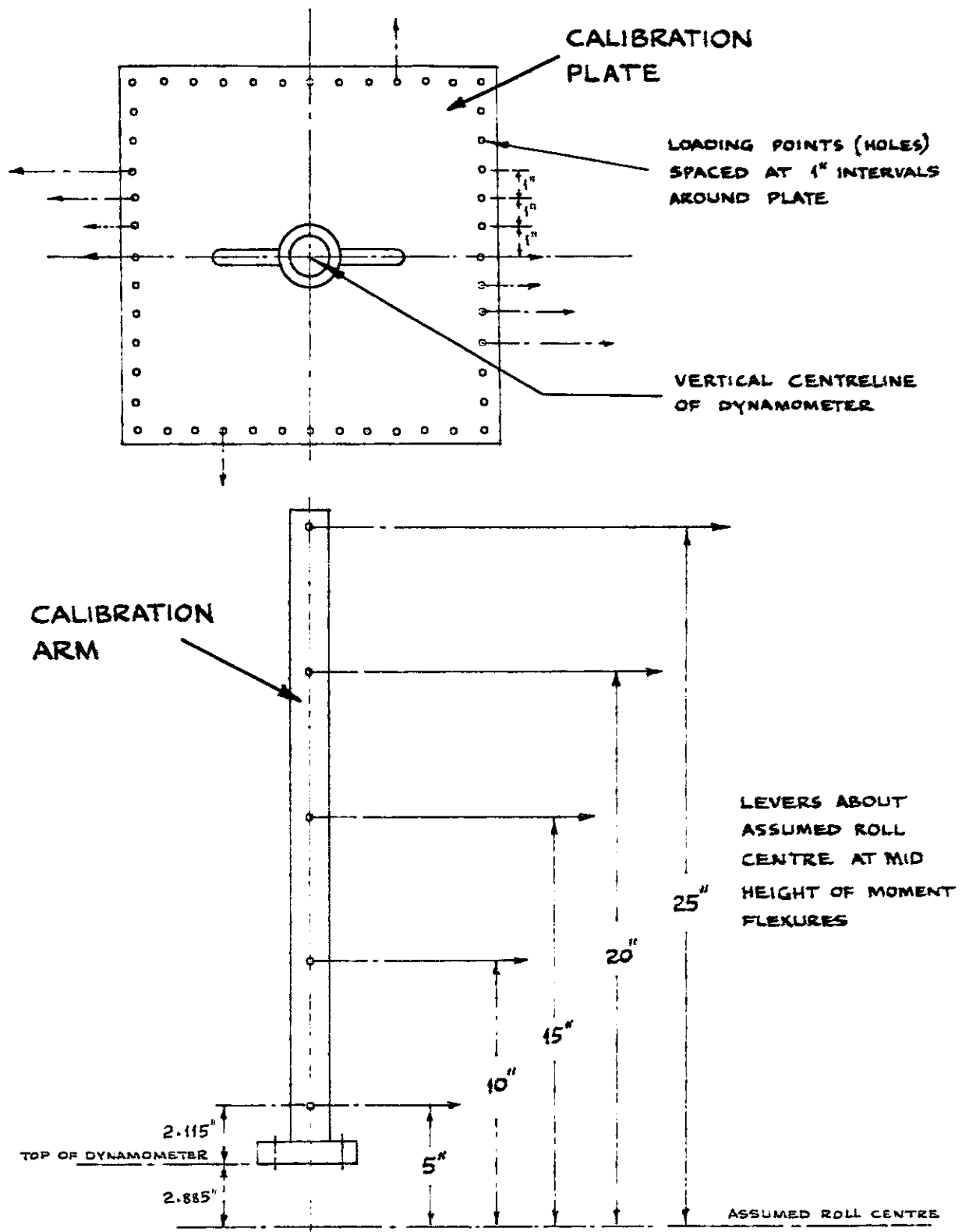
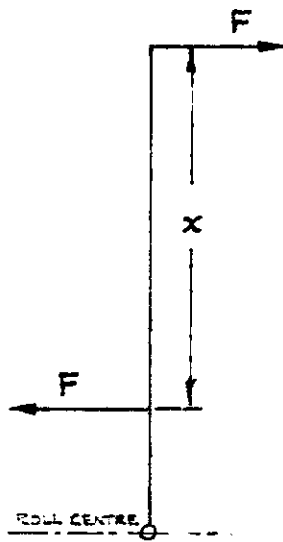


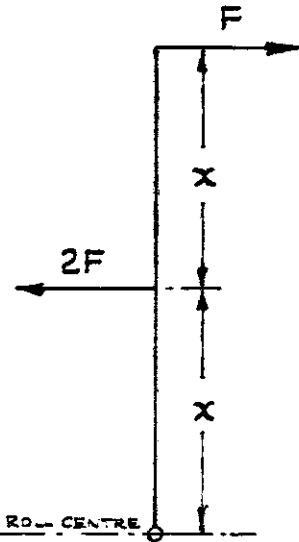
Fig. 26 POSITIONS OF LOADING POINTS ON CALIBRATION PLATE AND CALIBRATION ARM

	KEY DIAGRAMS	COMPONENTS	REMARKS
APPLICATION OF SINGLE COMPONENTS		$\pm D$	-
		$\pm L$	-
		$\pm MZ$	NOTE APPLICATION OF COUPLE TO ELIMINATE MX OR MY
		$\pm MX$ $\pm MY$	NOTE EQUAL AND OPPOSITE OFFSET LOAD REQUIRED TO ELIMINATE L OR D
APPLICATION OF COMBINATIONS OF COMPONENTS IN PAIRS		$L + D$	-
		$D + MY,$ $L + MX$	-
		$MZ + MX,$ $MZ + MY$	NOTE EQUAL AND OPPOSITE OFFSET LOAD REQUIRED TO ELIMINATE L OR D
		$MZ + D,$ $MZ + L$	NOTE APPLICATION OF COUPLE TO ELIMINATE MX OR MY, EXTRA PULLEY REQUIRED TO APPLY L OR D SEPARATELY
		$MX + D,$ $MY + L$	EXTRA PULLEY REQUIRED TO APPLY L OR D SEPARATELY
		$MX + MY$	(a) TWO EXTRA PULLEYS REQUIRED TO APPLY LOWER OFFSET LOADS. ALTERNATIVELY, (b) DYNAMOMETER ROTATED IN RIG WHEREBY D AND L ELIMINATED, AND MX AND MY OBTAINED BY RESOLUTION OF MOM AT $\beta$
APPLICATION OF ALL FIVE COMPONENTS		$L, D,$ $MZ, MX,$ $MY$	DYNAMOMETER ROTATED IN RIG WHEREBY SUITABLE SINGLE POINT LOAD WILL APPLY ALL FIVE COMPONENTS

Fig. 27 KEY DIAGRAMS SHOWING APPLICATIONS OF VARIOUS LOADS AND THEIR COMBINATIONS



(a) MOMENT =  $F \times x$   
 FORCE =  $F - F = 0$



(b) MOMENT =  $2F \times x - F \times 2x = 0$   
 FORCE =  $2F - F = F$

Fig. 28

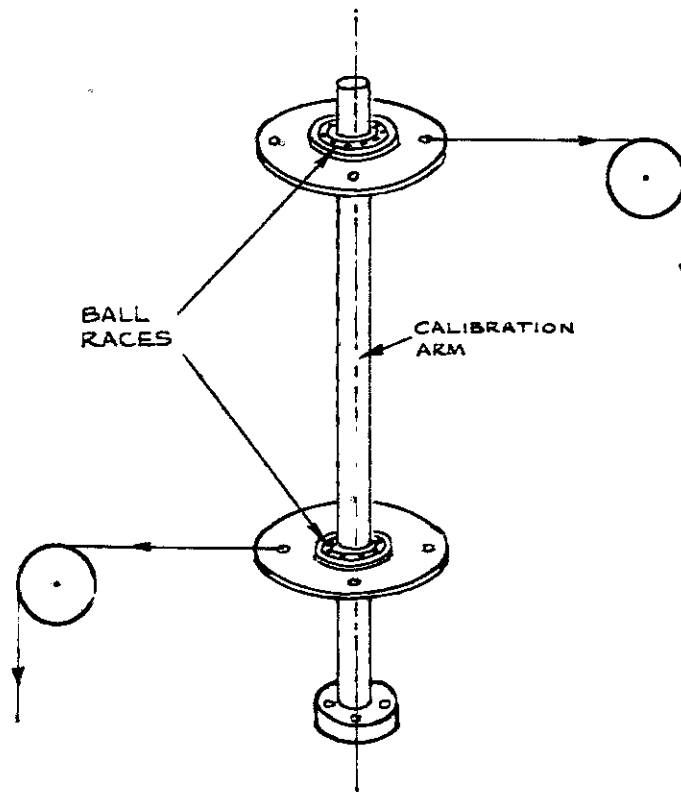


Fig. 29

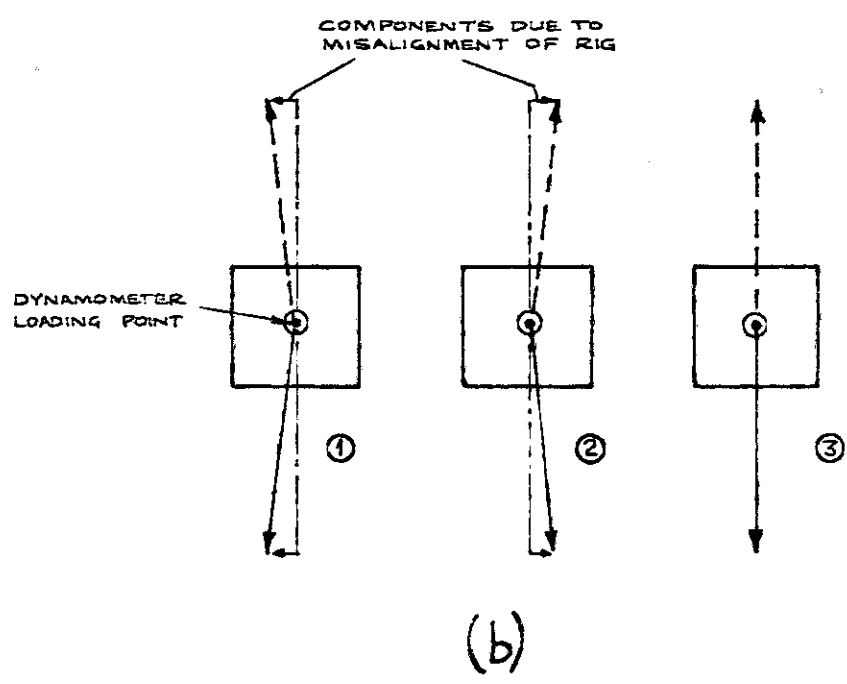
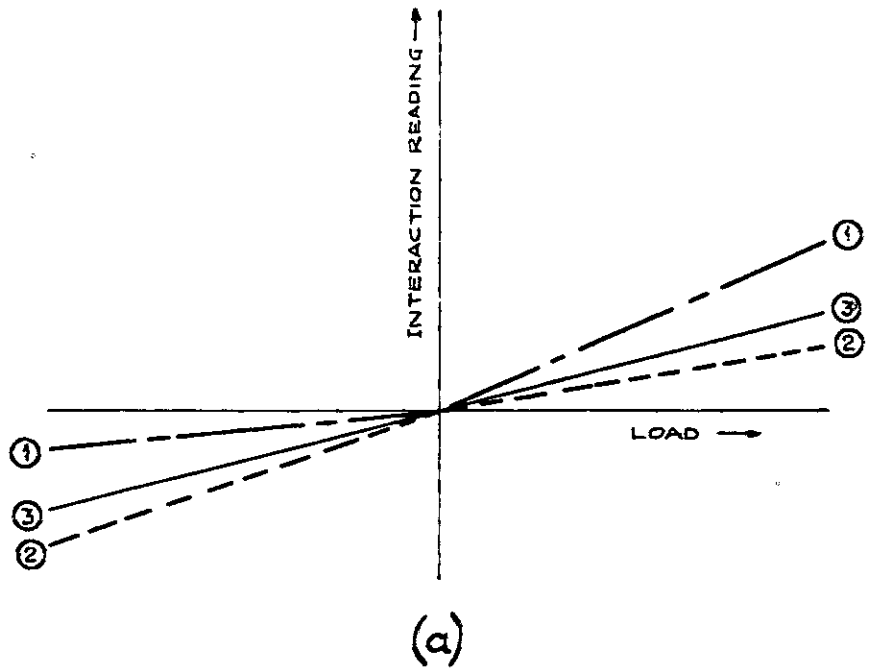


Fig. 30



	DYNAMOMETER			SKEG - CONNECTED TO ROTATIONAL BASE	
	LIFT 160 lbf. x 25 in LEVER TO ROLL CENTRE	DRAG 140 lbf. x 25 in LEVER TO ROLL CENTRE	TORQUE $\pm 1200$ lbf.in	LIFT 40 lbf. x 15 in LEVER TO ROLL CENTRE	DRAG 40 lbf. x 15 in LEVER TO ROLL CENTRE
RELATIVE TO FIXED BASE	0.045 in (1.14 mm)	0.044 in (1.12 mm)	MEAN $0.00013^\circ$ /lbf.in	0.007 in (0.19 mm)	0.010 in (0.25 mm)
RELATIVE TO ROTATIONAL BASE	0.012 in (0.30 mm)	0.010 in (0.25 mm)	—	0.003 in (0.08 mm)	0.005 in (0.13 mm)

Fig. 31 DEFLECTIONS OF DYNAMOMETER 5in ABOVE  
ROLL CENTRE FOR MAXIMUM LOADINGS

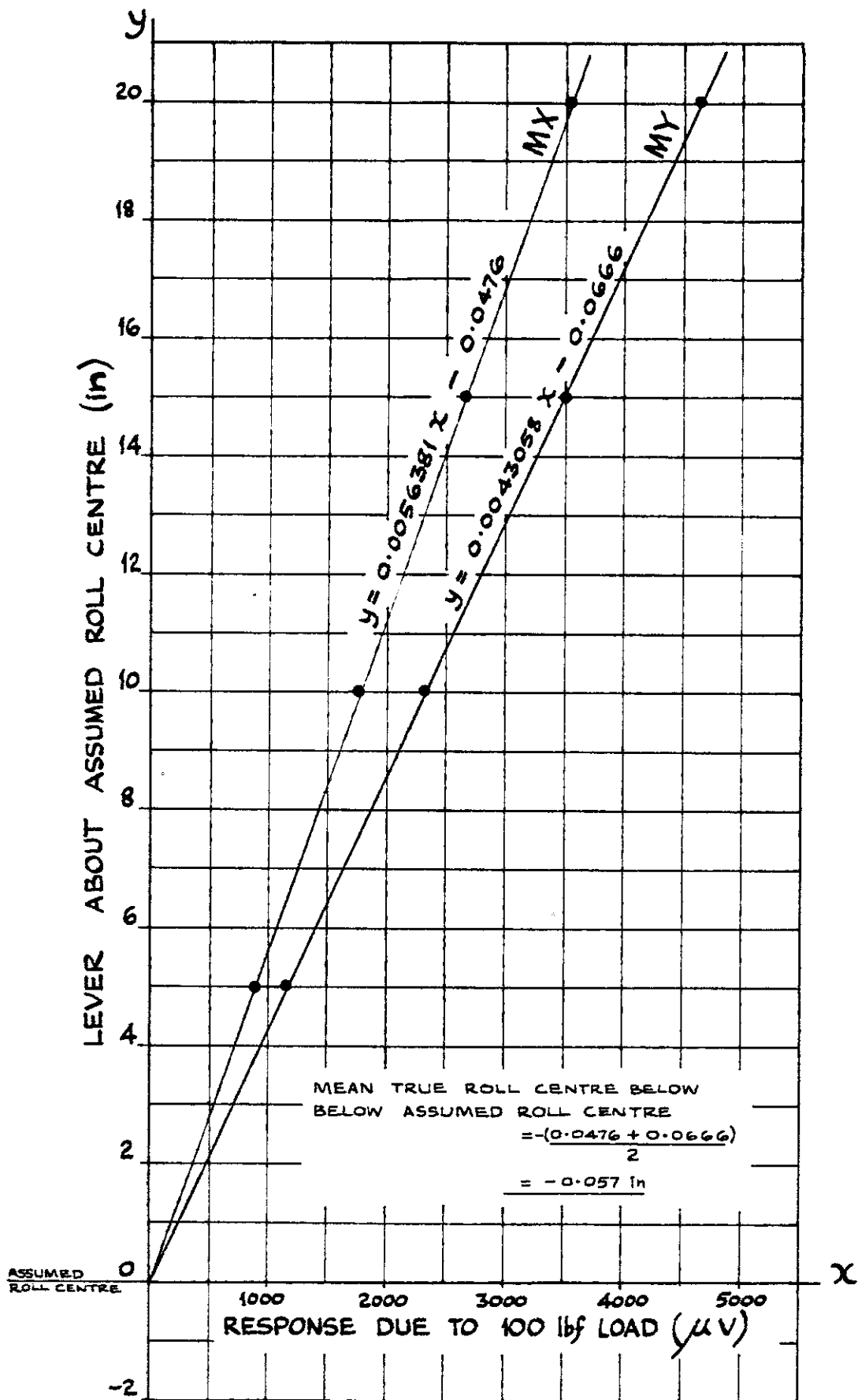


Fig. 32 DERIVATION OF TRUE ROLL CENTRE;  
 CROSS PLOTS OF RESPONSE DUE TO 100 lbf. LOAD  
 APPLIED AT VARYING LEVERS IN X AND Y DIRECTIONS.

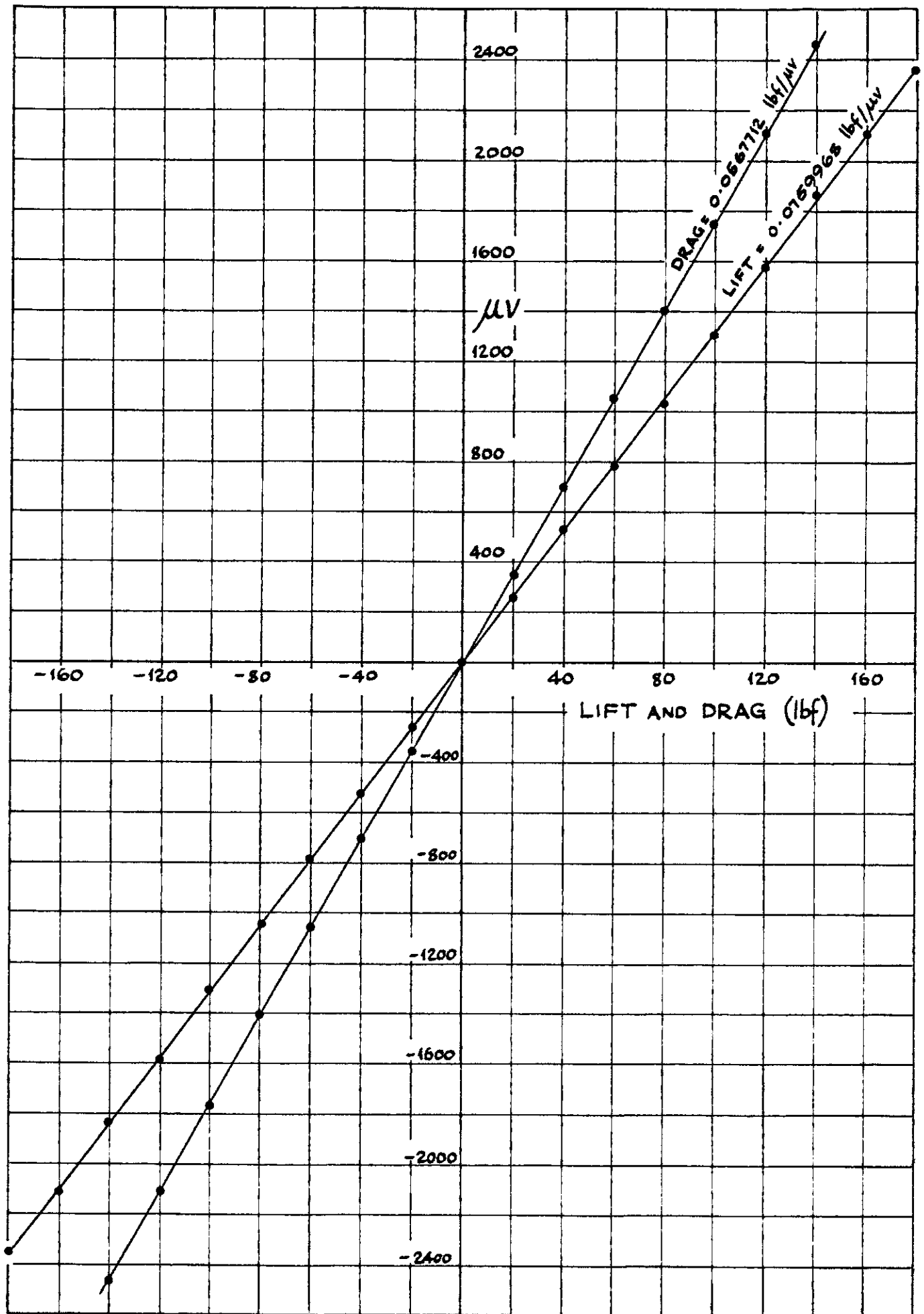


Fig. 33 LIFT AND DRAG CALIBRATION

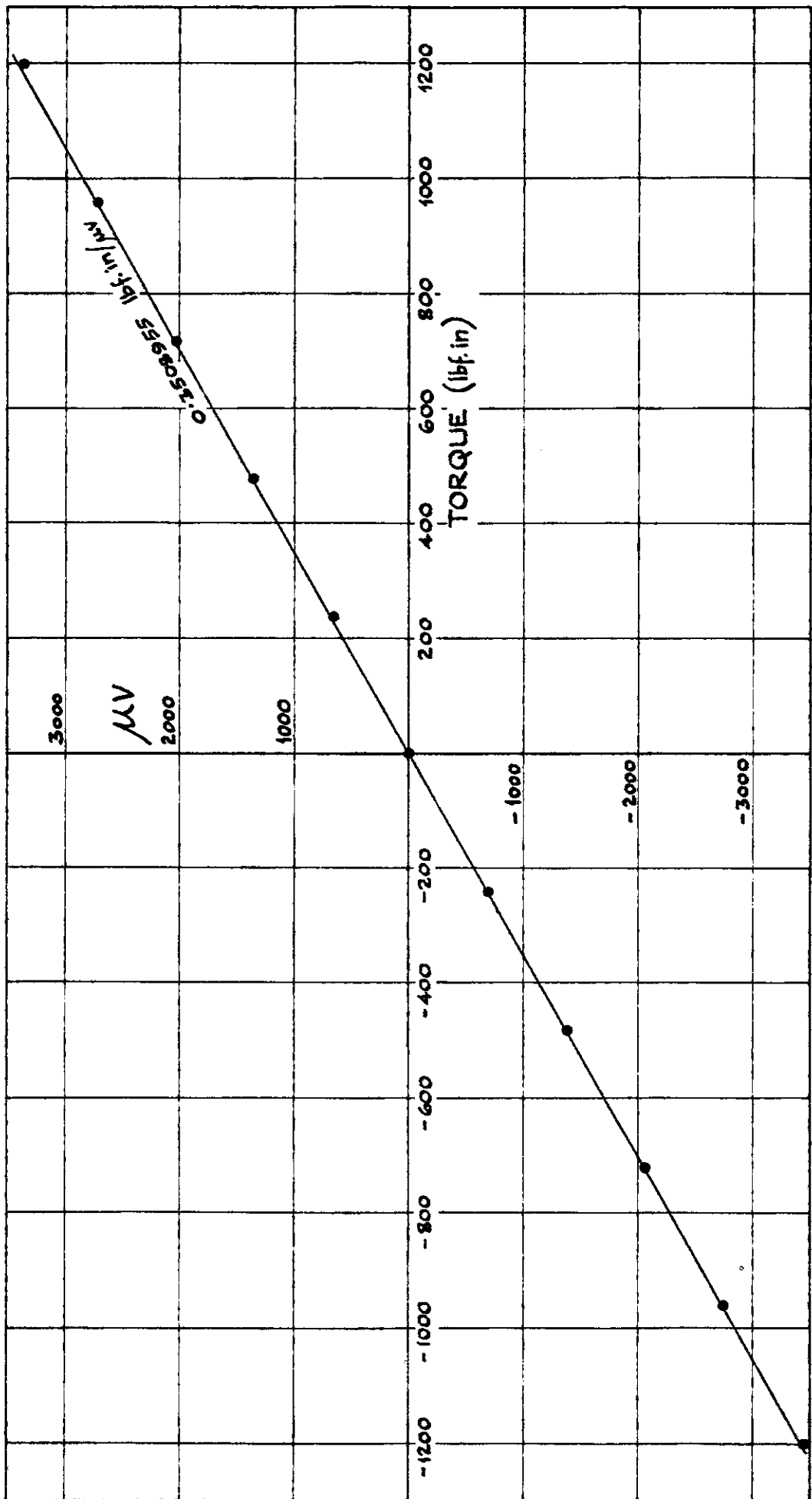


Fig. 34 TORQUE CALIBRATION

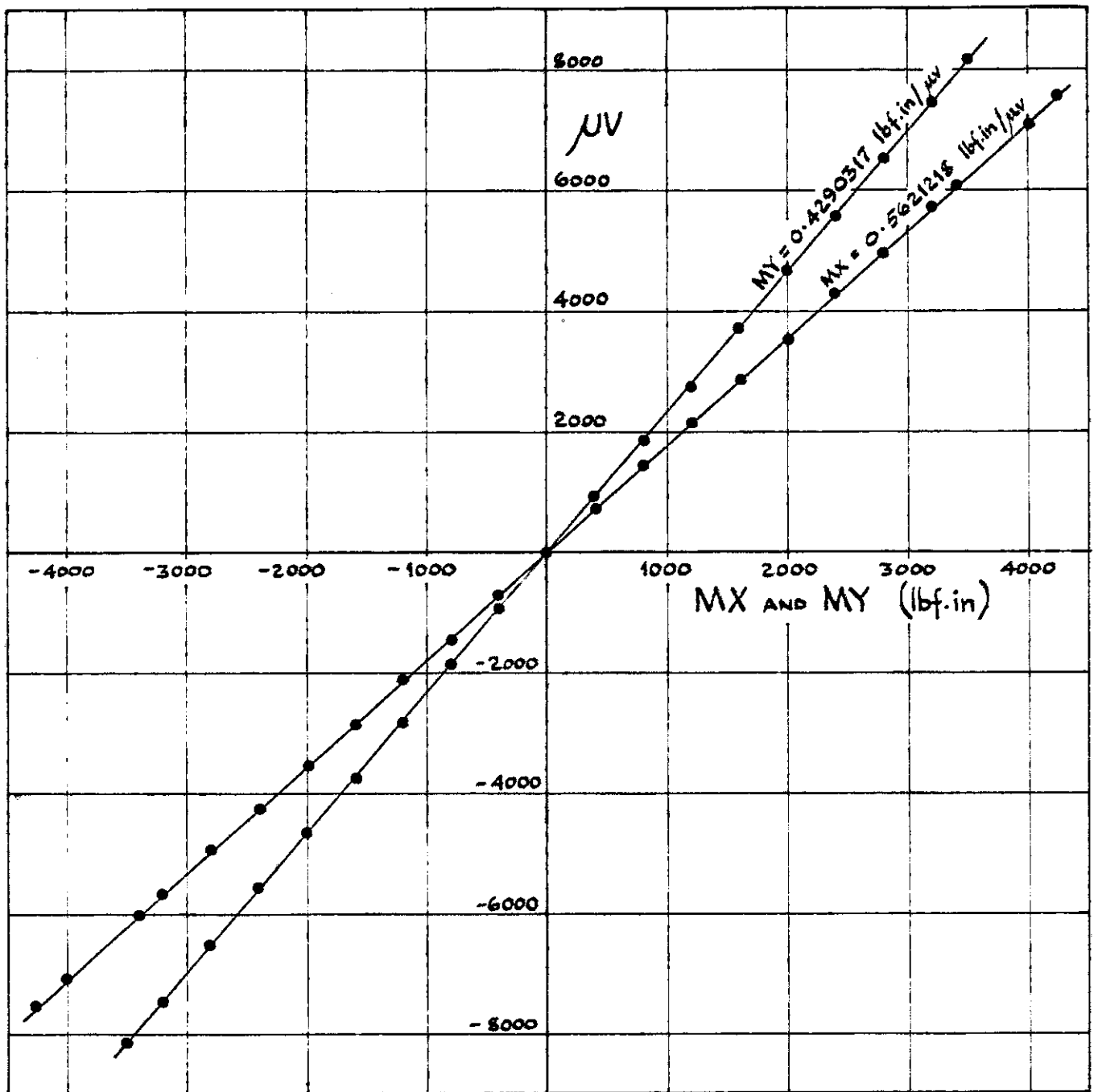
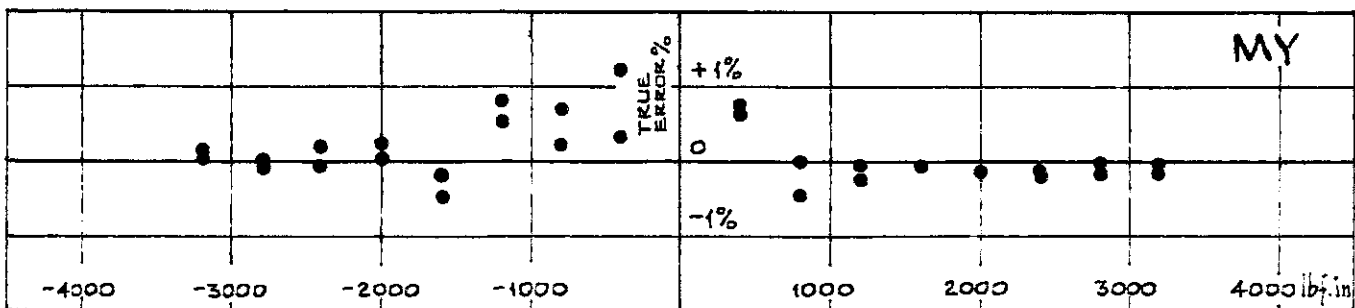
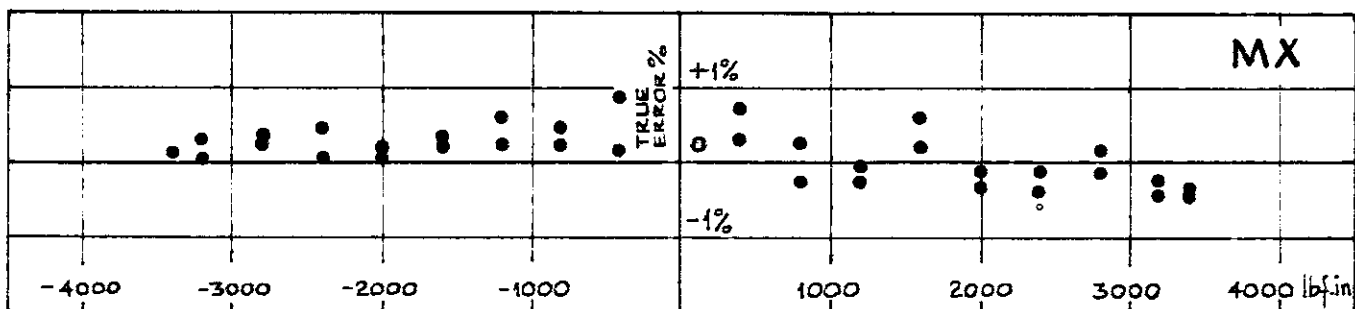
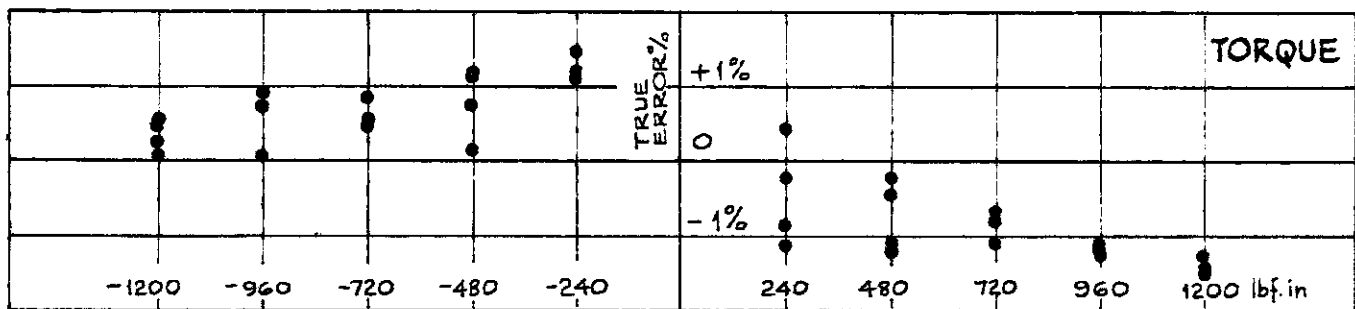
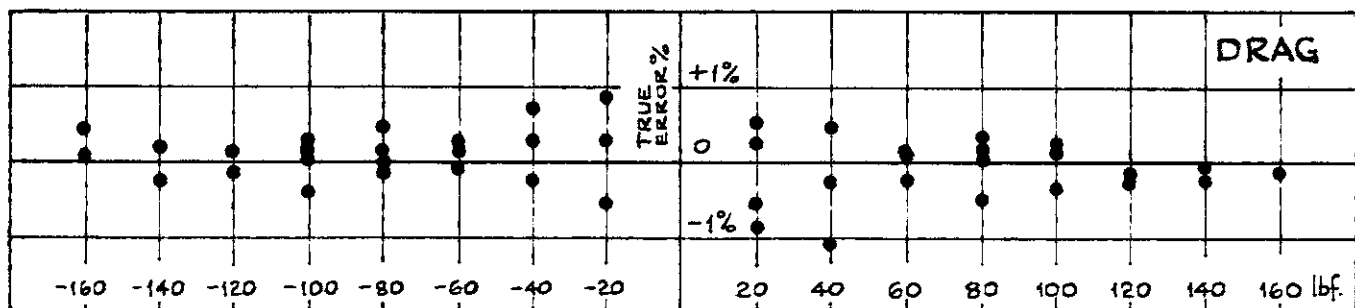
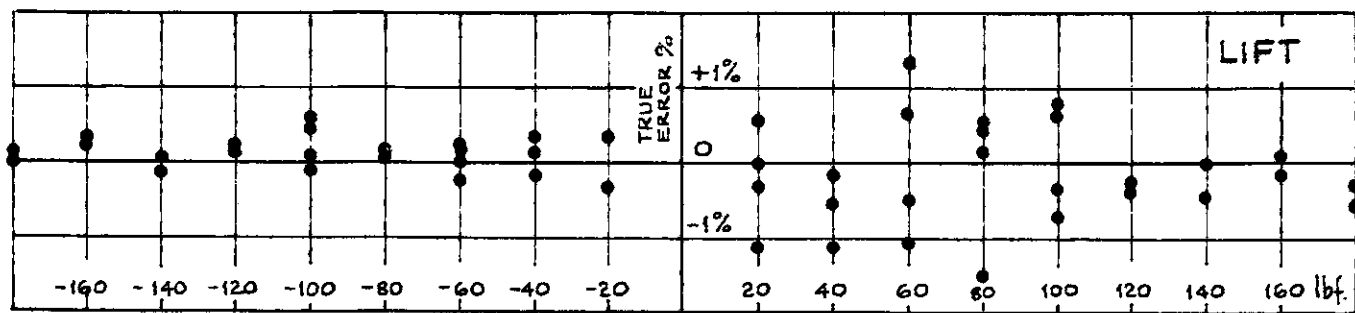


Fig. 35 MX AND MY CALIBRATION



**Fig. 36** TRUE ERRORS IN MEASURED DATA FOR EACH COMPONENT COMPARED WITH REGRESSION LINES

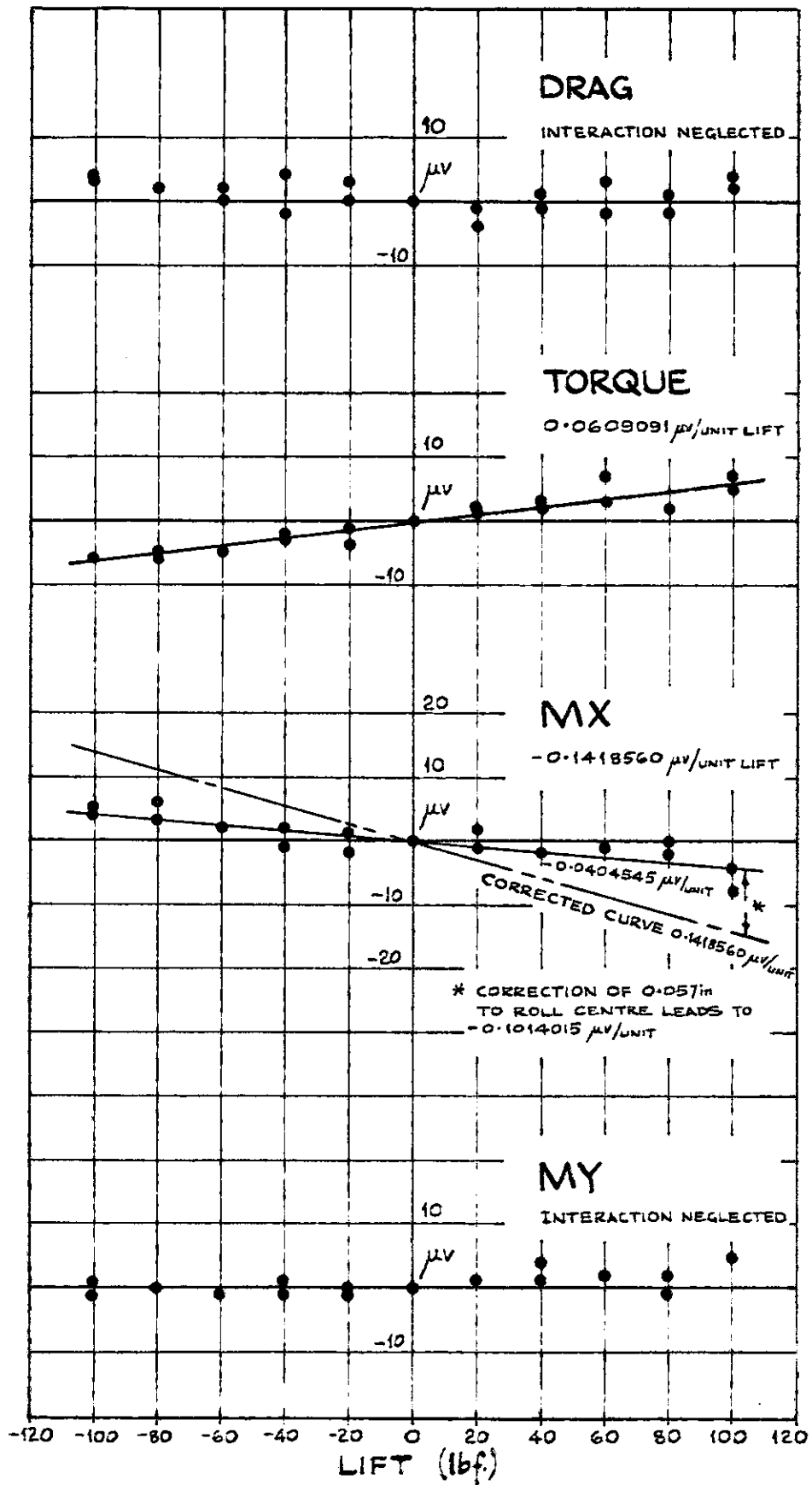


Fig. 37 INTERACTIONS CAUSED BY LIFT CALIBRATION DATA AND MEAN CURVES

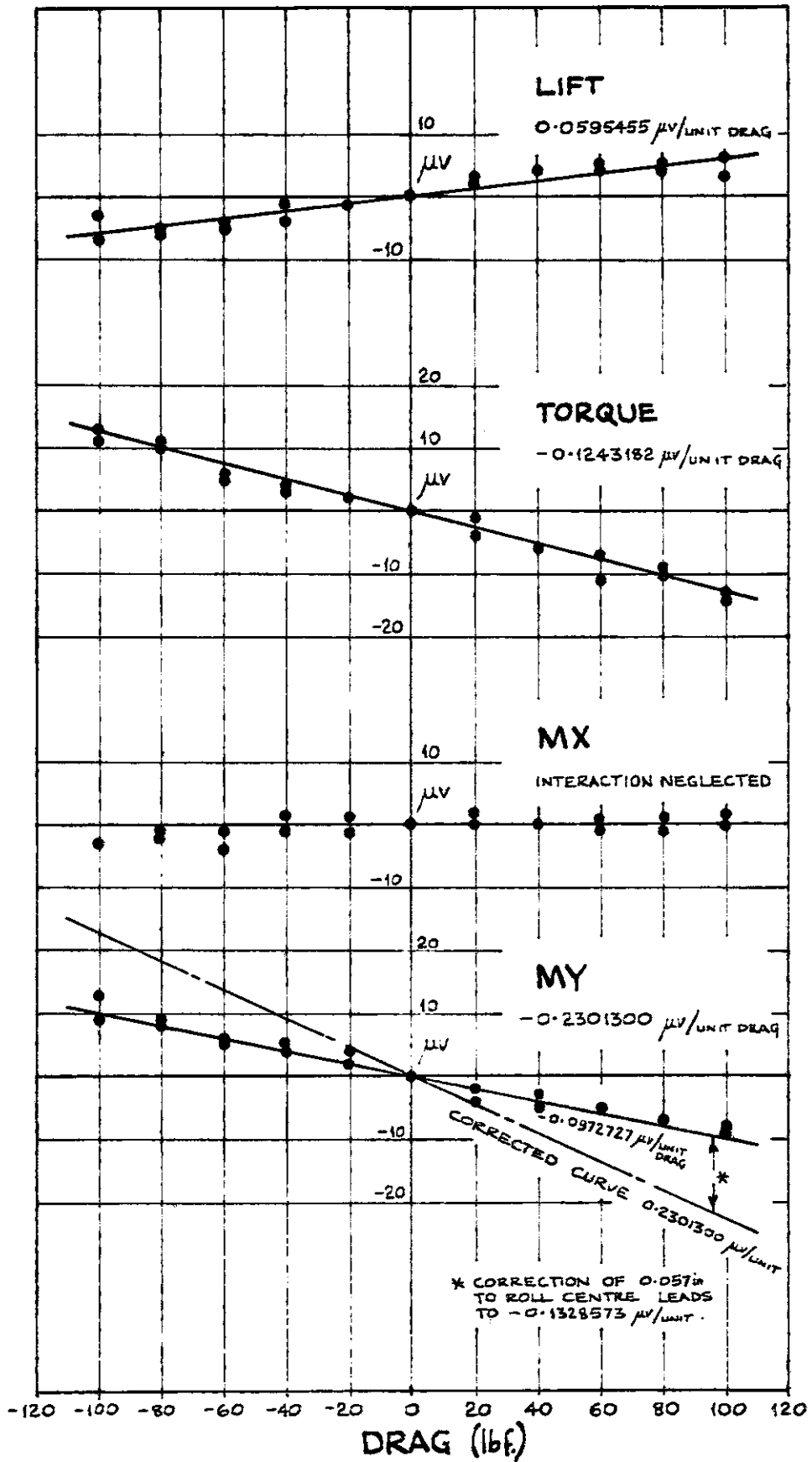


Fig. 38 INTERACTIONS CAUSED BY DRAG CALIBRATION DATA AND MEAN CURVES



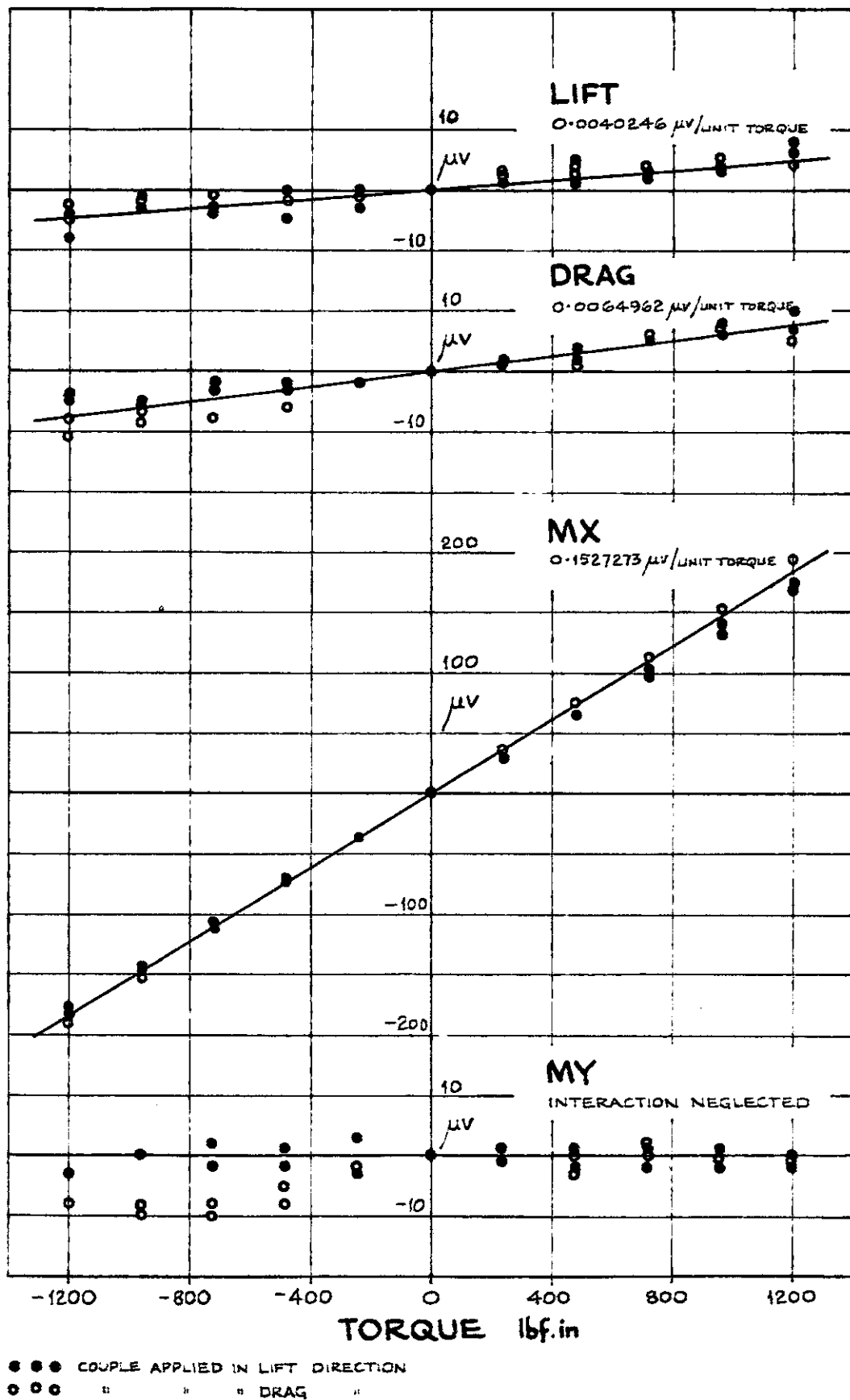


Fig. 39 INTERACTIONS CAUSED BY TORQUE CALIBRATION DATA AND MEAN CURVES

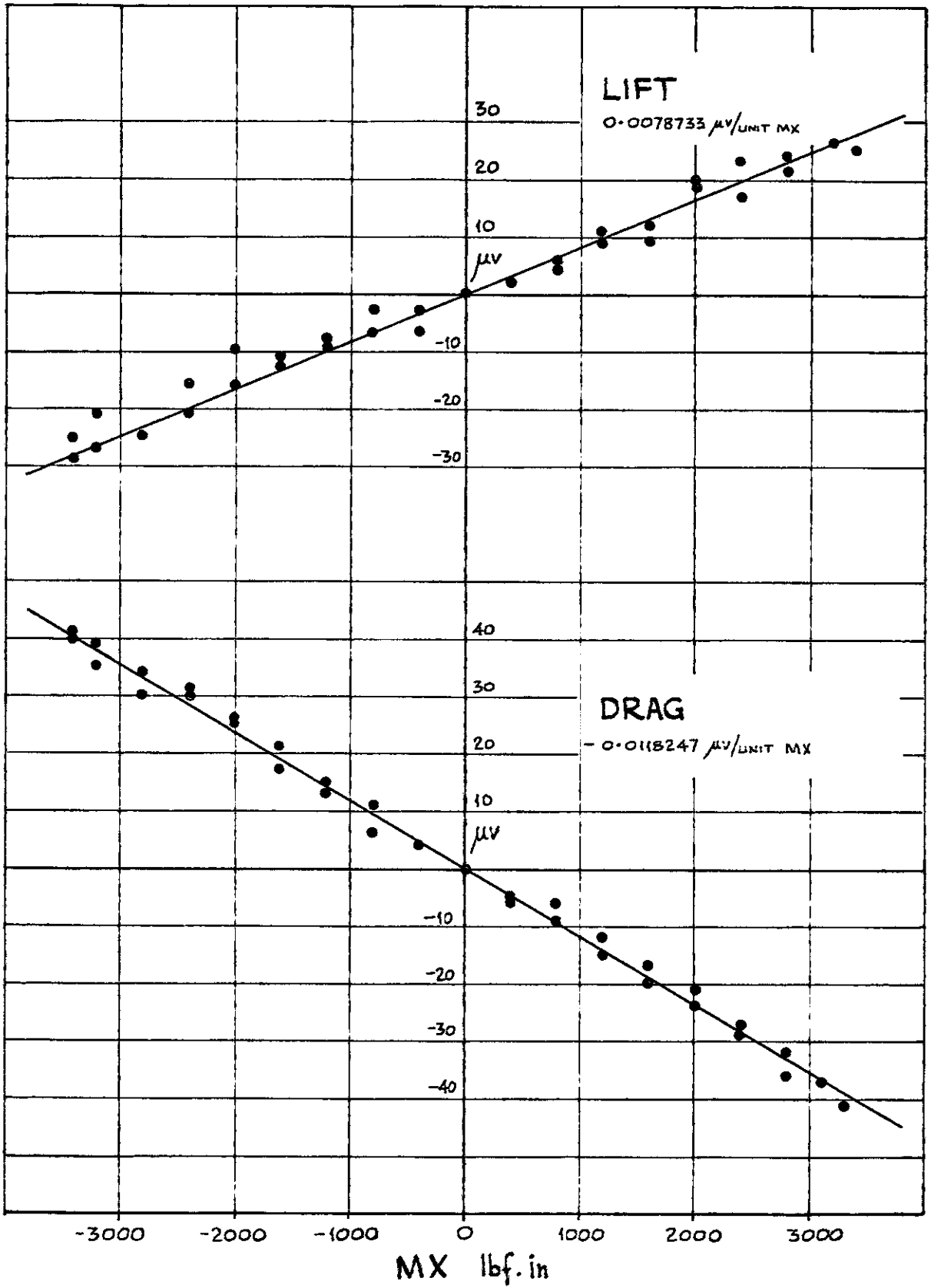


Fig. 40a INTERACTIONS CAUSED BY MX  
CALIBRATION DATA AND MEAN CURVES

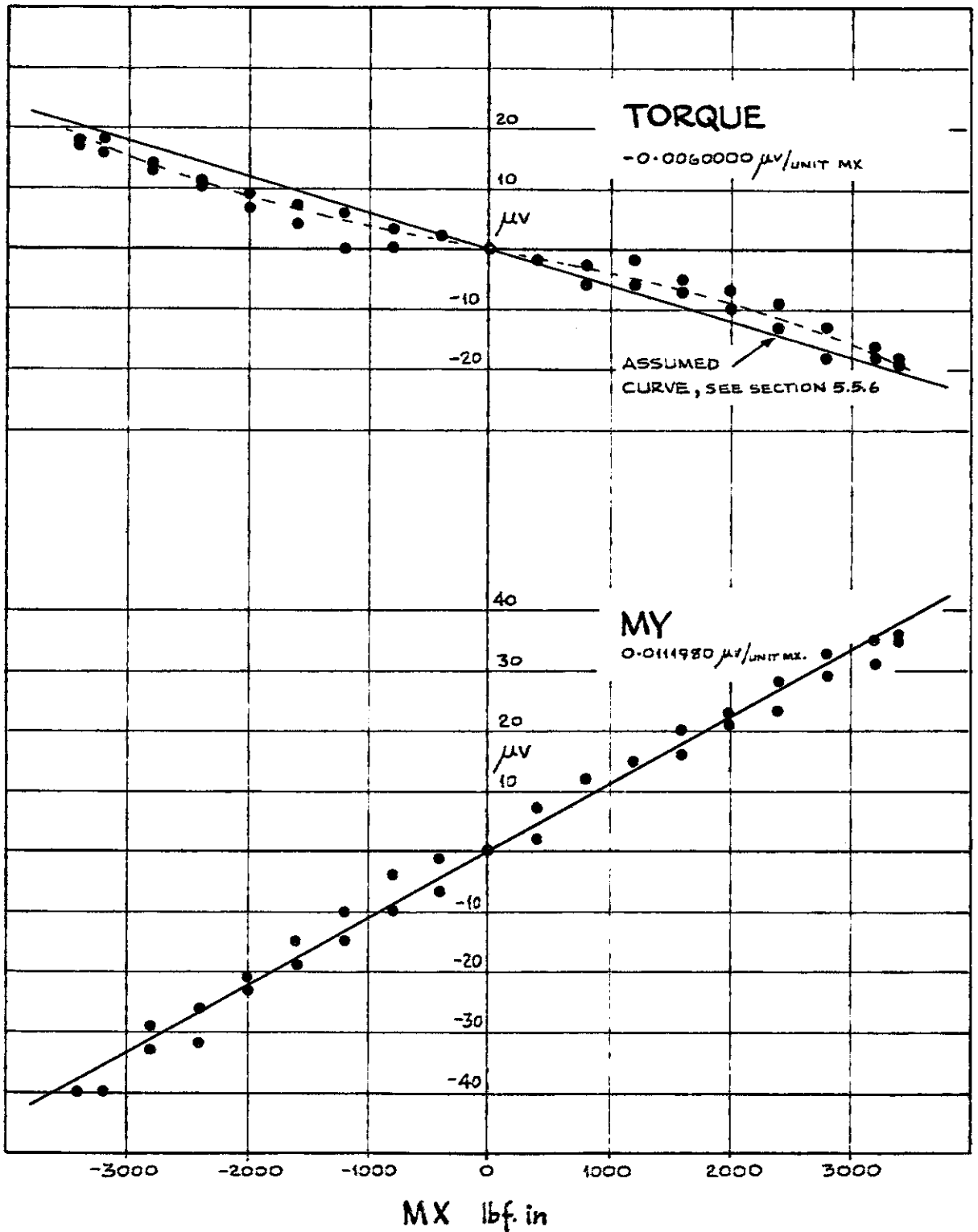


Fig. 40b INTERACTIONS CAUSED BY MX (cont'd)  
 CALIBRATION DATA AND MEAN CURVES

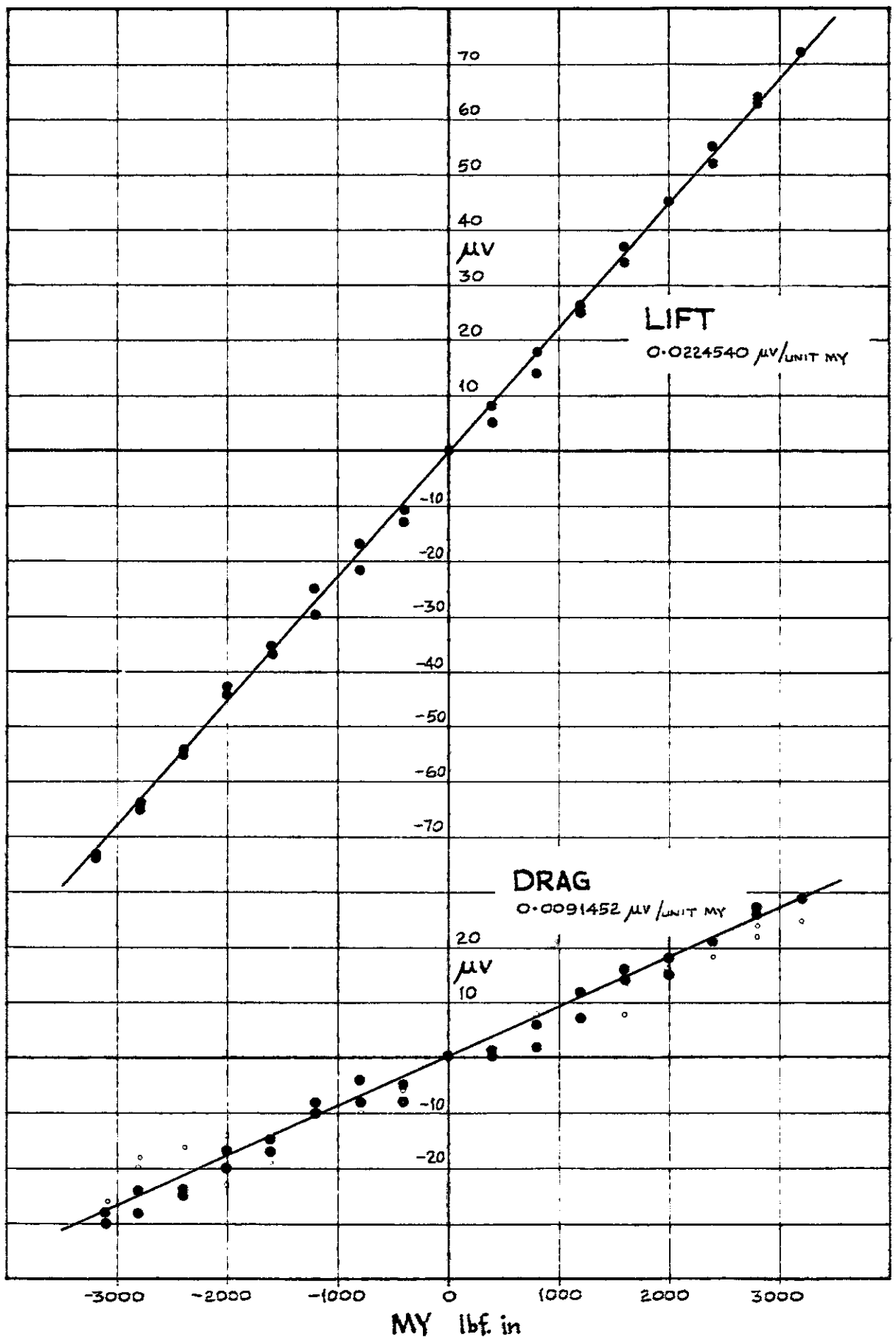


Fig. 41a INTERACTIONS CAUSED BY MY  
CALIBRATION DATA AND MEAN CURVES

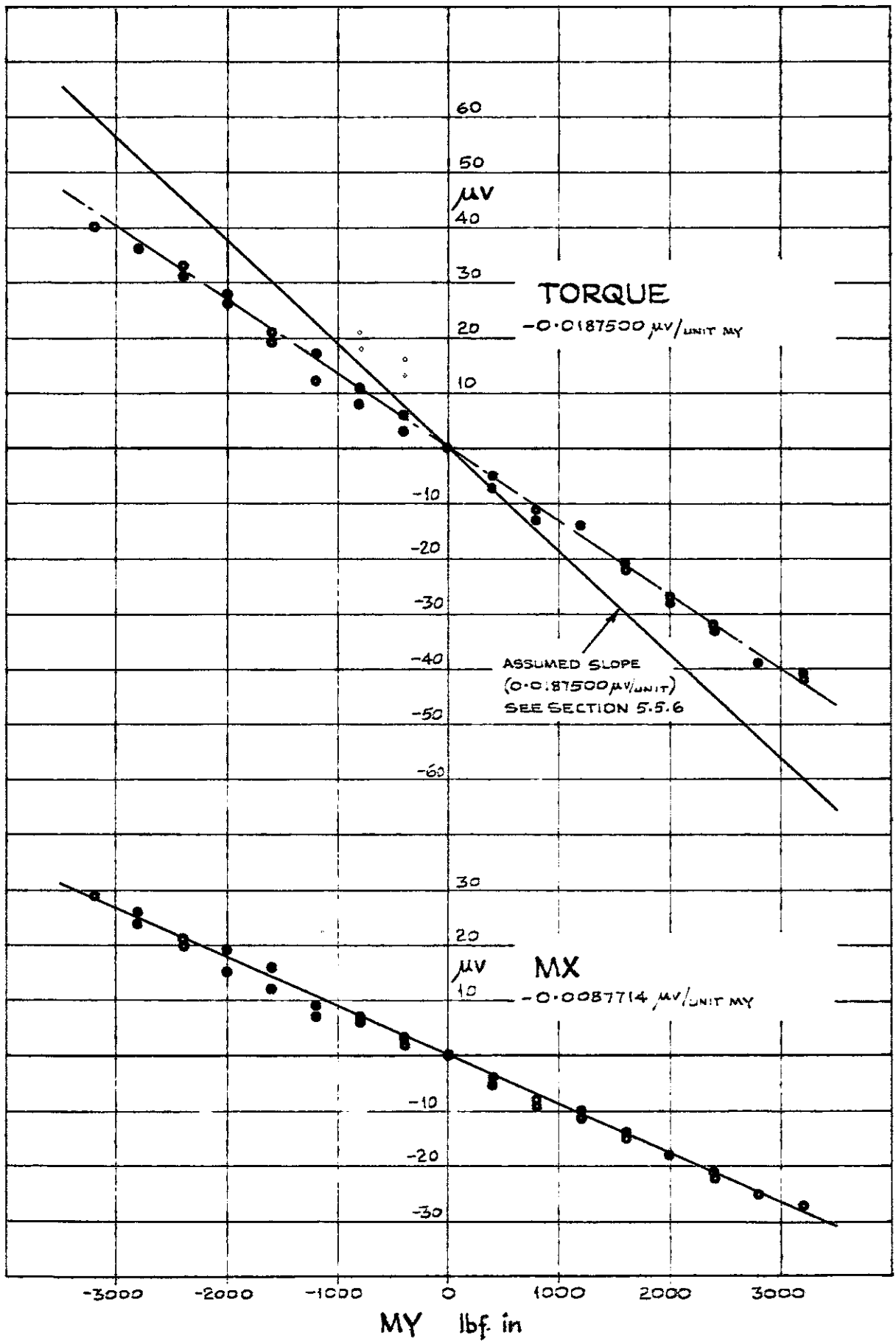
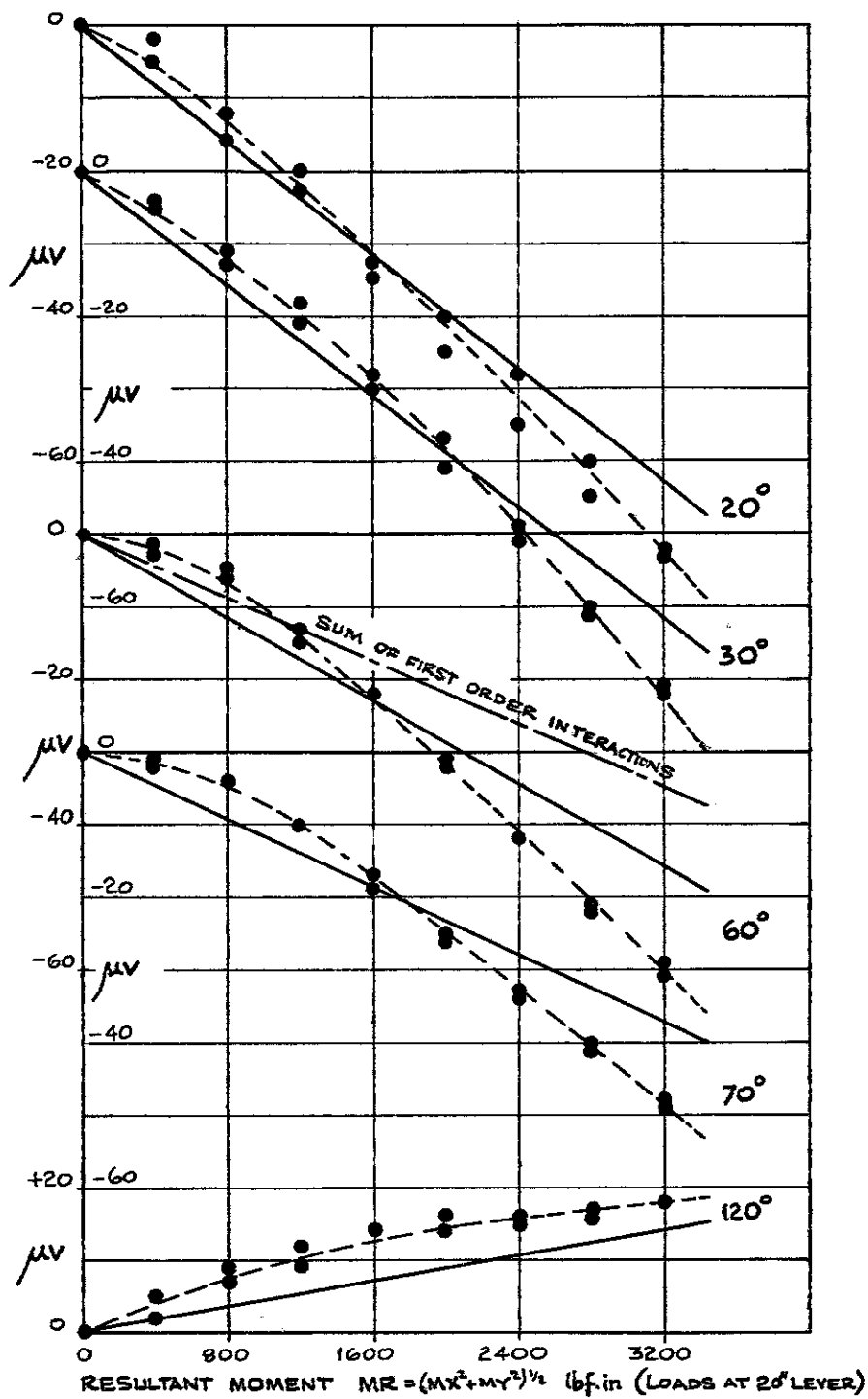


Fig. 41 b INTERACTIONS CAUSED BY MY (cont'd)  
 CALIBRATION DATA AND MEAN CURVES



-●-●-●- MEASURED INTERACTIONS  
 ——— ASSUMED INTERACTIONS

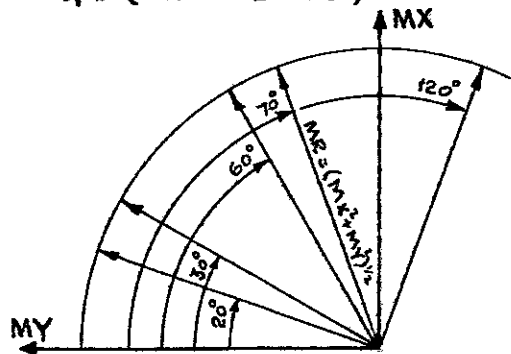
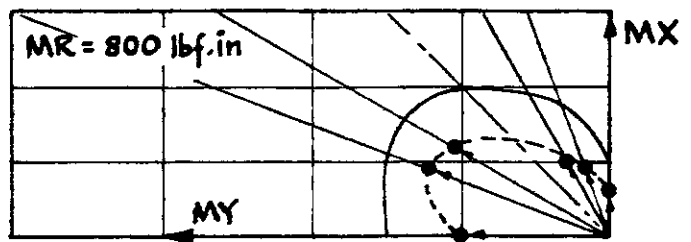
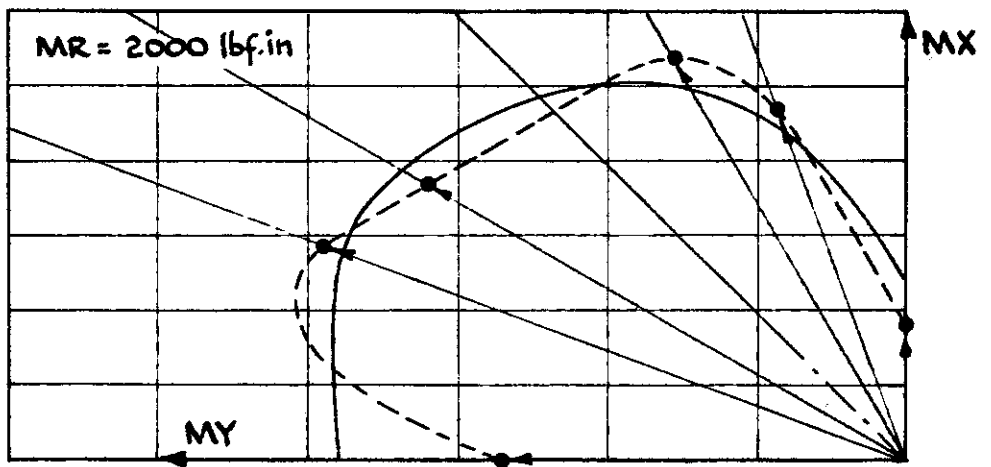
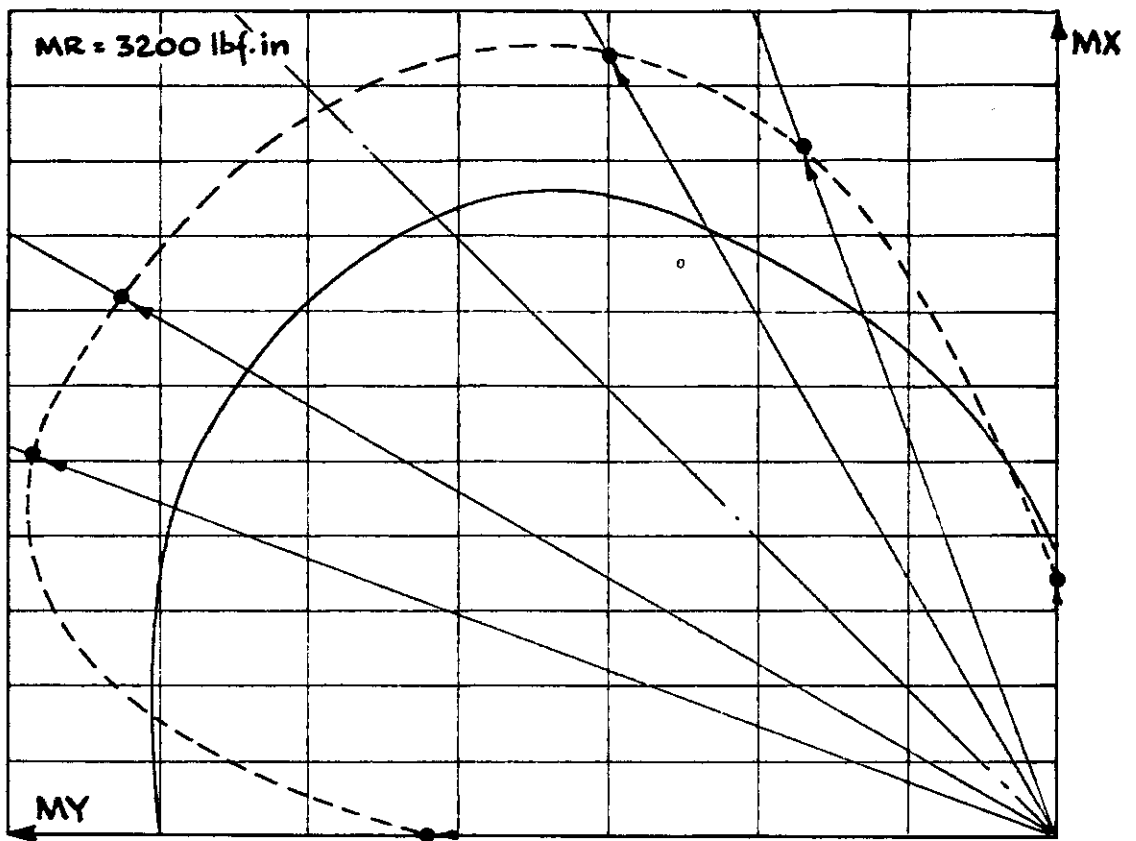


Fig. 42 TORQUE INTERACTIONS CAUSED BY  
 COMBINED MOMENTS (MX + MY)



-●-●-● MEASURED INTERACTION  
 ——— ASSUMED INTERACTION  
 SCALE : 2mm = 1μV

Fig. 43 POLAR DIAGRAMS OF TORQUE INTERACTIONS CAUSED BY (MX + MY) (DERIVED FROM Figs. 42, 41b, 40b)

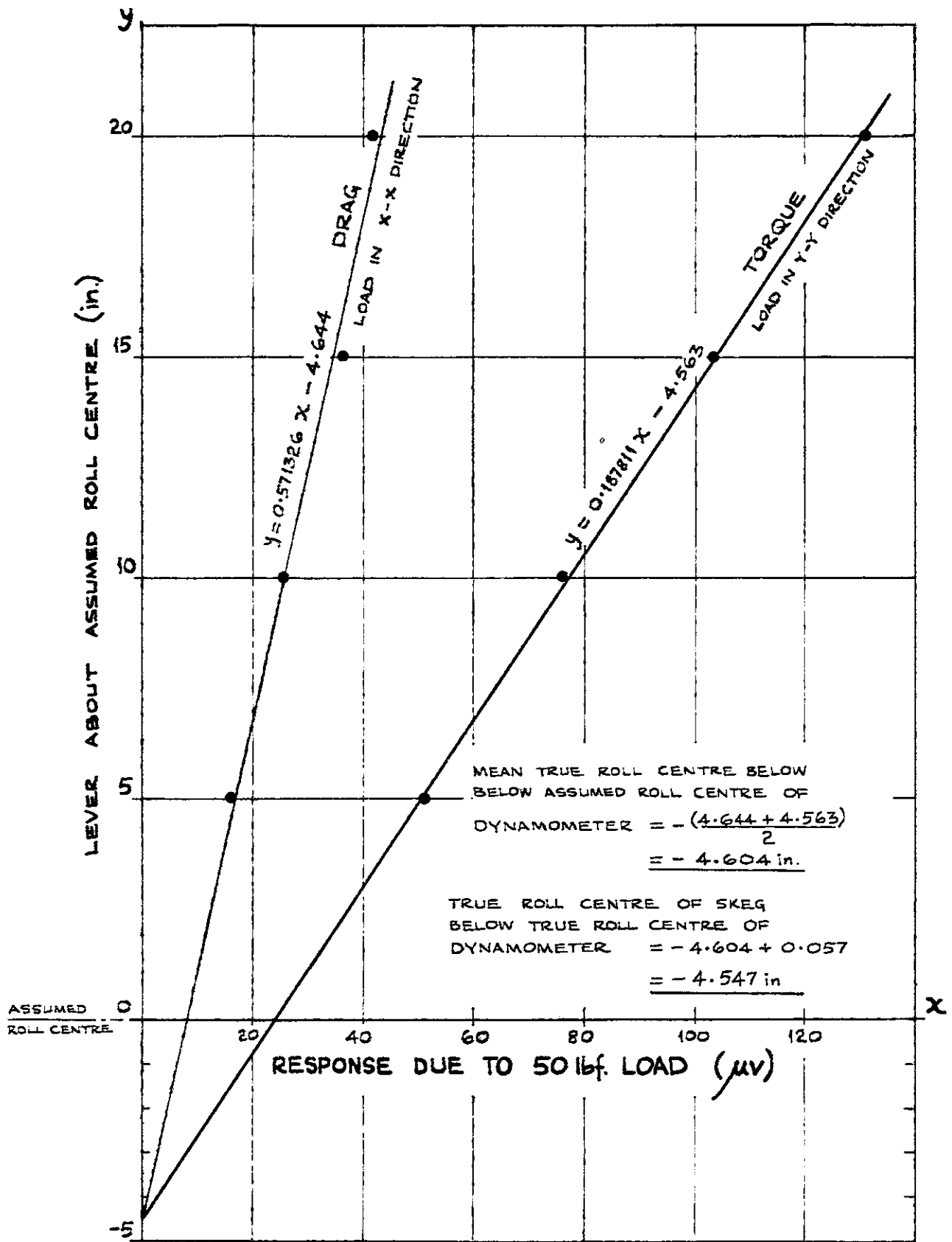


Fig. 44 DERIVATION OF TRUE ROLL CENTRE OF SKEG WHEN ATTACHED TO BASE  
CROSS PLOTS OF DRAG AND TORQUE RESPONSE CAUSED BY 50 lb. LOAD APPLIED TO SKEG AT VARYING LEVERS IN X AND Y DIRECTIONS



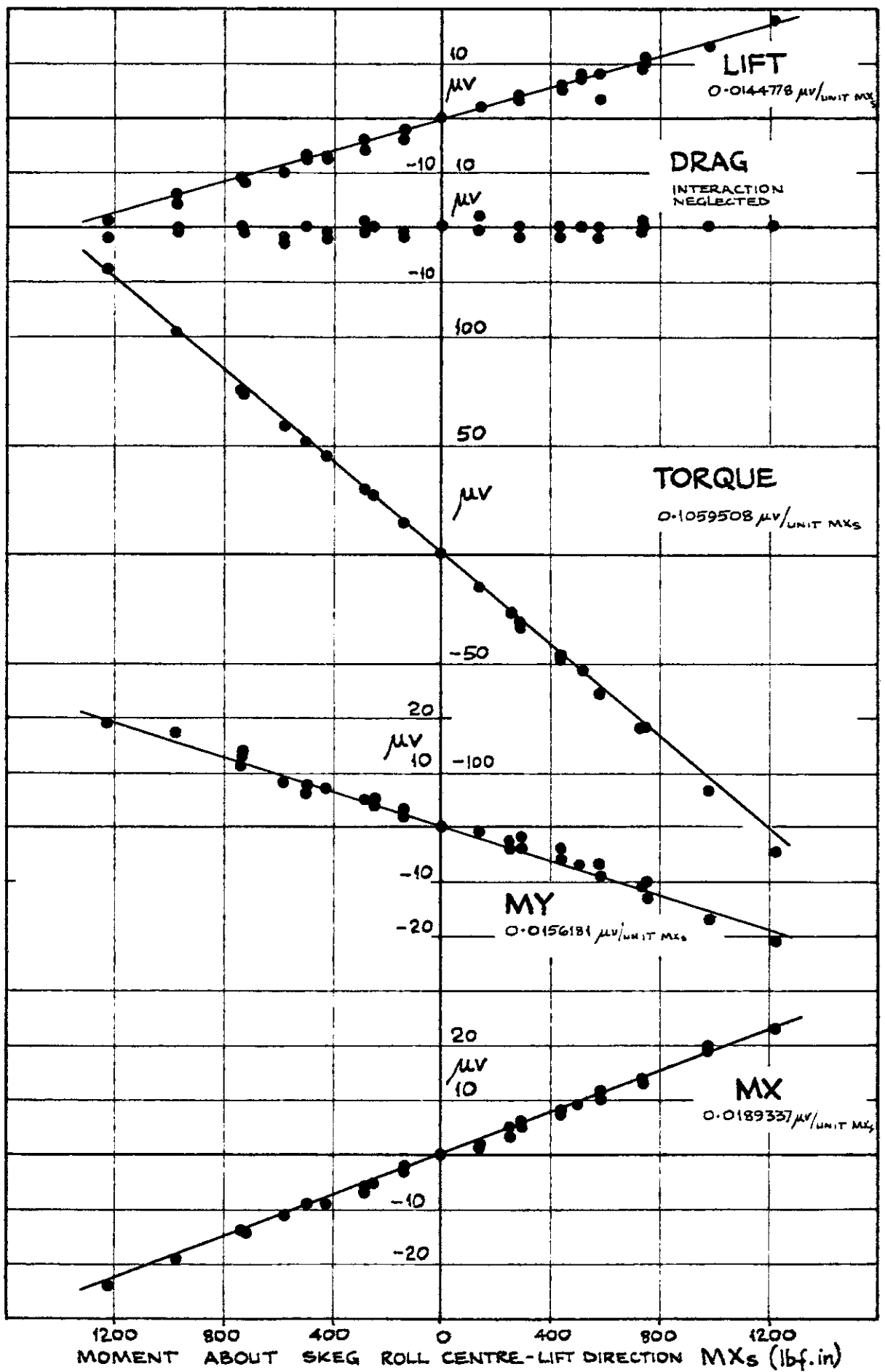


Fig.45 INTERACTIONS CAUSED BY SKEG LOADS:  
 LIFT DIRECTION  
 CALIBRATION DATA AND MEAN CURVES

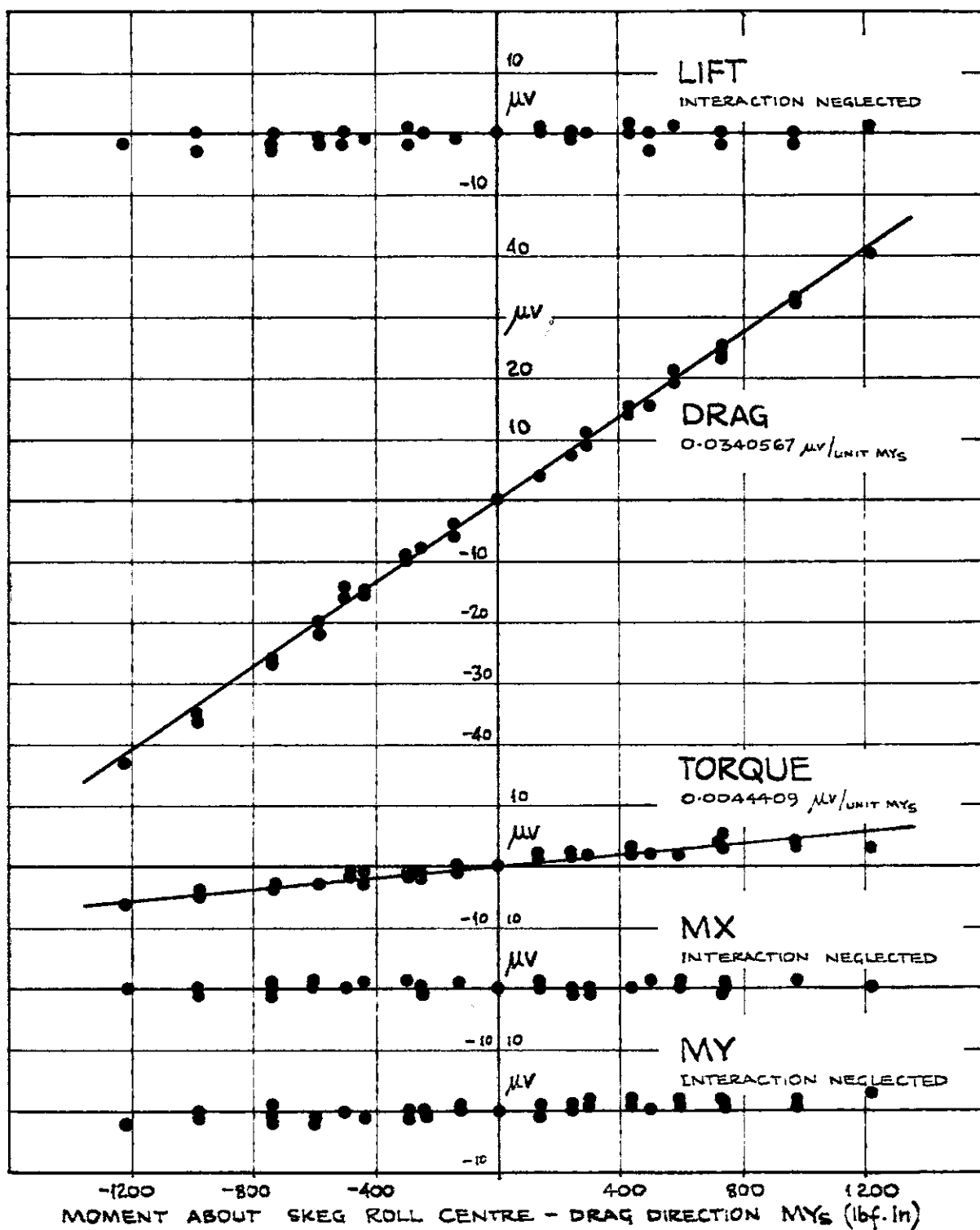


Fig. 46 INTERACTIONS CAUSED BY SKEG LOADS:  
 DRAG DIRECTION  
 CALIBRATION DATA AND MEAN CURVES

1 2 3 4 5 6 7 8 9 10 11 12 13 14 15 16 17 18 19 20 21 22 23 24 25 26 27 28 29 30 31 32 33 34 35 36 37 38 39 40 41 42 43 44 45 46 47 48 49 50

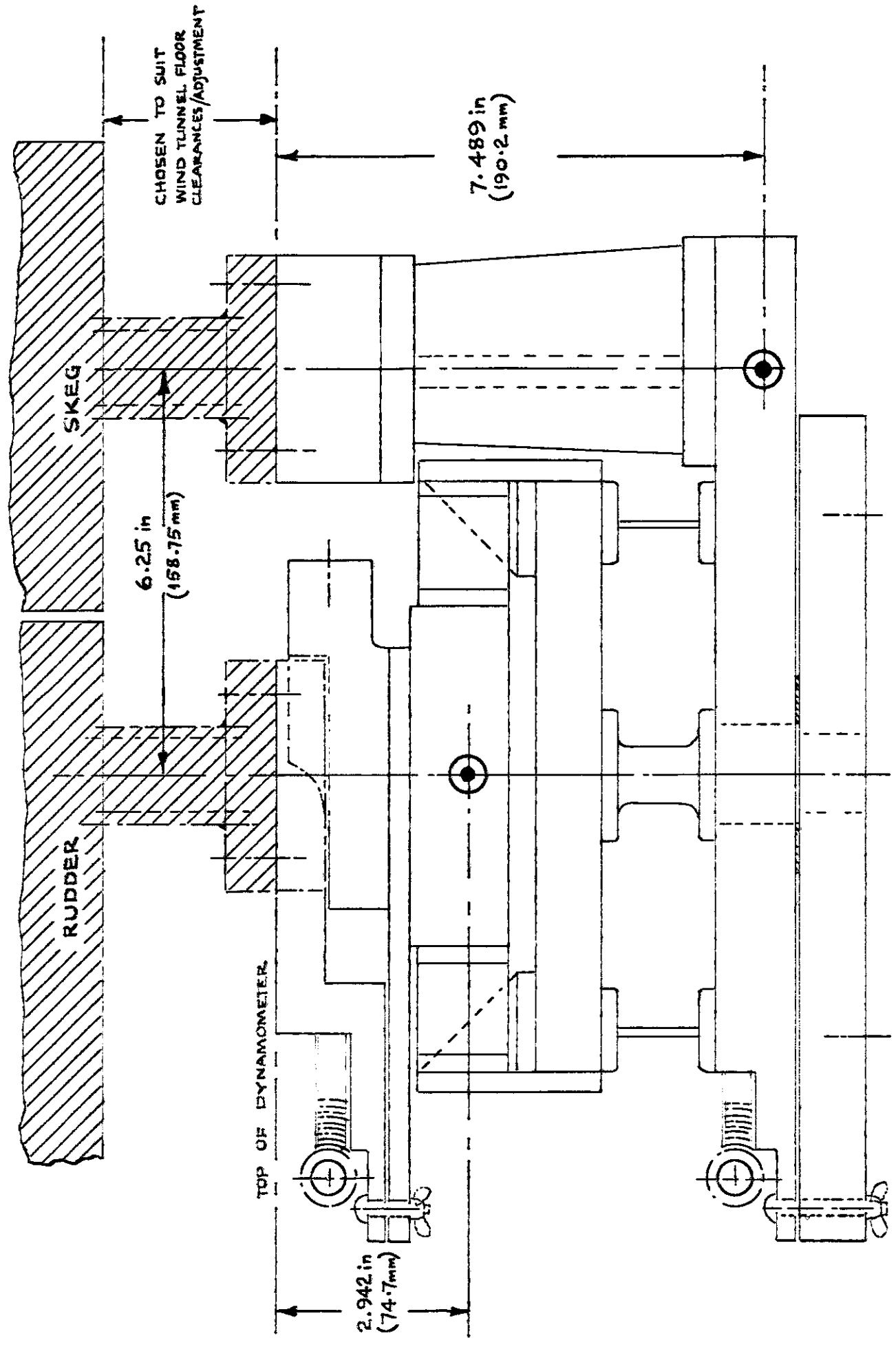


Fig. 47 TRUE ROLL CENTRES OF DYNAMOMETER

4 5 6 7 8 9 10 11 12 13 14 15 16 17 18 19 20 21 22 23 24 25 26 27 28 29 30 31 32 33 34 35 36 37 38 39 40 41 42 43 44 45 46 47 48 49 50 51 52 53 54 55 56 57 58 59 60 61 62 63 64 65 66 67 68 69 70 71 72 73 74 75 76 77 78 79 80 81 82 83 84 85 86 87 88 89 90 91 92 93 94 95 96 97 98 99 100

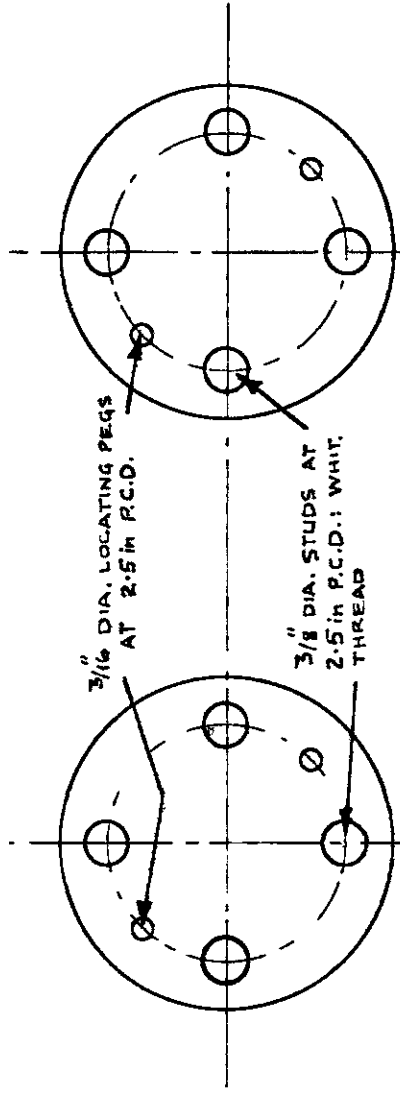
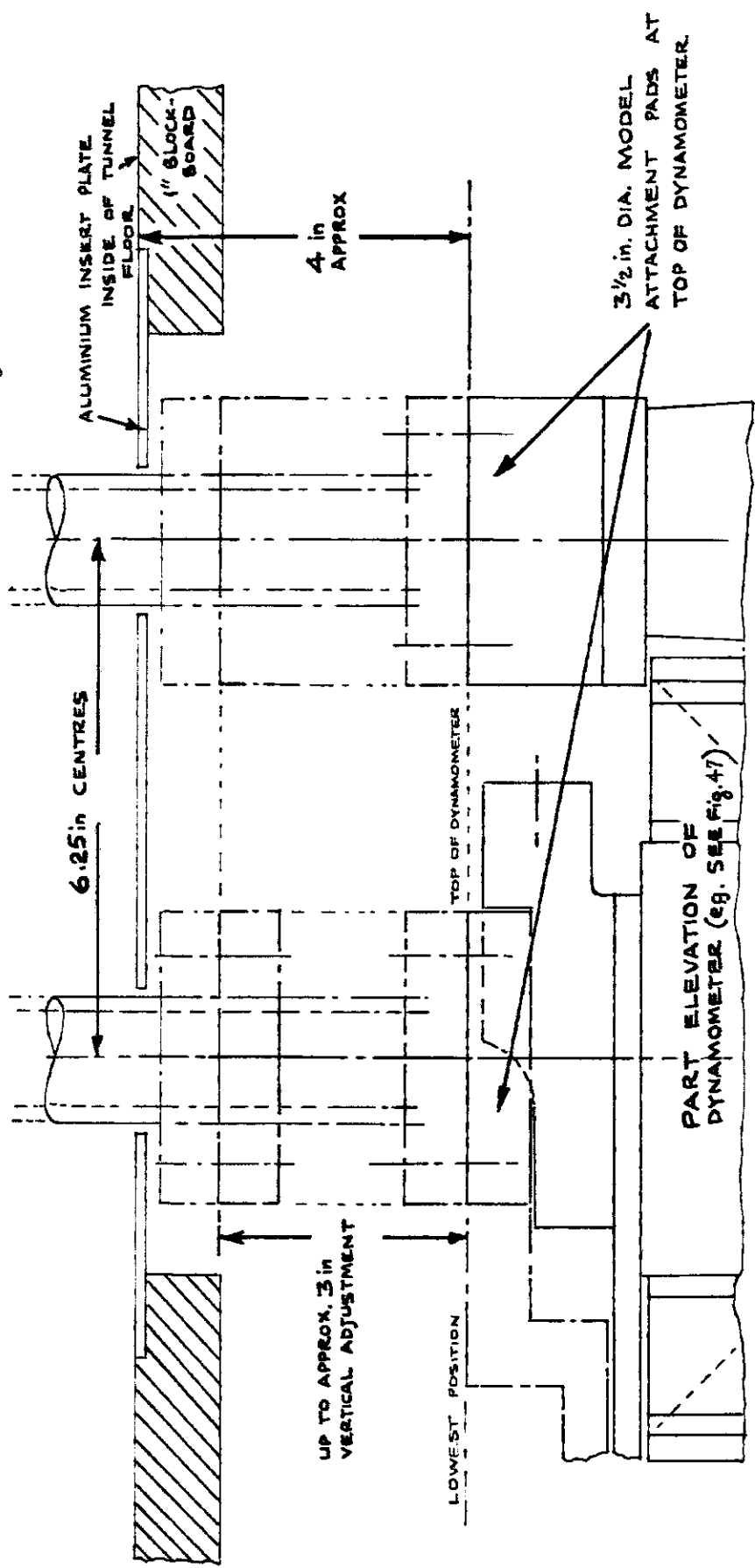


Fig. 48 MODEL CONNECTING PADS ON DYNAMOMETER, AND VERTICAL ADJUSTMENT

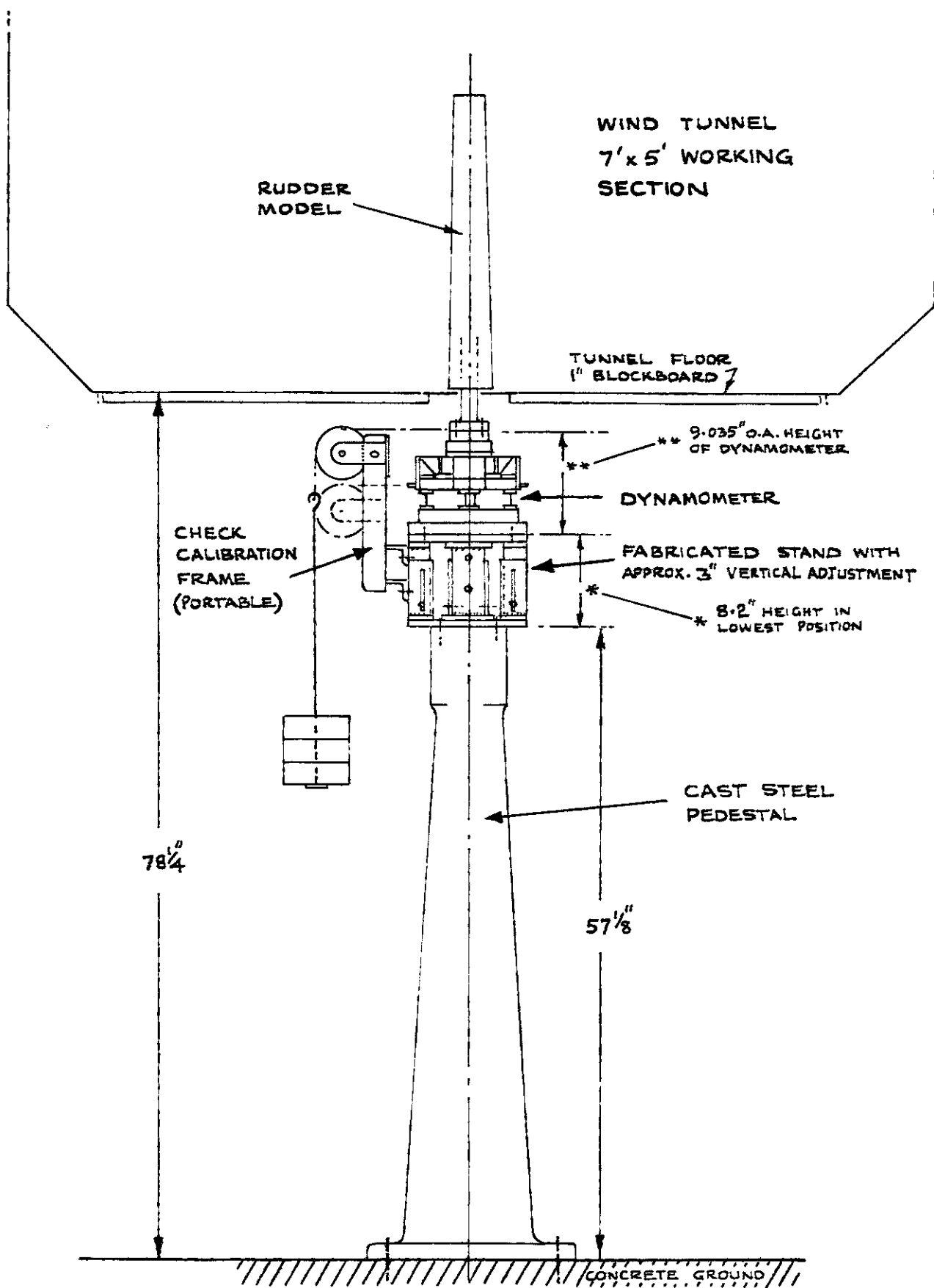


Fig. 49 OUTLINE DETAILS OF DYNAMOMETER  
IN WORKING POSITION

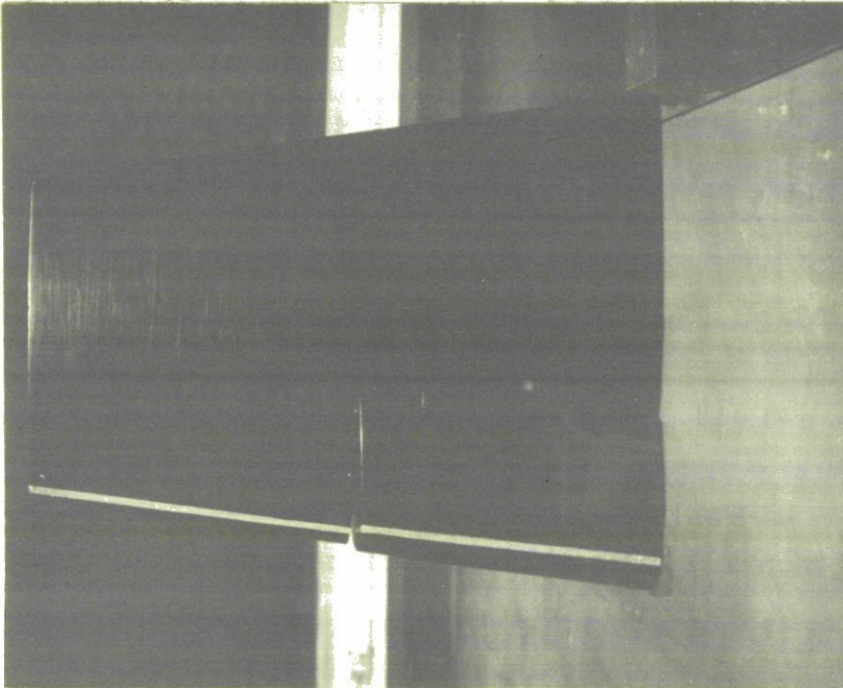


Fig. 50 SKEG RUDDER IN TUNNEL

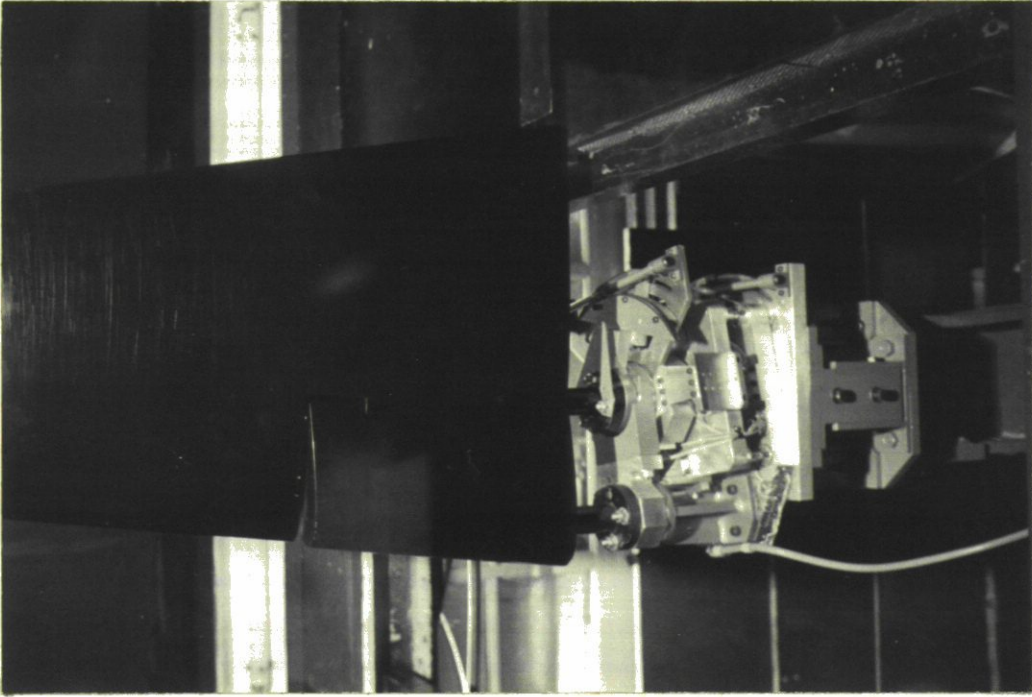


Fig. 51 SKEG RUDDER IN TUNNEL  
(FLOOR REMOVED SHOWING  
DYNAMOMETER)

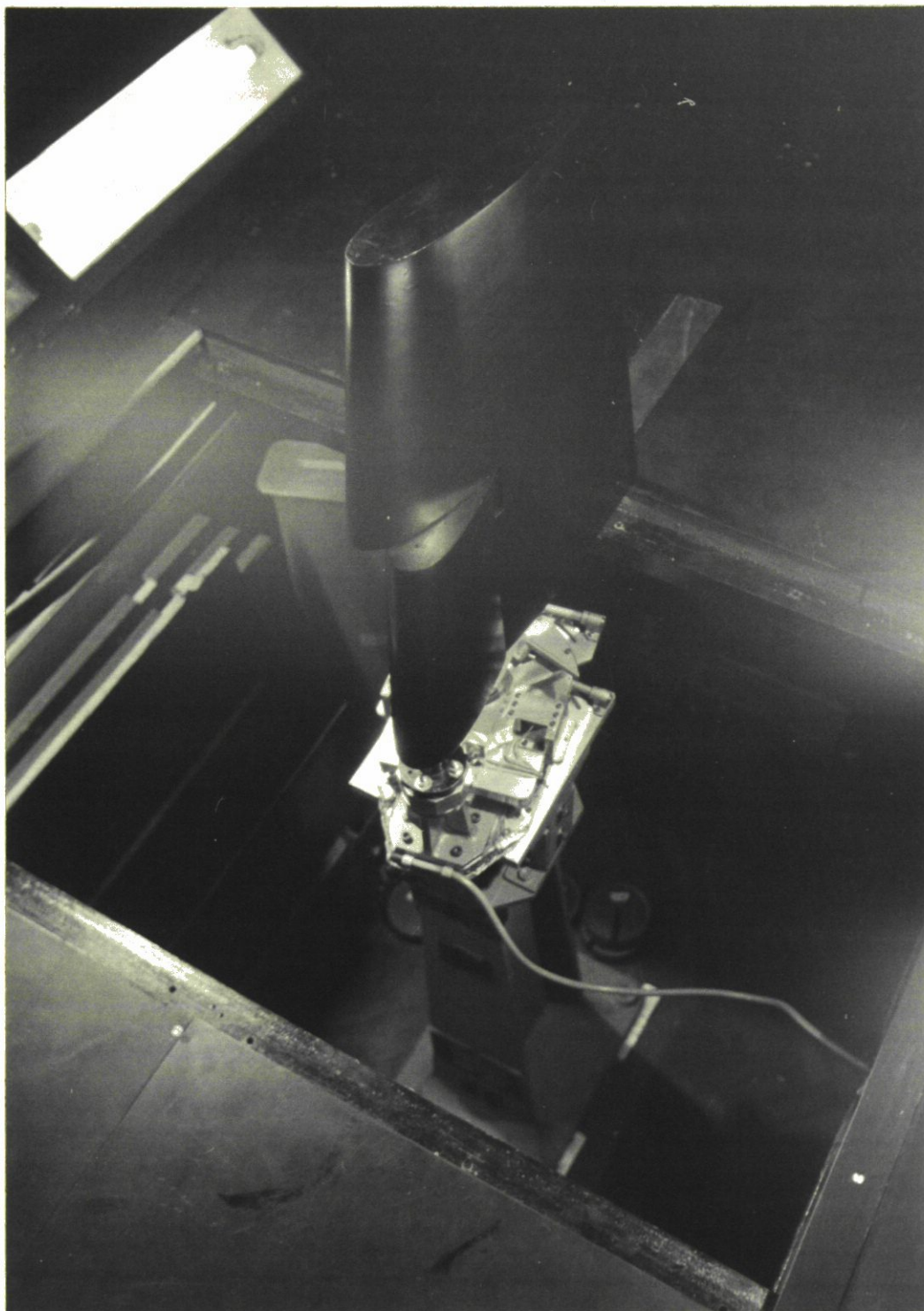
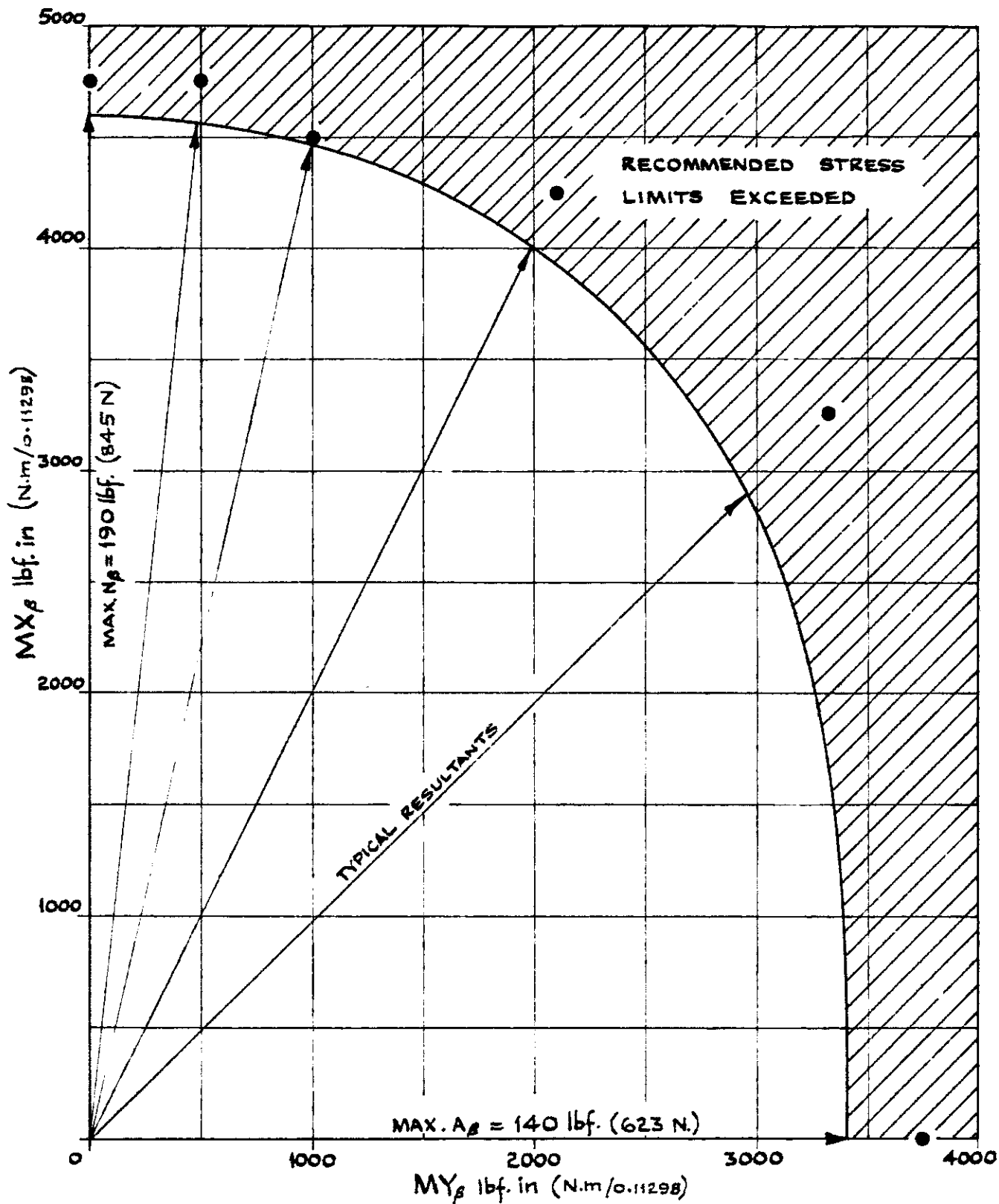


Fig. 52 SKEG RUDDER IN TUNNEL  
(TUNNEL FLOOR REMOVED SHOWING  
DYNAMOMETER AND PEDESTAL ATTACHMENT  
TO GROUND)



**NOTES:**

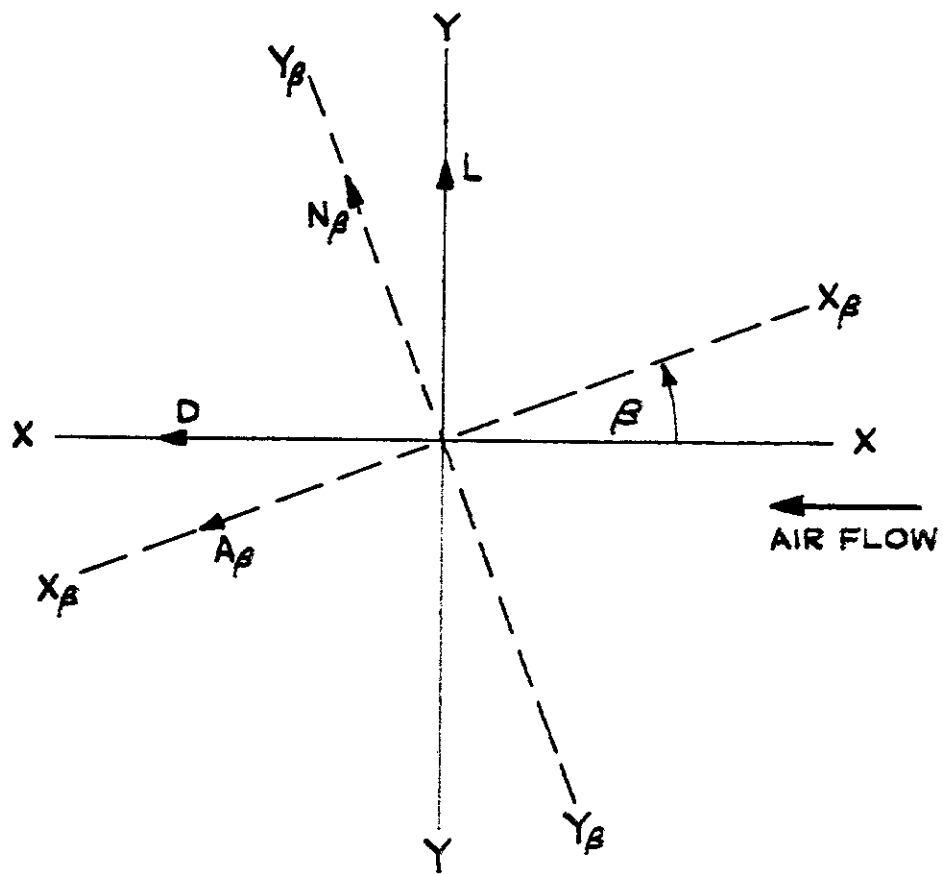
ONE QUADRANT SHOWN; COMBINATIONS APPLICABLE TO ALL FOUR QUADRANTS  
 ● ● ● PROOF LOAD DATA

MAXIMUM TORQUE OF 1200 lbf.in CAN BE SUPERIMPOSED ON ANY OF ABOVE MAXIMUM COMBINATIONS OF LOADINGS

LOADS CAN BE UP TO  $N_p = 190 \text{ lbf.}$  OR  $A_p = 140 \text{ lbf.}$  AND ANY COMBINATION OF THESE MAXIMA PROVIDED ABOVE COMBINATIONS OF MOMENTS ( $MX_p + MY_p$ ) ARE NOT EXCEEDED

**Fig. 53** MAXIMUM STATIC LOADS AND MOMENTS



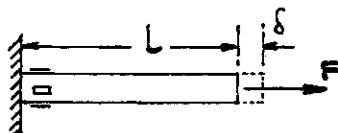


X AND Y ARE TUNNEL AXES  
 $X_{\beta}$  AND  $Y_{\beta}$  ARE DYNAMOMETER AXES

Fig. 54 RESOLUTION OF COMPONENTS

# FORCE MEASUREMENT

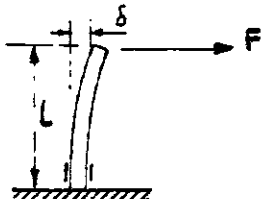
## ① AXIAL



$$\epsilon = \frac{\sigma}{E}$$

$$\delta = L \times \epsilon$$

## ② BENDING

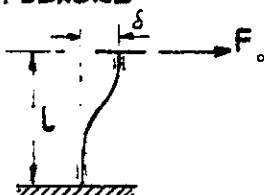


STRAIN AT ROOT DUE TO BENDING:

$$\epsilon = \frac{F \cdot L}{E \cdot I_y}$$

$$\delta = \frac{F \cdot L^3}{3E \cdot I}$$

## ③ CONTRA-FLEXURE

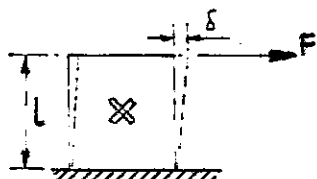


STRAIN AT ROOT DUE TO BENDING IN CONTRA-FLEXURE:

$$\epsilon = \frac{F \cdot L}{2E \cdot I_y}$$

$$\delta = \frac{F \cdot L^3}{12E \cdot I}$$

## ④ SHEAR



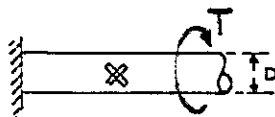
DIRECT STRAIN DUE TO SIMPLE SHEAR:

$$\epsilon_{45^\circ} = \frac{\phi}{2} = \frac{\delta}{2L} = \frac{q}{2G}$$

$$\delta = \frac{Lq}{G}$$

# MOMENT OR TORQUE MEASUREMENT

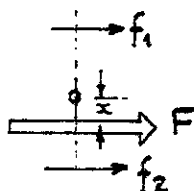
## ⑤ SHEAR



STRAIN DUE TO TORSIONAL SHEAR (ACTING AT 45° TO AXIS):

$$\epsilon_{45^\circ} = \frac{16T}{\pi \cdot D \cdot E}$$

⑥ ALTERNATIVELY, MOMENT OR TORQUE MAY BE DERIVED BY COMPUTING THE DIFFERENCES OF FORCES MEASURED BY ONE OF THE ABOVE METHODS



i.e. TOTAL FORCE =  $F = f_1 + f_2$   
AND MOMENT  $(F \cdot x) \propto (f_2 - f_1)$

A SUITABLE ARRANGEMENT OF STRAIN GAUGE BRIDGE CIRCUIT WILL GIVE A DIRECT READING OF MOMENT

Fig. 55

SOME FLEXURE TYPES WITH SUMMARY OF STRAINS AND DEFLECTIONS

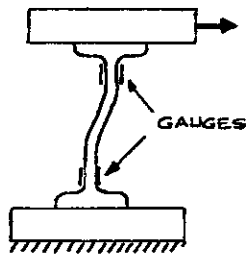


Fig. 56

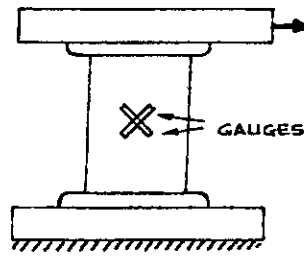


Fig. 57

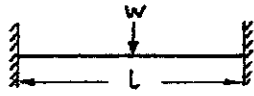


Fig. 58

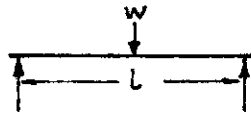


Fig. 59

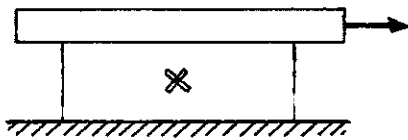


Fig. 60

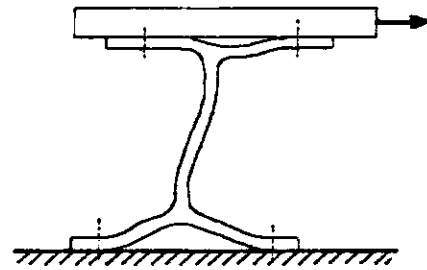


Fig. 61

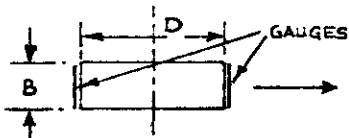


Fig. 62

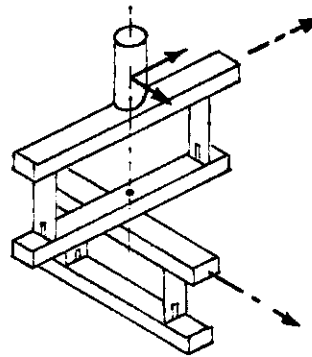


Fig. 63

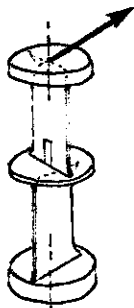


Fig. 64

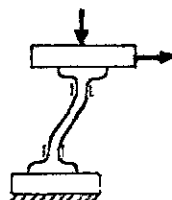


Fig. 65

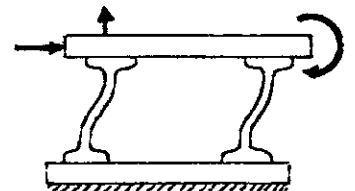


Fig. 66

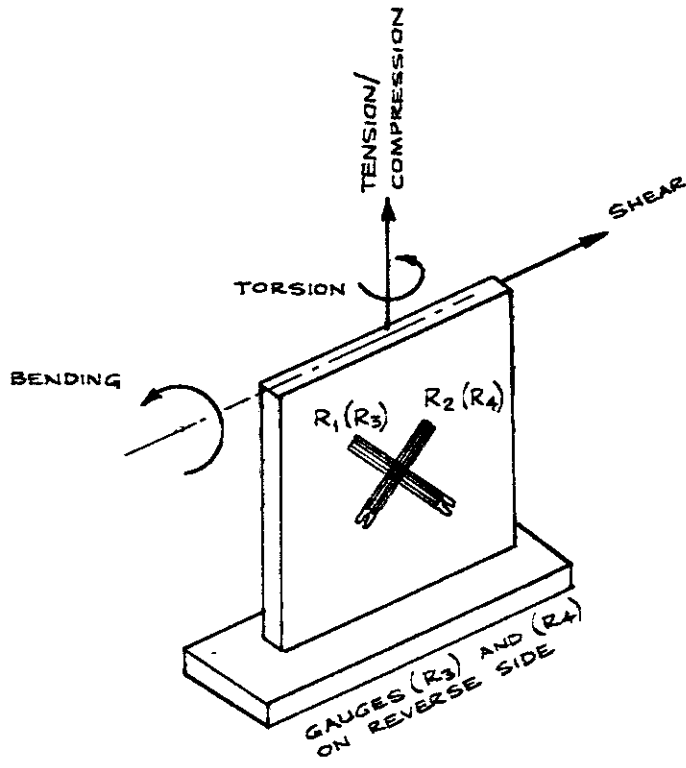
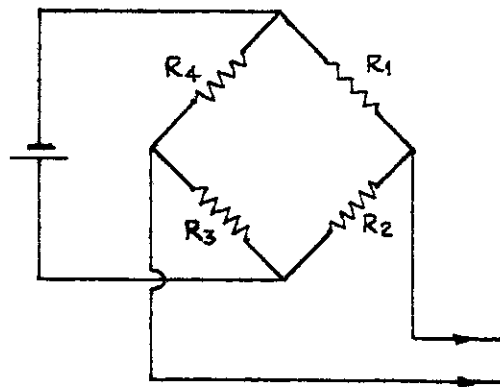


Fig. 67



FOR BRIDGE BALANCE :

$$\frac{R_1}{R_2} = \frac{R_4}{R_3}$$

Fig. 68

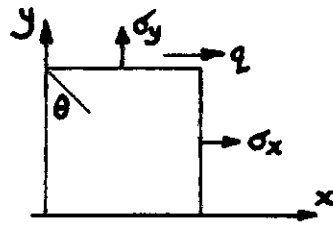


Fig. 69

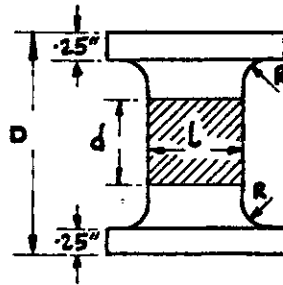


Fig. 70

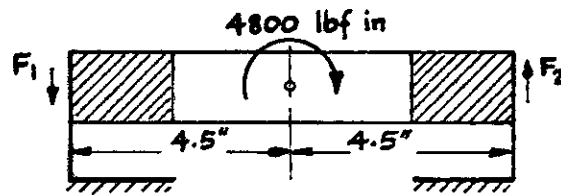


Fig. 71

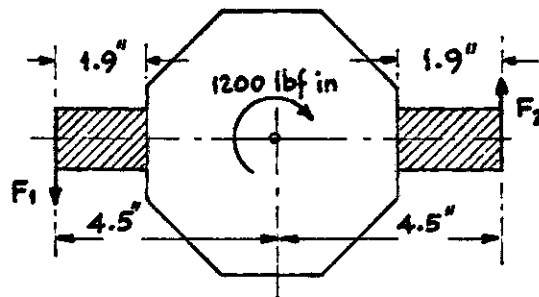


Fig. 72

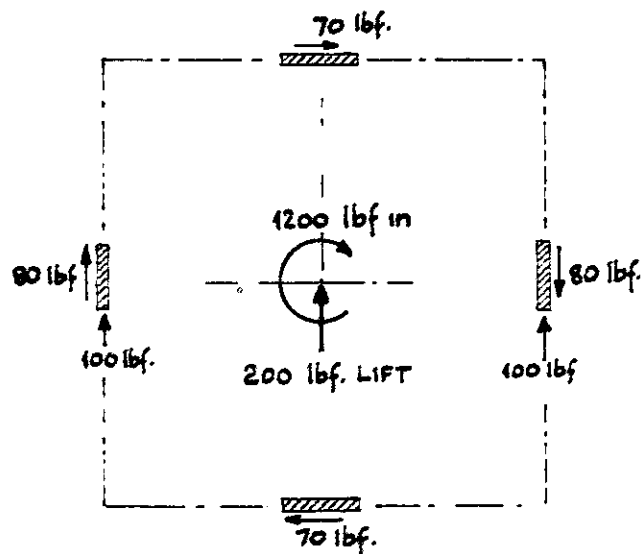


Fig. 73

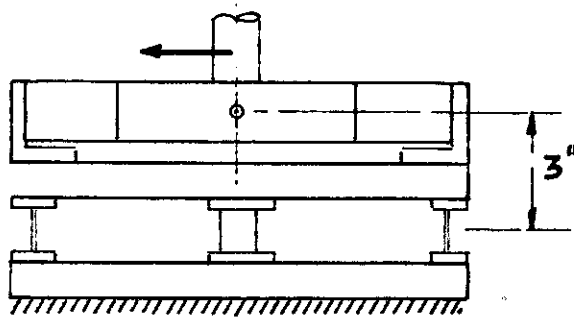


Fig. 74

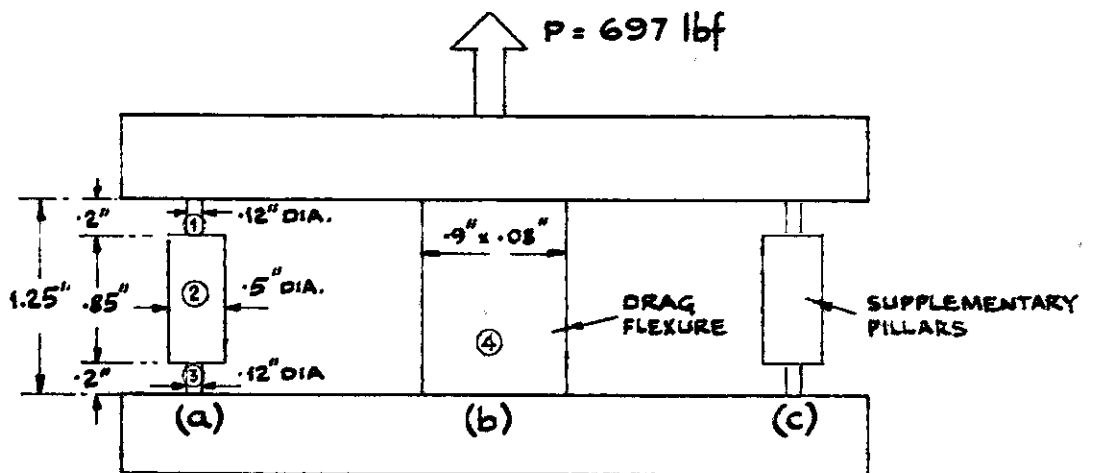
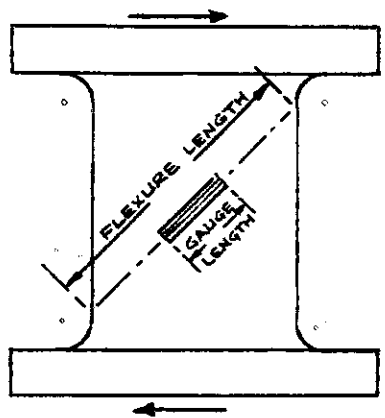
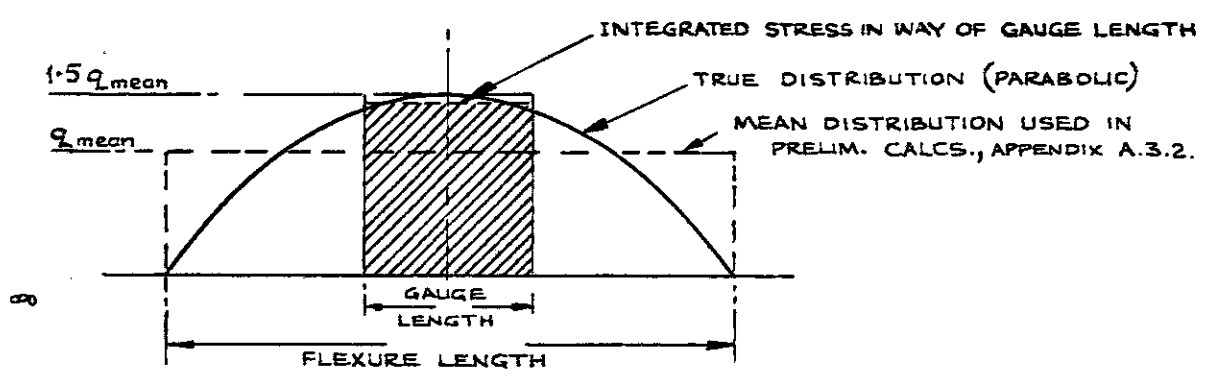


Fig. 75



	$\frac{\text{GAUGE LENGTH}}{\text{FLEXURE LENGTH}}$
LIFT FLEXURES	: 0.310
DRAG FLEXURES	: 0.297
TORQUE FLEXURES	: APPROX. AVERAGE OF LIFT AND DRAG
MOMENT FLEXURES	: 0.199



INTEGRATED STRESSES OVER GAUGE LENGTH FOR DIFFERENT FLEXURE TYPES :

LIFT GAUGES	: $q_{actual} = 1.46 q_{mean}$
DRAG GAUGES	: $q_{actual} = 1.45 q_{mean}$
TORQUE GAUGES	: $q_{actual} = 1.45 q_{mean}$ (APPROX.)
MOMENT GAUGES	: $q_{actual} = 1.48 q_{mean}$

Fig. 76 STRAIN DISTRIBUTION IN WAY OF GAUGES

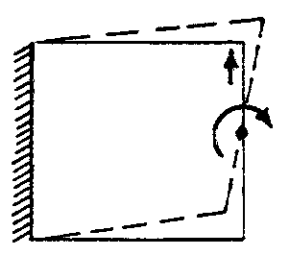


Fig. 77 INFLUENCE OF ROTATION ON MOMENT FLEXURES